

ABSTRACT

Peng Geng. Numerical and Theoretical Analysis of Falling Plume Caused by Bioconvection of Microorganisms and Its Applications (Under the direction of Dr. Andrey V. Kuznetsov)

The purpose of this research is to analytically and numerically investigate the formation and applications of bioconvection caused by microorganisms. The falling plumes in bioconvection with a suspension saturated with porous medium are studied theoretically. Utilizing bioconvection to mix and uniform solid particles are studied numerically. Large particle settling in bioconvection is also included in this research.

The formation of falling plumes as observed in suspensions of these bacteria in experiments is explained in this research. A suspension of motile oxytactic bacteria that consume oxygen and swim up the oxygen gradient is considered. A utilized model that is based on a quasi-steady approximation is established. Based on the approximate solution, a similarity solution of full governing equations that describe fluid flow as well as oxygen and cell transport in the plume is obtained.

Settling of small solid particles in a suspension of motile gyrotactic microorganisms is investigated numerically. Bioconvection induced by the upswimming of microorganisms enhances mixing between the particles and leads to a more uniform number density distribution of solid particles across the layer depth. The case that a bioconvection suspension that contains two types of particles is considered. It is found that the number density distribution of solid particles of one type impacts that of particles of the other type as well as that of microorganisms.

Settling of one or two large solid particles in a bioconvection flow induced by gyrotactic motile microorganisms is investigated as well. Chimera method is utilized to generate subgrids around the moving particles. Equations for calculating values on moving boundaries in the streamfunction-vorticity formulation are developed. It is demonstrated that bioconvection can either accelerate or decelerate settling of the particle depending on the initial position of the particle relative to the plume

center. Settling of one particle can displace bioconvection plume and change its shape. Introducing the second particle can either further displace the plume or make this displacement smaller depending on the initial releasing positions of the first and second particles.

**Numerical and Theoretical Analysis of Falling Plume Caused by
Bioconvection of Microorganisms and Its Applications**

Peng Geng

A dissertation submitted to the Graduate Faculty of

North Carolina State University

In partial fulfillment of the

Requirements for the degree of

Doctor of Philosophy

In

MECHANICAL ENGINEERING

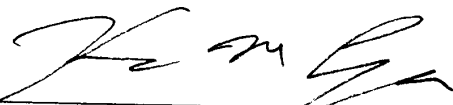
Raleigh, NC

2005

Approved by:


ANDREY V. KUZNETSOV
Chair of Advisory Committee


TAREK ECHEKKI


KEVIN M. LYONS


H. T. TRAN

UMI Number: 3195117

UMI[®]

UMI Microform 3195117

Copyright 2006 by ProQuest Information and Learning Company.
All rights reserved. This microform edition is protected against
unauthorized copying under Title 17, United States Code.

ProQuest Information and Learning Company
300 North Zeeb Road
P.O. Box 1346
Ann Arbor, MI 48106-1346

To my dearest mom and dad

BIOGRAPHY

Peng Geng was born in Beijing, People's Republic of China in 1977. After he received his B.S. degree in Engineering Mechanics from Tsinghua University of China in 2000, he went to University of Kansas, where he received his M.S. degree in Mechanical Engineering in 2001. Peng joined North Carolina State University, Raleigh, NC, in January 2002. He is a member of ASME.

ACKNOWLEDGEMENTS

First of all I would like to thank my advisor, Dr. Andrey V. Kuznetsov for his tremendous amount of help during my studies at NC State University. His enthusiasm and attitude in research guided me to complete my research and dissertation.

I gratefully acknowledge the support of this work by NASA Office of Biological and Physical Research, Physical Sciences Division. Thanks also go out to the committee members, Dr. Tarek Echehki, Dr. Kevin M. Lyons, and Dr. Hien T. Tran. I am grateful for their suggestions and comments for my research and dissertation.

Special mention goes to my colleague, Mr. Sid Becker, for his continuous assistance, encouragement and friendship.

Great thanks are present to my dearest family, mom, dad and my elder brother. I could not have done all of this without your unconditional love.

TABLE OF CONTENTS

LIST OF TABLES	viii
LIST OF FIGURES	ix
1. INTRODUCTION	1
1.1 BACKGROUND OF BIOCONVECTION OF MICROORGANISMS	1
1.2 RESERCH ON <i>BIOCONVECTION SEDIMENTATION</i> OF SMALL SOLID PARTICLES	1
1.3 RESERCH ON <i>BIOCONVECTION SEDIMENTATION</i> OF LARGE SOLID PARTICLES	2
1.4 INTROUCTION OF PARTS AND CHAPTERS.....	2
REFERENCE.....	6
PART ONE: FALLING PLUME IN BIOCONVECTION OF OXYTACTIC BACTERIA IN POROUS MEDIUM.....	9
2. A SIMILARITY SOLUTION FOR A FALLING PLUME IN BIOCONVECTION OF OXYTACTIC BACTERIA IN A POROUS MEDIUM.....	10
ABSTRACT.....	10
2.1 INTRODUCTION	10
2.2 PROBLEM DISCRIPTION.....	12
2.3 RESULT AND DISCUSSION	18
2.4 CONCLUSIONS.....	20
ACKNOWLEDGEMENT	20
REFERENCES	20
3. ANALYTICAL INVESTIGATION OF A FALLING PLUME CAUSED BY BIOCONVECTION OF OXYTACTIC BACTERIA IN A FLUID SATURATED POROUS MEDIUM	22
ABSTRACT.....	22
3.1 INTRODUCTION	22
3.2 SIMILARITY TRANSFORMATION.....	24
3.3 SERIED SOLUTION FOR SMALL SIMILARITY VARIABLE.....	28
3.4 NUMERICAL RESULTS AND DISCUSSION	30
3.5 CONCLUSIONS.....	33
ACKNOWLEDGEMENTS	34
REFERENCES	34
PART TWO: INTERACTION BETWEEN MICROORGANISMS AND SMALL SOLID PARTICLES IN BIOCONVECTION SUSPENSION.....	36
4. THE INTERACTION OF BIOCONVECTION CAUSED BY GYROTACTIC MICROORGANISMS AND SETTLING OF SMALL SOLID PARTICLES	37
ABSTRACT.....	37
NOMENCLATURE	38
4.1 INTRODUCTION	41

4.2	GOVERNING EQUATIONS	44
4.3	RESULTS AND DISCUSSION	49
4.4	CONCLUSIONS.....	66
	ACKNOWLEDGEMENTS.....	67
	REFERENCES	67
5.	SETTLING OF BIDISPERSED SMALL SOLID PARTICLES IN A DILUTE SUSPENSION CONTAINUNG GYROTACTIC MICROORGANISMS	69
	ABSTRACT.....	69
	NOMENCLATURE	70
5.1	INTRODUCTION	74
5.2	GOVERNING EQUATIONS.....	76
5.3	RESULTS AND DISCUSSION	83
5.4	CONCLUSIONS.....	98
	ACKNOWLEDGEMENTS.....	98
	REFERENCES	98
6.	INTRODUCING THE CONCEPT OF EFFECTIVE DIFFUSIVITY TO EVALUATE THE EFFECT OF BIOCONVECTION ON SMALL SOLID PARTICLES	100
	ABSTRACT.....	100
	NOMENCLATURE	101
6.1	INTRODUCTION	105
6.2	GOVERNING EQUATIONS.....	107
6.3	RESULTS AND DISCUSSION.....	114
6.4	CONCLUSIONS.....	126
	ACKNOWLEDGEMENTS.....	127
	REFERENCES	127
PART THREE: DYNAMICS OF LARGE SOLID PARTICLES IN		
BIOCONVECTION FLOW CAUSED BY MOTILE GYROTACTIC		
MICROORGANISMS..... 130		
7.	DIRECT NUMERICAL SIMULATION OF SETTLING OF A LARGE SOLID PARTICLE DURING BIOCONVECTION.....	131
	ABSTRACT.....	131
	NOMENCLATURE	132
7.1	INTRODUCTION	135
7.2	GOVERNING EQUATIONS.....	137
7.3.	RESULTS AND DISCUSSION	147
7.4	CONCLUSIONS.....	158
8.	DYNAMICS OF LARGE SOLID PARTICLES IN BIOCONVECTIVE SEDIMENTATION.....	161
	ABSTRACT.....	161
8.1	INTRODUCTION	162
8.2	GOVERNING EQUATIONS.....	164

8.3	RESULTS AND DISCUSSION	171
8.4	CONCLUSIONS.....	187
	REFERENCE.....	187
9	CONCLUSIONS.....	190
9.1	REMARKS ON FALLING BIOCONVECTION PLUME.....	190
9.2	REMARKS ON SMALL SOLD PARTICLES SETTLING IN BIOCONVECTION	190
9.3	REMARKS ON LARGE SOLD PARTICLES SETTLING IN BIOCONVECTION	191
9.4	RECOMMENDATIONS FOR FUTURE WORK.....	191

LIST OF TABLES

Table 4-1. Physical properties and geometrical parameters utilized in the computations.....	50
Table 4-2. Values of dimensionless parameters utilized in computations.....	51
Table 4-3. Maximum values of the dimensionless number densities of microorganisms and particles, as well as the maximum value of the dimensionless stream function in the computational domain for the case of $\Delta\rho_p / \Delta\rho_m = 5$ and $D_p^* = 0.1$ at different time (based on the data shown in Figs. 3-6)	58
Table 4-4. Maximum values of the dimensionless number densities of microorganisms and particles, as well as the maximum value of the dimensionless stream function in the computational domain at steady-state conditions for $\Delta\rho_p / \Delta\rho_m = 5$ for different diffusivities of solid particles (based on the data shown in Figs. 4-2, 4-5, 4-7, and 4-8)62	
Table 4-5. Maximum values of the dimensionless number densities of microorganisms and particles, as well as the maximum value of the dimensionless stream function in the computational domain at steady-state conditions for $D_p / D_m = 0.1$ for different densities of solid particles (based on the data shown in Figs. 4-2, 4-5, 4-9, and 4-10).....	65
Table 5-1. Physical properties and geometrical parameters utilized in computations.....	83
Table 5-2. Values of dimensionless parameters utilized in computations.....	84
Table 6-1. Physical properties, geometrical parameters, and values of dimensionless parameters utilized in computations	115
Table 6-2. Physical properties and values of dimensionless parameters of particles utilized in computations	115
Table 6-3. Effective diffusivities of solid particles of types 1 through 6 for monodispersed cases	121
Table 6-4. Effective diffusivities of solid particles of types 1 through 6 for bidispersed cases	125
Table 6-5. Effective diffusivities of solid particles of type 4 for bidispersed cases	126
Table 7-1. Physical properties, geometrical parameters, and values of dimensionless parameters utilized in computations	147
Table 7-2. Initial positions of the center of the particle for Cases A-E	148
Table 8-1. Physical properties, geometrical parameters, and values of dimensionless parameters utilized in computations	172
Table 8-2. Initial positions of particle centers for Cases A-D	173

LIST OF FIGURES

Figure 2-1. Schematic diagram of bioconvection plume in a fluid saturated porous medium 11	
Figure 2-2. Similarity solution for $\bar{Q} = 8.62 \times 10^{-6}$: (a) Dimensionless cell concentration, $N(\eta)$; (b) Dimensionless rate of change of oxygen concentration, $G'(\eta)$; (c) Dimensionless downward fluid filtration velocity, $F'(\eta)/\eta$	19
Figure 4-1. (a) Computational domain and boundary conditions (b) Swimming direction of a gyrotatic microorganism	43
Figure 4-2. Basic case: no solid particles, steady-state plume ($t^* = 0.49825$). (a) Dimensionless number of microorganisms, (b) Contours of dimensionless stream function, (c) Fluid velocity vector field, (d) Streamlines.....	52
Figure 4-3. Solid particles present, $\bar{n}_p/\bar{n}_m = 0.1$, $\Delta\rho_p/\Delta\rho_m = 5$, $D_p^* = 1/10$, $t^* = 0.19825$. (a) Dimensionless number density of microorganisms, (b) Dimensionless number density of particles, (c) Contours of dimensionless stream function, (d) Fluid velocity vector field	54
Figure 4-4. Same as Fig. 4-3, $t^* = 0.3$	55
Figure 4-5. Same as Fig. 4-3, $t^* = 0.49825$	56
Figure 4-6. Same as Fig. 4-3, $t^* = 0.59825$	57
Figure 4-7. Same as Fig. 4-3, $D_p/D_m = 0.2$ and $t^* = 0.49825$ (steady-state plume).....	60
Figure 4-8. Same as Fig. 4-3, $D_p/D_m = 1$ and $t^* = 0.49825$ (steady-state plume).....	61
Figure 4-9. Same as Fig. 4-3, $\Delta\rho_p/\Delta\rho_m = 10$, $D_p/D_m = 0.1$, and $t^* = 0.49825$ (steady-state plume)	63
Figure 4-10. Same as Fig. 4-3, $\Delta\rho_p/\Delta\rho_m = 20$, $D_p/D_m = 0.1$, and $t^* = 0.49825$ (steady-state plume)	64
Figure 4-11. Distributions of the dimensionless number density of solid particles the middle of the chamber (at $x^* = 0$) computed with no bioconvection and with bioconvection. (a) n_p^* at $x^* = 0$ for cases displayed in Figs. 4-5, 4-7, and 4-8; (b1) n_p^* at $x^* = 0$ for cases displayed in Figs. 4-5, 4-9, and 4-10; (b2) Same as (b1), enlarged scale to show number density of solid particles close to the bottom of the chamber.....	66
Figure 5-1. Computational domain and boundary conditions	82
Figure 5-2. Distributions of the dimensionless number densities of microorganisms, (n_m^*), particles of type 1, ($(n_p^*)_1$), particles of type 2, ($(n_p^*)_2$), and the ratio of the difference between densities of the suspension and water to that of water, ($\Delta\rho/\rho_0$), at different moments of time: (a) $t^* = 0.001$, (b) $t^* = 0.25$, (c) $t^* = 0.30$, (d) $t^* = 0.65$, (e) $t^* = 1.2$, (f) $t^* = 3.2$	93
Figure 5-3. Nonuniformities of number density distributions of microorganisms ((a1) and (a2)), particles of type 1 ((b1) and (b2)), and particles of type 2 (c)	97
Figure 6-1. Computational domain and boundary conditions	112
Figure 6-2. Steady state distributions of the dimensionless number density of particles of type 4 in a bidispersed suspension of particles of types 1 & 4 (a) the case with bioconvection,	

computations are based on real diffusivity of solid particles, (b) the case without bioconvection, computations are based on effective diffusivity of solid particles	117
Figure 6-3. Nonuniformities of number density distributions of solid particles in a monodispersed suspension with and without bioconvection (effective diffusivities are utilized for the cases without bioconvection) (a) particles of type 1, (b) particles of type 2, (c) particles of type 3, (d) particles of type 4, (e) particles of type 5, (f) particles of type 6.....	119
Figure 6-4. Number density distributions of particles of types 1 and 6 in monodispersed suspensions (a1) particles of type 1 at $t^* = 0$, (a2) particles of type 1 at $t^* = 0.275$, (a3) particles of type 1 at $t^* = 5.0$, (b1) particles of type 6 at $t^* = 0$, (b2) particles of type 6 at $t^* = 0.5$, (b3) particles of type 6 at $t^* = 5.0$	120
Figure 6-5. Effect of particle density on effective diffusivity of solid particles in monodispersed and bidispersed suspensions. In a bidispersed case, particles of type 4 are always presented in the suspension while the other particle type is changing from 1 to 6. This figure shows effective diffusivities of the second particle type (1 through 6), while effective diffusivity of particles of type 4 in a bidispersed suspension is shown in Fig. 6-7	121
Figure 6-6. Nonuniformities of number density distributions of solid particles in a bidispersed suspension with and without bioconvection (effective diffusivities are utilized for the cases without bioconvection) (a) particles of type 1 & 4, (b) particles of type 2 & 4, (c) particles of type 3 & 4, (d) particles of type 4 & 4, (e) particles of type 5 & 4, (f) particles of type 6 & 4.....	124
Figure 6-7. Values of effective diffusivities for solid particles of type 4 in a bidispersed suspension. (The other particle type in the bidispersed suspension is changing from 1 through 6. Their effective diffusivities are shown in Figure 5.)	126
Figure 7-1. Schematic diagram of a large particle settling in developed bioconvection flow	136
Figure 7-2. Chimera grid system: (a) global and subgrid mesh, (b) subgrid mesh.....	141
Figure 7-3. Steady-state bioconvection plume: (a) Dimensionless number density of microorganisms, (b) Contour lines of the dimensionless vorticity, (c) Contour lines of the dimensionless streamfunction	145
Figure 8-1. (a) Schematic diagram of two large particles settling in a bioconvection flow; (b) Chimera grid system, global and subgrid meshes; (c) Chimera grid system, subgrid mesh	163
Figure 8-2. Steady-state bioconvection plume: (a) Dimensionless number density of microorganisms, (b) Contour lines of the dimensionless vorticity, (c) Contour lines of the dimensionless streamfunction, (d) Vector field of fluid velocity	173
Figure 8-3. Case A, $t = 1.0 s$: (a) Dimensionless number density of microorganisms, (b) Contour lines of the dimensionless vorticity, (c) Contour lines of the dimensionless streamfunction, (d) Vector field of fluid velocity	175
Figure 8-4. Case B: (a) Dimensionless number density of microorganisms, (b) Contour lines of dimensionless vorticity, (c) Contour lines of dimensionless streamfunction, (d) Vector field of fluid velocity.....	177
Figure 8-5. Case C: (a) Dimensionless number density of microorganisms, (b) Contour lines of dimensionless vorticity, (c) Contour lines of dimensionless streamfunction, (d) Vector field of fluid velocity.....	181

Figure 8-6. Case D: (a) Dimensionless number density of microorganisms, (b) Contour lines of dimensionless vorticity, (c) Contour lines of dimensionless streamfunction, (d) Vector field of fluid velocity..... 183

Figure 8-7. Paths of particle centers for (a) Case B, (b) Case C, (c) Case D and (d) Paths of the center of the Particle 1 for Cases A-D 184

Figure 8-8. Dimensionless velocity in the y direction at the center of the particles (a) Particle 1, (b) Particle 2..... 186

1. INTRODUCTION

1.1 BACKGROUND OF BIOCONVECTION OF MICROORGANISMS

Bioconvection is a phenomenon caused by collective swimming in a particular direction of motile microorganisms. Most significant results in the area of bioconvection were obtained over the last two decades ([1], [2], [3], [4], [5]). Two types of microorganisms are widely considered in bioconvection: motile oxytactic bacteria and motile gyrotactic microorganisms. Oxytactic bacteria such as *Bacillus subtilis*, consume oxygen and swim up oxygen gradients. In a deep chamber, because of the limited diffusivity of oxygen, oxygen concentration is high only in a thin cell-rich upper boundary layer. Since bacteria are heavier than water, the cell-rich upper boundary layer becomes unstable and bioconvection plumes develop. Gyrotaxis is the behavior typical for algae, whose swimming direction is against gravity in still water, but once bioconvection develops, their swimming direction is determined by the balance of two torques: the viscous torque acting on a body placed in a shear flow and the torque that is generated by gravity because the center of mass of a typical alga is displaced from its center of buoyancy. The density of regions of downflow becomes larger than that of regions of upflow.

Two similarity solutions for a falling plume in bioconvection of oxytactic bacteria in a porous medium are covered in Part One (Chapters 2-3); the applications of using gyrotactic microorganisms on mixing settling small solid particles is covered in Part Two (Chapters 4-6); the application of using gyrotactic microorganisms on settling large solid particles is covered in Part Three (Chapters 7-8).

1.2 RESEARCH ON BIOCONVECTION SEDIMENTATION OF SMALL SOLID PARTICLES

Despite a considerable number of theoretical and experimental works on bioconvection, the effect of bioconvection on settling of small solid particles has never been studied before. This is an interesting topic because it deals with a possible application of bioconvection: the utilization of bioconvection to

slow down settling and enhance mixing between particles. The advantage of bioconvection is that it provides a simple mechanism for enhancing mixing and slowing down settling in very small fluid volumes ([10], [11]). This may be important, for example, in the pharmaceutical and biotechnological industries to enhance mixing in microvolumes of a fluid. Biotechnology is increasingly involved with large numbers of experiments, such as analyses of DNA or drugs, screening of patients, and combinatorial synthesis, all of which are processes that often require handling microvolumes of fluids. The settling of *monodispersed* and *bidispersed* small solid particles in a suspension of motile gyrotactic microorganisms is investigated. It was found that the mixing induced by bioconvection leads to a more uniform number density distribution of solid particles along the height of the chamber.

1.3 RESEARCH ON BIOCONVECTION SEDIMENTATION OF LARGE SOLID PARTICLES

The application of bioconvection is naturally extended from mixing small particles to large particles, in which the computational becomes to a much harder one that contains multi-connected domain with moving boundaries. Chimera method is utilized to decompose the moving domain. A new numerical method is developed to simulate the boundary conditions in Streamfunction-vorticity formulation. The results of this chapter bring to light the interaction between large particles and bioconvection plumes which may be utilized in controlling sedimentation in microvolumes. The bioconvection plume that is caused by gyrotactic microorganisms is already fully developed during the sedimentation of large particles. Gyrotactic behavior causes these microorganisms to accumulate in the regions of most rapid downflow. The effect of periodic boundary condition on particle sedimentation is studied and found that the vertical boundaries of the domain pushed the particle away from the periodic boundary.

1.4 INTRODUCTION OF PARTS AND CHAPTERS

This dissertation consists of three parts and nine chapters. Each one of Chapters 2-8 is mainly a published or submitted chapter and is relatively independent of each other. In Part One, which includes Chapters 2 and 3, the existence of bioconvection plume in a porous medium saturated with a suspension of oxytactic bacteria is theoretically predicted. Similarity solutions that describe fluid flow as well as oxygen and cell transport in the plume are obtained. Part Two, which includes Chapters 4 – 6, numerically investigates settling of small solid particles in a suspension of motile gyrotactic microorganisms. Bioconvection induced by the upswimming of microorganisms enhances mixing between the particles and leads to a more uniform number density distribution of solid particles across the layer depth. An optimal size and density of particles are found that effectively slow down bioconvection. A very useful parameter called the *effective diffusivity* of solid particles is firstly introduced to evaluate the effect of bioconvection to enhance mixing of small solid particles. Part Three, which includes Chapters 7-8, investigates the case that large solid particles settling in microorganisms suspension. It is demonstrated that the introduction of a single large particle displaces bioconvection plume and changes its shape. The introduction of two particles on the same side of the bioconvection plume further displaces the plume while the introduction of two particles on opposite sides reduces this displacement.

Chapter 2 (published as ref. [12]) analytically investigates a similarity solution for a falling bioconvection plume in a deep chamber filled with a fluid saturated porous medium. The existence of bioconvection plume in a porous medium saturated with a suspension of oxytactic bacteria is theoretically predicted. The utilized model is based on a quasi-steady approximation which assumes that the timescale for the development of bioconvection plume is much smaller than the timescale for the depletion of the cell-rich upper boundary layer.

Chapter 3 (published as ref. [13]) investigates a similarity solution of full governing equations (without utilizing the boundary layer approximation) that describe fluid flow as well as oxygen and cell transport in the plume is obtained. The resulting ordinary differential equations are singular when

the similarity variable approaches zero; therefore, a series solution of these ordinary differential equations, which is valid for small values of the similarity variable, is obtained. This series solution is used as a starting point for a numerical solution, which makes it possible to investigate the plume for the whole range of values of the similarity variable.

Chapter 4 (published as ref. [13]) numerically investigates the settling of small solid particles in a suspension of motile gyrotactic microorganisms. The particles are assumed to be sufficiently small, so that the Brownian diffusion is not completely negligible. The formation of almost regular patterns and gyrotactic plumes in algal suspensions is documented in numerous experimental papers ([15 – 18]). Despite a considerable number of theoretical and experimental works on bioconvection, the effect of bioconvection on settling of small solid particles has never been studied before. Computational results show that bioconvection induced by the upswimming of microorganisms enhances mixing between the particles and leads to a more uniform number density distribution of solid particles across the layer depth.

Chapter 5 (published as ref. [19]) numerically considers a bidispersed suspension of small solid particles that have different densities and settling velocities in a fluid that contains motile gyrotactic microorganisms. The introduction of the second type of small solid particles (that have a different density than particles of the first type) into the suspension that already contains microorganisms and particles of the first type does not have much influence on the number density distribution of microorganisms. However, the number density distribution of particles of the first type becomes more non-uniform. This suggests a useful method of adjusting the number density distribution of particles in bioconvection by introducing particles of a different density. It is interesting that this does not significantly impact bioconvection. Furthermore, bioconvection is more efficient in mixing solid particles, which have smaller settling velocity. With bioconvection, number densities of particles attain their steady-state distributions much faster than without bioconvection.

Chapter 6 (published as ref. [20]) firstly introduces a very useful parameter named the *effective diffusivity* of solid particles is firstly introduced to evaluate the effect of bioconvection to enhance mixing of small solid particles. With the application of *effective diffusivity* of solid particles, numerical results show that: 1) In a monodispersed suspension, increasing the density of particles increases the nonuniformity of the number density distribution of particles, which means that bioconvection is less effective in mixing suspensions of heavy particles than it is in mixing suspensions of light particles. 2) In a bidispersed suspension, the introduction of a second particle type decreases the effect of mixing by the bioconvection flow thus making the particle distribution more nonuniform.

Chapter 7 (submitted as ref. [21]) investigates settling of a large solid particle in bioconvection flow caused by gyrotactic microorganisms. A subgrid is generated around the moving particle, which is called the Chimera method, is utilized. A numerical method based on the streamfunction-vorticity formulation for the case of a multi-connected domain with moving boundaries is developed. The particle settling changes the shape and location of the bioconvection plume. The particle settling is also affected by bioconvection.

Chapter 8 (submitted as ref. [22]) investigates settling of two large solid particles in bioconvection flow caused by gyrotactic microorganisms. It is demonstrated that the introduction of a single large particle displaces bioconvection plume and changes its shape. The introduction of two particles on the same side of the bioconvection plume further displaces the plume while the introduction of two particles on opposite sides reduces this displacement. The influence of the bioconvection plume on the particles' settling paths is investigated.

REFERENCE

1. Pedley, T.J., Hill, N.A., and Kessler, J.O. (1988), "The growth of bioconvection patterns in a uniform suspension of gyrotactic microorganisms," *J. Fluid Mech.*, Vol. 195, pp. 223-338.
2. Ghorai, S. and Hill, N.A. (1999), "Development and stability of gyrotactic plumes in bioconvection," *J. Fluid Mech.*, Vol. 400, pp. 1-31.
3. Pedley, T.J. and Kessler, J.O. (1987), "The orientation of spheroidal microorganisms swimming in a flow field," *Proc. R. Soc. Lond.*, Vol. B231, pp. 47-70.
4. Pedley, T.J. and Kessler, J.O. (1990), "A new continuum model for suspensions of gyrotactic microorganisms," *Journal of Fluid Mechanics*, Vol. 212, pp. 155-182.
5. Pedley, T.J. and Kessler, J.O. (1992), "Hydrodynamic phenomena in suspensions of swimming microorganisms," *Ann. Rev. Fluid Mech.*, Vol. 24, pp. 313-358.
6. Kessler, J.O.: The external dynamics of swimming microorganisms. Progress in Phycological Research **4**, pp. 257-307, Bristol: Biopress 1986.
7. Hillesdon, A.J., Pedley, T.J., Kessler, J.O.: The development of concentration gradients in a suspension of chemotactic bacteria. Bull. Math. Biol. **57**, 299-344 (1995).
8. Kessler, J.O., Hoelzer, M.A., Pedley, T.J., Hill, N.A.: Functional patterns of swimming bacteria. In Mechanics and Physiology of Animal Swimming, L. Maddock, Q. Bone, and J.M.V. Rayner, eds., pp. 3-12, Cambridge University Press 1994.

9. Metcalfe, A.M., Pedley, T.J.: Falling Plumes in Bacterial Bioconvection. *J. Fluid Mech.* **445**, 121-149 (2001).
10. Ghorai, S. and Hill, N.A. (1999), "Development and stability of gyrotactic plumes in bioconvection," *J. Fluid Mech.*, Vol. 400, pp. 1-31.
11. Ghorai, S. and Hill, N.A. (2000), "Periodic arrays of gyrotactic plumes in bioconvection," *Physics of Fluids*, Vol. 12, pp. 5-22.
12. A.V. Kuznetsov, A.A. Avramenko, and P. Geng, A Similarity Solution for a Falling Plume in Bioconvection of Oxytactic Bacteria in a Porous Medium, *International Communications in Heat and Mass Transfer*, vol. 30, pp. 37-46, 2003.
13. A.V. Kuznetsov, A.A. Avramenko, and P. Geng, Analytical Investigation of a Falling Plume Caused by Bioconvection of Oxytactic Bacteria in a Fluid Saturated Porous Medium, *International Journal of Engineering Science*, vol. 42, pp. 557-569, 2004.
14. A.V. Kuznetsov and P. Geng, The interaction of bioconvection caused by gyrotactic microorganisms and settling of small solid particles, *International Communications in Heat and Mass Transfer*, **15**, **4**, 328 (2005)
15. Kessler, J.O. (1985a), "Hydrodynamic focusing of motile algal cells," *Nature*, Vol. 313, pp. 218-220
16. Kessler, J.O. (1985b), "Co-operative and concentrative phenomena of swimming microorganisms," *Contemp. Phys.*, Vol. 26, pp. 147-166.
17. Kessler, J.O., Wiseley, D.A., Remick, K.E., Marthaler, D.E. (1997), "Individual and collective dynamics of swimming bacteria," *Proceedings of the Workshop "Traffic and*

Granular Flow'97", M. Schreckenberg and D.E. Wolf (Eds.), Springer, New York, pp. 37-51.

18. Kessler, J.O., Burnett, G.D., and Remick, K.E. (2000), "Mutural dynamics of swimming microorganisms and their fluid habitat," *Nonlinear Science at the Dawn of the 21st Century*, P.L. Christiansen, M.P. Sorensen, and A.C. Scott (Eds.), Springer, New York, pp. 409-426.
19. Geng P. and Kuznetsov A.V., Settling of Bidispersed Small Solid Particles in a Dilute Suspension Containing Gyrotactic Microorganisms, *International Journal of Engineering Science* **43**, 992 (2005).
20. Geng P. and Kuznetsov A.V., Introducing the Concept of Effective Diffusivity to Evaluate the Effect of Bioconvection on Small Solid particles, *I. J. Trans. Phenomena*, **7**, 321 (2005).
21. Geng, P. and Kuznetsov, A.V., Direct Numerical Simulation of Settling of a Large Solid Particle During Bioconvection, *International Journal of Numerical Methods in Fluids*, under review.
22. Geng, P. and Kuznetsov, A.V., Direct Numerical Simulation of Settling of a Large Solid Particle during Bioconvection, *Physics of Fluid*, under review.

PART ONE

FALLING PLUME IN BIOCONVECTION OF OXYTACTIC

BACTERIA IN POROUS MEDIUM

2. A SIMILARITY SOLUTION FOR A FALLING PLUME IN BIOCONVECTION OF OXYTACTIC BACTERIA IN A POROUS MEDIUM

ABSTRACT

The objective of this chapter is to present a similarity solution for a falling bioconvection plume in a deep chamber filled with a fluid saturated porous medium. A suspension of motile oxytactic bacteria, such as *Bacillus subtilis*, which swim up the oxygen gradient, is considered. In a deep chamber, because of the limited diffusivity of oxygen, oxygen concentration is high only in a thin cell-rich upper boundary layer. Since bacteria are heavier than water, the cell-rich upper boundary layer becomes unstable and bioconvection plumes develop. The bioconvection plume carries oxygen and cells from this cell-rich upper boundary layer to the lower region of the chamber.

2.1 INTRODUCTION

In Metcalfe and Pedley's recent paper [1], a theory of bioconvection in a suspension of the oxytactic bacteria *Bacillus subtilis*, which consume oxygen and swim up oxygen gradients, was developed. The objective of their research was to explain the formation of falling plumes as observed in suspensions of these bacteria in the experiments described in Kessler et al. [2] and Hillesdon et al. [3].

Metcalfe and Pedley [1] considered an initially well-mixed suspension in a deep chamber. The bottom and edges of the chamber are sealed but its upper free surface is open to the air. Since the chamber is deep, the oxygen concentration below a certain depth is too small for the bacteria to be active. The experimental results demonstrate that there is a thin, cell-rich upper boundary layer caused by bacterial swimming up the oxygen gradient towards the free surface. The lower part of the chamber is

too far from the free surface; therefore, only very little oxygen can reach this region by diffusion. For this reason, the bacteria in this region become inactive when they consume all of the dissolved oxygen. The falling plumes provide a convective transport mechanism for oxygen from the upper boundary layer. As a result, some of the inactive cells in the lower region of the chamber are resuscitated by the oxygen carried by the falling plumes.

The goal of this chapter is to extend the theory developed in Metcalfe and Pedley [1] to the case where the chamber is filled with a fluid saturated porous medium of uniform porosity. Despite the potential of porous media to control bioconvection, the number of publications on bioconvection in porous media is very limited. An experimental paper by Kessler [4] addressed the utilization of a porous medium (a surgical cotton wool) to suppress bioconvection instability. Kuznetsov and Avramenko [5] developed a criterion for the critical permeability value of a porous medium. To the best of the authors' knowledge, bioconvection of oxytactic bacteria in porous media, which is addressed in this chapter, has never been investigated before.

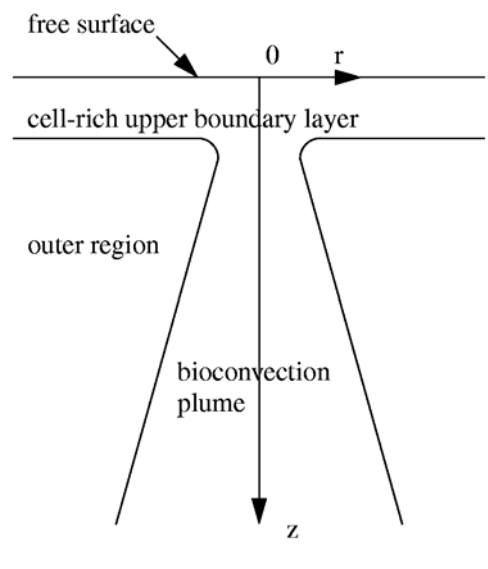


Figure 2-1. Schematic diagram of bioconvection plume in a fluid saturated porous medium

2.2 PROBLEM DISCRPTION

In this chapter, an axisymmetric falling plume is investigated. Following Metcalfe and Pedley [1], the orientation of bacteria by viscous forces in a shear flow (gyrotaxis) is neglected, and it is assumed that the cells are swimming in a strictly vertical direction and that their upswimming velocity is proportional to the gradient of oxygen concentration:

$$\mathbf{V} = bW_c H(C) \nabla C \quad (2.1)$$

where b has dimensions of length, W_c has dimensions of velocity (the product bW_c assumed to be constant), $H(C)$ is the step function, and C is the dimensionless oxygen concentration defined as

$$C = \frac{\tilde{C} - \tilde{C}_{\min}}{\tilde{C}_0 - \tilde{C}_{\min}} \quad (2.2)$$

where \tilde{C} is the oxygen concentration, \tilde{C}_0 is the concentration of oxygen at the free surface (assumed to be the same as the initial oxygen concentration), and \tilde{C}_{\min} is a minimum concentration of oxygen required for the bacteria to be active.

Governing equations for this problem are given below.

Conservation of Cells

$$\nabla \cdot (n\mathbf{U} + n\mathbf{V}) = \nabla \cdot (D_n \nabla n) \quad (2.3)$$

where n is the concentration of cells, \mathbf{U} is the filtration velocity vector, and $D_n = D_{n0} H(C)$ is the cell diffusivity (the diffusion term models the random aspects of cell swimming). Equation (2.3) accounts for three possible mechanisms of the transport of the cells: by convection, by upswimming, and by diffusion.

The plume in the upper part of the chamber, where the oxygen concentration is larger than \tilde{C}_{min} and all bacteria are actively swimming, is considered. In this part of the chamber $C > 0$; therefore, the step function, $H(C)$, identically equals to unity and Eq. (2.3) can be presented as:

$$\begin{aligned} & \left(v + bW_c \frac{\partial C}{\partial z} \right) \frac{\partial n}{\partial z} + \left(u + bW_c \frac{\partial C}{\partial r} \right) \frac{\partial n}{\partial r} + bW_c n \left(\frac{\partial^2 C}{\partial z^2} + \frac{\partial^2 C}{\partial r^2} + \frac{1}{r} \frac{\partial C}{\partial r} \right) \\ & = D_n \left(\frac{\partial^2 n}{\partial z^2} + \frac{\partial^2 n}{\partial r^2} + \frac{1}{r} \frac{\partial n}{\partial r} \right) \end{aligned} \quad (2.4)$$

where r is the radial coordinate, z is the vertically downward coordinate, u is the radial velocity component, and v is the vertical velocity component.

In the upper part of the chamber, the plume is narrow and Eq. (2.4) can be parabolized by neglecting terms containing $\frac{\partial^2 C}{\partial z^2}$, $\frac{\partial^2 n}{\partial z^2}$, and $\frac{\partial C}{\partial z} \frac{\partial n}{\partial z}$. This is consistent with the scaling analysis and parabolization performed in Metcalfe and Pedley [1]. This results in the following cell conservation equation:

$$v \frac{\partial n}{\partial z} + \left(u + bW_c \frac{\partial C}{\partial r} \right) \frac{\partial n}{\partial r} + bW_c n \left(\frac{\partial^2 C}{\partial r^2} + \frac{1}{r} \frac{\partial C}{\partial r} \right) = D_n \left(\frac{\partial^2 n}{\partial r^2} + \frac{1}{r} \frac{\partial n}{\partial r} \right) \quad (2.5)$$

Conservation of Oxygen

$$\nabla \cdot (\tilde{C}\mathbf{U}) = D_C \nabla^2 \tilde{C} - \gamma \quad (2.6)$$

where D_C is the oxygen diffusivity and the term $-\gamma$ describes the consumption of oxygen by the bacteria. To account for the reduction of cell activity in the lower part of the chamber, where cell concentration is smaller than in the upper layer, it is assumed that $\gamma = \gamma_0 (n/n_{fs}) H(C)$, where n_{fs} is the concentration of bacteria at the free surface (assumed to be constant) and γ_0 is a constant characterizing the rate of oxygen consumption by the bacteria.

$$v \frac{\partial C}{\partial z} + u \frac{\partial C}{\partial r} = D_c \left(\frac{\partial^2 C}{\partial z^2} + \frac{\partial^2 C}{\partial r^2} + \frac{1}{r} \frac{\partial C}{\partial r} \right) - \frac{\gamma}{\Delta C} \quad (2.7)$$

Neglecting the term $\frac{\partial^2 C}{\partial z^2}$, Eq. (2.7) is parabolized as:

$$v \frac{\partial C}{\partial z} + u \frac{\partial C}{\partial r} = D_c \left(\frac{\partial^2 C}{\partial r^2} + \frac{1}{r} \frac{\partial C}{\partial r} \right) - \frac{\gamma}{\Delta C}, \quad (2.8)$$

where $\Delta C = \tilde{C}_0 - \tilde{C}_{\min}$.

z-momentum equation

$$\frac{\partial p}{\partial z} + \frac{\mu}{K} v - n \theta \Delta \rho g = 0, \quad (2.9)$$

where p is the pressure; K is the permeability of the porous medium; θ is the average volume of the bacterium; $\Delta \rho$ is the density difference, $\rho_{cell} - \rho_0$; μ is the dynamic viscosity, assumed to be approximately the same as that of water; and ρ_0 is the density of water.

r-momentum equation

$$\frac{\partial p}{\partial r} + \frac{\mu}{K} u = 0 \quad (2.10)$$

Continuity Equation

$$\nabla \cdot \mathbf{U} = 0 \quad (2.11)$$

or

$$\frac{1}{r} \frac{\partial(ru)}{\partial r} + \frac{\partial(v)}{\partial z} = 0 \quad (2.12)$$

Eliminating the pressure from (2.9) and (2.10) results in:

$$\frac{\mu}{K} \left(\frac{\partial v}{\partial r} - \frac{\partial u}{\partial z} \right) - \frac{\partial n}{\partial r} \theta \Delta \rho g = 0. \quad (2.13)$$

Equations (2.5), (2.8), (2.12), and (2.13) must be solved subject to the following boundary conditions. Utilizing symmetry about $r=0$, the following boundary conditions are imposed at $r=0$:

$$\frac{\partial n}{\partial r} = 0, \quad \frac{\partial C}{\partial r} = 0, \quad u = 0, \quad \frac{\partial v}{\partial r} = 0 \quad (2.14)$$

At $r \rightarrow \infty$ the following boundary conditions are imposed:

$$n \rightarrow 0, \quad \frac{\partial C}{\partial r} \rightarrow 0, \quad v \rightarrow 0 \quad (2.15)$$

Following Metcalfe and Pedley [1], a similarity solution to Eqs. (2.5), (2.8), (2.12), and (2.13) is investigated. Assuming that R is the radius of the plume, the following scaling is utilized:

$$R \propto z^a, \quad v \propto z^b, \quad n \propto z^c, \quad C \propto z^d, \quad \text{and} \quad u \propto z^{a+b-1} \quad (2.16)$$

Substitution Eqs. (2.16) into Eqs. (2.5), (2.8), (2.12), and (2.13) and equating the powers of z , the following solution is obtained: $a=1$, $b=-1$, $c=-1$, and $d=0$. The similarity variable η is then defined as:

$$\eta = \frac{r}{z} \quad (2.17)$$

The new dimensionless functions $N(\eta)$, $G(\eta)$, and $F(\eta)$ are introduced as:

$$n = \frac{K^{1/2}}{\theta} z^{-1} N(\eta), \quad C = G(\eta), \quad \psi = \frac{\mu}{\rho} z F(\eta), \quad u = \frac{\mu}{\rho} z^{-1} \left[F'(\eta) - \frac{F(\eta)}{\eta} \right], \quad v = \frac{\mu}{\rho} \frac{z^{-1}}{\eta} F'(\eta) \quad (2.18)$$

where stream function is defined as $\partial \psi / \partial r = v r$ and $\partial \psi / \partial z = -u r$.

Continuity Eq. (2.12) is automatically satisfied. Substituting Eqs. (2.18) into Eqs. (2.5), (2.8), and (2.13), the following equations for the dimensionless functions $N(\eta)$, $G(\eta)$, and $F(\eta)$ are obtained:

$$N'' + \left[\frac{1}{\eta} (1 + \text{Sc}F) - \text{Pe} G' \right] N' + \left[\frac{\text{Sc}F'}{\eta} - \text{Pe} \frac{1}{\eta} G' - \text{Pe} G'' \right] N = 0 \quad (2.19)$$

$$G'' + \frac{1}{\eta} \left(1 + \text{Sc} \frac{D_n}{D_c} F \right) G' - \beta N^2 = 0 \quad (2.20)$$

$$(1 + \eta^2) F'' - \frac{F'}{\eta} - \text{Ar} \eta N' = 0 \quad (2.21)$$

where prime denotes the derivative with respect to η and

$$Pe = \frac{W_c b}{D_n}, \quad Sc = \frac{\mu}{\rho D_n}, \quad Ar = \frac{gK^{3/2} \rho \Delta \rho}{\mu^2}, \quad \beta = \frac{K \gamma_0}{D_c n_{fs} \Delta C \theta^2} \quad (2.22)$$

In Eqs. (2.22), Pe is the Peclet number, Sc is the Schmidt number, Ar is the Archimedes number, and β is the dimensionless parameter that represents the strength of oxygen consumption relative to its diffusion.

Equations (2.19)-(2.21) must be solved subject to the following boundary conditions, which are obtained by transforming the boundary conditions given by Eqs. (2.14) and (2.15):

$$\text{At } \eta = 0: \quad N' = 0, \quad G' = 0, \quad F' - \frac{F}{\eta} = 0, \quad \frac{F''}{\eta} - \frac{F'}{\eta^2} = 0 \quad (2.23)$$

$$\text{As } \eta \rightarrow \infty: \quad N = 0, \quad G' = 0, \quad \frac{F'}{\eta} = 0 \quad (2.24)$$

An additional condition that the solution must obey can be obtained from Eq. (2.5), which can be recast as:

$$\frac{\partial}{\partial r} \left(r n u + b W_c r n \frac{\partial C}{\partial r} - D_n r \frac{\partial n}{\partial r} \right) + r \frac{\partial}{\partial z} (n v) = 0 \quad (2.25)$$

Integrating Eq. (2.25) from $r = 0$ to $r = \infty$ and utilizing boundary conditions yields

$$Q = \int_0^{\infty} v n r dr = \text{constant} \quad (2.26)$$

This condition, first obtained in Metcalfe and Pedley [1], physically means cells do not swim into or out of the plume; therefore, the flux of the cells in the z -direction is the same in any cross-section of the plume for any value of z .

It is easy to check that the similarity solution defined by Eqs. (2.18) satisfies this condition. Indeed, substituting the first and the fifth of Eqs. (2.18) into Eq. (2.26), the following is obtained:

$$Q = \frac{K^{1/2}}{\theta} \frac{\mu}{\rho} \int_0^{\infty} z^{-2} \frac{F'}{\eta} N r dr = \frac{K^{1/2}}{\theta} \frac{\mu}{\rho} \int_0^{\infty} F' N d\eta = \text{constant} \quad (2.27)$$

where Q is the flux of the bacteria in the z -direction.

Equation (2.27) can be recast as

$$\int_0^{\infty} F' N d\eta = \frac{Q\theta\rho}{K^{1/2}\mu} = \bar{Q} \quad (2.28)$$

where \bar{Q} is the dimensionless flux of the bacteria in the z -direction.

This condition must be used along with boundary conditions (2.23) and (2.24) in numerical integration of Eqs. (2.19)-(2.21).

Equations (2.19)-(2.21) as well as boundary conditions (2.23) are singular at $\eta = 0$. To initiate the numerical solution a series solution must be obtained for small η . The following series expansions are assumed for functions $N(\eta)$, $G'(\eta)$, and $F(\eta)$:

$$N(\eta) = \sum_{i=0}^{\infty} n_i \eta^i, \quad G'(\eta) = \sum_{i=0}^{\infty} g_i \eta^i, \quad F(\eta) = \sum_{i=0}^{\infty} f_i \eta^i \quad (2.29)$$

Boundary conditions at $\eta = 0$ given by Eqs. (2.23) yield to the following relations:

$$n_1 = g_0 = f_0 = f_1 = f_3 = 0 \quad (2.30)$$

It is assumed that $n_0 \neq 0$ and $f_2 \neq 0$ to provide for non-zero concentration of bacteria and nonzero axial fluid velocity in the center of the plume. The solution is obtained in terms of n_0 and f_2 as:

$$N(\eta) = n_0 - \frac{1}{4} (2f_2 n_0 \text{Sc} - n_0^3 \text{Pe}\beta) \eta^2 \\ + \frac{n_0}{64D_C} [2D_C f_2 \text{Sc} (2 + 4f_2 \text{Sc} + \text{Ar} n_0 \text{Sc}) - n_0^2 (2f_2 \{6D_C + D_n\} + \text{Ar} D_C n_0) \text{Pe}\text{Sc}\beta + 4D_C n_0^4 \text{Pe}^2 \beta^2] \eta^4$$

$$\begin{aligned}
& + \frac{1}{2304D_C^2} \left(-2D_C^2 f_2 n_0 \text{Sc} \{24 + \text{Sc}(24f_2^2 \text{Sc} - \text{Ar}n_0[14 + \text{Ar}n_0 \text{Sc}]) + f_2[36 + 22\text{Ar}n_0 \text{Sc}]\} \right) \\
& + n_0^3 \text{Pe} \text{Sc} \beta \{8D_n^2 f_2^2 \text{Sc} + 2D_C D_n f_2 [4 + 26f_2 \text{Sc} + 3\text{Ar}n_0 \text{Sc}] \\
& + D_C^2 (176f_2^2 \text{Sc} + \text{Ar}n_0 [12 + \text{Ar}n_0 \text{Sc}]) + f_2 [44 + 52\text{Ar}n_0 \text{Sc}]\} \\
& - D_C n_0^5 \{148D_C f_2 + 30D_n f_2 + 15\text{Ar}D_C n_0 + 2\text{Ar}D_n n_0\} \text{Pe}^2 \text{Sc} \beta^2 + 36D_C^2 n_0^7 \text{Pe}^3 \beta^3 \eta^6
\end{aligned} \tag{2.31}$$

$$\begin{aligned}
G'(\eta) &= \frac{1}{2} n_0^2 \beta \eta + \frac{n_0^2 \beta}{8D_C} [-f_2 \text{Sc}(2D_C + D_n) + D_C n_0^2 \text{Pe} \beta] \eta^3 \\
& + \frac{n_0^2 \beta}{192D_C^2} [2f_2 \text{Sc} \{2D_C (D_C + D_n) + (2f_2 [4D_C^2 + 2D_C D_n + D_n^2] + \text{Ar}D_C [D_C + D_n] n_0) \text{Sc}\} \\
& - D_C n_0^2 \{20D_C f_2 + 6D_n f_2 + \text{Ar}(D_C + D_n) n_0\} \text{Pe} \text{Sc} \beta + 6D_C^2 n_0^4 \text{Pe}^2 \beta^2] \eta^5
\end{aligned} \tag{2.32}$$

$$\begin{aligned}
F(\eta) &= f_2 \eta^2 + \frac{1}{16} [-2f_2 (2 + \text{Ar}n_0 \text{Sc}) + \text{Ar}n_0^3 \text{Pe} \beta] \eta^4 \\
& + \frac{1}{384D_C} [2D_C f_2 \{24 + \text{Ar}n_0 \text{Sc} (14 + 4f_2 \text{Sc} + \text{Ar}n_0 \text{Sc})\} \\
& - \text{Ar}n_0^3 \text{Pe} \{2D_n f_2 \text{Sc} + D_C (12 + 12f_2 \text{Sc} + \text{Ar}n_0 \text{Sc})\} \beta + 4\text{Ar}D_C n_0^5 \text{Pe}^2 \beta^2] \eta^6
\end{aligned} \tag{2.33}$$

2.3 RESULT AND DISCUSSION

Computations are performed for the following values of dimensionless parameters: $\text{Ar}=1$, $D_n / D_C = 1$, $\text{Pe} = 10$, $\text{Sc} = 20$, and $\beta = 10^6$. For $0 \leq \eta \leq 0.01$ computations are performed utilizing the series solution (2.31)-(2.33), and for $\eta > 0.01$ Eqs. (2.19)-(2.21) are solved numerically. Details of the computational procedure are discussed in Metcalfe and Pedley [1]. The solution is displayed in Figs. 2-2(a-c).

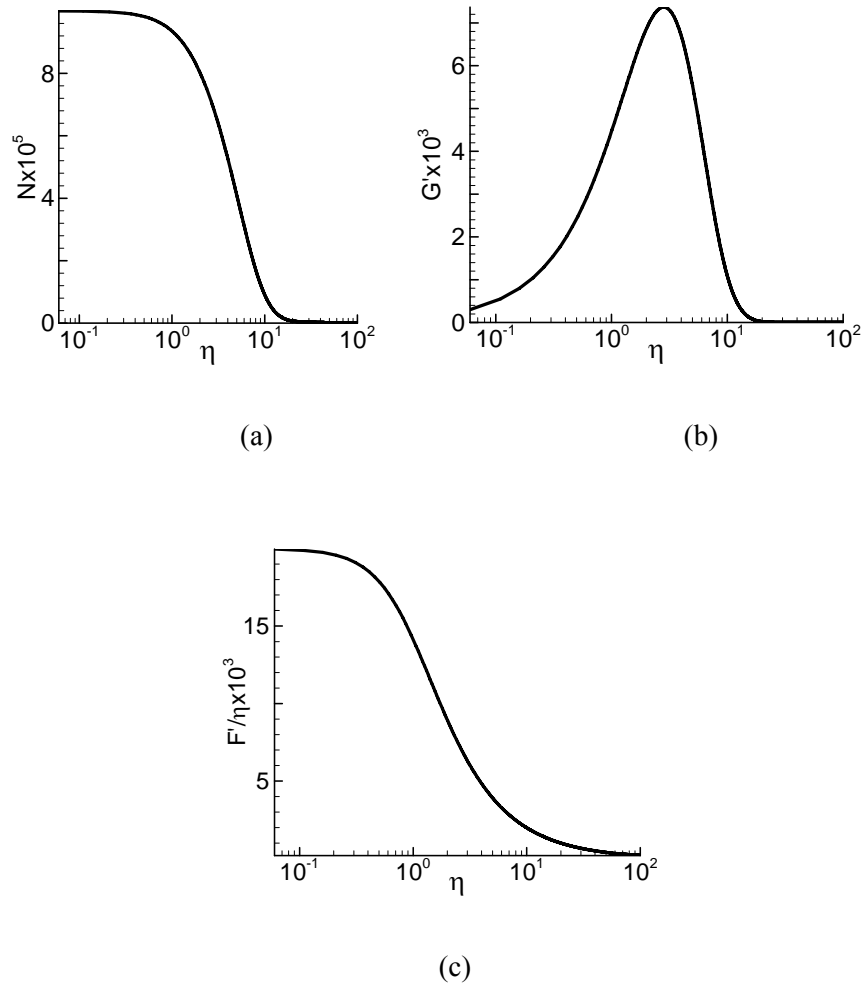


Figure 2-2. Similarity solution for $\bar{Q} = 8.62 \times 10^{-6}$: (a) Dimensionless cell concentration, $N(\eta)$; (b) Dimensionless rate of change of oxygen concentration, $G'(\eta)$; (c) Dimensionless downward fluid filtration velocity, $F'(\eta)/\eta$

Figure 2-2(a) displays the dimensionless concentration of bacteria, $N(\eta)$. As expected, the cell concentration is maximum in the center of the plume and decreases toward its edge. Figure 2-2(b) displays the dimensionless rate of change of oxygen concentration, $G'(\eta)$, which takes on its maximum at some distance from the center of the plume. This is in agreement with the clear fluid results presented in [1] and can be explained by the reduction of oxygen concentration in the center of the plume because of the large concentration of the cells that consume oxygen. Figure 2-2(c) displays

the dimensionless downward fluid filtration velocity, $F'(\eta)/\eta$, which takes on its maximum in the center of the plume and decreases to zero at the edge of the plume.

2.4 CONCLUSIONS

The existence of bioconvection plume in a porous medium saturated with a suspension of oxytactic bacteria is theoretically predicted. The utilized model is based on a quasi-steady approximation which assumes that the timescale for the development of bioconvection plume is much smaller than the timescale for the depletion of the cell-rich upper boundary layer. Further experimental research is needed to confirm the theoretical predictions of this chapter.

ACKNOWLEDGEMENT

AVK gratefully acknowledges the grant # NAG3-2706 awarded to him by NASA Office of Biological and Physical Research, Physical Sciences Division. The authors also acknowledge the NATO Expert Visit Grant (PST.EV.978144). Critical comments of Prof. D.A. Nield are greatly appreciated.

REFERENCES

1. A.M. Metcalfe and T.J. Pedley, *J. Fluid Mech.* **445**, 121 (2001).
2. J.O. Kessler, M.A. Hoelzer, T.J. Pedley, and N.A. Hill, in L. Maddock, Q. Bone, and J.M.V. Rayner (eds.), *Mechanics and Physiology of Animal Swimming*, pp.3-12, Cambridge University Press (1994).
3. A.J. Hillesdon, T.J. Pedley, and J.O. Kessler, *Bull. Math. Biol.* **57**, 299 (1995).

4. J.O. Kessler, *Progress in Phycological Research* **4**, 257 (1986). A.V. Kuznetsov and A.A. Avramenko, *International Communications in Heat and Mass Transfer* **29**, 175 (2002).

3. ANALYTICAL INVESTIGATION OF A FALLING PLUME CAUSED BY BIOCONVECTION OF OXYTACTIC BACTERIA IN A FLUID SATURATED POROUS MEDIUM

ABSTRACT

This chapter investigates a bioconvection plume in a suspension of oxytactic bacteria in a deep chamber filled with a fluid saturated porous medium. The plume transports oxygen from the upper boundary layer, which is rich in cells and oxygen, to the lower part of the chamber, which is depleted of both cells and oxygen. A similarity solution of full governing equations (without utilizing the boundary layer approximation) that describe fluid flow as well as oxygen and cell transport in the plume is obtained. The resulting ordinary differential equations are singular when the similarity variable approaches zero; therefore, a series solution of these ordinary differential equations, which is valid for small values of the similarity variable, is obtained. This series solution is used as a starting point for a numerical solution which makes it possible to investigate the plume for the whole range of values of the similarity variable.

3.1 INTRODUCTION

Bioconvection is a convection motion of fluid that results from the density gradient created by collective swimming in a particular direction of motile microorganisms that are heavier than the fluid. Although bioconvection is a beautiful phenomenon to observe (Kessler [1, 2], Kessler et al. [3, 4], and Harashima et al. [5]), in many practical situations bioconvection must be controlled or suppressed. For example, the property of motile microorganisms to swim in a particular direction may be used to concentrate the cells, purify cultures, separate different subpopulations (separate fast swimmers from slow swimmers and non-swimmers), or separate living and dead cells. In these

applications, bioconvection would prevent successful separation because it would cause mixing between different types of cells.

Porous media can be used to control bioconvection. In [6], Kessler suggested and experimentally proved that a porous medium (surgical cotton) can be utilized to suppress bioconvection in order to separate (eliminate) fungus from *Dunaliella* cultures and to concentrate vigorous cells of *Chlamydomonas nivalis* and *Chlamydomonas rosae*. These examples demonstrate the importance of investigating bioconvection in porous media and understanding the effect of porous media on bioconvection.

Hillesdon et al. [7] and Kessler et al. [8] describe experiments that show the formation of falling plumes in a deep chamber (7 to 8 mm in depth) that contains a suspension of oxytactic bacteria *Bacillus subtilis*. These bacteria consume oxygen and swim up the oxygen gradient as they require certain minimum concentration of oxygen to be active. Since the diffusivity of oxygen in water is very small, sufficient amounts of oxygen can penetrate by diffusion only in the upper fluid layer. In the lower part of the chamber, the bacteria consume all the oxygen keeping the oxygen concentration very low; therefore, the bacteria in this region become inactive. The chamber is thus divided into two regions, the upper cell-rich boundary layer, which contains actively swimming cells, and the lower region of the chamber, where concentration of oxygen is smaller than the minimum concentration and cells are therefore inactive. Since the bacteria are heavier than water, the upper cell-rich boundary layer becomes unstable, which results in the formation of falling plumes that carry cells and oxygen into the lower part of the chamber. The plumes provide for an additional convective transport mechanism into the depth of the chamber, which is more efficient than the diffusion transport mechanism. The oxygen transported by falling plumes resuscitates some of inactive cells in the lower part of the chamber.

Once bioconvection instability has developed, the falling plumes will eventually deplete the upper boundary layer of oxygen and bacteria. However, the timescale for the development of bioconvection

plumes is much smaller than for the depletion of the upper boundary layer. Therefore, the plume can be assumed quasi-steady and concentrations of oxygen and bacteria at the free surface can be assumed constant. Utilizing these assumptions, Metcalfe and Pedley [9] obtained a similarity solution for a falling plume in a suspension of oxytactic bacteria in a clear (of solid material) fluid. In a communication by Kuznetsov et al. [10], a falling plume in a suspension of oxytactic bacteria in a fluid saturated porous medium was investigated. The analyses presented in [9] and [10] were based on the parabolization of governing equations that describe fluid dynamics as well as cell and oxygen transport in the plume. This chapter attempts to obtain a similarity solution for the bioconvection plume in a porous medium utilizing full equations; without neglecting any terms and without parabolizing them.

3.2 SIMILARITY TRANSFORMATION

Symmetries of Eqs. (2.4), (2.7), (2.12), and (2.13) are investigated by utilizing the Lie group theory. Following the procedure described in Olver [12] it is established that these equations have a symmetry group of scaling with the following infinitesimal generator:

$$q = r \frac{\partial}{\partial r} + z \frac{\partial}{\partial z} - u \frac{\partial}{\partial u} - v \frac{\partial}{\partial v} - n \frac{\partial}{\partial n} \quad (3.1)$$

Following [12], it is established that the utilization of infinitesimal generator given by Eq. (3.2) results in the following self-similar transformation. The similarity variable η is defined as:

$$\eta = \frac{r}{z} \quad (3.2)$$

and the new dimensionless functions $N(\eta)$, $G(\eta)$, and $F(\eta)$ are defined as:

$$n = \frac{K^{1/2}}{\theta} z^{-1} N(\eta), \quad C = G(\eta), \quad \psi = \frac{\mu}{\rho} z F(\eta), \quad u = \frac{\mu}{\rho} z^{-1} \left[F'(\eta) - \frac{F(\eta)}{\eta} \right], \quad v = \frac{\mu}{\rho} \frac{z^{-1}}{\eta} F'(\eta) \quad (3.3)$$

where the streamfunction is defined as $\partial\psi / \partial r = vr$ and $\partial\psi / \partial z = -ur$.

The continuity Eq. (2.12) is automatically satisfied. Substituting Eqs. (3.1) into Eqs. (2.4), (2.7), and (2.13), the following equations for the dimensionless functions $N(\eta)$, $G(\eta)$, and $F(\eta)$ are obtained:

$$\begin{aligned} (1 + \eta^2)N'' + \left[4\eta + \frac{1}{\eta}(1 + ScF) - PeG'(1 + \eta^2) \right] N' \\ + \left[2 + \frac{ScF'}{\eta} - Pe\frac{1}{\eta}G' - PeG''(1 + \eta^2) - 3\eta PeG' \right] N = 0 \end{aligned} \quad (3.4)$$

$$(1 + \eta^2)G'' + \left(\frac{1}{\eta} + \frac{Sc}{\eta} \frac{D_n}{D_c} F + 2\eta \right) G' - \beta N^2 = 0 \quad (3.5)$$

$$(1 + \eta^2)F'' - \frac{F'}{\eta} - Ar\eta N' = 0 \quad (3.6)$$

where prime denotes the derivative with respect to η and

$$Pe = \frac{W_c b}{D_n}, \quad Sc = \frac{\mu}{\rho D_n}, \quad Ar = \frac{gK^{3/2} \rho \Delta \rho}{\mu^2}, \quad \beta = \frac{K\gamma_0}{D_c n_{fs} \Delta C \theta^2} \quad (3.7)$$

In Eqs. (3.7), Pe is the Peclet number, Sc is the Schmidt number, Ar is the Archimedes number, and β is the dimensionless parameter that represents the strength of oxygen consumption relative to its diffusion.

Equations (3.4)-(3.6) must be solved subject to the following boundary conditions that are obtained by transforming the boundary conditions given by Eqs. (2.14) and (2.15):

At $\eta = 0$:

$$N' = 0, G' = 0, F' - \frac{F}{\eta} = 0, \frac{F''}{\eta} - \frac{F'}{\eta^2} = 0 \quad (3.8)$$

As $\eta \rightarrow \infty$:

$$N = 0, G' = 0, \frac{F'}{\eta} = 0 \quad (3.9)$$

An additional condition that the solution must obey can be obtained from Eq. (2.4). Integrating this equation with respect to r from zero to infinity and rearranging, the following is obtained:

$$\int_0^{\infty} \frac{\partial}{\partial r} \left[r v n + r b W_c n \frac{\partial C}{\partial r} - r D_n \frac{\partial n}{\partial r} \right] dr + \int_0^{\infty} \frac{\partial}{\partial z} \left[r v n + r b W_c n \frac{\partial C}{\partial z} - r D_n \frac{\partial n}{\partial z} \right] dr = 0 \quad (3.10)$$

The first integral identically equals zero due to boundary conditions (2.14) and (2.15). It should be noted that for the first integral to be zero, the following condition must be satisfied:

$$r \frac{\partial n}{\partial r} \rightarrow 0 \quad \text{as} \quad r \rightarrow \infty \quad (3.11)$$

Although this condition does not formally follow from boundary conditions (2.14) and (2.15), it comes from the physics of the process and properties of the solution of Eqs. (3.4)-(3.6).

From Eq. (3.10) it follows that the integral below is a constant (takes on the same value at any cross-section independent of z):

$$Q = 2\pi \int_0^{\infty} \left[r v n + r b W_c n \frac{\partial C}{\partial z} - r D_n \frac{\partial n}{\partial z} \right] dr = \text{constant} \quad (3.11)$$

This integral characterizes the flux of the cells in the plume in the z -direction due to advection by the bulk flow (the first term in this integral), due to the cells swimming up the oxygen gradient (the second term, the cell swimming velocity is given by Eq. (2.1)), and due to cell diffusion (the third term). Equation (3.11) thus means that the total flux of the cells in the z -direction due to these three factors is the same in any cross-section of the plume for any value of z . The case of parabolized equations was investigated in Metcalfe and Pedley [9] for a plume in a clear fluid and in Kuznetsov et al. [10] for a plume in a porous medium. It is interesting that the analysis of parabolized equations results in a cell flux condition in the following form [9, 10]:

$$Q = 2\pi \int_0^{\infty} [rvn] dr = \text{constant} \quad (3.12)$$

which means that parabolization of equations results in neglecting the effect of cell swimming and cell diffusion on the total cell flux in the plume.

Each term in Eq. (3.27) can be expressed in terms of similarity functions. The first term is:

$$\int_0^{\infty} (zv)(zn) \frac{r}{z} d\left(\frac{r}{z}\right) = \int_0^{\infty} \left(\frac{\mu}{\rho} \frac{F'(\eta)}{\eta}\right) \left(\frac{K^{1/2}}{\theta} N(\eta)\right) \eta d\eta \quad (3.13)$$

The second term is:

$$\int_0^{\infty} rbW_c n \frac{\partial C}{\partial z} dr = - \int_0^{\infty} \frac{r}{z} bW_c (nz) G' \frac{r}{z^2} z d\left(\frac{r}{z}\right) = - \int_0^{\infty} bW_c \left(\frac{K^{1/2}}{\theta} N(\eta)\right) \eta^2 G' d\eta \quad (3.14)$$

Finally, the third term is:

$$- \int_0^{\infty} rD_n \frac{\partial n}{\partial z} dr = \int_0^{\infty} \frac{r}{z} D_n \frac{K^{1/2}}{\theta} \left(\frac{N(\eta)}{z^2} + N'(\eta) \frac{r}{z^3}\right) z^2 d\left(\frac{r}{z}\right) = \int_0^{\infty} \eta D_n \frac{K^{1/2}}{\theta} [N(\eta) + N'(\eta)\eta] d\eta \quad (3.15)$$

Adding equations (3.13)-(3.15), the following expression for Q through similarity functions is obtained:

$$\begin{aligned}
Q &= 2\pi \int_0^{\infty} \left[r\nu n + rbW_c n \frac{\partial C}{\partial z} - rD_n \frac{\partial n}{\partial z} \right] dr \\
&= 2\pi \int_0^{\infty} \left[\left(\frac{\mu}{\rho} \frac{F'(\eta)}{\eta} \right) \left(\frac{K^{1/2}}{\theta} N(\eta) \right) \eta - bW_c \left(\frac{K^{1/2}}{\theta} N(\eta) \right) \eta^2 G' + \eta D_n \frac{K^{1/2}}{\theta} (N(\eta) + N'(\eta)\eta) \right] d\eta \\
&= 2\pi \frac{K^{1/2}}{\theta} \int_0^{\infty} \left[\frac{\mu}{\rho} N F' - bW_c \eta^2 N G' + \eta D_n (N + N'\eta) \right] d\eta = \text{constant} \tag{3.16}
\end{aligned}$$

Equation (3.16) can be recast in the dimensionless form as:

$$\bar{Q} = \frac{Q\theta\rho}{2\pi\mu K^{1/2}} = \int_0^{\infty} \left[N F' - \frac{bW_c\rho}{\mu} \eta^2 N G' + \frac{D_n\rho}{\mu} \eta (N + N'\eta) \right] d\eta = \text{constant} \tag{3.17}$$

or

$$\bar{Q} = \int_0^{\infty} \left[N F' - \text{PeSc}^{-1} \eta^2 N G' + \text{Sc}^{-1} \eta (N + N'\eta) \right] d\eta = \text{constant} \tag{3.18}$$

where \bar{Q} is the dimensionless flux of cells in z -direction.

This condition must be used along with boundary conditions (3.8) and (3.9) in numerical integration of Eqs. (3.3)-(3.6).

3.3 SERIED SOLUTION FOR SMALL SIMILARITY VARIABLE

Equations (3.4)-(3.6) as well as boundary conditions (3.8) are singular at $\eta = 0$. To initiate the numerical solution a series solution must be obtained for small η . The following series expansions are assumed for functions $N(\eta)$, $G'(\eta)$, and $F(\eta)$:

$$N(\eta) = \sum_{i=0}^6 n_i \eta^i, \quad G'(\eta) = \sum_{i=0}^6 g_i \eta^i, \quad F(\eta) = \sum_{i=0}^6 f_i \eta^i \quad (3.19)$$

Boundary conditions at $\eta = 0$ given by Eqs. (3.8) yield to the following relations:

$$n_1 = g_0 = f_0 = f_1 = f_3 = 0 \quad (3.20)$$

It is assumed that $n_0 \neq 0$ and $f_2 \neq 0$ to provide for non-zero concentration of bacteria and nonzero axial fluid velocity in the center of the plume. The solution is obtained in terms of n_0 and f_2 as:

$$\begin{aligned} N(\eta) = & n_0 + \frac{1}{4} n_0 (-2 - 2f_2 \text{Sc} + n_0^2 \text{Pe} \beta) \eta^2 \\ & + \frac{1}{64 D_C} (2D_C n_0 (12 + \text{Sc}(\text{Ar} n_0 + f_2 (18 + 4f_2 \text{Sc} + \text{Ar} n_0 \text{Sc}))) \\ & - n_0^3 \text{Pe} (2D_n f_2 \text{Sc} + D_C (18 + 12f_2 \text{Sc} + \text{Ar} n_0 \text{Sc})) \beta + 4D_C n_0^5 \text{Pe}^2 \beta^2) \eta^4 \\ & + \frac{1}{2304 D_C^2} (-2D_C^2 n_0 (360 + \text{Sc}(24f_2^3 \text{Sc}^2 + \text{Ar} n_0 [66 + \text{Ar} n_0 \text{Sc}]) \\ & + 2f_2^2 \text{Sc}(126 + 11\text{Ar} n_0 \text{Sc}) + f_2 [660 + \text{Ar} n_0 \text{Sc}(90 + \text{Ar} n_0 \text{Sc})])) \\ & + n_0^3 \text{Pe} \{8D_n^2 f_2^2 \text{Sc}^2 + 2D_C D_n \text{Sc} [2\text{Ar} n_0 + f_2 (62 + 26f_2 \text{Sc} + 3\text{Ar} n_0 \text{Sc})] \\ & + D_C^2 (660 + \text{Sc}(176f_2^2 \text{Sc} + \text{Ar} n_0 [94 + \text{Ar} n_0 \text{Sc}] + f_2 [760 + 52\text{Ar} n_0 \text{Sc}])) \} \beta \\ & - D_C n_0^5 \text{Pe}^2 \{2D_n (15f_2 + \text{Ar} n_0) \text{Sc} + D_C (254 + 148f_2 \text{Sc} + 15\text{Ar} n_0 \text{Sc}) \} \beta^2 + 36D_C^2 n_0^7 \text{Pe}^3 \beta^3) \eta^6 \end{aligned} \quad (3.21)$$

$$G'(\eta) = \frac{1}{2} n_0^2 \beta \eta + \frac{n_0^2 \beta}{8 D_C} [-D_n f_2 \text{Sc} + D_C (-5 - 2f_2 \text{Sc} + n_0^2 \text{Pe} \beta)] \eta^3$$

$$\begin{aligned}
& + \frac{1}{192D_C^2} \left[n_0^2 \beta (4D_n^2 f_2^2 \text{Sc}^2 + D_C D_n \text{Sc} (2\text{Ar} n_0 + 2f_2 (22 + 4f_2 \text{Sc} + \text{Ar} n_0 \text{Sc}) - n_0^2 (6f_2 + \text{Ar} n_0) \text{Pe} \beta) \right. \\
& + D_C^2 (132 + 2\text{Sc}(\text{Ar} n_0 + f_2 (46 + 8f_2 \text{Sc} + \text{Ar} n_0 \text{Sc})) \\
& \left. - n_0^2 \text{Pe} (46 + 20f_2 \text{Sc} + \text{Ar} n_0 \text{Sc}) \beta + 6n_0^4 \text{Pe}^2 \beta^2) \right] \eta^5 \tag{3.22}
\end{aligned}$$

$$\begin{aligned}
F(\eta) &= f_2 \eta^2 + \frac{1}{16} \left[-2f_2 (2 + \text{Ar} n_0 \text{Sc}) + \text{Ar} n_0 (-2 + n_0^2 \text{Pe} \beta) \right] \eta^4 \\
& + \frac{1}{384D_C} \left[2D_C \left\{ 24(f_2 + \text{Ar} n_0) + \text{Ar} n_0 (30f_2 + \text{Ar} n_0) \text{Sc} + \text{Ar} f_2 n_0 (4f_2 + \text{Ar} n_0) \text{Sc}^2 \right\} \right. \\
& \left. - \text{Ar} n_0^3 \text{Pe} \left\{ 2D_n f_2 \text{Sc} + D_C (30 + 12f_2 \text{Sc} + \text{Ar} n_0 \text{Sc}) \right\} \beta + 4\text{Ar} D_C n_0^5 \text{Pe}^2 \beta^2 \right] \eta^6 \tag{3.23}
\end{aligned}$$

3.4 NUMERICAL RESULTS AND DISCUSSION

For computational results displayed in Figs. 3.1-3.3 the following parameter values are utilized: $\text{Ar}=1$, $D_n/D_C=1$, $\text{Pe}=10$, $\text{Sc}=20$, and $\beta=10^6$. Since Eqs. (3.4)-(3.6) and boundary conditions (3.8) are singular at $\eta=0$, to initiate numerical solution a series solution given by Eqs. (3.21)-(3.23) is used. The utilization of this series solution requires an assumption concerning the values of n_0 and f_2 that are present as parameters in this series solution. Values of n_0 and f_2 are initially guessed and then their values are iteratively improved by the Shooting Method until the boundary conditions at $\eta \rightarrow \infty$ and the integral condition given by Eq. (3.18) are satisfied. Utilizing this series solution, computations are performed up to $\eta=0.01$. At $\eta=0.01$, values of $N(\eta)$, $N'(\eta)$, $G'(\eta)$, $F(\eta)$, and $F'(\eta)$ are evaluated utilizing the series solution. These values are used as the initial condition for the

numerical solution. For $\eta > 0.01$, Eqs. (3.4)-(3.6) are solved numerically utilizing RKF45 ordinary differential equation solver.

Figure 3-1 displays the dimensionless cell concentration, $N(\eta)$, for different values of the dimensionless cell flux in z -direction, \bar{Q} . The increase of \bar{Q} corresponds to larger concentration of cells, as expected. The width of the plume slightly decreases with the increase of \bar{Q} .

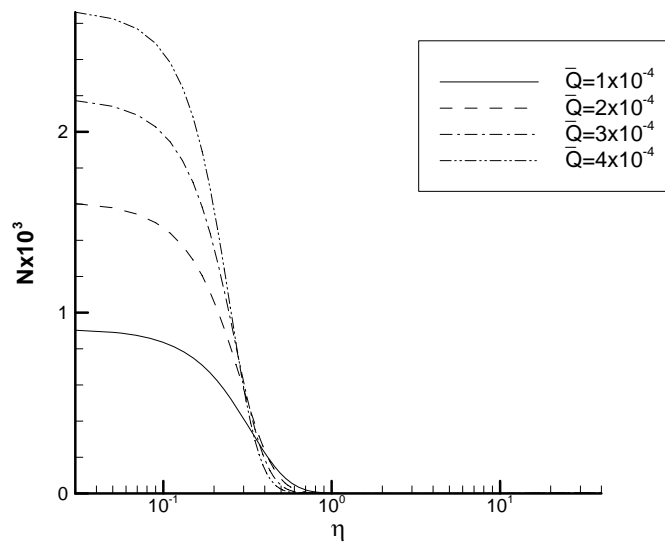
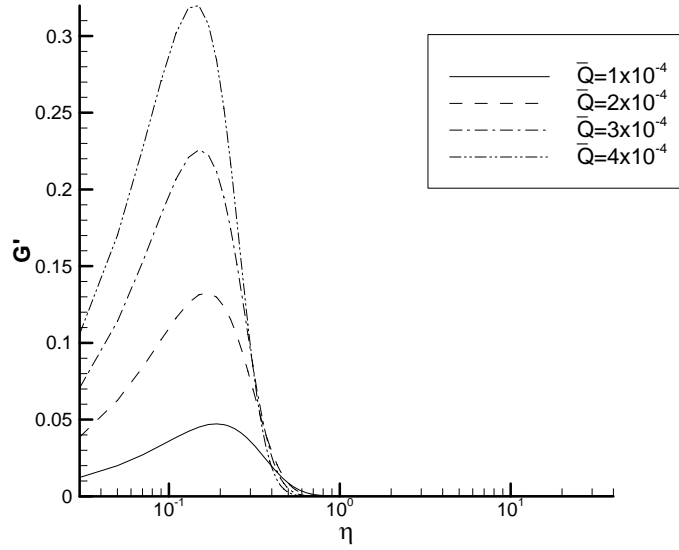
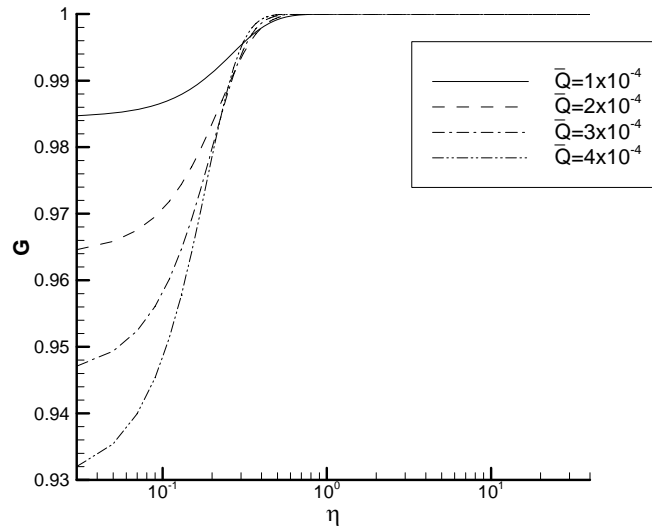


Figure 3-1. Similarity solution: Dimensionless cell concentration, $N(\eta)$

Figure 3-2(a) displays the dimensionless rate of change of oxygen concentration, $G'(\eta)$, and Fig. 3-2(b) displays the dimensionless oxygen concentration, $G(\eta)$, which is computed by integrating $G'(\eta)$ assuming that $G(\infty)=1$. The oxygen concentration decreases toward the center of the plume. This happens because the center of the plume has the largest concentration of cells that consume oxygen.



(a)



(b)

Figure 3-2. Similarity solution: (a) Dimensionless rate of change of oxygen concentration, $G'(\eta)$; (b) Dimensionless oxygen concentration, $G(\eta)$, computed assuming that $G(\infty)=1$

This result is in agreement with the clear fluid results obtained in Metcalfe and Pedley [9]. The increase of \bar{Q} increases the number of the cells in the plume which increases the rate of oxygen consumption; therefore, the increase of \bar{Q} leads to smaller oxygen concentration in the center of the plume. It should be noted that the proposed model is valid only as long as $C > 0$ (or $\tilde{C} > \tilde{C}_{min}$),

which is true only in the upper part of the plume, where oxygen concentration around the plume is relatively high. In the lower part of the chamber, the oxygen concentration in the bulk of the fluid is smaller than \tilde{C}_{min} , and the plume will provide the convective mechanism for the oxygen and cell transport into the lower part of the chamber. However, the solution obtained in this chapter is valid only as long as $\tilde{C} > \tilde{C}_{min}$, and this explains why the oxygen concentration in the center of the plume is a little smaller than at its edges.

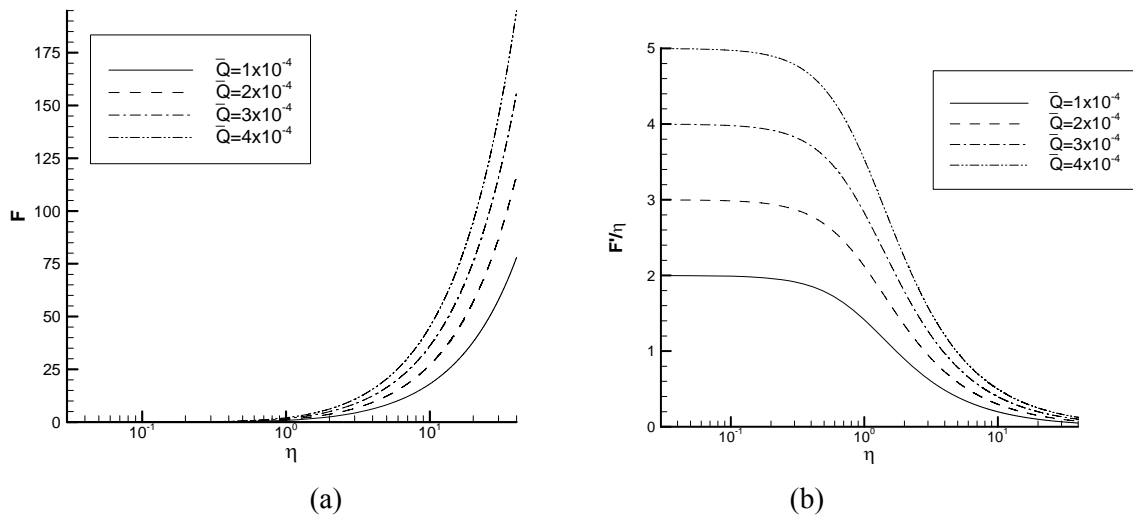


Figure 3-3. Similarity solution: (a) Dimensionless streamfunction, $F(\eta)$; (b) Dimensionless downward fluid filtration velocity, $F'(\eta)/\eta$

Figure 3-3(a) displays the dimensionless streamfunction, $F(\eta)$, while Fig. 3-3(b) displays the dimensionless downward fluid filtration velocity, $F'(\eta)/\eta$. The downward fluid velocity increases as \bar{Q} increases, as expected; the axial velocity takes its maximum value in the center of the plume and decreases to zero at the edge of the plume.

3.5 CONCLUSIONS

A similarity solution of full (non-parabolized) equations describing a falling bioconvection plume in a suspension of oxytactic bacteria in a fluid saturated porous medium is obtained. The obtained

numerical solutions reveal that the cell concentration increases from the periphery of the plume toward its center. Contrary to this, the oxygen concentration decreases from the periphery of the plume toward its center. The downward filtration velocity takes on its maximum value in the center of the plume.

ACKNOWLEDGEMENTS

AVK gratefully acknowledges the grant # NAG3-2706 awarded to him by NASA Office of Biological and Physical Research, Physical Sciences Division. The authors also acknowledge the NATO Expert Visit Grant (PST.EV.978144). Critical comments of Prof. D.A. Nield are greatly appreciated.

REFERENCES

1. Kessler, J.O.: Hydrodynamic focusing of motile algal cells. *Nature* **313**, 218-220 (1985).
2. Kessler, J.O.: Cooperative and concentrative phenomena of swimming microorganisms. *Contemp. Phys.* **26**, 147-166 (1985).
3. Kessler, J.O., Wiseley, D.A., Remick, K.E., Marthaler, D.E.: Individual and collective dynamics of swimming bacteria, *Proceedings of the Workshop "Traffic and Granular Flow'97"*, M. Schreckenberg and D.E. Wolf, eds, Springer, New York, pp. 37-51 (1997).
4. Kessler, J.O., Burnett, G.D., Remick, K.E.: Mutual dynamics of swimming microorganisms and their fluid habitat, In *Nonlinear Science at the Dawn of the 21st Century*, P.L. Christiansen, M.P. Sorensen and A.C. Scott, eds, pp. 409-426, New York: Springer 2000.
5. Harashima, A., Watanabe, M., Fujishiro, I.: Evolution of bioconvection patterns in a culture of motile flagellates, *Phys. Fluids* **31**, 764-755 (1988).

6. Kessler, J.O.: The external dynamics of swimming microorganisms. *Progress in Phycological Research* **4**, pp. 257-307, Bristol: Biopress 1986.
7. Hillesdon, A.J., Pedley, T.J., Kessler, J.O.: The development of concentration gradients in a suspension of chemotactic bacteria. *Bull. Math. Biol.* **57**, 299-344 (1995).
8. Kessler, J.O., Hoelzer, M.A., Pedley, T.J., Hill, N.A.: Functional patterns of swimming bacteria. In *Mechanics and Physiology of Animal Swimming*, L. Maddock, Q. Bone, and J.M.V. Rayner, eds., pp. 3-12, Cambridge University Press 1994.
9. Metcalfe, A.M., Pedley, T.J.: Falling Plumes in Bacterial Bioconvection. *J. Fluid Mech.* **445**, 121-149 (2001).
10. Kuznetsov, A.V., Avramenko, A.A., Geng, P.: A similarity solution for a falling plume in bioconvection of oxytactic bacteria in a porous medium. *International Communications in Heat and Mass Transfer*, submitted.
11. Pedley, T.J., Hill, N.A., Kessler, J.O.: The growth of bioconvection patterns in a uniform suspension of gyrotactic microorganisms. *J. Fluid Mech.* **195**, 223-338 (1988).
12. Olver, P.: *Applications of Lie Groups to Differential Equations*. New York: Springer 1985.

PART TWO

INTERACTION BETWEEN MICROORGANISMS AND

SMALL SOLID PARTICLES IN BIOCONVECTION

SUSPENSION

4. THE INTERACTION OF BIOCONVECTION CAUSED BY GYROTACTIC MICROORGANISMS AND SETTLING OF SMALL SOLID PARTICLES

ABSTRACT

The purpose of this chapter is to investigate the settling of small solid particles in a suspension of motile gyrotactic microorganisms. The particles are assumed to be sufficiently small, so that the Brownian diffusion is not completely negligible. Bioconvection induced by the upswimming of microorganisms enhances mixing between the particles and leads to a more uniform number density distribution of solid particles across the layer depth.

NOMENCLATURE

a	radius of a micro-organism, m
B	time scale for the reorientation of microorganisms by the gravitational torque against viscous torque, $4\pi\mu a^3 / (mgh)$, s
D_m	diffusivity of microorganisms, m ² /s
D_p	diffusivity of solid particles due to Brownian diffusion and interactions with microorganisms, m ² /s
D_p^*	ratio of the diffusivity of solid particles to diffusivity of microorganisms, D_p / D_m
g	gravity vector, 9.81 m/s ²
G	gyrotaxis number, BD_m / L^2
h	displacement of the center of mass of a gyrotactic micro-organism from its center of buoyancy, m
H	height of the chamber, m
J_m^*	dimensionless flux of microorganisms, defined by equation (4-18a)
J_p^*	dimensionless flux of solid particles, defined by equation (4-18b)
L	width of the chamber, m
n_m	number density of microorganisms, 1/m ³
\bar{n}_m	average number density of microorganisms, 1/m ³
n_m^*	dimensionless number density of microorganisms, n_m / \bar{n}_m
n_p	number density of solid particles, 1/m ³
\bar{n}_p	average number density of solid particles, 1/m ³
n_p^*	dimensionless number density of solid particles, n_p / \bar{n}_p

\bar{n}_p^*	ratio of the average number density of particles to that of microorganisms, \bar{n}_p / \bar{n}_m
$\hat{\mathbf{p}}$	unit vector indicating the direction of swimming of gyrotactic microorganisms
p_e	excess pressure (above hydrostatic), Pa
R_m	Rayleigh number for microorganisms, $\bar{n}_m \theta_m \Delta \rho_m g L^3 / (\rho_0 \nu D_m)$
R_p	Rayleigh number for solid particles, $\bar{n}_m \theta_p \Delta \rho_p g L^3 / (\rho_0 \nu D_m)$
S_c	Schmidt number, ν / D_m
t	time, s
t^*	dimensionless time, $D_m t / L^2$
u	horizontal velocity component, m/s
v	vertical velocity component, m/s
\mathbf{v}	velocity vector, m/s
W_m	average swimming velocity of microorganisms (assumed to be constant), m/s
W_m^*	dimensionless average swimming velocity of microorganisms, $W_m L / D_m$
W_p	particle settling velocity, m/s
W_p^*	dimensionless particle settling velocity, $W_p L / D_p$
x	horizontal coordinate, m
x^*	dimensionless horizontal coordinate, x / L
$\hat{\mathbf{x}}$	unit vector in the x -direction
y	vertical coordinate, m
y^*	dimensionless vertical coordinate, y / L

\hat{y} unit vector in the y -direction

Greek symbols

$\Delta\rho_m$ density difference between microorganisms and water, $\rho_m - \rho_0$, kg/m^3

$\Delta\rho_p$ density difference between solid particles and water, $\rho_p - \rho_0$, kg/m^3

ζ horizontal component of vorticity, $1/s$

ζ^* dimensionless horizontal component of vorticity, $\zeta L^2 / D_m$

θ_m volume of a micro-organism, m^3

θ_p volume of a particle, m^3

Θ angle between the vertical axis and the swimming velocity of microorganisms

λ aspect ratio of the chamber, H / L

μ dynamic viscosity, assumed to be approximately the same as that of water, $\text{kg}/(m\ s)$

ν kinematics viscosity, assumed to be approximately the same as that of water, m^2/s

ρ_0 density of water, kg/m^3

ρ_m density of microorganisms, kg/m^3

ρ_p density of solid particles, kg/m^3

ψ stream function, m^2/s

ψ^* dimensionless stream function, ψ / D_m

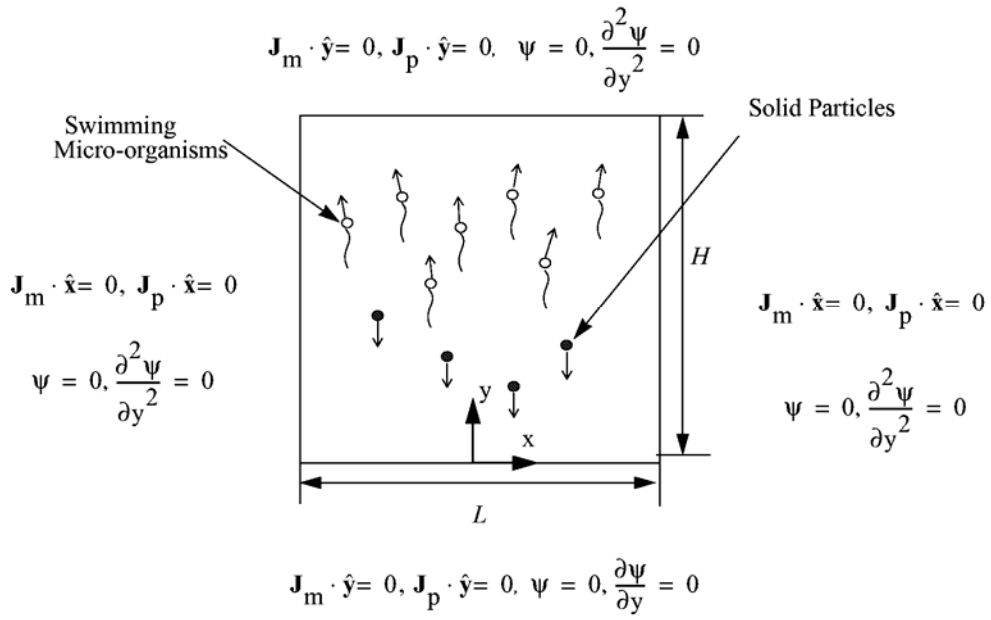
4.1 INTRODUCTION

Bioconvection is a phenomenon caused by collective swimming in a particular direction of motile microorganisms. Most significant results in the area of bioconvection were obtained over the last two decades (Pedley et al., 1988; Ghorai and Hill, 1999; Pedley and Kessler, 1987, 1990, 1992). Gyrotactic microorganisms (this behavior is typical for many species of algae) swim against gravity in still water, but once bioconvection develops, their swimming direction is determined by the balance of two torques: the viscous torque acting on a body placed in a shear flow and the torque that is generated by gravity because the center of mass of a typical alga is displaced from its center of buoyancy. Algae are approximately 5% denser than water; gyrotactic behavior results in their swimming towards the regions of most rapid downflow. Therefore, the regions of downflow become denser than the regions of upflow. Buoyancy increases the upward velocity in the regions of upflow and downward velocity in the regions of downflow, thus enhancing velocity fluctuations and inducing macroscopic convective fluid motion (Pedley et al., 1988; Ghorai and Hill, 1999, 2000). The formation of almost regular patterns and gyrotactic plumes in algal suspensions is documented in numerous experimental papers (Kessler, 1985a, 1985b and Kessler et al. 1997, 2000).

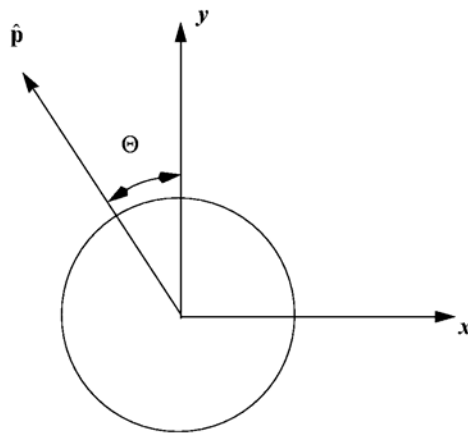
Despite a considerable number of theoretical and experimental works on bioconvection, the effect of bioconvection on settling of small solid particles has never been studied before. This is an interesting topic because it deals with a possible application of bioconvection: the utilization of bioconvection to slow down settling and enhance mixing between particles. The advantage of bioconvection is that it provides a simple mechanism for enhancing mixing and slowing down settling in very small fluid volumes (Ghorai and Hill, 1999, 2000, for example, studied bioconvection in a chamber as small as 5mm×5mm). This may be important, for example, in the pharmaceutical industry or for the development of new medical tests. This statement implies microorganisms not interfering with the test and surviving the presence of reactants.

This research is concentrated on investigating the settling of solid particles in a dilute suspension that contains both gyrotactic microorganisms (whose number density is n_m) and small particles (whose density is n_p) in a two-dimensional chamber of depth H and width L whose side walls are assumed to be shear-free. Both microorganisms and particles are heavier than water. The particles are small, so that the Brownian diffusion is not completely negligible. If diffusion were completely negligible, all particles would eventually end up at the bottom of the chamber. It is also assumed that particle diffusivity, caused by the Brownian motion, is enhanced by the interaction between the particles and the swimming microorganisms. Because the suspension is dilute, this interaction is expected to be weak. Nevertheless, it cannot be completely neglected; therefore, it is modeled here by increasing the particle diffusivity as compared to its value predicted by the Einstein correlation. Stability analysis of this suspension is carried out in Kuznetsov and Avramenko (2004).

The computational domain is shown schematically in Fig. 1(a). The width of the domain is L (the coordinate x varies from $-L/2$ to $L/2$) and the height of the domain is H (the coordinate y varies from 0 to H). The top boundary is assumed to be stress-free and the bottom boundary is rigid (the no-slip condition is imposed there). The side walls are stress-free to model periodic condition; a wider computational domain would produce several identical plumes, it is assumed that the plume spacing is L . The question how solid particles may affect the wavelengths of bioconvection patterns requires further investigation.



(a)



(b)

Figure 4-1. (a) Computational domain and boundary conditions (b) Swimming direction of a gyrotatic microorganism

4.2 GOVERNING EQUATIONS

4.2.1 DIMENSIONAL GOVERNING EQUATIONS

Governing equations are written by extending equations given in Ghorai and Hill (1999, 2000) to account for solid particles. The cross-effect between microorganisms and solid particles movement is neglected because the suspension is dilute (volume concentrations of both microorganisms and solid particles are much smaller than unity). Very slow motion associated with bioconvection flows justifies the creeping flow assumption and allows neglecting the inertia terms in these equations.

x and y- momentum equations:

$$\rho_0 \frac{\partial u}{\partial t} = -\frac{\partial p_e}{\partial x} + \mu \left(\frac{\partial^2 u}{\partial x^2} + \frac{\partial^2 u}{\partial y^2} \right) \quad (4.1)$$

$$\rho_0 \frac{\partial \mathbf{v}}{\partial t} = -\frac{\partial p_e}{\partial y} + \mu \left(\frac{\partial^2 \mathbf{v}}{\partial x^2} + \frac{\partial^2 \mathbf{v}}{\partial y^2} \right) - n_m \theta_m \Delta \rho_m \mathbf{g} - n_p \theta_p \Delta \rho_p \mathbf{g} \quad (4.2)$$

Continuity equation:

$$\frac{\partial u}{\partial x} + \frac{\partial \mathbf{v}}{\partial y} = 0 \quad (4.3)$$

Conservation of motile microorganisms:

$$\frac{\partial (n_m)}{\partial t} = -\text{div}(n_m \mathbf{v} + n_m W_m \hat{\mathbf{p}} - D_m \nabla n_m) \quad (4.4)$$

Conservation of solid particles:

$$\frac{\partial (n_p)}{\partial t} = -\text{div} \left(n_p \mathbf{v} + n_p W_p \frac{\mathbf{g}}{|\mathbf{g}|} - D_p \nabla n_p \right) \quad (4.5)$$

where D_m is the diffusivity of microorganisms (this assumes that all random motions of the microorganisms can be approximated by a diffusive process); D_p is the diffusivity of particles due to the Brownian motion and interactions with microorganisms (D_p is smaller than D_m , but still not zero); n_m is the number density of motile microorganisms; n_p is the number density of solid particles; p_e is the excess pressure above hydrostatic; $\hat{\mathbf{p}}$ is the unit vector indicating the direction of swimming of microorganisms (equations for this vector are given in Pedley et al., 1988); t is the time; u and v are the x and y -velocity components, respectively; \mathbf{v} is the velocity vector, (u,v) ; $W_m \hat{\mathbf{p}}$ is the vector of microorganisms' average swimming velocity relative to the fluid (W_m is assumed to be constant); $W_p \frac{\mathbf{g}}{|\mathbf{g}|}$ is the vector of particles' settling velocity relative to the fluid (W_p is assumed to be constant, the particles settle straight downward); x and y are the Cartesian coordinates (x is the horizontal coordinate and y is the vertical coordinate); $\Delta\rho_m$ is the density difference between microorganisms and water, $\rho_m - \rho_0$; $\Delta\rho_p$ is the density difference between particles and water, $\rho_p - \rho_0$; θ_m is the volume of a micro-organism; θ_p is the volume of a particle; μ is the dynamic viscosity, assumed to be approximately the same as that of water; and ρ_0 is the density of water.

For spherical particles the settling velocity can be found according to the Stokes law (Batchelor, 1982), as:

$$W_p = \frac{\theta_p \Delta\rho_p \mathbf{g}}{6\pi\mu \left(\frac{3}{4} \frac{\theta_p}{\pi}\right)^{1/3}} \quad (4.7)$$

According to Ghorai and Hill (2000), vector $\hat{\mathbf{p}}$ that determines the swimming direction of a gyrotactic micro-organism can be given in terms of the angle Θ between the vertical axis and the

vector of swimming velocity of the micro-organism (cf. Fig. 4-1(b)), so that $\hat{\mathbf{p}} = (p_x, p_y) = (-\sin \Theta, \cos \Theta)$. Angle Θ satisfies the following equation:

$$\frac{d\Theta}{dt} = \frac{B\zeta - \sin \Theta}{2B} \quad (4.8)$$

where ζ is the horizontal component of vorticity and B is the time scale for the reorientation of microorganisms by the gravitational torque against viscous resistance. Parameter B was called the “gyrotactic orientation parameter” by Pedley and Kessler (1987), it is defined as:

$$B = \frac{4\pi\mu a^3}{mgh} \quad (4.9)$$

where h is the displacement of the center of mass of a gyrotactic micro-organism from its center of buoyancy, m is the mass of the micro-organism, and a is the radius of the micro-organism.

4.2.2 DIMENSIONLESS GOVERNING EQUATION

Utilizing the stream function-vorticity formulation, the governing equations can be recast in dimensionless form as follows:

$$\zeta^* = -\nabla^2 \psi^* \quad (4.10)$$

$$S_c^{-1} \left(\frac{\partial \zeta^*}{\partial t^*} + \mathbf{u}^* \frac{\partial \zeta^*}{\partial x^*} + \mathbf{v}^* \frac{\partial \zeta^*}{\partial y^*} \right) = \nabla^2 \zeta^* - \left(R_m \frac{\partial n_m^*}{\partial x^*} + R_p \frac{\partial n_p^*}{\partial x^*} \right) \quad (4.11)$$

$$\frac{\partial n_m^*}{\partial t^*} = -\nabla \cdot \left[n_m^* (\mathbf{v}^* + W_m^* \hat{\mathbf{p}}) - \nabla n_m^* \right] \quad (4.12)$$

$$\frac{\partial n_p^*}{\partial t^*} = -\nabla \cdot \left[n_p^* \left(\mathbf{v}^* + W_p^* \frac{\mathbf{g}}{|\mathbf{g}|} \right) - D_p^* \nabla n_p^* \right] \quad (4.13)$$

In Ghorai and Hill (1999, 2000) it is shown that vector $\hat{\mathbf{p}}$ can be computed as:

$$\hat{\mathbf{p}} = \begin{cases} \left(-\kappa - (\kappa^2 - 1)^{1/2}, 0 \right), & \kappa < -1 \\ \left(-\kappa, (1 - \kappa^2)^{1/2} \right), & |\kappa| \leq 1 \\ \left(-\kappa + (\kappa^2 - 1)^{1/2}, 0 \right), & \kappa > 1 \end{cases} \quad (4.14)$$

where $\kappa = B\zeta = G\zeta^*$.

The dimensionless variables in equations (4.10)-(4.13) are:

$$\begin{aligned} x^* &= \frac{x}{L}; \quad y^* = \frac{y}{L}; \quad t^* = \frac{D_m}{L^2} t; \quad u^* = \frac{\partial \psi^*}{\partial y^*}; \quad v^* = -\frac{\partial \psi^*}{\partial x^*}; \quad \mathbf{v}^* = \mathbf{v} \frac{L}{D_m}; \\ W_m^* &= W_m \frac{L}{D_m}; \quad W_p^* = W_p \frac{L}{D_m}; \quad n_m^* = \frac{n_m}{\bar{n}_m}; \quad n_p^* = \frac{n_p}{\bar{n}_m}; \\ S_c &= \frac{\nu}{D_m}; \quad G = \frac{BD_m}{L^2}; \quad R_m = \frac{\bar{n}_m \theta_m \Delta \rho_m g L^3}{\rho_0 \nu D_m}; \quad R_p = \frac{\bar{n}_m \theta_p \Delta \rho_p g L^3}{\rho_0 \nu D_m}; \quad D_p^* = \frac{D_p}{D_m} \end{aligned} \quad (4.15)$$

4.2.3 INITIAL AND BOUNDARY CONDITIONS

Equations (4.10)-(4.13) must be solved subject to the following boundary conditions (cf. Fig. 4-1(a)).

No-slip boundary condition is imposed at the bottom wall while the top boundary and the side walls are assumed to be impermeable to the fluid and stress-free. The assumption that the top surface is stress-free implies that the surface tension is negligible and microorganisms do not form a packed layer at the top surface. Under these assumptions the boundary conditions can be presented as:

$$\psi^* = 0 \text{ at } y^* = 0, \lambda \text{ and } x^* = \pm 0.5, \quad (4.16a)$$

where λ is the aspect ratio, H/L ,

$$\frac{\partial \psi^*}{\partial y^*} = 0 \text{ at } y^* = 0, \quad (4.16b)$$

$$\frac{\partial^2 \psi^*}{\partial y^{*2}} = 0 \text{ at } y^* = \lambda, \text{ and } \frac{\partial^2 \psi^*}{\partial x^{*2}} = 0 \text{ at } x^* = \pm 0.5. \quad (4.16c)$$

All four boundaries of the domain are also impermeable to the fluid, microorganisms, and solid particles; therefore, normal fluxes of microorganisms and solid particles are zero through all these boundaries:

$$\mathbf{J}_m^* \cdot \hat{\mathbf{y}} = 0 \text{ and } \mathbf{J}_p^* \cdot \hat{\mathbf{y}} = 0 \text{ at } y^* = 0, \lambda \quad (4.17a)$$

$$\mathbf{J}_m^* \cdot \hat{\mathbf{x}} = 0 \text{ and } \mathbf{J}_p^* \cdot \hat{\mathbf{x}} = 0 \text{ at } x^* = \pm 0.5, \quad (4.17b)$$

where $\hat{\mathbf{x}}$ and $\hat{\mathbf{y}}$ are the unit vectors in the x - and y -directions, respectively,

$$\mathbf{J}_m^* = n_m^* (\mathbf{v}^* + W_m^* \hat{\mathbf{p}}) - \nabla n_m^* \quad (4.18a)$$

is the dimensionless flux of microorganisms and

$$\mathbf{J}_p^* = n_p^* \left(\mathbf{v}^* + W_p^* \frac{\mathbf{g}}{|\mathbf{g}|} \right) - D_p^* \nabla n_p^* \quad (4.18b)$$

is the dimensionless flux of solid particles.

Initially, at $t^* = 0$, it is assumed that the fluid is motionless and the number density distributions of microorganisms and solid particles are uniform. As in Ghorai and Hill (1999, 2000), small perturbations to these uniform distributions are utilized to ensure that the plume forms in the middle of the computational domain. This results in the following initial condition:

$$\psi^* = 0, \zeta^* = 0, n_m^* = 1 + \varepsilon \cos\left(m \pi x^*\right), n_p^* = \frac{\bar{n}_p}{\bar{n}_m} + \varepsilon \cos\left(m \pi x^*\right) \quad (4.19)$$

where $\varepsilon = 10^{-5}$ and $m = 2$.

4.2.4 NUMERICAL PROCEDURE

A conservative finite-difference scheme is used to discretize the governing equations. An implicit scheme with Euler backward differencing in time and central differencing in space is utilized to obtain the transient solutions. A line-by-line tridiagonal matrix algorithm with relaxation is used together with an iteration technique to solve the nonlinear discretized equations. A staggered uniform grid with the stream function and vorticity stored in one set of nodes and the number densities of microorganisms and solid particles stored in another set of nodes is utilized. The grid is chosen so that the number density nodes lie in the interior of the computational domain only, whereas those of the stream function and vorticity lie in the interior and at the boundary of the domain. The mesh size is 36×36 . Computations are performed at the North Carolina Supercomputing Center utilizing an Origin 2400 workstation. CPU time required to investigate plume development until it attains steady-state for 36×36 uniform mesh is about 10 hours. Grid independence of the solution was checked by performing a test computation utilizing a uniform 72×72 mesh, and the maximum variation of the fluid velocity did not exceed 3%.

4.3 RESULTS AND DISCUSSION

Values of physical properties and geometrical parameters utilized in the computations are summarized in Table 4-1. Values of dimensionless groups that correspond to these parameter values

are given in Table 4-2. The values of particle diffusivity are taken larger than those following from the Einstein's relation that determines the diffusivity of small particles due to the Brownian motion. This is done to account for additional random motions of particles that may result from their interactions with swimming microorganisms (a particle may be either directly hit by a micro-organism or it can enter a propulsive stream caused by a swimming micro-organism).

Table 4-1. Physical properties and geometrical parameters utilized in the computations

Average number density of microorganisms	\bar{n}_m	10^{12} cells/m ³
Average number density of solid particles	\bar{n}_p	10^{11} cells/m ³
Density of water	ρ_0	10^3 kg/m ³
Specific gravity of microorganisms	$\Delta\rho_m/\rho_0$	0.05
Specific gravity of solid particles	$\Delta\rho_p/\rho_0$	Fig 4.3-4.8: 0.25 Fig 4.9: 0.5 Fig 4.10: 1
Volume of a micro-organism	θ_m	5×10^{-16} m ³
Volume of a particle	θ_p	5×10^{-16} m ³
Average swimming velocity of microorganisms	W_c	10^{-4} m/s
Particle settling velocity (calculated according to equation (4.7))	W_p	Fig 4.3-4.8: 1.32×10^{-5} m/s Fig 4.9: 2.64×10^{-5} m/s Fig 4.10: 5.28×10^{-5} m/s
Diffusivity of microorganisms	D_m	5×10^{-8} m ² /s
Diffusivity of particles	D_p	Fig 4.3-4.6, 4.9, 4.10: 5×10^{-9} m ² /s Fig 4.7: 1×10^{-8} m ² /s Fig 4.8: 5×10^{-8} m ² /s
Gyrotaxis orientation parameter	B	5 s
Kinematic viscosity of the suspension	ν	10^{-6} m ² /s
Height of the computational domain	H	0.005 m
Width of the computational domain	L	0.005 m

Table 4-2. Values of dimensionless parameters utilized in computations.

Dimensionless average swimming velocity of microorganisms	$W_m^* = W_m \frac{L}{D_m}$	10
Dimensionless particles settling velocity	$W_p^* = W_p \frac{L}{D_m}$	Fig 4.3-4.8: 1.32 Fig 4.9: 2.64 Fig 4.10: 5.28
Schmidt number	$S_c = \frac{\nu}{D_m}$	20
Gyrotaxis number	$G = \frac{BD_m}{L^2}$	10^{-2}
Rayleigh number for microorganisms	$R_m = \frac{\bar{n}_m \theta_m \Delta \rho_m g L^3}{\rho_0 \nu D_m}$	612.5
Rayleigh number for solid particles	$R_p = \frac{\bar{n}_m \theta_p \Delta \rho_p g L^3}{\rho_0 \nu D_m}$	Fig 4.3-4.8: 3062.5 Fig 4.9: 6125 Fig 4.10: 12250
Dimensionless diffusivity of particles	$D_p^* = \frac{D_p}{D_m}$	Fig 4.3-4.6, 4.9, 4.10: 0.1 Fig 4.7: 0.2 Fig 4.8: 1
Aspect ratio	$\lambda = \frac{H}{L}$	1
Dimensionless average concentration of particles	$\bar{n}_p^* = \frac{\bar{n}_p}{\bar{n}_m}$	0.1

The major aim of the presented computations is to investigate the effect of solid particles on bioconvection as well as the effect of bioconvection on number density distribution of solid particles in the chamber. Without bioconvection, solid particles have exponential distribution across the chamber's depth with the largest number density at the bottom of the chamber (the particles do not all settle to the bottom because of the Brownian diffusion). The particle number density distribution can be obtained by integrating equation (4.13) for the case when $\mathbf{v}^* = \partial n_p^* / \partial t^* = 0$, as:

$$n_p^*(y^*) = -\frac{1}{D_p^*} \frac{\exp\left(-\frac{1}{D_p^*} W_p^* (1-y^*)\right)}{\exp\left(-\frac{1}{D_p^*} W_p^*\right) - 1} \bar{n}_p^* W_p^* \quad (4.20)$$

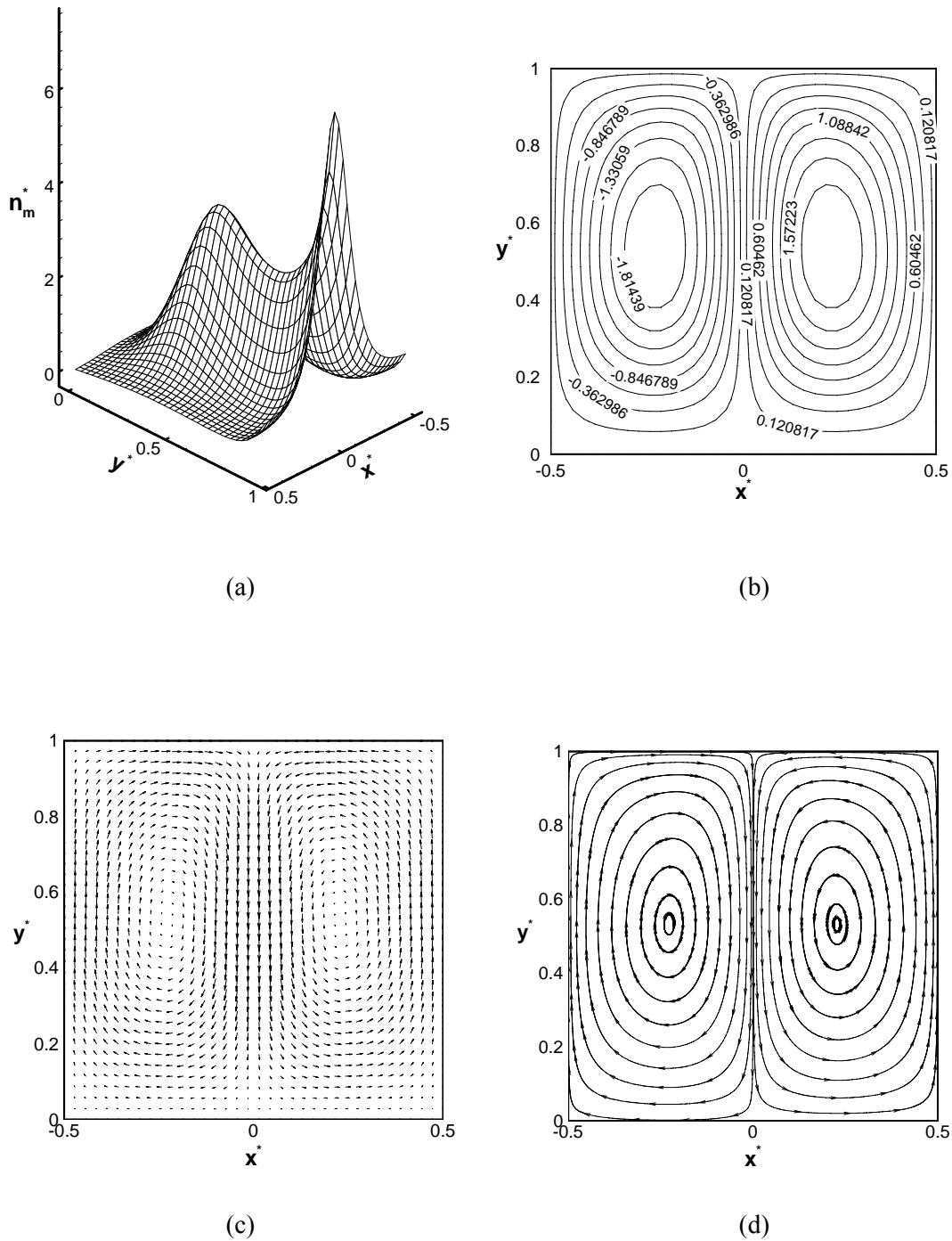


Figure 4-2. Basic case: no solid particles, steady-state plume ($t^* = 0.49825$). (a) Dimensionless number of microorganisms, (b) Contours of dimensionless stream function, (c) Fluid velocity vector field, (d) Streamlines

To evaluate the effect of solid particles on bioconvection, the basic case when there are no solid particles in the suspension is first investigated. Figures 4-2(a)-(d) show the dimensionless number density of microorganisms (a), the contours of the dimensionless stream function (b), the fluid velocity vector field (c), and the flow streamlines (d) for the case of no solid particles when bioconvection plume attains its steady-state (as shown below, this happens at $t^* = 0.49825$).

Figures 4-3 to 4-6 display the case with solid particles, computations are carried out for $\Delta\rho_p / \Delta\rho_m = 5$ and $D_p / D_m = 0.1$. As shown in Table 4-2, for all computations with particles it is assumed that the average number density of particles is ten times smaller than that of microorganisms, $\bar{n}_p / \bar{n}_m = 0.1$. Since the case with solid particles is of major interest for this investigation, Figs. 4-3 to 4-6 show the development of the bioconvection plume: Fig. 4-3 shows the plume at $t^* = 0.19825$, Fig. 4-4 shows the plume at $t^* = 0.3$, Fig. 4-5 shows the plume at $t^* = 0.49825$, and Fig. 4-6 shows the plume at $t^* = 0.59825$. In Figs. 4-3 to 4-6, figure (a) shows the dimensionless number density of microorganisms, figure (b) shows the dimensionless number density of particles, figure (c) shows contours of the dimensionless stream function, and figure (d) shows the fluid velocity vector field. Table 4-3 shows the maximum values of the dimensionless number densities of microorganisms and particles, $(n_m^*)_{\max}$ and $(n_p^*)_{\max}$, and the maximum value of the dimensionless stream function, $(\psi^*)_{\max}$. As Table 4-3 shows, these three parameters change by no more than 2.3% between $t^* = 0.49825$ and $t^* = 0.59825$. Therefore, it is assumed that at $t^* = 0.49825$ the plume attains its steady-state.

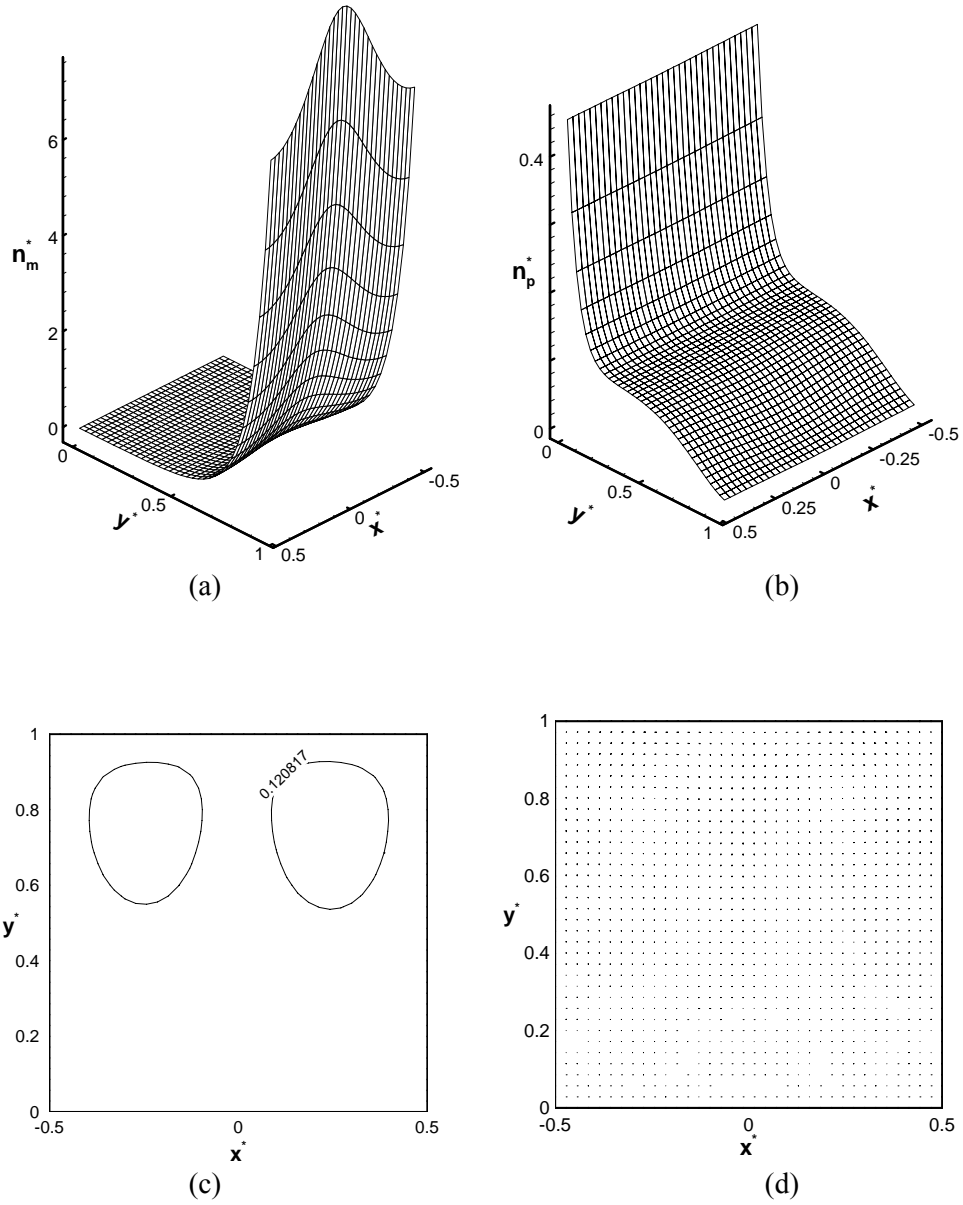


Figure 4-3. Solid particles present, $\bar{n}_p/\bar{n}_m = 0.1$, $\Delta\rho_p/\Delta\rho_m = 5$, $D_p^* = 1/10$, $t^* = 0.19825$. (a) Dimensionless number density of microorganisms, (b) Dimensionless number density of particles, (c) Contours of dimensionless stream function, (d) Fluid velocity vector field

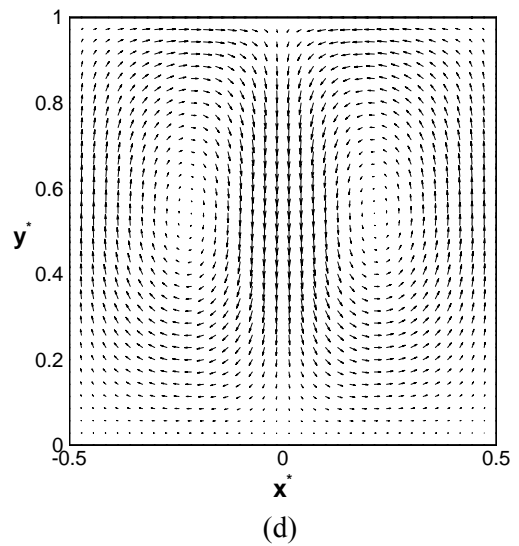
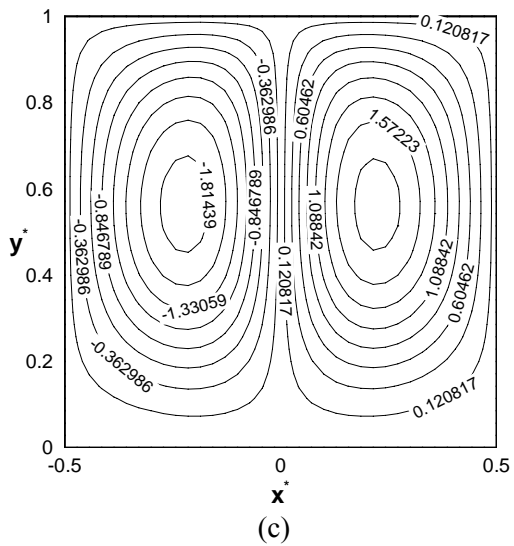
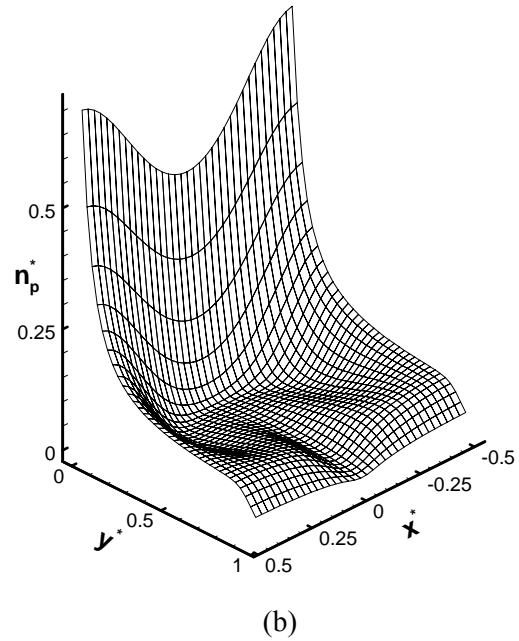
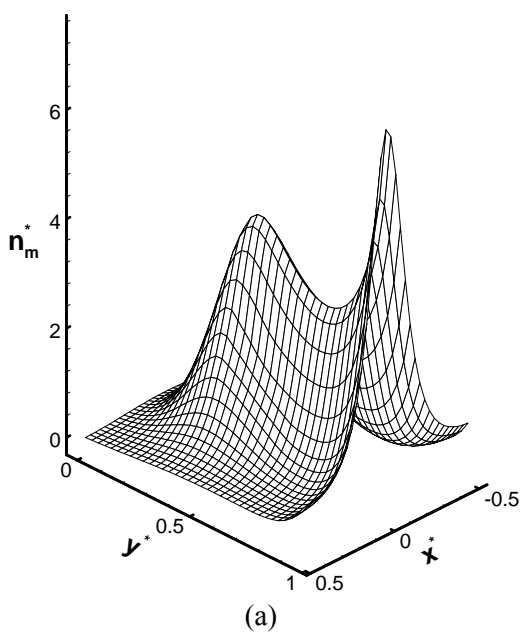
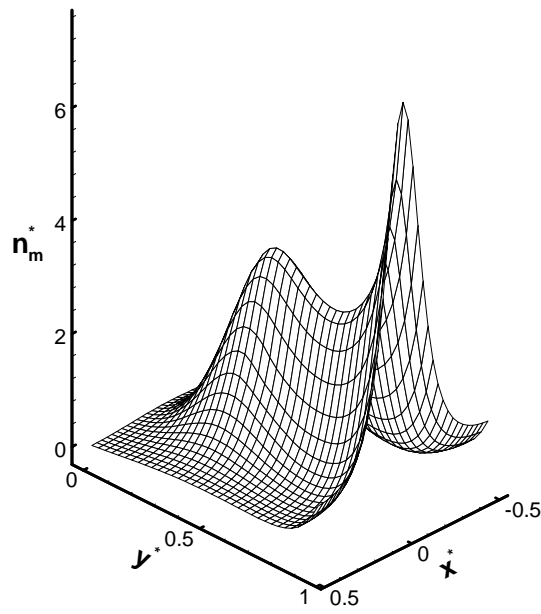
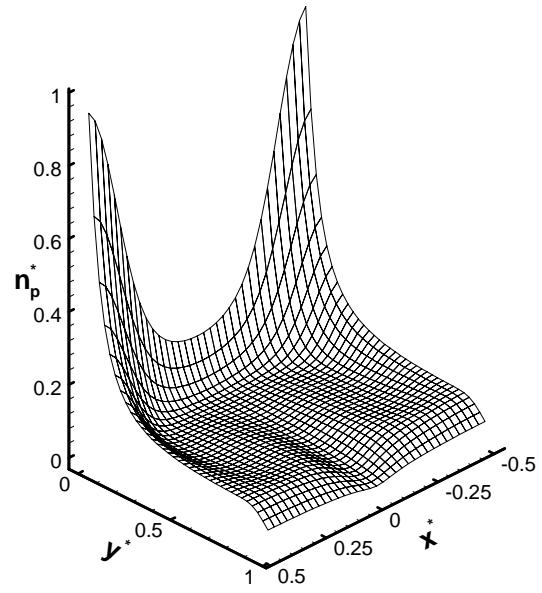


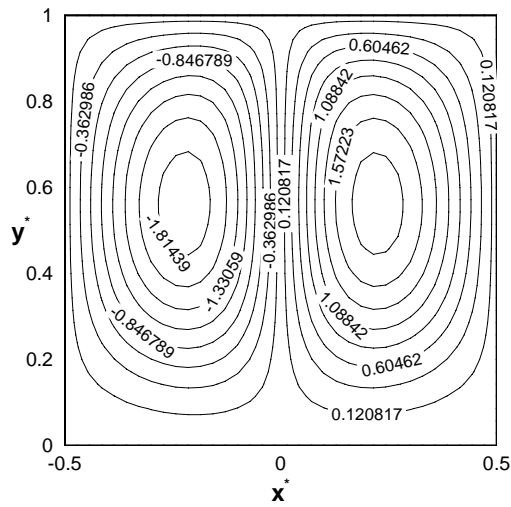
Figure 4-4. Same as Fig. 4-3, $t^* = 0.3$



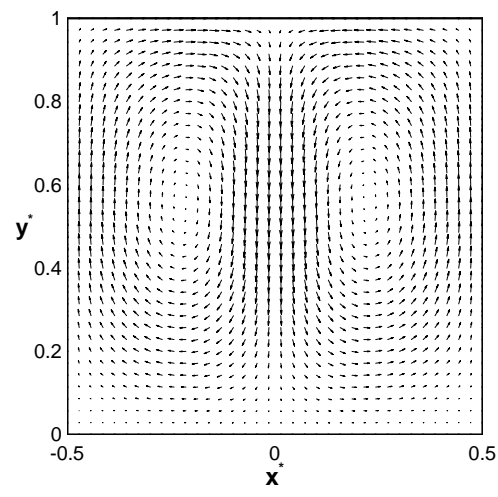
(a)



(b)



(c)



(d)

Figure 4-6. Same as Fig. 4-3, $t^* = 0.59825$

Table 4-3. Maximum values of the dimensionless number densities of microorganisms and particles, as well as the maximum value of the dimensionless stream function in the computational domain for the case of $\Delta\rho_p / \Delta\rho_m = 5$ and $D_p^* = 0.1$ at different time (based on the data shown in Figs. 3-6)

t^*	$(n_m^*)_{\max}$	$(n_p^*)_{\max}$	$(\psi^*)_{\max}$
0.19825	10.0561	0.453481	0.213259
0.30000	6.90995	0.700287	2.05947
0.49825	7.38435	0.962994	1.9235
0.59825	7.37157	0.941157	1.95196

Figures 4-7 and 4-8 display the steady-state bioconvection plumes for the case of $\Delta\rho_p / \Delta\rho_m = 5$ when $D_p / D_m = 0.2$ and 1, respectively. Table 4-4 summarizes the maximum values of the dimensionless number densities of microorganisms and particles, $(n_m^*)_{\max}$ and $(n_p^*)_{\max}$, and the maximum value of the dimensionless stream function, $(\psi^*)_{\max}$, for the basic case of no solid particles (Fig. 4-2) and cases with solid particles (Figs. 4-5, 4-7, and 4-8) for different diffusivities of the particles (all cases with particles shown in Table 4-4 are computed for $\Delta\rho_p / \Delta\rho_m = 5$). Number density of microorganisms takes on its maximum value at the top of the computational domain, while number density of solid particles takes on its maximum value at the bottom of the domain. According to boundary conditions (Eq. (4-16a)), the stream function takes on zero value at the boundaries of the domain. Since the stream function field is similar for all computed cases, the maximum value of the stream function indicates, on average, how strong the fluid velocity in the domain is. Figures 4-5, 4-7, and 4-8 and Table 4-4 show that the increase of diffusivity of solid particles results in a more uniform distribution of the particles over the depth of the chamber. A much more interesting conclusion is obtained by comparing the values of $(\psi^*)_{\max}$ for the case of no solid particles and the cases with solid

particles of different diffusivities. For all computed cases, the value of $(\psi^*)_{\max}$ is the largest for the case with no solid particles, which indicates that the presence of solid particles slows down bioconvection. Bioconvection is slowed down more efficiently by larger particles that, according to the Einstein relation, have smaller diffusivity and, therefore, concentrate near the bottom of the chamber. This unexpected result has a simple physical explanation. Bioconvection is caused by unstable density stratification that is created by the upswimming of microorganisms that are heavier than water. Very small particles (nanoparticles) that have very large diffusivity and whose distribution across the depth of the chamber is almost uniform have no impact on density stratification and, therefore, have no impact on bioconvection. Larger particles with smaller diffusivity concentrate near the bottom of the chamber. Since the particles are heavier than water, they create a more stable density stratification partly compensating for the increase of density in the upper fluid layer caused by the upswimming of microorganisms. Therefore, larger particles slow down bioconvection more effectively than very small particles. Figure 4-11(a) shows number density distributions of small particles at steady-state computed for two cases: with no bioconvection (computed utilizing equation (4-20)) and with bioconvection (in this case number density distribution is shown in the middle of the chamber, at $x^* = 0$). Number density distributions shown in Fig. 4-11(a) correspond to the cases that are displayed in Figs. 4-5, 4-7, and 4-8 and summarized in Table 4-4. It can be seen that if particle diffusivity is very large (the case of $D_p / D_m = 1$), the number density distribution of such solid particles across the depth of the chamber is almost uniform, which explains why these particles do not have considerable impact on bioconvection. However, the conclusion that larger particles slow down bioconvection is true only if the particles are not very large (which would imply that they have negligible diffusivity) or very heavy (which would imply that they have very large settling velocity). Such particles do not have any impact on bioconvection because they simply settle down to the bottom. This means that there is an optimum size (optimum diffusivity) of solid particles when they slow down bioconvection most efficiently.

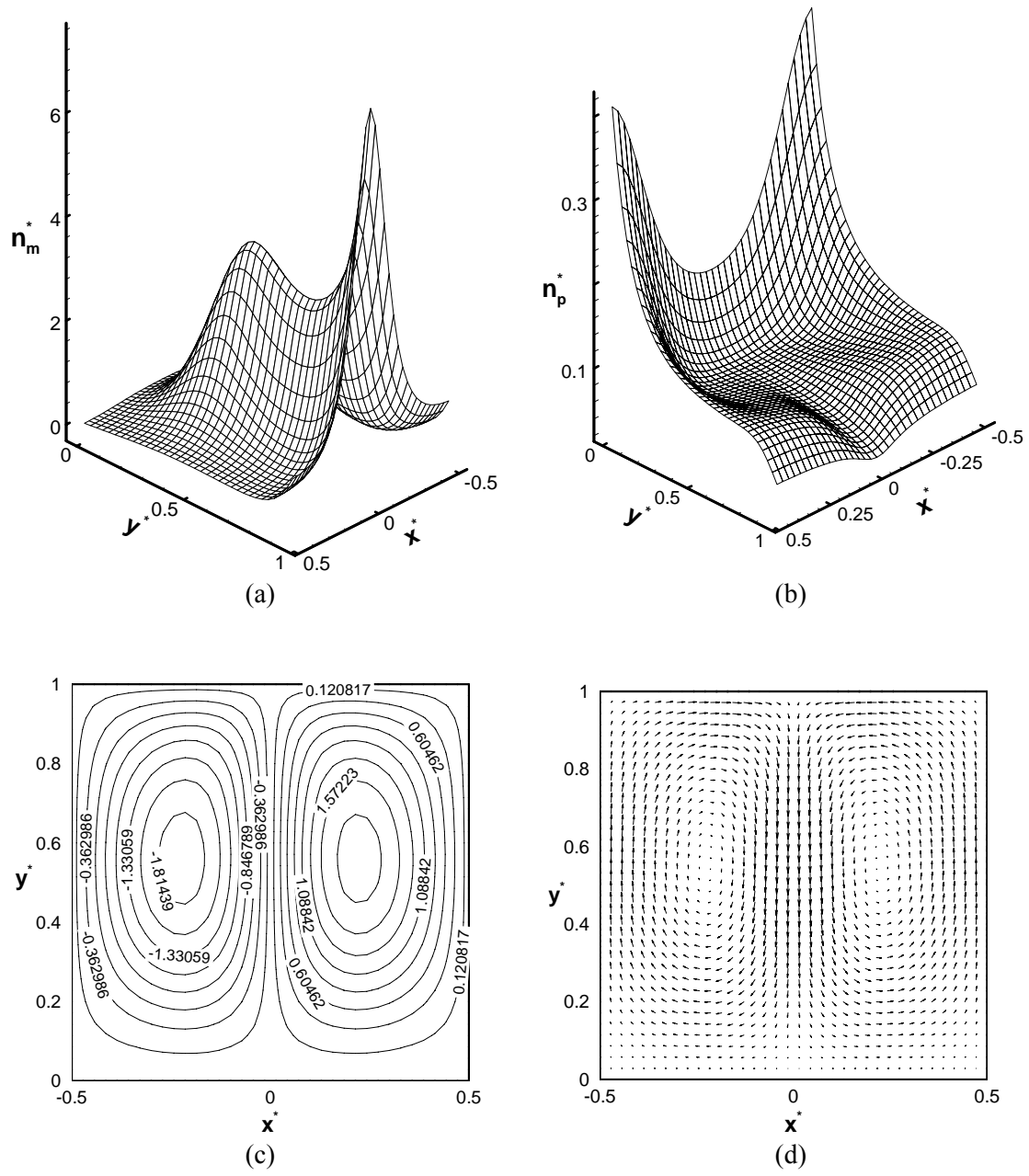


Figure 4-7. Same as Fig. 4-3, $D_p/D_m = 0.2$ and $t^* = 0.49825$ (steady-state plume)

Table 4-4. Maximum values of the dimensionless number densities of microorganisms and particles, as well as the maximum value of the dimensionless stream function in the computational domain at steady-state conditions for $\Delta\rho_p / \Delta\rho_m = 5$ for different diffusivities of solid particles (based on the data shown in Figs. 4-2, 4-5, 4-7, and 4-8)

	$(n_m^*)_{\max}$	$(n_p^*)_{\max}$	$(\psi^*)_{\max}$
No solid particles	6.79392	0	2.05603
$D_p / D_m = 1$	7.01507	0.158789	2.00139
$D_p / D_m = 0.2$	7.36259	0.410833	1.93294
$D_p / D_m = 0.1$	7.38435	0.962994	1.9235

Figures 4-9 and 4-10 display the steady-state bioconvection plumes for the case of $D_p / D_m = 0.1$ when $\Delta\rho_p / \Delta\rho_m = 10$ and 20, respectively. Table 4-5 summarizes the maximum values of the dimensionless number densities of microorganisms and particles, $(n_m^*)_{\max}$ and $(n_p^*)_{\max}$, and the maximum value of the dimensionless stream function, $(\psi^*)_{\max}$, for the basic case of no solid particles (Fig. 4-2) and cases with solid particles (Figs. 4-5, 4-9, and 4-10) for different densities of the particles (all cases with particles shown in Table 5 are computed for $D_p / D_m = 0.1$). Table 4-5 shows that when particles become too heavy and, therefore, settle too fast, they have almost no impact on bioconvection. Number density distributions of solid particles in the middle of the chamber that are shown in Figs. 4-11(b1, b2) correspond to the cases that are displayed in Figs. 4-5, 4-9, and 4-10 and summarized in Table 4-5. (Figure 4-11(b2) shows number density distributions of solid particles close to the bottom of the chamber on an enlarged scale.) Figures 4-11(b1, b2) show that heavy particles, because of their large settling velocity, just concentrate near the bottom of the chamber (there are

almost no particles in the rest of the domain). This explains why very heavy particles (the case of $\Delta\rho_p / \Delta\rho_m = 20$) have almost no impact on bioconvection.

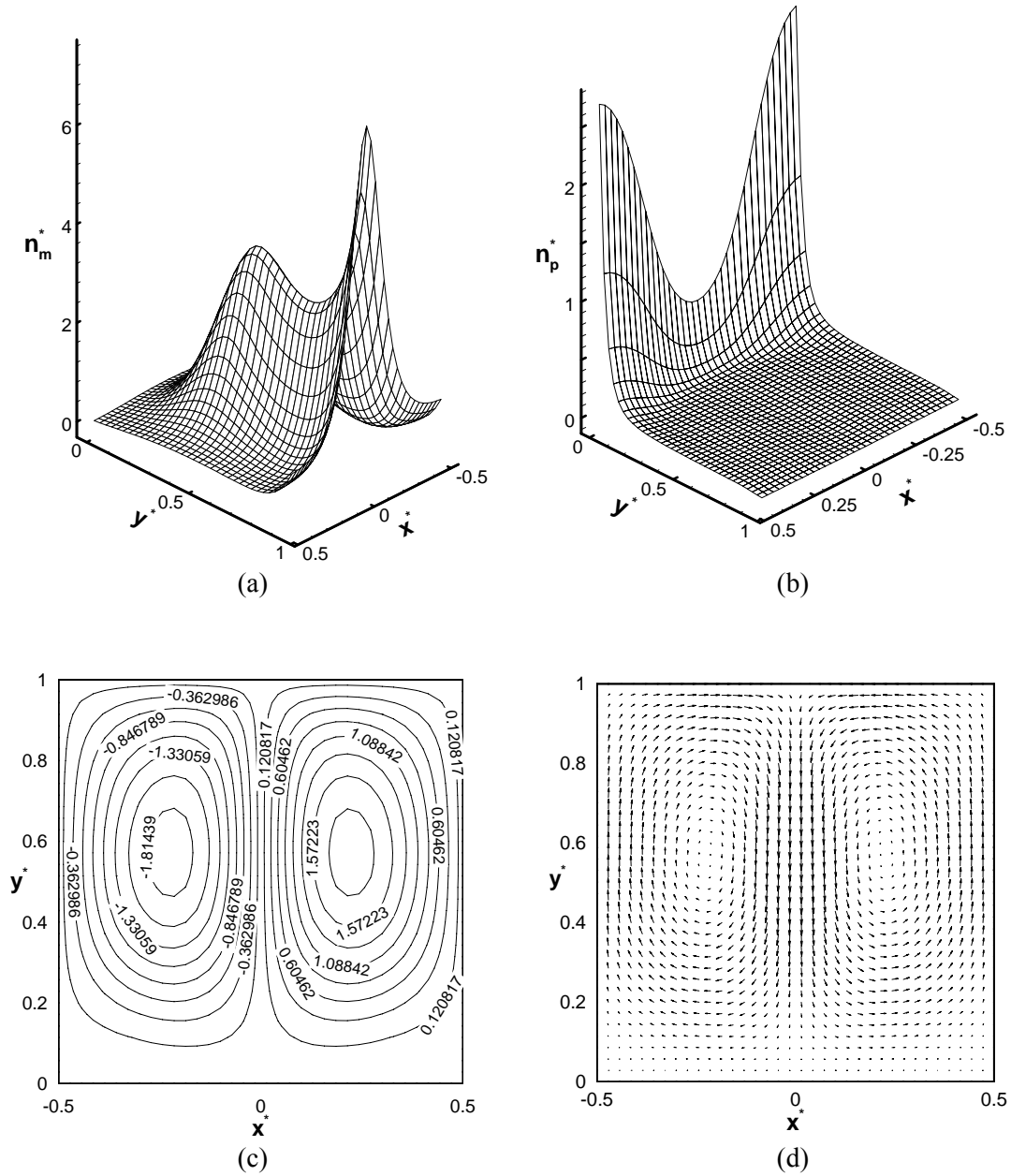


Figure 4-9. Same as Fig. 4-3, $\Delta\rho_p / \Delta\rho_m = 10$, $D_p / D_m = 0.1$, and $t^* = 0.49825$ (steady-state plume)

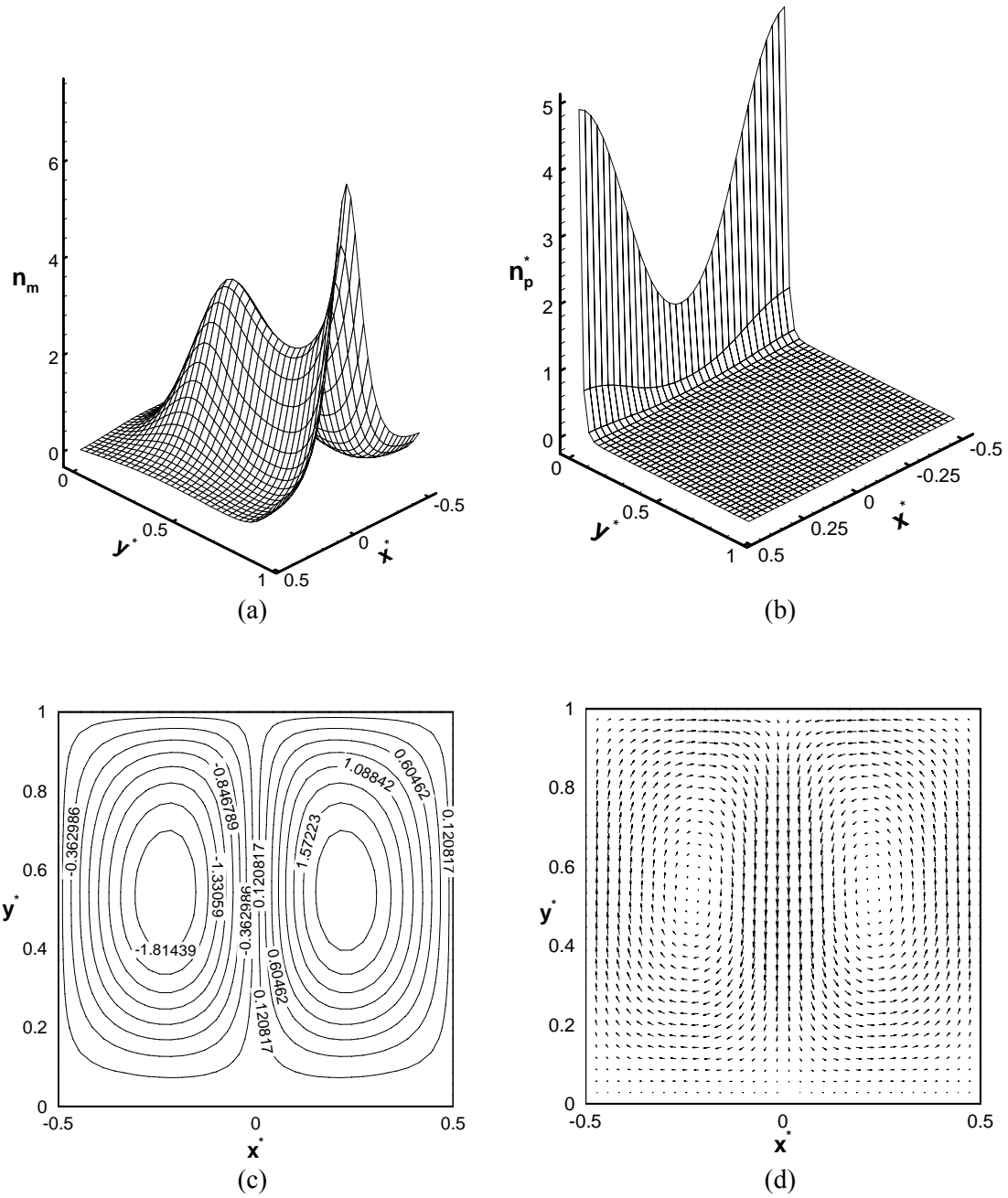
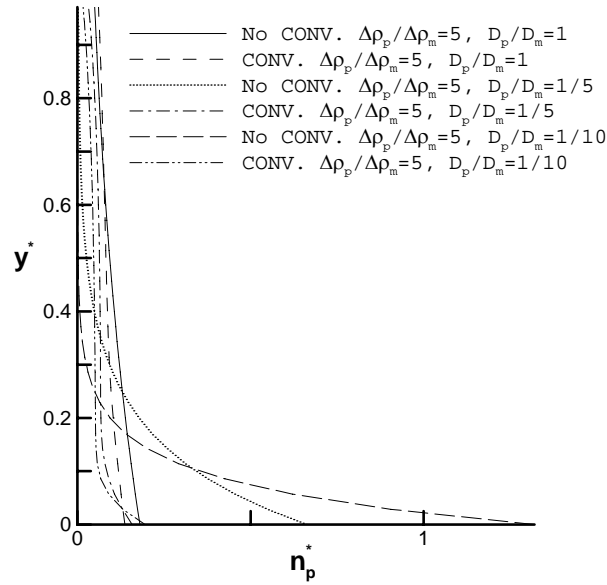


Figure 4-10. Same as Fig. 4-3, $\Delta\rho_p / \Delta\rho_m = 20$, $D_p / D_m = 0.1$, and $t^* = 0.49825$ (steady-state plume)

Table 4-5. Maximum values of the dimensionless number densities of microorganisms and particles, as well as the maximum value of the dimensionless stream function in the computational domain at steady-state conditions for $D_p / D_m = 0.1$ for different densities of solid particles (based on the data shown in

Figs. 4-2, 4-5, 4-9, and 4-10)

	$(n_m^*)_{\max}$	$(n_p^*)_{\max}$	$(\psi^*)_{\max}$
No solid particles	6.79392	0	2.05603
$\Delta\rho_p / \Delta\rho_m = 5$	7.38435	0.962994	1.9235
$\Delta\rho_p / \Delta\rho_m = 10$	7.25841	2.69321	1.93613
$\Delta\rho_p / \Delta\rho_m = 20$	6.81734	4.90278	2.04411



(a)

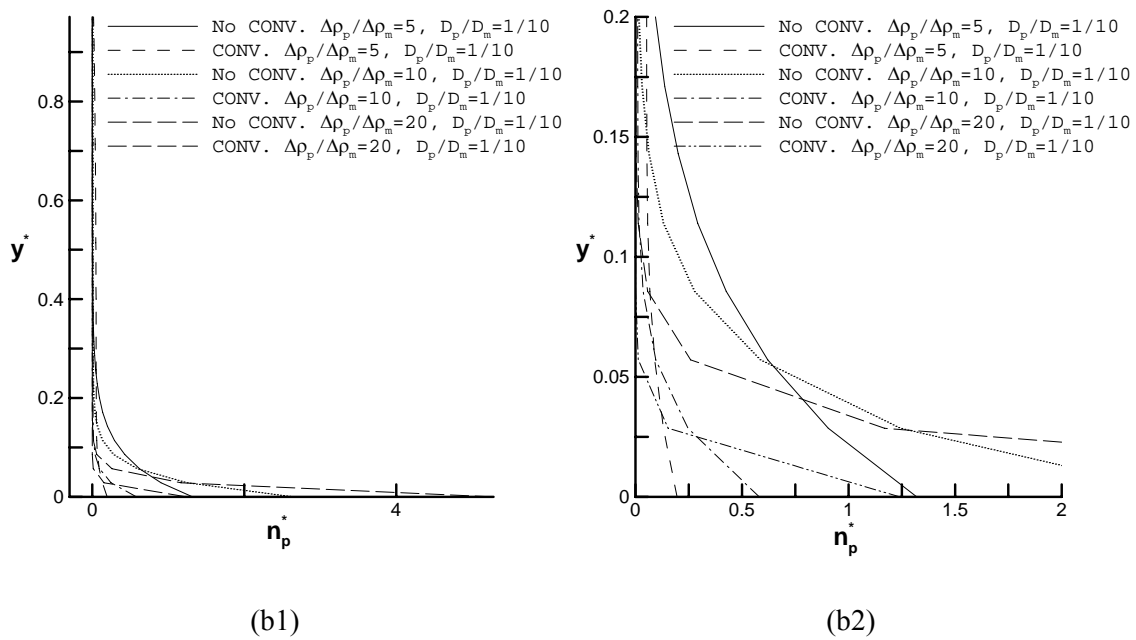


Figure 4-11. Distributions of the dimensionless number density of solid particles the middle of the chamber (at $x^* = 0$) computed with no bioconvection and with bioconvection. (a) n_p^* at $x^* = 0$ for cases displayed in Figs. 4-5, 4-7, and 4-8; (b1) n_p^* at $x^* = 0$ for cases displayed in Figs. 4-5, 4-9, and 4-10; (b2) Same as (b1), enlarged scale to show number density of solid particles close to the bottom of the chamber

4.4 CONCLUSIONS

It is established that small solid particles that are heavier than water slow down bioconvection. This is attributed to the fact that solid particles create a more stable density stratification than microorganisms alone. Extremely small particles (nanoparticles) that have negligible settling velocity do not have any noticeable impact on bioconvection, very large particles (that have negligible diffusivity) or very heavy particles (that have very large settling velocity) also do not have any impact on bioconvection because they simply settle to the bottom. However, if the particles are of the optimal size and density (gravitational settling must compete with Brownian diffusion to create an exponential number density distribution of solid particles with the maximum at the bottom of the chamber), these particles can effectively slow down bioconvection. On the other hand, bioconvection

makes number density distribution of solid particles more uniform. Further experimental research is needed to confirm the theoretical predictions of this chapter.

ACKNOWLEDGEMENTS

AVK gratefully acknowledges the grant # NAG3-2706 awarded to him by NASA Office of Biological and Physical Research, Physical Sciences Division. The authors also acknowledge the assistance of the North Carolina Supercomputing Center (NCSC) under an Advanced Computing Resources Grant. Critical comments of Prof. D.A. Nield are greatly appreciated.

REFERENCES

1. Batchelor, G.K. (1982), "Sedimentation in a dilute polydisperse system of interacting spheres. Part 1. General theory," *J. Fluid Mech.*, Vol. 119, pp. 379-408.
2. Ghorai, S. and Hill, N.A. (1999), "Development and stability of gyrotactic plumes in bioconvection," *J. Fluid Mech.*, Vol. 400, pp. 1-31.
3. Ghorai, S. and Hill, N.A. (2000), "Periodic arrays of gyrotactic plumes in bioconvection," *Physics of Fluids*, Vol. 12, pp. 5-22.
4. Kessler, J.O. (1985a), "Hydrodynamic focusing of motile algal cells," *Nature*, Vol. 313, pp. 218-220
5. Kessler, J.O. (1985b), "Co-operative and concentrative phenomena of swimming microorganisms," *Contemp. Phys.*, Vol. 26, pp. 147-166.

6. Kessler, J.O., Burnett, G.D., and Remick, K.E. (2000), "Mutural dynamics of swimming microorganisms and their fluid habitat," *Nonlinear Science at the Dawn of the 21st Century*, P.L. Christiansen, M.P. Sorensen, and A.C. Scott (Eds.), Springer, New York, pp. 409-426.
7. Kessler, J.O., Wiseley, D.A., Remick, K.E., Marthaler, D.E. (1997), "Individual and collective dynamics of swimming bacteria," *Proceedings of the Workshop "Traffic and Granular Flow'97"*, M. Schreckenberg and D.E. Wolf (Eds.), Springer, New York, pp. 37-51.
8. Kuznetsov, A.V., and Avramenko, A.A. (2004), "Effect of small particles on the stability of bioconvection in a suspension of gyrotactic microorganisms in a layer of finite depth," *International Communications in Heat and Mass Transfer*, Vol. 31, pp. 1-10.
9. Pedley, T.J., Hill, N.A., and Kessler, J.O. (1988), "The growth of bioconvection patterns in a uniform suspension of gyrotactic microorganisms," *J. Fluid Mech.*, Vol. 195, pp. 223-338.
10. Pedley, T.J. and Kessler, J.O. (1987), "The orientation of spheroidal microorganisms swimming in a flow field," *Proc. R. Soc. Lond.*, Vol. B231, pp. 47-70.
11. Pedley, T.J. and Kessler, J.O. (1990), "A new continuum model for suspensions of gyrotactic microorganisms," *Journal of Fluid Mechanics*, Vol. 212, pp. 155-182.
12. Pedley, T.J. and Kessler, J.O. (1992), "Hydrodynamic phenomena in suspensions of swimming microorganisms," *Ann. Rev. Fluid Mech.*, Vol. 24, pp. 313-358.

5. SETTLING OF BIDISPERSED SMALL SOLID PARTICLES IN A DILUTE SUSPENSION CONTAINUNG GYROTACTIC MICROORGANISMS

ABSTRACT

The motivation of this chapter is to investigate the feasibility of the utilization of bioconvection for enhancing mixing in a suspension of small solid particles. This may be important in microfluidic applications relevant to biotechnology and medicine, such as analyses of DNA or drugs, screening of patients, and combinatorial synthesis. Traditionally, the mixing of fluids in microvolumes has been limited to diffusion. Due to the microscopic size of the organisms involved in bioconvection, bioconvective flows are a prospective and novel design for microfluidic mixing. This chapter considers a bidispersed suspension of small solid particles that have different densities and settling velocities in a fluid that contains motile gyrotactic microorganisms. The particles are assumed to be sufficiently small so that their Brownian diffusion is not negligible. It is found that the number density distribution of solid particles of one type impacts that of particles of the other type as well as that of microorganisms.

NOMENCLATURE

a	radius of a micro-organism, m
A	area of the chamber, m^2
B	time scale for the reorientation of microorganisms by the gravitational torque against viscous torque, $4\pi\mu a^3 / (mgh)$, s
D_m	diffusivity of microorganisms, m^2/s
$(D_p)_1$	diffusivity of solid particles of type 1 due to Brownian motion and interactions with microorganisms, m^2/s
$(D_p)_2$	diffusivity of solid particles of type 2 due to Brownian motion and interactions with microorganisms, m^2/s
$(D_p^*)_1$	ratio of the diffusivity of solid particles of type 1 to that of microorganisms, $(D_p)_1 / D_m$
$(D_p^*)_2$	ratio of the diffusivity of solid particles of type 2 to that of microorganisms, $(D_p)_2 / D_m$
\mathbf{g}	gravity vector, 9.81 m/s^2
G	gyrotaxis number, BD_m / L^2
h	displacement of the center of mass of a gyrotactic micro-organism from its center of buoyancy, m
H	height of the chamber, m
\mathbf{J}_m^*	dimensionless flux of microorganisms, defined by equation (5.17a)
$(\mathbf{J}_p^*)_1$	dimensionless flux of solid particles of type 1, defined by equation (5.17b)
$(\mathbf{J}_p^*)_2$	dimensionless flux of solid particles of type 2, defined by equation (5.17c)

L	width of the chamber, m
n_m	number density of microorganisms, $1/m^3$
\bar{n}_m	average number density of microorganisms, $1/m^3$
n_m^*	dimensionless number density of microorganisms, n_m / \bar{n}_m
$(n_p)_1$	number density of solid particles of type 1, $1/m^3$
$(\bar{n}_p)_1$	average number density of solid particles of type 1, $1/m^3$
$(n_p^*)_1$	dimensionless number density of solid particles of type 1, $(n_p)_1 / \bar{n}_m$
$(\bar{n}_p^*)_1$	ratio of the average number density of particles of type 1 to that of microorganisms, $(\bar{n}_p)_1 / \bar{n}_m$
$(n_p)_2$	number density of solid particles of type 2, $1/m^3$
$(\bar{n}_p)_2$	average number density of solid particles of type 2, $1/m^3$
$(n_p^*)_2$	dimensionless number density of solid particles of type 2, $(n_p)_2 / \bar{n}_m$
$(\bar{n}_p^*)_2$	ratio of the average number density of particles of type 2 to that of microorganisms, $(\bar{n}_p)_2 / \bar{n}_m$
\hat{p}	unit vector indicating the direction of swimming of gyrotactic microorganisms
p_e	excess pressure (above hydrostatic), Pa
R_m	Rayleigh number for microorganisms, $\bar{n}_m \theta_m \Delta \rho_m g L^3 / (\rho_0 \nu D_m)$
$(R_p)_1$	Rayleigh number for solid particles of type 1, $\bar{n}_m (\theta_p)_1 (\Delta \rho_p)_1 g L^3 / (\rho_0 \nu D_m)$
$(R_p)_2$	Rayleigh number for solid particles of type 2, $\bar{n}_m (\theta_p)_2 (\Delta \rho_p)_2 g L^3 / (\rho_0 \nu D_m)$
S_c	Schmidt number, ν / D_m
t	time, s

t^*	dimensionless time, $D_m t / L^2$
u	horizontal velocity component, m/s
v	vertical velocity component, m/s
\mathbf{V}	velocity vector, m/s
\mathbf{V}^*	dimensionless velocity vector, $\mathbf{V}L / D_m$
W_m	average swimming velocity of microorganisms (assumed to be constant), m/s
W_m^*	dimensionless average swimming velocity of microorganisms, $W_m L / D_m$
$(W_p)_1$	settling velocity of particles of type 1, m/s
$(W_p^*)_1$	dimensionless settling velocity of particles of type 1, $(W_p)_1 L / D_p$
$(W_p)_2$	settling velocity of particles of type 2, m/s
$(W_p^*)_2$	dimensionless settling velocity of particles of type 2, $(W_p)_2 L / D_p$
x	horizontal coordinate, m
x^*	dimensionless horizontal coordinate, x / L
$\hat{\mathbf{x}}$	unit vector in the x -direction
y	vertical coordinate, m
y^*	dimensionless vertical coordinate, y / L
$\hat{\mathbf{y}}$	unit vector in the y -direction

Greek symbols

$\Delta(\bar{n}_m^*)$ nonuniformity of number density distribution of microorganisms, defined by Eq. (5.21a)

$\Delta(\bar{n}_p^*)_1$ nonuniformity of number density distribution of particles of type 1, defined by Eq. (5.21b)

$\Delta(\bar{n}_p^*)_2$	nonuniformity of number density distribution of particles of type 2, defined by Eq. (5.21c)
$\Delta\rho$	density difference between suspension and pure water, $\rho_{suspension} - \rho_0$, kg/m ³
$\Delta\rho_m$	density difference between microorganisms and water, $\rho_m - \rho_0$, kg/m ³
$(\Delta\rho_p)_1$	density difference between solid particles of type 1 and water, $(\rho_p)_1 - \rho_0$, kg/m ³
$(\Delta\rho_p)_2$	density difference between solid particles of type 2 and water, $(\rho_p)_2 - \rho_0$, kg/m ³
ζ	horizontal component of vorticity, 1/s
ζ^*	dimensionless horizontal component of vorticity, $\zeta L^2 / D_m$
θ_m	volume of a micro-organism, m ³
$(\theta_p)_1$	volume of a particle of type 1, m ³
$(\theta_p)_2$	volume of a particle of type 2, m ³
λ	aspect ratio of the chamber, H / L
μ	dynamic viscosity, assumed to be approximately the same as that of water, kg/(m s)
ν	kinematics viscosity, assumed to be approximately the same as that of water, m ² /s
ρ_0	density of water, kg/m ³
ρ_m	density of microorganisms, kg/m ³
$(\rho_p)_1$	density of solid particles of type 1, kg/m ³
$(\rho_p)_2$	density of solid particles of type 2, kg/m ³
$\rho_{suspension}$	density of the suspension that contains particles and microorganisms
ψ	stream function, m ² /s
ψ^*	dimensionless stream function, ψ / D_m

5.1 INTRODUCTION

The aim of this chapter is to investigate the feasibility of utilizing bioconvection to enhance the mixing of a bidispersed suspension of small solid particles. This may be important in possible applications of bioconvection in the pharmaceutical and bio-technological industries to enhance mixing in microvolumes of a fluid. Biotechnology is increasingly involved with large numbers of experiments, such as analyses of DNA or drugs, screening of patients, and combinatorial synthesis, all of which are processes that often require handling microvolumes of fluids.

The investigation of bioconvection is relevant to biotechnology in innumerable applications. One example of this is microfluidics. Microfluidics is the ability to move, pump, mix, and otherwise manipulate microvolumes of fluids. This is applicable to pharmaceuticals, public health, laboratory testing, agriculture, etc. At the microscopic scale, controlled mixing of fluids becomes something of a challenge as the associated Reynolds number is so small that the flows do not become turbulent. Traditionally, the mixing of fluids on such a small scale has been limited to diffusion. Due to the microscopic size of the organisms involved in bioconvection (a typical cell volume is $10^{-16} m^3$), bioconvective flows would seem an ideal and novel design for microfluidic mixing.

The term bioconvection is used to describe the phenomenon of spontaneous pattern formation in suspensions of motile microorganisms. Over the last two decades, many significant results in this area, such as Pedley et al. [1], Ghorai and Hill [2], and Pedley and Kessler [3-5], were obtained. Microorganisms may swim in a certain direction due to different stimuli such as phototaxis, chemotaxis, and gyrotaxis. This chapter considers microorganisms that exhibit gyrotactic behavior. Gyrotaxis is the behavior typical for algae, whose swimming direction is determined by the balance of gravitational and viscous torques. Algae are approximately 3-5% denser than water; gyrotactic behavior results in their swimming towards the regions of most rapid downflow. Therefore, the density of regions of downflow becomes larger than that of regions of upflow. Buoyancy increases

velocities in both upflow and downflow regions, thus enhancing velocity fluctuations and inducing macroscopic convective fluid motion (Pedley et al. [1], Ghorai and Hill [2, 6]). The formation of gyrotactic plumes with regular patterns in algal suspensions is described in numerous experimental papers (Kessler [7-10]).

Kuznetsov and Geng [11] investigated the settling of *monodispersed* small solid particles in a suspension of motile gyrotactic microorganisms. It was found that the mixing induced by bioconvection leads to a more uniform number density distribution of solid particles along the height of the chamber. The aim of this chapter is to investigate the behavior of a *bidispersed* suspension of small solid particles.

Weiland and McPherson [12] and Fessas and Weiland [13] suggested an interesting technique for improving sedimentation rates of solid particles. They suggested adding a second buoyant particulate phase to the suspension. It turns out that the presence of buoyant particles leads to a rapid separation of the two types of particles into large-scale convection streams, which occur in the vertical direction. The velocity of these streams adds to the normal settling velocity of heavy particles, thus increasing their sedimentation rate. We would like to emphasize that our computations are restricted to the case when both types of particles are heavier than water; therefore, in our case, these streams do not occur.

This research is concentrated on investigating the evolution of number density distributions of microorganisms and particles in a dilute suspension that contains gyrotactic microorganisms (whose number density is n_m) and small particles of types 1 and 2 (whose densities are $(n_p)_1$ and $(n_p)_2$, respectively) in a two-dimensional chamber. The depth of the chamber is H and the width is L . The side walls of the chamber are assumed to be shear-free to model the periodic condition (it is assumed that there are other plumes and that the typical distance between the plumes is L). Microorganisms and particles of both types are slightly heavier than water. Both particles are sufficiently small so that their Brownian diffusion prevents their complete settling to the bottom of the chamber.

The computational domain and boundary conditions are shown schematically in Fig. 1. The width of the domain is L (the coordinate x is changing from $-L/2$ to $L/2$) and the height of the domain is H (the coordinate y is changing from 0 to H). Initially, the microorganisms and particles of both types are uniformly distributed in a chamber and the fluid is motionless. The free surface is assumed to be stress-free and the bottom wall is rigid (a hydrodynamic no-slip condition is imposed there). The side walls are stress-free to model the periodic condition, as discussed above. No flux of microorganisms or particles is allowed through any of the chamber's boundaries.

5.2 GOVERNING EQUATIONS

5.2.1 Dimensional Governing Equations

Governing equations are obtained by extending the equations given in Ghorai and Hill [2, 6] to account for the buoyancy force induced by bidispersed solid particles. Since the Reynolds number is much smaller than unity, inertia terms in these equations are neglected:

x and y- momentum equations:

$$\rho_0 \frac{\partial u}{\partial t} = -\frac{\partial p_e}{\partial x} + \mu \left(\frac{\partial^2 u}{\partial x^2} + \frac{\partial^2 u}{\partial y^2} \right) \quad (5.1)$$

$$\rho_0 \frac{\partial \mathbf{v}}{\partial t} = -\frac{\partial p_e}{\partial y} + \mu \left(\frac{\partial^2 \mathbf{v}}{\partial x^2} + \frac{\partial^2 \mathbf{v}}{\partial y^2} \right) - n_m \theta_m \Delta \rho_m \mathbf{g} - (n_p)_1 (\theta_p)_1 (\Delta \rho_p)_1 \mathbf{g} - (n_p)_2 (\theta_p)_2 (\Delta \rho_p)_2 \mathbf{g} \quad (5.2)$$

Continuity equation:

$$\frac{\partial u}{\partial x} + \frac{\partial v}{\partial y} = 0 \quad (5.3)$$

Conservation of motile microorganisms:

$$\frac{\partial(n_m)}{\partial t} = -\text{div}(n_m \mathbf{V} + n_m W_m \hat{\mathbf{p}} - D_m \nabla n_m) \quad (5.4)$$

Conservation of solid particles:

$$\frac{\partial(n_p)_1}{\partial t} = -\text{div}\left((n_p)_1 \mathbf{V} + (n_p)_1 (W_p)_1 \frac{\mathbf{g}}{|\mathbf{g}|} - (D_p)_1 \nabla(n_p)_1\right) \quad (5.5a)$$

$$\frac{\partial(n_p)_2}{\partial t} = -\text{div}\left((n_p)_2 \mathbf{V} + (n_p)_2 (W_p)_2 \frac{\mathbf{g}}{|\mathbf{g}|} - (D_p)_2 \nabla(n_p)_2\right) \quad (5.5b)$$

where D_m is the diffusivity of microorganisms (this assumes that all random motions of microorganisms can be approximated by a diffusive process); $(D_p)_1$ and $(D_p)_2$ are the diffusivities of particles of type 1 and 2, respectively (both $(D_p)_1$ and $(D_p)_2$ are smaller than D_m , but still not zero; the diffusivity of particles results from the Brownian motion and interactions with microorganisms); n_m is the number density of motile microorganisms; $(n_p)_1$ and $(n_p)_2$ are the number densities of particles of type 1 and 2, respectively; p_e is the excess pressure (above hydrostatic); $\hat{\mathbf{p}}$ is the unit vector indicating the direction of swimming of microorganisms (equations for this vector are given in Pedley et al. [1]); t is the time; u and v are the x and y -velocity components, respectively; \mathbf{V} is the velocity vector, (u, v) ; $W_m \hat{\mathbf{p}}$ is the vector of microorganisms' average swimming velocity (W_m is assumed to be constant); $(W_p)_1 \frac{\mathbf{g}}{|\mathbf{g}|}$ and $(W_p)_2 \frac{\mathbf{g}}{|\mathbf{g}|}$ are the vectors of settling velocities relative to the fluid of particles of type 1 and 2, respectively ($(W_p)_1$ and $(W_p)_2$ are assumed to be constant, both particles settle straight downward); x and y are the Cartesian coordinates (x is the horizontal coordinate and y is the vertical coordinate); $\Delta\rho_m$ is the density difference between microorganisms and water, $\rho_m - \rho_0$; $(\Delta\rho_p)_1$ is the density difference between

particles of type 1 and water, $(\rho_p)_1 - \rho_0$; $(\Delta\rho_p)_2$ is the density difference between particles of type 2 and water, $(\rho_p)_2 - \rho_0$; θ_m is the volume of a micro-organism; $(\theta_p)_1$ and $(\theta_p)_2$ are the volumes of particles of type 1 and 2, respectively; μ is the dynamic viscosity of the suspension, assumed to be approximately the same as that of water since the suspension is dilute; and ρ_0 is the density of water.

According to the Stokes law (Batchelor [14]), the settling velocity of spherical particles can be found as:

$$(W_p)_1 = \frac{(\theta_p)_1 (\Delta\rho_p)_1 g}{6\pi\mu \left(\frac{3}{4} \frac{(\theta_p)_1}{\pi} \right)^{1/3}} \quad (5.7a)$$

$$(W_p)_2 = \frac{(\theta_p)_2 (\Delta\rho_p)_2 g}{6\pi\mu \left(\frac{3}{4} \frac{(\theta_p)_2}{\pi} \right)^{1/3}} \quad (5.7b)$$

5.2.2 Dimensionless Governing Equations

Utilizing stream function-vorticity formulation, the governing equations can be recast in the dimensionless form as follows:

$$\zeta^* = -\nabla^2 \psi^* \quad (5.8)$$

$$S_c^{-1} \left(\frac{\partial \zeta^*}{\partial t^*} + u^* \frac{\partial \zeta^*}{\partial x^*} + v^* \frac{\partial \zeta^*}{\partial y^*} \right) = \nabla^2 \zeta^* - \left(R_m \frac{\partial n_m^*}{\partial x^*} + (R_p)_1 \frac{\partial (n_p)_1^*}{\partial x^*} + (R_p)_2 \frac{\partial (n_p)_2^*}{\partial x^*} \right) \quad (5.9)$$

$$\frac{\partial n_m^*}{\partial t^*} = -\nabla \cdot [n_m^* (\mathbf{V}^* + W_m^* \hat{\mathbf{p}})] - \nabla n_m^* \quad (5.10)$$

$$\frac{\partial(n_p^*)_1}{\partial t^*} = -\nabla \cdot \left[(n_p^*)_1 \left(\mathbf{v}^* + (W_p^*)_1 \frac{\mathbf{g}}{|\mathbf{g}|} \right) - (D_p^*)_1 \nabla(n_p^*)_1 \right] \quad (5.11a)$$

$$\frac{\partial(n_p^*)_2}{\partial t^*} = -\nabla \cdot \left[(n_p^*)_2 \left(\mathbf{v}^* + (W_p^*)_2 \frac{\mathbf{g}}{|\mathbf{g}|} \right) - (D_p^*)_2 \nabla(n_p^*)_2 \right] \quad (5.11b)$$

In Ghorai and Hill [2, 6] it is shown that vector $\hat{\mathbf{p}}$, which determines the swimming direction of microorganisms, can be computed as:

$$\hat{\mathbf{p}} = \begin{cases} \left(-\kappa - (\kappa^2 - 1)^{1/2}, 0 \right), & \kappa < -1 \\ \left(-\kappa, (1 - \kappa^2)^{1/2} \right), & |\kappa| \leq 1 \\ \left(-\kappa + (\kappa^2 - 1)^{1/2}, 0 \right), & \kappa > 1 \end{cases} \quad (5.12)$$

where $\kappa = B\zeta = G\zeta^*$. According to equation (5.12), unit vector $\hat{\mathbf{p}}$ is a function of vorticity. At the initial moment of time, when fluid is motionless, this vector is directed vertically upward (which implies that at the initial moment all microorganisms are swimming vertically upward); however, as bioconvection develops and the vorticity field becomes non-zero, the direction of this vector deviates from strictly vertical; it changes with time and also depends on the location in the chamber.

Parameter B is called the “gyrotactic orientation parameter”. It is defined by Pedley and Kessler [3] as:

$$B = \frac{4\pi\mu a^3}{mgh} \quad (5.13)$$

where h is the displacement of the center of mass of a gyrotactic micro-organism from its center of buoyancy, m is the mass of the micro-organism, and a is the radius of the micro-organism.

The dimensionless variables in equations (5.8)-(5.11) are defined as:

$$\begin{aligned}
 x^* &= \frac{x}{L}; \quad y^* = \frac{y}{L}; \quad t^* = \frac{D_m}{L^2} t; \quad u^* = \frac{\partial \psi^*}{\partial y^*}; \quad v^* = -\frac{\partial \psi^*}{\partial x^*}; \quad \mathbf{V}^* = \mathbf{V} \frac{L}{D_m}; \\
 W_m^* &= W_m \frac{L}{D_m}; \quad (W_p^*)_1 = (W_p)_1 \frac{L}{D_m}; \quad (W_p^*)_2 = (W_p)_2 \frac{L}{D_m}; \\
 n_m^* &= \frac{n_m}{\bar{n}_m}; \quad (n_p^*)_1 = \frac{(n_p)_1}{\bar{n}_m}; \quad (n_p^*)_2 = \frac{(n_p)_2}{\bar{n}_m}; \quad S_c = \frac{\nu}{D_m}; \quad G = \frac{BD_m}{L^2}; \\
 R_m &= \frac{\bar{n}_m \theta_m \Delta \rho_m g L^3}{\rho_0 \nu D_m}; \quad (R_p)_1 = \frac{\bar{n}_m (\theta_p)_1 (\Delta \rho_p)_1 g L^3}{\rho_0 \nu D_m}; \quad (R_p)_2 = \frac{\bar{n}_m (\theta_p)_2 (\Delta \rho_p)_2 g L^3}{\rho_0 \nu D_m}; \\
 (D_p^*)_1 &= \frac{(D_p)_1}{D_m}; \quad (D_p^*)_2 = \frac{(D_p)_2}{D_m}
 \end{aligned} \tag{5.14}$$

5.2.2 Initial and Boundary Conditions

Equations (5.8)-(5.11) must be solved subject to the following boundary conditions (see Fig. 5-1). A no-slip boundary condition is imposed at the bottom wall, while the top boundary and the side walls are assumed impermeable to the fluid and stress-free. Under these assumptions the boundary conditions can be presented as:

$$\psi^* = 0 \text{ at } y^* = 0, \quad \lambda \text{ and } x^* = \pm 0.5, \tag{5.15a}$$

where λ is the aspect ratio of the chamber, H/L ,

$$\frac{\partial \psi^*}{\partial y^*} = 0 \text{ at } y^* = 0, \tag{5.15b}$$

$$\frac{\partial^2 \psi^*}{\partial y^{*2}} = 0 \text{ at } y^* = \lambda, \text{ and } \frac{\partial^2 \psi^*}{\partial x^{*2}} = 0 \text{ at } x^* = \pm 0.5. \tag{5.15c}$$

Normal fluxes of microorganisms and solid particles are zero through all boundaries of the chamber:

$$\mathbf{J}_m^* \cdot \hat{\mathbf{y}} = 0, (\mathbf{J}_p^*)_1 \cdot \hat{\mathbf{y}} = 0 \text{ and } (\mathbf{J}_p^*)_2 \cdot \hat{\mathbf{y}} = 0 \text{ at } y^* = 0, \lambda \quad (5.16a)$$

$$\mathbf{J}_m^* \cdot \hat{\mathbf{x}} = 0, (\mathbf{J}_p^*)_1 \cdot \hat{\mathbf{x}} = 0 \text{ and } (\mathbf{J}_p^*)_2 \cdot \hat{\mathbf{x}} = 0 \text{ at } x^* = \pm 0.5, \quad (5.16b)$$

where $\hat{\mathbf{x}}$ and $\hat{\mathbf{y}}$ are the unit vectors in the x - and y -directions, respectively,

$$\mathbf{J}_m^* = n_m^* (\mathbf{V}^* + W_m^* \hat{\mathbf{p}}) - \nabla n_m^* \quad (5.17a)$$

is the dimensionless flux of microorganisms,

$$(\mathbf{J}_p^*)_1 = (n_p^*)_1 \left(\mathbf{V}^* + (W_p^*)_1 \frac{\mathbf{g}}{|\mathbf{g}|} \right) - (D_p^*)_1 \nabla (n_p^*)_1 \quad (5.17b)$$

is the dimensionless flux of solid particles of type 1 and

$$(\mathbf{J}_p^*)_2 = (n_p^*)_2 \left(\mathbf{V}^* + (W_p^*)_2 \frac{\mathbf{g}}{|\mathbf{g}|} \right) - (D_p^*)_2 \nabla (n_p^*)_2 \quad (5.17c)$$

is the dimensionless flux of solid particles of type 2.

Initially, at $t^* = 0$, the fluid is assumed motionless and the number density distributions of microorganisms and solid particles are assumed uniform. As in Ghorai and Hill [2, 6], small perturbations to these uniform distributions are utilized to ensure that the plume forms in the middle of the computational domain. This results in the following initial condition:

$$\psi^* = 0, \zeta^* = 0, n_m^* = 1 + \varepsilon \cos(m \pi x^*), (n_p^*)_1 = \frac{(\bar{n}_p)_1}{\bar{n}_m} + \varepsilon \cos(m \pi x^*),$$

$$(n_p^*)_2 = \frac{(\bar{n}_p)_2}{\bar{n}_m} + \varepsilon \cos(m \pi x^*) \quad (5.18)$$

where $\varepsilon = 10^{-5}$ and $m = 2$.

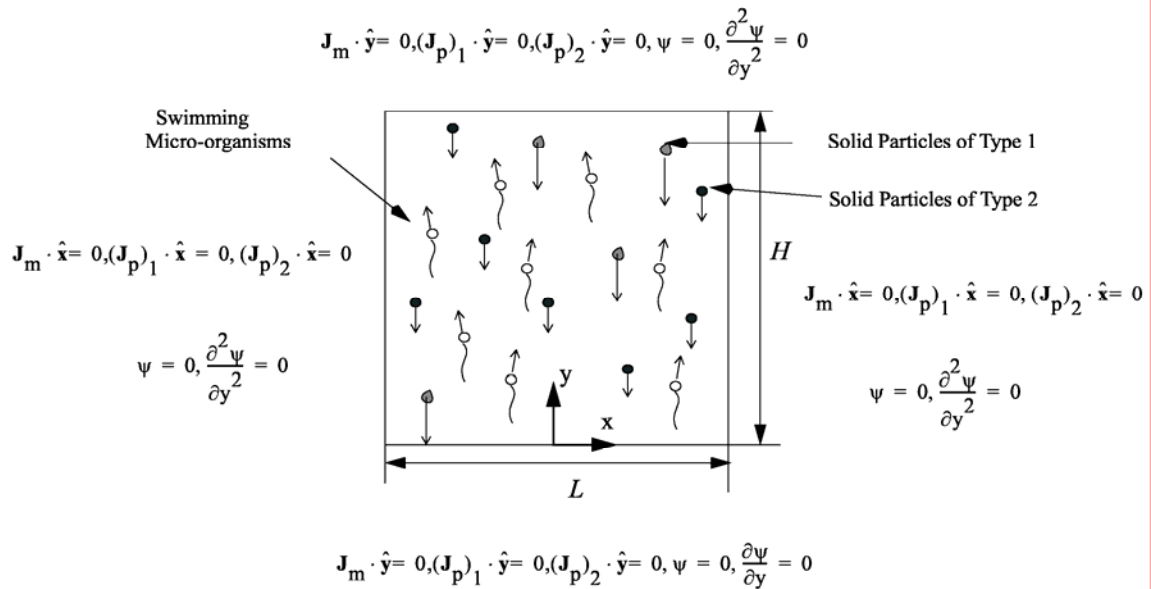


Figure 5-1. Computational domain and boundary conditions

5.2.4 Numerical Procedure

A conservative finite-difference scheme is used to discretize the governing equations. An implicit scheme with Euler backward differencing in time and central differencing in space is utilized to obtain the transient solutions. A line-by-line tridiagonal matrix algorithm with relaxation is used together with an iteration technique to solve the nonlinear discretized equations. A staggered uniform grid with the stream function and vorticity stored in one set of nodes and the number densities of microorganisms and solid particles stored in another set of nodes is utilized. The grid is chosen so that the number density nodes lie in the interior of the computational domain only, whereas those of the stream function and vorticity lie in the interior and at the boundary of the domain. Computations are performed at the North Carolina State University IBM p690 super computer. CPU time required to investigate plume development until it attains its steady-state for a 36×36 uniform mesh is about 15 hours.

5.3 RESULTS AND DISCUSSION

Values of physical properties and geometrical parameters utilized in computations are summarized in Table 5-1. Values of dimensionless groups that correspond to these parameter values are given in Table 5-2. The diffusivities of particles of both types are taken to be about 250 times larger than those following from the Einstein's relation that determines the diffusivity of small particles due to the Brownian motion. This is done for three reasons: 1) To account for additional random motions of particles that may result from their interactions with swimming microorganisms (a particle may be either directly hit by a micro-organism or it can enter a propulsive stream caused by a swimming micro-organism); 2) It has been shown (Acricos et al. [15]) that placing a particle in a shear flow results in the particle exhibiting additional diffusivity in the streamwise direction; 3) To introduce artificial diffusivity in order to avoid excessive stiffness of the numerical problem.

Table 5-1. Physical properties and geometrical parameters utilized in computations

Average number density of microorganisms	\bar{n}_m	10^{12} cells/m ³
Average number density of solid particles of type 1	$(\bar{n}_p)_1$	10^{15} cells/m ³
Average number density of solid particles of type 2	$(\bar{n}_p)_2$	10^{15} cells/m ³
Density of water	ρ_0	10^3 kg/m ³
Density of microorganisms	ρ_m	1.05×10^3 kg/m ³
Density of particles of type 1	$(\rho_p)_1$	21×10^3 kg/m ³
Density of particles of type 2	$(\rho_p)_2$	6×10^3 kg/m ³
Volume of a micro-organism	θ_m	5×10^{-16} m ³
Volume of a particle of type 1	$(\theta_p)_1$	5×10^{-21} m ³
Volume of a particle of type 2	$(\theta_p)_2$	5×10^{-21} m ³
Average swimming velocity of microorganisms	W_m	10^{-4} m/s
Settling velocity of particles of type 1 (calculated according to equation (7a))	$(W_p)_1$	4.9011×10^{-7} m/s
Settling velocity of particles of type 2	$(W_p)_2$	

(calculated according to equation (7b))		1.2253×10^{-7} m/s
Diffusivity of microorganisms	D_m	5×10^{-8} m ² /s
Diffusivity of particles of type 1	$(D_p)_1$	5×10^{-10} m ² /s
Diffusivity of particles of type 2	$(D_p)_2$	5×10^{-10} m ² /s
Gyrotaxis orientation parameter	B	5 s
Kinematic viscosity of the suspension	ν	10^{-6} m ² /s
Height of the computational domain	H	0.005 m
Width of the computational domain	L	0.005 m

Table 5-2. Values of dimensionless parameters utilized in computations

Dimensionless average swimming velocity of microorganisms	$W_m^* = W_m \frac{L}{D_m}$	10.000
Dimensionless settling velocity of particles of type 1	$(W_p^*)_1 = (W_p)_1 \frac{L}{D_m}$	4.9001
Dimensionless settling velocity of particles of type 2	$(W_p^*)_2 = (W_p)_2 \frac{L}{D_m}$	1.2253
Schmidt number	$S_c = \frac{\nu}{D_m}$	20
Gyrotaxis number	$G = \frac{BD_m}{L^2}$	10^{-2}
Rayleigh number for microorganisms	$R_m = \frac{\bar{n}_m \theta_m \Delta \rho_m g L^3}{\rho_0 \nu D_m}$	612.5
Rayleigh number for solid particles of type 1	$(R_p)_1 = \frac{\bar{n}_m (\theta_p)_1 (\Delta \rho_p)_1 g L^3}{\rho_0 \nu D_m}$	2.45
Rayleigh number for solid particles of type 2	$(R_p)_2 = \frac{\bar{n}_m (\theta_p)_2 (\Delta \rho_p)_2 g L^3}{\rho_0 \nu D_m}$	0.6125
Dimensionless diffusivity of particles of type 1	$(D_p^*)_1 = \frac{(D_p)_1}{D_m}$	0.01
Dimensionless diffusivity of particles of type 2	$(D_p^*)_2 = \frac{(D_p)_2}{D_m}$	0.01
Aspect ratio	$\lambda = \frac{H}{L}$	1

Dimensionless average concentration of particles of type 1	$(\bar{n}_p^*)_1 = \frac{(\bar{n}_p)_1}{\bar{n}_m}$	1000.0
Dimensionless average concentration of particles of type 2	$(\bar{n}_p^*)_2 = \frac{(\bar{n}_p)_2}{\bar{n}_m}$	1000.0

The aim of the computations presented in this chapter is to investigate the impact of solid particles on bioconvection as well as the effect of solid particles of type 2 on number density distribution of solid particles of type 1. Without bioconvection, solid particles would have exponential distribution across the chamber's depth with the largest number density at the bottom of the chamber. The particle number density distribution can be obtained by integrating equation (5.11) for the case when

$\mathbf{V}^* = \partial n_p^* / \partial t^* = 0$, as:

$$(n_p^*)_1(y^*) = \frac{1}{(D_p^*)_1} \frac{\exp\left(\frac{1}{(D_p^*)_1} (W_p^*)_1 (1-y^*)\right)}{\exp\left(\frac{1}{(D_p^*)_1} (W_p^*)_1\right) - 1} (\bar{n}_p^*)_1 (W_p^*)_1 \quad (5.19a)$$

$$(n_p^*)_2(y^*) = \frac{1}{(D_p^*)_2} \frac{\exp\left(\frac{1}{(D_p^*)_2} (W_p^*)_2 (1-y^*)\right)}{\exp\left(\frac{1}{(D_p^*)_2} (W_p^*)_2\right) - 1} (\bar{n}_p^*)_2 (W_p^*)_2 \quad (5.19b)$$

In computations presented in Figs. 5-2(a)-(f) and 5-3(a)-(c), particles of type 1 are characterized by the following parameters: $(\rho_p)_1 = 21 \times 10^3 \text{ kg/m}^3$, $(D_p)_1 / D_m = 0.01$, and $(\theta_p)_1 / \theta_m = 1 \times 10^{-5}$.

Particles of type 2 are characterized by the following parameters: $(\rho_p)_2 = 6 \times 10^3 \text{ kg/m}^3$, $(D_p)_2 / D_m = 0.01$, and $(\theta_p)_2 / \theta_m = 1 \times 10^{-5}$. As shown in Table 2, for all computations with particles

it is assumed that the average number density of particles of each type is one thousand times larger

than that of microorganisms: $(\bar{n}_p)_1 / \bar{n}_m = 1000$ and $(\bar{n}_p)_2 / \bar{n}_m = 1000$. The total volume fraction of the solid phase (including particles of both types and microorganisms) in the fluid is 5.1×10^{-4} , which means that the suspension is indeed dilute. Suspensions in which volume fraction of the solid phase is less than 1% can be modeled as dilute suspensions [16].

If bioconvection was neglected and diffusivity of solid particles was assumed negligible, it would take 170 minutes for a single particle of type 1 to settle from the top of the chamber to the bottom (to go the vertical distance of 0.5 cm). It would take 680 minutes for a particle of type 2 to go the same distance. From computations that are shown later on, which do account for bioconvection, one can see that it takes much shorter time for the number densities of solid particles to attain their steady-state distributions.

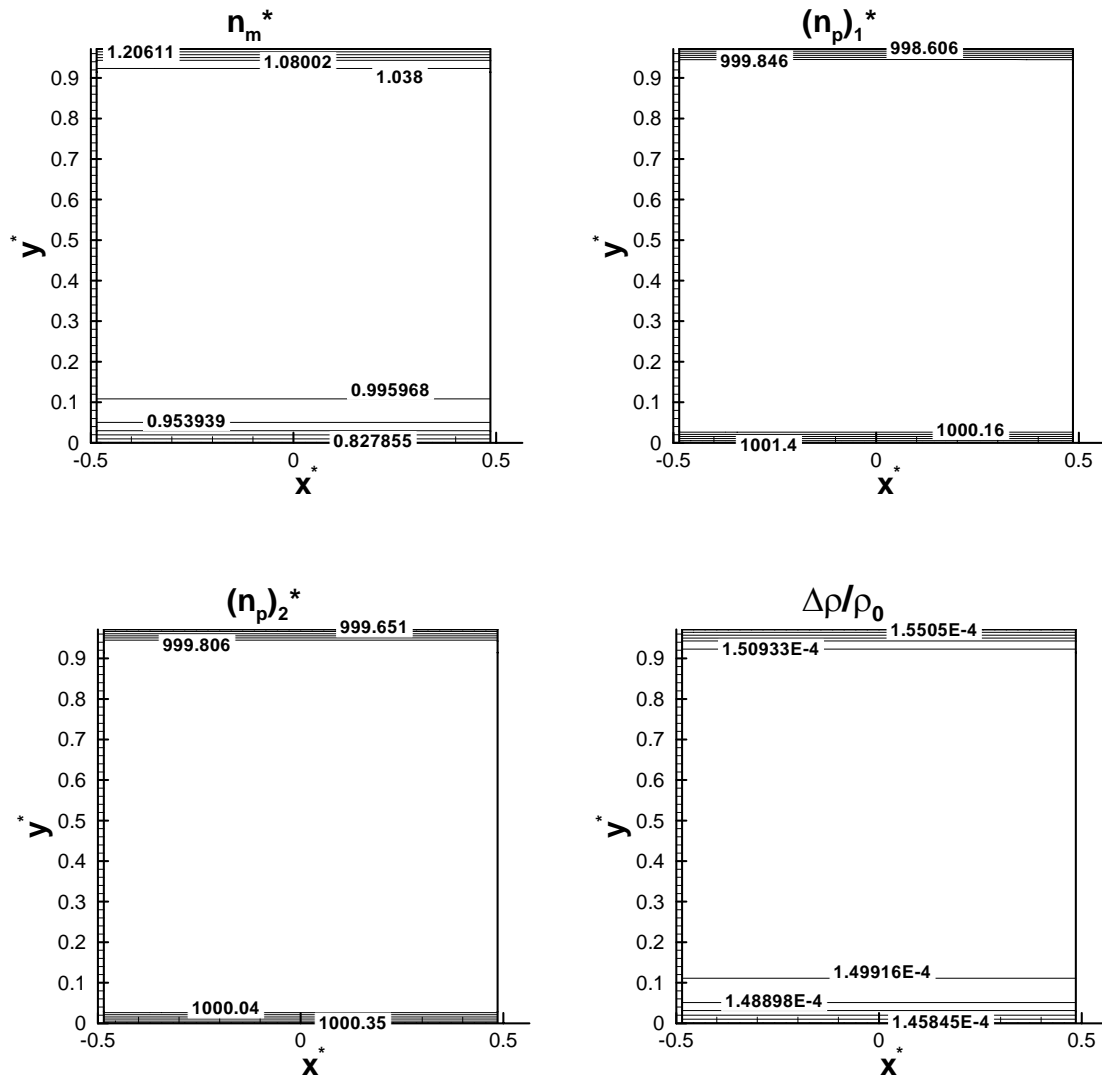
Figures 5-2(a)-(f) show the dimensionless number density of microorganisms, n_m^* , the dimensionless number density of particles of type 1, $(n_p^*)_1$, the dimensionless number density of particles of type 2, $(n_p^*)_2$, and the ratio of the difference between densities of the suspension and water to that of water, $\Delta\rho/\rho_0$, at different moments of time ($t^* = 0.001, 0.25, 0.30, 0.65, 1.2, 3.2$, respectively). $\Delta\rho/\rho_0$, which is shown in Fig. 5-2, is calculated as:

$$\frac{\Delta\rho}{\rho_0} = \frac{\rho_{suspension} - \rho_0}{\rho_0} = n_m \theta_m \frac{\Delta\rho_m}{\rho_0} + (n_p)_1 (\theta_p)_1 \frac{(\Delta\rho_p)_1}{\rho_0} + (n_p)_2 (\theta_p)_2 \frac{(\Delta\rho_p)_2}{\rho_0} \quad (5.20)$$

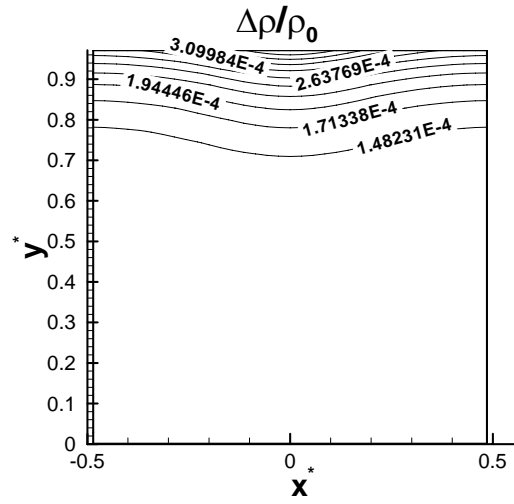
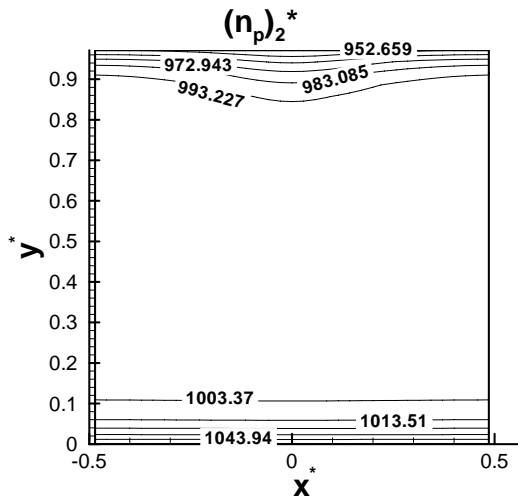
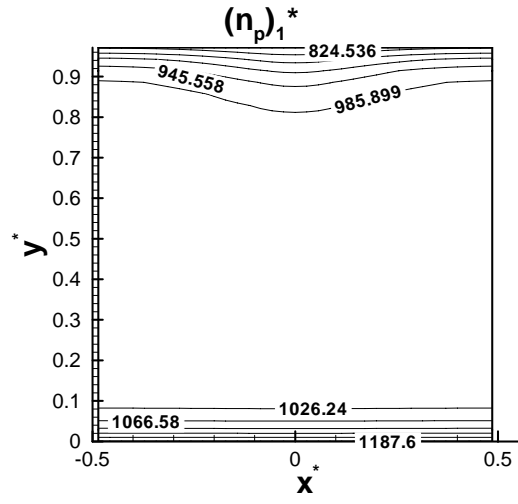
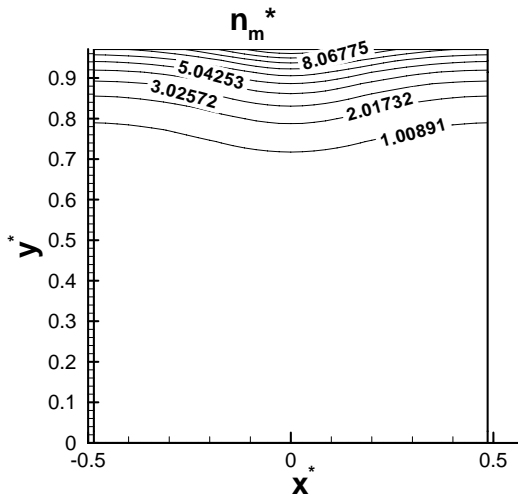
Since bioconvection is induced by unstable density stratification caused by the upswimming of microorganisms, the distribution of $\Delta\rho/\rho_0$ characterizes the driving mechanism of bioconvection. Bioconvection will proceed only as long as $\Delta\rho/\rho_0$ has a local maximum in the upper region of the chamber, which manifests unstable density stratification.

In Figs. 5-2(a)-(f), number density distributions start their development from the initial uniform distributions. Initially, there is no convection, microorganisms just swim upward and particles simply settle downward, as seen in Fig. 5-2(a). The upswimming of microorganisms results in a maximum value of $\Delta\rho/\rho_0$ occurring at the upper surface of the chamber. In Figure 5-2(b), which is computed for $t^* = 0.25$, one can see how the plume begins to develop in the upper part of the chamber. The number density of microorganisms takes on its maximum value in the center of the upper surface of the chamber, where it is not uniform any more as it was at $t^* = 0.001$ (cf. Fig. 5-2(a)). Number density distributions of solid particles are affected by bioconvection as well. The number densities of particles take on their maximum values at the bottom of the chamber; the minimum values occur at the center of the upper surface of the chamber. As seen in Fig. 5-2(c), at a later stage of plume development (at $t^* = 0.3$) microorganisms concentrate in the center of the upper part of the chamber, $\Delta\rho/\rho_0$ takes on its maximum value at the upper surface in the center of the chamber, the fluid in the center starts moving downward (because of the bouyancy force), and the bioconvection plume develops over the whole height of the chamber. The plume involves microorganisms and particles of both types in a convective motion, enhances mixing in the suspension, and makes number density distributions more uniform. The local maxima of particle number densities occur in the center of the chamber. Figure 5-2(d) shows that the number density of microorganisms has not changed much compared to what it was in Fig 5-2(c). This is because the number density of microorganisms is already close to its steady-state. Particles are getting involved in convection as they settle down. Maximum number densities of particles occur at the corners near the bottom of the chamber. Particles of type 1 exhibit larger number density at the bottom of the chamber than particles of type 2. That is because particles of type 1 have a larger density than particles of type 2; therefore, their settling velocity is larger than that of particles of type 2. The minimum concentrations of particles occur near the center of the upper surface of the chamber. Particles of type 2 have a more uniform concentration than particles of type 1. This shows that bioconvection produces a more significant mixing effect on

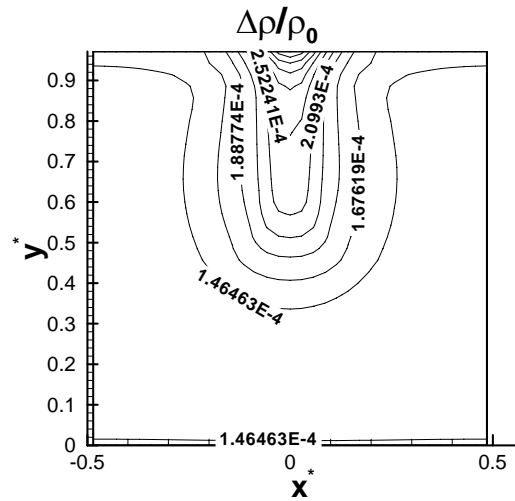
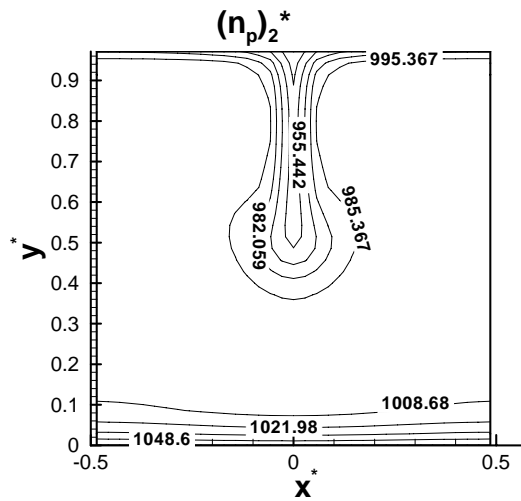
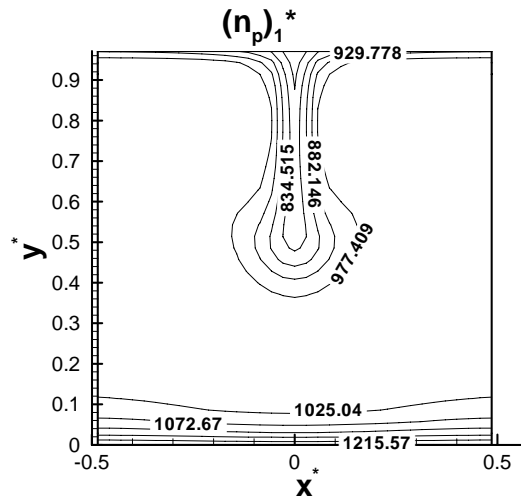
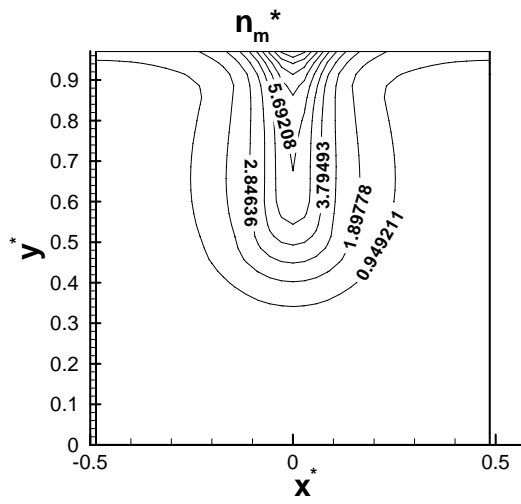
particles that have smaller settling velocity. As particles are settling down, more particles concentrate in the lower part of the chamber. This can be seen in Figs. 5-2(e)-(f). From analyzing Figs. 5-2(e) and 5-2(f), one can conclude that the maximum difference in particle number densities between corresponding points is less than 10^{-4} . Therefore, it is reasonable to say that Fig. 5-2(f) shows the steady-state of the process. At steady-state, the global maximum of $\Delta\rho/\rho_0$ gets shifted to the bottom of the chamber. However, a local maximum of $\Delta\rho/\rho_0$ at the upper boundary remains, and this drives bioconvection.



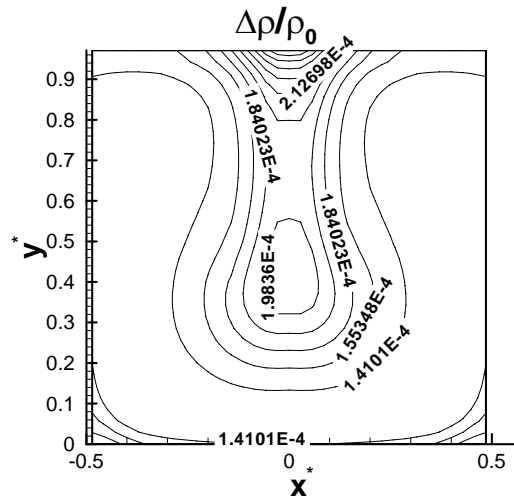
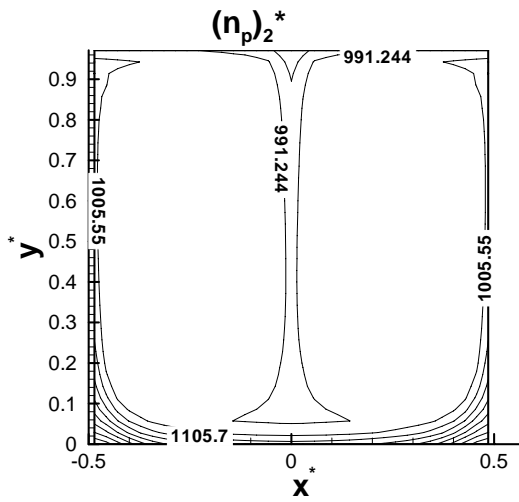
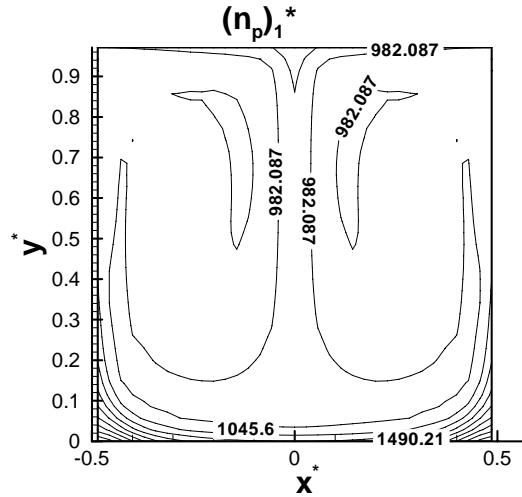
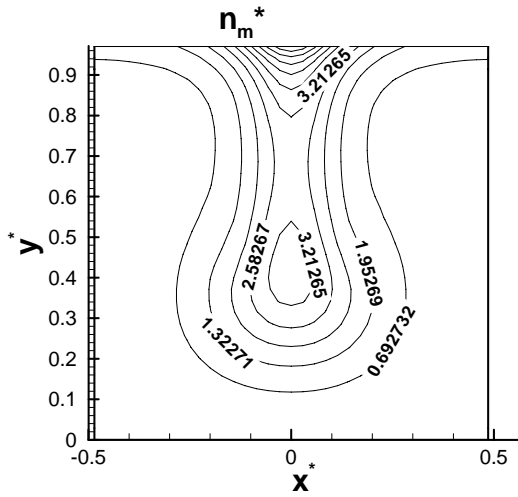
(a) $t^* = 0.001$



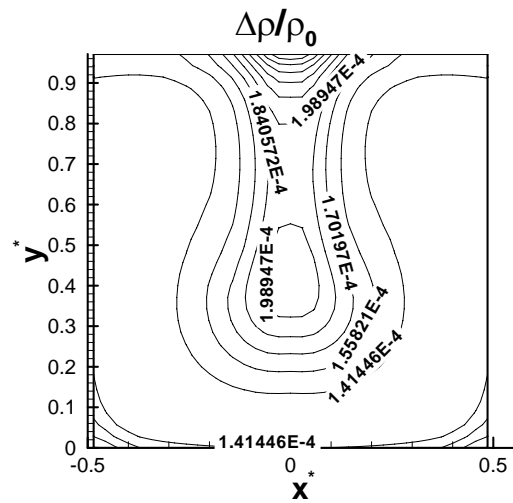
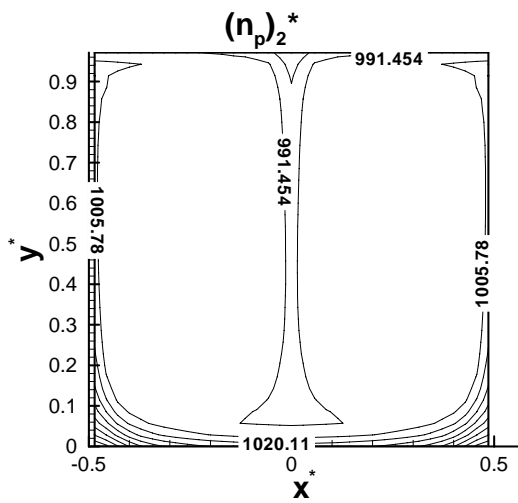
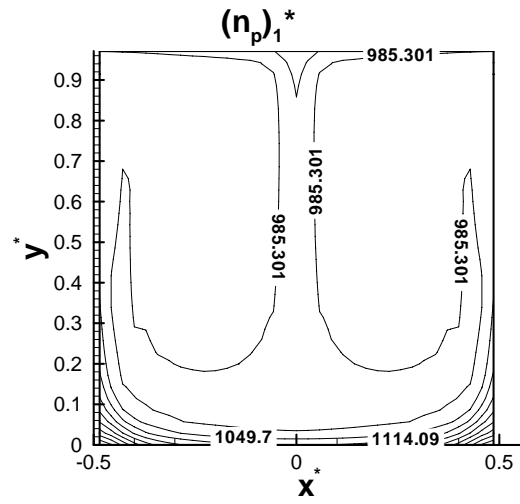
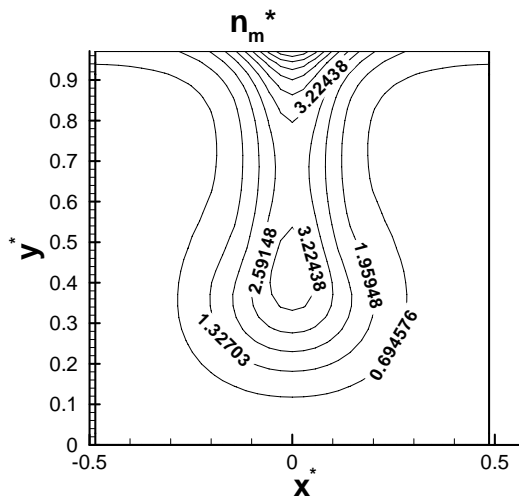
(b) $t^* = 0.25$



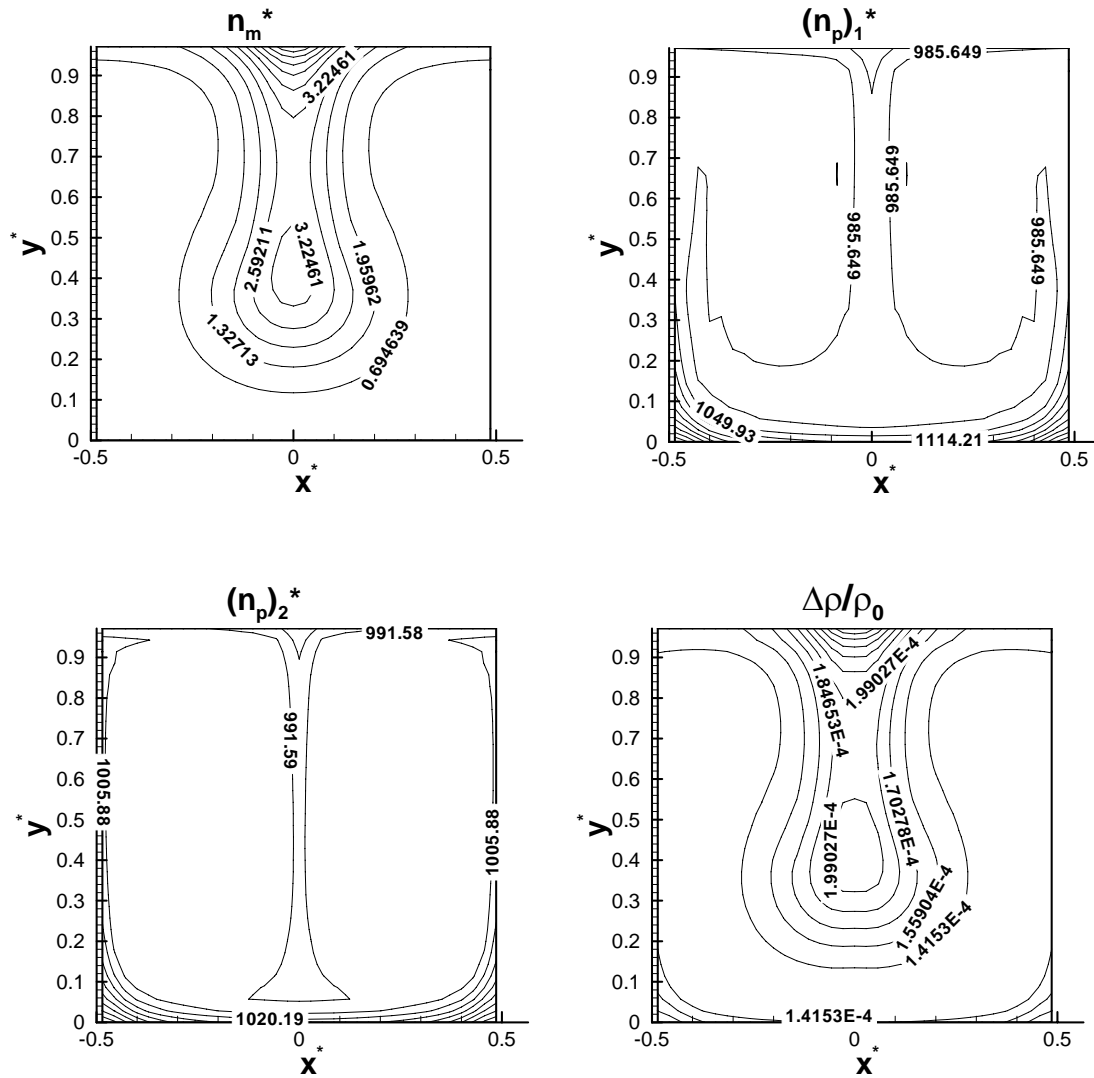
(c) $t^* = 0.30$



(d) $t^* = 0.65$



(e) $t^* = 1.2$



(f) $t^* = 3.2$

Figure 5-2. Distributions of the dimensionless number densities of microorganisms, (n_m^*) , particles of type 1, $((n_p)_1^*)$, particles of type 2, $((n_p)_2^*)$, and the ratio of the difference between densities of the suspension and water to that of water, $(\Delta\rho/\rho_0)$, at different moments of time: (a) $t^* = 0.001$, (b) $t^* = 0.25$, (c) $t^* = 0.30$, (d) $t^* = 0.65$, (e) $t^* = 1.2$, (f) $t^* = 3.2$

One of the aims of this chapter is to investigate whether bioconvection helps to make the number density distribution of solid particles more uniform. To evaluate how far or close the number density distribution is from the uniform one, a parameter called *nonuniformity* is introduced. This is a dimensionless parameter that characterizes how far a number density distribution is from the uniform

one. Nonuniformities of number density distributions of microorganisms, solid particles of type 1, and solid particles of type 2, respectively, are defined as follows:

$$\Delta(\bar{n}_m^*) = \left\{ \frac{1}{A \bar{n}_m^*} \int_A [n_m^*(x, y) - \bar{n}_m^*]^2 dA \right\}^{1/2} \quad (5.21a)$$

$$\Delta(\bar{n}_p^*)_1 = \left\{ \frac{1}{A (\bar{n}_p^*)_1} \int_A [(n_p^*)_1(x, y) - (\bar{n}_p^*)_1]^2 dA \right\}^{1/2} \quad (5.21b)$$

$$\Delta(\bar{n}_p^*)_2 = \left\{ \frac{1}{A (\bar{n}_p^*)_2} \int_A [(n_p^*)_2(x, y) - (\bar{n}_p^*)_2]^2 dA \right\}^{1/2} \quad (5.21c)$$

where A is the dimensionless area of the chamber. The nonuniformity parameters defined by Eqs. (5.21a-c) make it possible to measure the distance between the number density distribution of (for example) particles of type 1 that occurs at a certain moment of time and the uniform distribution of these particles that occurs at $t = 0$. (The reader will note that the definition of nonuniformity given by Eqs. (5.21a-c) is equivalent to the distance between functions in the L^2 -space.)

Figures 5-3(a)-(c) display nonuniformity versus time for the cases when the suspension includes solid particles only (no microorganisms), solid particles of one type and microorganisms (the two monodispersed cases), and solid particles of both types and microorganisms (the bidispersed case). Figure 5-3(a) displays the nonuniformity of number density distribution of microorganisms versus time. Figure 5-3(b) shows the nonuniformity of number density distribution of particles of type 1 versus time. Figure 5-3(c) displays the nonuniformity of number density distribution of particles of type 2 versus time. Figure 5-3(a1) shows that the nonuniformity of number density distribution of microorganisms for the case of a bidispersed suspension is slightly larger than that for the two cases with monodispersed particles (of types 1 and 2, respectively). To show the behavior of the

nonuniformity of microorganisms for $t^* > 0.2$ more clearly, Fig. 5-3(a2) displays the same curves that have already been shown in Fig. 5-3(a1) using a larger scale for both vertical and horizontal axes. The difference between the monodispersed and bidispersed cases is explained as follows. It occurs because increasing the number of particles in the suspension makes density stratification more stable (heavy particles concentrate at the bottom of the chamber), thus decreasing the intensity of bioconvection. The number density distribution of microorganisms is more non-uniform for the case of a bidispersed suspension of solid particles (there are twice more particles, and, therefore, bioconvection is weaker). It is also interesting that oscillations of nonuniformity are observed in Fig. 5-2(a2), which indicates that the steady-state of the plume is approached in an oscillatory manner rather than monotonically.

A dramatic change in the nonuniformity of number density distribution of particles of type 1 between the case that does not have microorganisms in the suspension and the two cases that do have microorganisms in the suspension is displayed in Fig. 5-3(b1). The nonuniformity of number density distribution of particles of type 1 is much smaller if microorganisms are present in the suspension. With bioconvection, the particles need a much shorter time to attain the steady-state distribution compared to the case with no bioconvection. Figures 5-3(b1) and (c) show that at $t^* = 3.2$ the number densities of particles of types 1 and 2 for the cases without microorganisms are still far from their steady-states. However, for the cases with microorganisms, particles are mixed more efficiently and attain their steady-state distributions much faster. Furthermore, the number density of solid particles of type 1 is more non-uniform if solid particles of type 2 are introduced in the suspension. To see the difference between the monodispersed and the bidispersed cases more clearly, Fig. 5-3(b2) shows the same curves that are displayed in Fig. 5-3(b1) using a larger scale for the vertical axis. Figure 5-3(c) shows that the nonuniformity of number density distribution of particles of type 1, for the case of the suspension that does not contain microorganisms, is larger than for the two other cases that do contain microorganisms in the suspension. This figure also shows that the nonuniformity of the number

density distribution of particles of type 2 in a bidispersed suspension is higher than that in a monodispersed suspension of particles of type 2 only. The difference is larger than that in Figs. 5-3(b1) and (b2), meaning that *microorganisms* have a more profound effect on the number density distribution of particles that have smaller settling velocity (particles of type 2) than on particles that have larger settling velocity (particles of type 1). It is also seen that *solid particles* with a larger density (particles of type 1) have a more profound effect on the number density distribution of particles with a smaller density (particles of type 2).

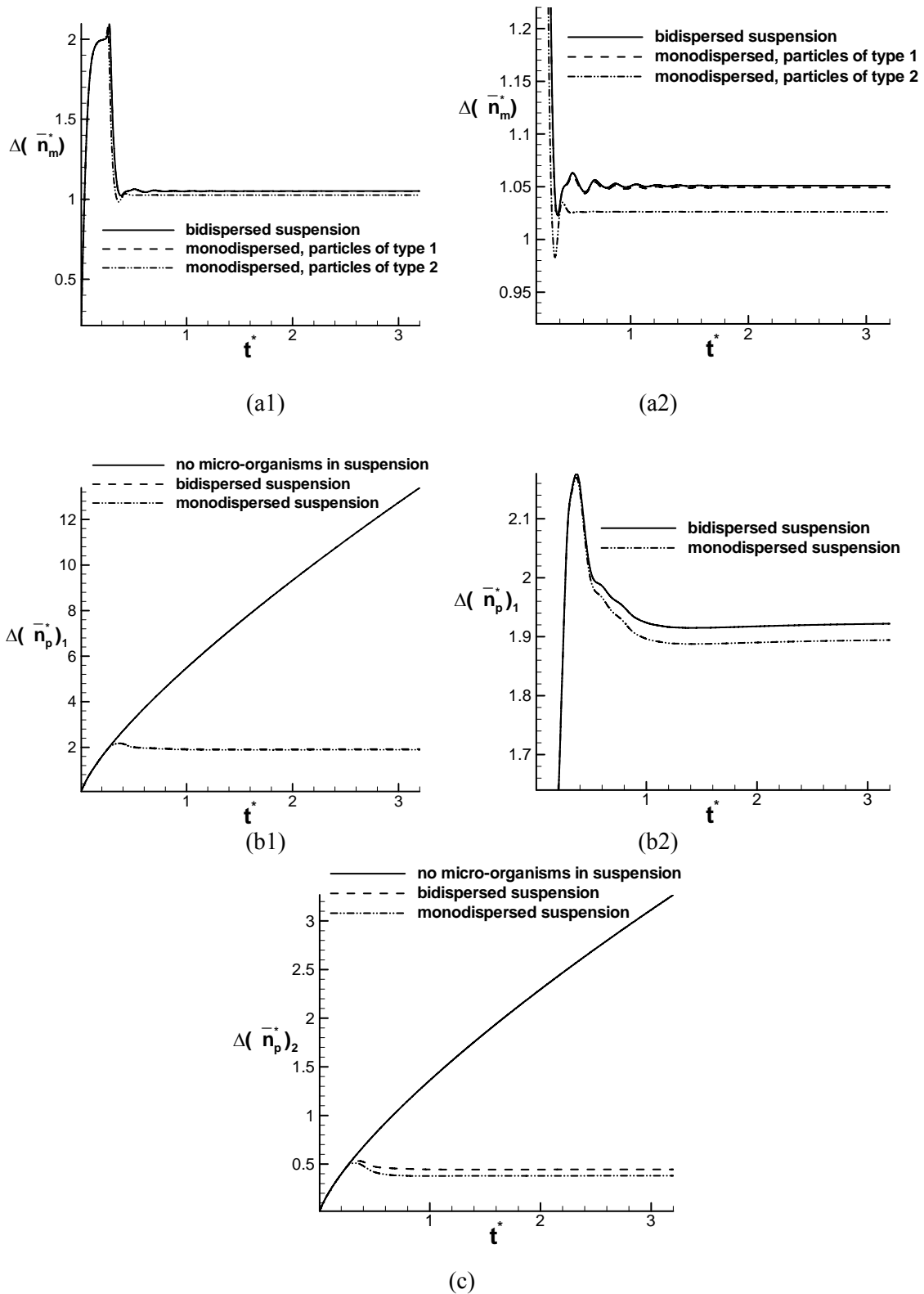


Figure 5-3. Nonuniformities of number density distributions of microorganisms ((a1) and (a2)), particles of type 1 ((b1) and (b2)), and particles of type 2 (c)

5.4 CONCLUSIONS

The introduction of the second type of small solid particles (that have a different density than particles of the first type) into the suspension that already contains microorganisms and particles of the first type does not have much influence on the number density distribution of microorganisms. However, the number density distribution of particles of the first type becomes more non-uniform. This suggests a useful method of adjusting the number density distribution of particles in bioconvection by introducing particles of a different density. It is interesting that this does not significantly impact bioconvection. Furthermore, bioconvection is more efficient in mixing solid particles which have smaller settling velocity. With bioconvection, number densities of particles attain their steady-state distributions much faster than without bioconvection. Further experimental research is needed to confirm the numerical predictions of this chapter.

ACKNOWLEDGEMENTS

AVK gratefully acknowledges the grant # NAG3-2706 awarded to him by NASA Office of Biological and Physical Research, Physical Sciences Division.

REFERENCES

- 1 T.J. Pedley, N.A. Hill, J.O. Kessler, The growth of bioconvection patterns in a uniform suspension of gyrotactic microorganisms, *J. Fluid Mech.* 195 (1988) 223-338.
- 2 S. Ghorai, N.A. Hill, Development and stability of gyrotactic plumes in bioconvection, *J. Fluid Mech.* 400 (1999) 1-31.
- 3 T.J. Pedley, J.O. Kessler, The orientation of spheroidal microorganisms swimming in a flow field, *Proc. R. Soc. Lond.* B231 (1987) 47-70.
- 4 T.J. Pedley, J.O. Kessler, A New Continuum Model for Suspensions of Gyrotactic Microorganisms, *Journal of Fluid Mechanics* 212 (1990) 155-182.
- 5 T.J. Pedley, J.O. Kessler, Hydrodynamic phenomena in suspensions of swimming microorganisms, *Ann. Rev. Fluid Mech.* 24 (1992) 313-358.

- 6 S. Ghorai, N.A. Hill, Periodic arrays of gyrotactic plumes in bioconvection, *Physics of Fluids* 12 (2000) 5-22.
- 7 J.O. Kessler, Hydrodynamic focusing of motile algal cells, *Nature* 313 (1985) 218-220.
- 8 J.O. Kessler, Co-operative and concentrative phenomena of swimming microorganisms, *Contemp. Phys.* 26 (1985) 147-166.
- 9 J.O. Kessler, G.D. Burnett, K.E. Remick, Mutual dynamics of swimming microorganisms and their fluid habitat, in: P.L. Christiansen, M.P. Sorensen, and A.C. Scott (Eds.), *Nonlinear Science at the Dawn of the 21st Century*, Springer, New York, 2000, pp. 409-426.
- 10 J.O. Kessler, D.A. Wiseley, K.E. Remick, D.E. Marthaler, Individual and collective dynamics of swimming bacteria, in: M. Schreckenberg and D.E. Wolf (Eds.), *Proceedings of the Workshop "Traffic and Granular Flow'97"*, Springer, New York, 1997, pp. 37-51.
- 11 P. Geng and A.V. Kuznetsov, Effect of Small Solid Particles on the Development of Bioconvection Plumes, *International Communications in Heat and Mass Transfer*, vol. 31, No. 5, pp. 629-639, 2004
- 12 R.H. Weiland, R.R. McPherson, Accelerating settling by addition of buoyant particles, *Ind. Engr. Chem. Fundls.* (1979) 18, 45-49.
- 13 Y.P. Fessas, R.H. Weiland, The settling of suspensions promoted by rigid buoyant particles, *International Journal of Multiphase Flow* (1984) 10 485-507.
- 14 G.K. Batchelor, Sedimentation in a dilute polydisperse system of interacting spheres. Part 1. General theory, *J. Fluid Mech.* 119 (1982) 379-408.
- 15 A. Acrivos, G.K. Batchelor, E.J. Hinch, D.L. Koch, R. Mauri, Longitudinal shear-induced diffusion of spheres in a dilute suspension, *J. Fluid Mech.* 240 (1992) 651-657.
- 16 Martin Rhodes, Pneumatic transport of powders, *Educational Resources for Particles Technology* (2001) 2, No. 2, Article # 1.

6. INTRODUCING THE CONCEPT OF EFFECTIVE DIFFUSIVITY TO EVALUATE THE EFFECT OF BIOCONVECTION ON SMALL SOLID PARTICLES

ABSTRACT

The effect of bioconvection to enhance mixing of small solid particles is evaluated by introducing a new parameter called the *effective diffusivity* of solid particles. The effective diffusivity is computed by matching (at steady state) the nonuniformities of number density distributions of small solid particles computed with and without bioconvection. Applications of bioconvection to enhance mixing of small solid particles may include microfluidic applications relevant to biotechnology and medicine, such as the analysis of blood samples when only limited volumes of blood can be extracted. Other applications including analyses of DNA or drugs, screening of patients, and combinatorial synthesis are very interesting as well. This chapter considers monodispersed and bidispersed suspensions of small particles in a fluid that contains motile gyrotactic microorganisms. The particles are assumed to be sufficiently small so that their Brownian diffusion is not negligible. It is shown that the *effective diffusivity* is a good parameter to evaluate the mixing effect of bioconvection.

NOMENCLATURE

a	radius of a microorganism, m
A	area of a vertical cross-section of the chamber, m^2
B	time scale for the reorientation of microorganisms by the gravitational torque against viscous torque, $4\pi\mu a^3 / (mgh)$, s
D_m	diffusivity of microorganisms, m^2/s
$(D_p)_i$	diffusivity of solid particles of type i due to Brownian diffusion and interactions with microorganisms, m^2/s
$(D_p^*)_i$	ratio of the diffusivity of solid particles of type i to that of microorganisms, $(D_p)_i / D_m$
$(D_p^*)_i'$	dimensionless effective diffusivity of particles of type i
\mathbf{g}	gravity vector, 9.81 m/s^2
G	gyrotaxis number, BD_m / L^2
h	displacement of the center of mass of a gyrotactic micro-organism from its center of buoyancy, m
H	height of the chamber, m
\mathbf{J}_m^*	dimensionless flux of microorganisms, defined in equation (6.17a)
$(\mathbf{J}_p^*)_i$	dimensionless flux of solid particles of type i , defined in equation (6.17b)
L	width of the chamber, m
n_m	number density of microorganisms, $1/m^3$
\bar{n}_m	average number density of microorganisms, $1/m^3$
n_m^*	dimensionless number density of microorganisms, n_m / \bar{n}_m

$(n_p)_i$	number density of solid particles of type i , $1/m^3$
$(\bar{n}_p)_i$	average number density of solid particles of type i , $1/m^3$
$(n_p^*)_i$	dimensionless number density of solid particles of type i , $(n_p)_i / \bar{n}_m$
$(\bar{n}_p^*)_i$	ratio of the average number density of particles of type i to that of microorganisms, $(\bar{n}_p)_i / \bar{n}_m$
$(n_p^*)_i$	dimensionless number density of solid particles of type i in the suspension without microorganisms
$\hat{\mathbf{p}}$	unit vector indicating the direction of swimming of gyrotactic microorganisms
p_e	excess pressure (above hydrostatic), Pa
R_m	Rayleigh number for microorganisms, $\bar{n}_m \theta_m \Delta \rho_m g L^3 / (\rho_0 \nu D_m)$
$(R_p)_i$	Rayleigh number for solid particles of type i , $\bar{n}_m (\theta_p)_i (\Delta \rho_p)_i g L^3 / (\rho_0 \nu D_m)$
S_c	Schmidt number, ν / D_m
t	time, s
t^*	dimensionless time, $D_m t / L^2$
u	horizontal velocity component, m/s
v	vertical velocity component, m/s
\mathbf{V}	velocity vector, m/s
\mathbf{V}^*	dimensionless velocity vector, $\mathbf{V} L / D_m$
W_m	average swimming velocity of microorganisms (assumed to be constant), m/s
W_m^*	dimensionless average swimming velocity of microorganisms, $W_m L / D_m$
$(W_p)_i$	settling velocity of particles of type i , m/s
$(W_p^*)_i$	dimensionless settling velocity of particles of type i , $(W_p)_i L / D_p$

x	horizontal coordinate, m
x^*	dimensionless horizontal coordinate, x/L
\hat{x}	unit vector in the x -direction
y	vertical coordinate, m
y^*	dimensionless vertical coordinate, y/L
\hat{y}	unit vector in the y -direction

Greek symbols

$\Delta(\bar{n}_m^*)$	nonuniformity of the number density distribution of microorganisms, defined in Eq. (6.19a)
$\Delta(\bar{n}_p)_i^*$	nonuniformity of the number density distribution of particles of type i , defined in Eq. (6.19b)
$\Delta(\bar{n}'_p)_i^*$	nonuniformity of the number density distribution of particles of type i in a suspension without microorganisms
$\Delta\rho$	density difference between the suspension and pure water, $\rho_{suspension} - \rho_0$, kg/m ³
$\Delta\rho_m$	density difference between microorganisms and water, $\rho_m - \rho_0$, kg/m ³
$(\Delta\rho_p)_i$	density difference between solid particles of type i and water, $(\rho_p)_i - \rho_0$, kg/m ³
ζ	horizontal component of vorticity, 1/s
ζ^*	dimensionless horizontal component of vorticity, $\zeta L^2 / D_m$
θ_m	volume of a microorganism, m ³
$(\theta_p)_i$	volume of a particle of type i , m ³
λ	aspect ratio of the chamber, H/L
μ	dynamic viscosity, assumed to be approximately the same as that of water, kg/(m s)

ν	kinematics viscosity, assumed to be approximately the same as that of water, m^2/s
$\rho_{suspension}$	density of the suspension, kg/m^3
ρ_0	density of water, kg/m^3
ρ_m	density of microorganisms, kg/m^3
$(\rho_p)_i$	density of solid particles of type i , kg/m^3
ψ	stream function, m^2/s
ψ^*	dimensionless stream function, ψ / D_m

6.1 INTRODUCTION

Biotechnology is increasingly involved with large numbers of experiments, which often require handling microvolumes of fluids. Utilizing bioconvection to enhance mixing of small solid particles may be very useful in pharmaceutical and bio-technological applications. A typical study volume in this chapter is $10^{-9} m^3$ while $10^{-8} m^3$ is the minimum volume for most conventional biochemistry microvolume analyzers (Kashiwagi and Sakoda, 2001).

The term bioconvection is used to describe the phenomenon of the spontaneous pattern formation in suspensions of living microorganisms. Due to the microscopic size of the organisms involved in bioconvection (a typical cell volume is $10^{-16} m^3$), bioconvective flows would seem an ideal and novel design for microfluidic mixing. Many significant results in bioconvection, such as Pedley et al. (1988), Ghorai and Hill (1999), and Pedley and Kessler (1987, 1990, 1992), were obtained over the last two decades. However, using bioconvection to enhance mixing of small solid particles has not yet been studied in sufficient detail.

Motile microorganisms may swim in a particular direction due to different stimuli such as phototaxis, chemotaxis, and gyrotaxis. This chapter considers gyrotactic microorganisms. Gyrotaxis is the behavior typical for algae, whose swimming direction is determined by the balance of gravitational and viscous torques. Gyrotactic behavior results in the accumulation of the algae in the regions of most rapid downflow. Because the algae are 3-5% more dense than water, the density of regions of downflow becomes larger than that of regions of upflow. Buoyancy increases velocities in both upflow and downflow regions, thus velocity fluctuations are enhanced and a macroscopic convective fluid motion is induced (Pedley et al., 1988; Ghorai and Hill, 1999, 2000). This macroscopic convection fluid motion causes the development of bioconvection plumes. Numerous experimental papers (Kessler, 1985a, 1985b; Kessler et al., 1997, 2000) have described the formation of gyrotactic plumes with regular patterns in algal suspensions.

Kuznetsov and Geng (2003) investigated the settling of *monodispersed* (all particles have the same size and density) small solid particles in a suspension of motile gyrotactic microorganisms. It was found that the mixing induced by bioconvection leads to a more uniform number density distribution of solid particles along the height of the chamber. Geng and Kuznetsov (2003) studied the setting of *bidispersed* (the suspension includes two different particle types of different sizes and densities) small solid particles in a suspension of microorganisms as well as the effect of particle density ratio. Neither of the above two studies considered a method to quantify the effect that bioconvection has on making the distribution of solid particles more uniform.

This chapter introduces a new parameter, the *effective diffusivity*, and uses it to evaluate the effect of bioconvection to enhance mixing of both monodispersed and bidispersed suspensions of small solid particles. A higher effective diffusivity compared to the real diffusivity of solid particles shows that bioconvection has a profound effect on mixing.

Here *effective diffusivity* is calculated from the evolution of number density distributions of microorganisms (n_m) and number density distributions of small particles of types i ($(n_p)_i$) in a dilute suspension. The bioconvection plume formations are assumed to occur periodically and it is assumed that the distance between consecutive plumes is L . To model the mixing a two-dimensional chamber of height H and width L (to represent the distance between plumes) is utilized. The side walls of the chamber are assumed to be shear-free in order to model the plumes' assumed periodic condition.

The computational domain and boundary conditions are shown schematically in Fig. 1. The width of the domain is L (the coordinate x varies from $-L/2$ to $L/2$) and the height of the domain is H (the coordinate y varies from 0 to H). Initially the microorganisms and particles are uniformly distributed in the chamber and the fluid is motionless. The free surface is assumed to be stress-free and the bottom wall is rigid (a hydrodynamic no-slip condition is imposed there). The side walls are stress-

free to model the periodic condition, as discussed above. No flux of microorganisms or particles is allowed through any of the chamber's boundaries.

6.2 GOVERNING EQUATIONS

6.2.1 Dimensional Governing Equations

To account for the buoyancy force induced by the solid particles governing equations are derived by modifying the governing equations that are given in Ghorai and Hill (1999, 2000). Inertia terms in these equations are neglected because the Reynolds number is much smaller than unity:

x and y- momentum equations:

$$\rho_0 \frac{\partial u}{\partial t} = -\frac{\partial p_e}{\partial x} + \mu \left(\frac{\partial^2 u}{\partial x^2} + \frac{\partial^2 u}{\partial y^2} \right) \quad (6.1)$$

$$\rho_0 \frac{\partial v}{\partial t} = -\frac{\partial p_e}{\partial y} + \mu \left(\frac{\partial^2 v}{\partial x^2} + \frac{\partial^2 v}{\partial y^2} \right) - n_m \theta_m \Delta \rho_m g - \sum_i (n_p)_i (\theta_p)_i (\Delta \rho_p)_i g \quad (6.2)$$

where the subscript i denotes the particle type. In this chapter, particle types are marked as 1, 2, 3, 4, 5, and 6. In monodispersed cases there is only one component in the summation. In bidispersed cases there are two particle types in the summation depending on which two are present, such as 1 and 4, or 2 and 4, etc.

Continuity equation:

$$\frac{\partial u}{\partial x} + \frac{\partial v}{\partial y} = 0 \quad (6.3)$$

Conservation of motile microorganisms:

$$\frac{\partial (n_m)}{\partial t} = -\text{div}(n_m \mathbf{V} + n_m W_m \hat{\mathbf{p}} - D_m \nabla n_m) \quad (6.4)$$

Conservation of solid particles of type i :

$$\frac{\partial (n_p)_i}{\partial t} = -\text{div} \left((n_p)_i \mathbf{V} + (n_p)_i (W_p)_i \frac{\mathbf{g}}{|\mathbf{g}|} - (D_p)_i \nabla (n_p)_i \right) \quad (6.5)$$

where D_m is the diffusivity of microorganisms (this assumes that all random motions of microorganisms can be approximated by a diffusive process); $(D_p)_i$ is the diffusivity of particles of type i (all $(D_p)_i$ are smaller than D_m , but still not zero; the diffusivity of particles results from the Brownian motion and interactions with microorganisms); n_m is the number density of motile microorganisms; $(n_p)_i$ is the number densities of particles of type i ; p_e is the excess pressure (above hydrostatic); $\hat{\mathbf{p}}$ is the unit vector indicating the direction of swimming of microorganisms (equations for this vector are given in Pedley et al., 1988); t is the time; u and v are the x and y -velocity components, respectively; \mathbf{V} is the velocity vector, (u, v) ; $W_m \hat{\mathbf{p}}$ is the vector of microorganisms' average swimming velocity (W_m is assumed to be constant); $(W_p)_i \frac{\mathbf{g}}{|\mathbf{g}|}$ is the vector of settling velocity (relative to the fluid) of particles of type i (for all particles types, $(W_p)_i \frac{\mathbf{g}}{|\mathbf{g}|}$ is assumed to be constant, particles settle straight downward); x and y are the Cartesian coordinates (x is the horizontal coordinate and y is the vertical coordinate); $\Delta \rho_m$ is the density difference between microorganisms and water, $\rho_m - \rho_0$; $(\Delta \rho_p)_i$ are the density difference between particles of type i and water, $(\rho_p)_i - \rho_0$; θ_m is the volume of a micro-organism; $(\theta_p)_i$ is the volume of a particle of type i ; μ is the dynamic viscosity of the suspension, assumed to be approximately the same as that of water since the suspension is dilute; and ρ_0 is the density of water.

According to the Stokes law (Batchelor, 1982), the settling velocity of spherical particles can be found as:

$$(W_p)_i = \frac{(\theta_p)_i (\Delta \rho_p)_i g}{6\pi\mu \left(\frac{3}{4} \frac{(\theta_p)_i}{\pi} \right)^{1/3}} \quad (6.7)$$

6.2.2 Dimensionless Governing Equations

Utilizing the stream function-vorticity formulation, the governing equations can be recast in the dimensionless form as follows:

$$\zeta^* = -\nabla^2 \psi^* \quad (6.8)$$

$$S_c^{-1} \left(\frac{\partial \zeta^*}{\partial t^*} + u^* \frac{\partial \zeta^*}{\partial x^*} + v^* \frac{\partial \zeta^*}{\partial y^*} \right) = \nabla^2 \zeta^* - \left(R_m \frac{\partial n_m^*}{\partial x^*} + (R_p)_1 \frac{\partial (n_p^*)_1}{\partial x^*} + (R_p)_2 \frac{\partial (n_p^*)_2}{\partial x^*} \right) \quad (6.9)$$

$$\frac{\partial n_m^*}{\partial t^*} = -\nabla \cdot [n_m^* (\mathbf{V}^* + W_m^* \hat{\mathbf{p}})] - \nabla n_m^* \quad (6.10)$$

$$\frac{\partial (n_p^*)_i}{\partial t^*} = -\nabla \cdot \left[(n_p^*)_i \left(\mathbf{V}^* + (W_p^*)_i \frac{\mathbf{g}}{|\mathbf{g}|} \right) - (D_p^*)_i \nabla (n_p^*)_i \right] \quad (6.11)$$

Ghorai and Hill (1999, 2000) have shown that the vector $\hat{\mathbf{p}}$, which determines the swimming direction of microorganisms, can be computed as:

$$\hat{\mathbf{p}} = \begin{cases} \left(-\kappa - (\kappa^2 - 1)^{1/2}, 0 \right), & \kappa < -1 \\ \left(-\kappa, (1 - \kappa^2)^{1/2} \right), & |\kappa| \leq 1 \\ \left(-\kappa + (\kappa^2 - 1)^{1/2}, 0 \right), & \kappa > 1 \end{cases} \quad (6.12)$$

where $\kappa = B\zeta = G\zeta^*$. The parameter B is called the “gyrotactic orientation parameter.” It is defined in Pedley and Kessler (1987) as:

$$B = \frac{4\pi\mu a^3}{mgh} \quad (6.13)$$

where h is the displacement of the center of mass of a gyrotactic microorganism from its center of buoyancy, m is the mass of the microorganism, and a is the radius of a microorganism.

The dimensionless variables in equations (6.8)-(6.11) are defined as:

$$\begin{aligned} x^* &= \frac{x}{L}; \quad y^* = \frac{y}{L}; \quad t^* = \frac{D_m}{L^2}t; \quad u^* = \frac{\partial \psi^*}{\partial y^*}; \quad v^* = -\frac{\partial \psi^*}{\partial x^*}; \quad \mathbf{V}^* = \mathbf{V} \frac{L}{D_m}; \\ W_m^* &= W_m \frac{L}{D_m}; \quad (W_p^*)_i = (W_p)_i \frac{L}{D_m}; \quad n_m^* = \frac{n_m}{\bar{n}_m}; \quad (n_p^*)_i = \frac{(n_p)_i}{\bar{n}_m}; \quad S_c = \frac{v}{D_m}; \quad G = \frac{BD_m}{L^2}; \\ R_m &= \frac{\bar{n}_m \theta_m \Delta \rho_m g L^3}{\rho_0 \nu D_m}; \quad (R_p)_i = \frac{\bar{n}_m (\theta_p)_i (\Delta \rho_p)_i g L^3}{\rho_0 \nu D_m}; \quad (D_p^*)_i = \frac{(D_p)_i}{D_m} \end{aligned} \quad (6.14)$$

6.2.3 Initial and Boundary Conditions

Equations (6.8)-(6.11) must be solved subject to the following boundary conditions. The no-slip boundary condition is applied at the bottom wall. The top boundary and the side walls are assumed to be impermeable to the fluid and stress-free. Under these assumptions the boundary conditions can be presented as:

$$\psi^* = 0 \text{ at } y^* = 0, \lambda \text{ and } x^* = \pm 0.5, \quad (6.15a)$$

where λ is the aspect ratio of the chamber, H/L ,

$$\frac{\partial \psi^*}{\partial y^*} = 0 \text{ at } y^* = 0, \quad (6.15b)$$

$$\frac{\partial^2 \psi^*}{\partial y^{*2}} = 0 \text{ at } y^* = \lambda, \text{ and } \frac{\partial^2 \psi^*}{\partial x^{*2}} = 0 \text{ at } x^* = \pm 0.5. \quad (6.15c)$$

Normal fluxes of microorganisms and solid particles are zero through all boundaries of the chamber:

$$\mathbf{J}_m^* \cdot \hat{\mathbf{y}} = 0 \text{ and } (\mathbf{J}_p^*)_i \cdot \hat{\mathbf{y}} = 0 \text{ at } y^* = 0, \lambda \quad (6.16a)$$

$$\mathbf{J}_m^* \cdot \hat{\mathbf{x}} = 0 \text{ and } (\mathbf{J}_p^*)_i \cdot \hat{\mathbf{x}} = 0 \text{ at } x^* = \pm 0.5, \quad (6.16b)$$

where $\hat{\mathbf{x}}$ and $\hat{\mathbf{y}}$ are the unit vectors in the x - and y -directions, respectively,

$$\mathbf{J}_m^* = n_m^* (\mathbf{V}^* + W_m^* \hat{\mathbf{p}}) - \nabla n_m^* \quad (6.17a)$$

is the dimensionless flux of microorganisms,

$$(\mathbf{J}_p^*)_i = (n_p^*)_i \left(\mathbf{V}^* + (W_p^*)_i \frac{\mathbf{g}}{|\mathbf{g}|} \right) - (D_p^*)_i \nabla (n_p^*)_i \quad (6.17b)$$

is the dimensionless flux of solid particles of type i .

Initially, at $t^* = 0$, the fluid is assumed motionless and the number density distributions of microorganisms and solid particles are assumed uniform. As in Ghorai and Hill (1999, 2000), small perturbations to these uniform distributions are used to ensure that the plume forms in the middle of the computational domain:

$$\psi^* = 0, \zeta^* = 0, n_m^* = 1 + \varepsilon \cos(m \pi x^*), (n_p^*)_i = \frac{(\bar{n}_p)_i}{\bar{n}_m} + \varepsilon \cos(m \pi x^*) \quad (6.18)$$

where $\varepsilon = 10^{-5}$ and $m = 2$.

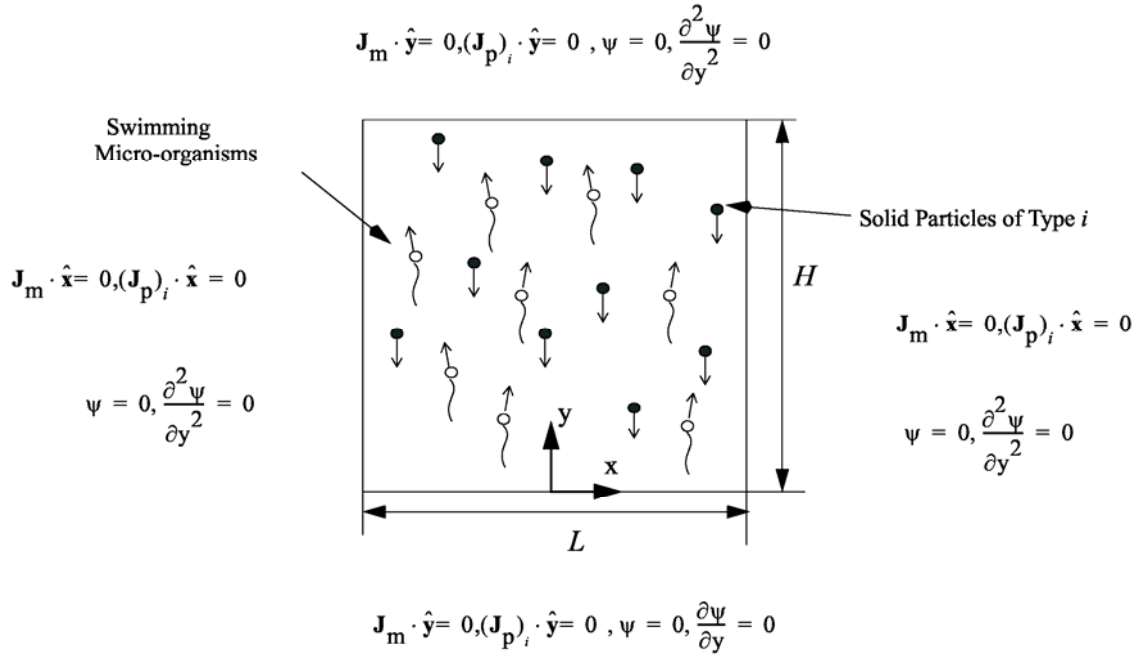


Figure 6-1. Computational domain and boundary conditions

6.2.4 Nonuniformity and Effective Diffusivity

To evaluate the effect that bioconvection has on the mixing of solid particles, a dimensionless parameter called *nonuniformity* (first introduced in Geng and Kuznetsov, 2003) is utilized. Nonuniformity characterizes the magnitude of deviation between the number density distribution of solid particles (or microorganisms) and the uniform distribution of these particles (or microorganisms). If the distribution of microorganisms or solid particles is uniform (such as in a well-mixed suspension), the *nonuniformity* of that distribution is identically equal to zero. Nonuniformities of number density distributions of microorganisms and solid particles of type i are defined as follows, respectively:

$$\Delta(\bar{n}_m^*) = \left\{ \frac{1}{A \bar{n}_m^*} \int_A [n_m^*(x, y) - \bar{n}_m^*]^2 dA \right\}^{1/2} \quad (6.19a)$$

$$\Delta(\bar{n}_p)_i^* = \left\{ \frac{1}{A (\bar{n}_p)_i^*} \int_A \left[(n_p)_i^*(x, y) - (\bar{n}_p)_i^* \right]^2 dA \right\}^{1/2} \quad (6.19b)$$

Effective diffusivity represents the magnitude of diffusivity required to achieve the same nonuniformity if bioconvection was not involved. The nonuniformity is used to calculate the effective diffusivity as follows. Both cases of mixing with and without bioconvection are considered. For the case with bioconvection the real diffusivity of solid particles is used. For the case without bioconvection the effective diffusivity is found. Effective diffusivity is found by matching nonuniformities between these two cases at steady-state and solving for the diffusivity for the case without bioconvection.

There are two physical effects that can prevent solid particles from concentrating at the bottom of the chamber: bioconvection and diffusion. Without bioconvection, solid particles settle until an exponential distribution across the chamber's depth is attained with the largest number density at the bottom of the chamber.

The particles number density distribution can be obtained by integrating equation (6.11) for the case when $\mathbf{V}^* = \partial n_p^* / \partial t^* = 0$, as:

$$(n_p^*)_i(y^*) = \frac{1}{(D_p^*)_i} \frac{\exp\left(\frac{1}{(D_p^*)_i} (W_p^*)_i (1 - y^*)\right)}{\exp\left(\frac{1}{(D_p^*)_i} (W_p^*)_i\right) - 1} (\bar{n}_p^*)_i (W_p^*)_i \quad (6.20)$$

Using Eq. (6.19b), nonuniformity of the number density distribution of solid particles of type i for the case without bioconvection, $\Delta(\bar{n}_p^*)_i$, can be calculated. To define effective diffusivity the nonuniformities of solid particles distributions are considered at steady-state. The nonuniformity of

solid particles for the case without bioconvection, $\Delta(\bar{n}_p)_i^*$, can be set equal to the nonuniformity of solid particles for the case with bioconvection, $\Delta(\bar{n}_p)_i^*$, by increasing the diffusivity of solid particles for the case without bioconvection. The value of diffusivity that matches the two nonuniformities is called the *effective diffusivity*, (D_p^*) . This is a dimensionless parameter that characterizes the effect of bioconvection on making the number density distribution of solid particles in the chamber more uniform.

6.2.5 Numerical Procedure

A conservative finite-difference scheme is utilized to discretize the governing equations. An implicit scheme with Euler backward differencing in time and central differencing in space is utilized to obtain the transient solutions. A line-by-line tridiagonal matrix algorithm and iteration technique with over relaxation is used to solve the nonlinear discretized equations. A staggered uniform grid is utilized in which the stream function and vorticity are stored in one nodal set while the number densities of microorganisms and solid particles are stored in another nodal set. The grid is chosen such that the number density nodes lie in the interior of the computational domain, while the stream function and vorticity nodes lie in the interior and at the boundary of the domain. Computations are performed at the North Carolina State University IBM p690 super computer. The CPU time required to investigate the plume development until it attains its steady-state for a 36×36 uniform mesh is about 20 hours.

6.3 RESULTS AND DISCUSSIONS

Values of physical properties, geometrical parameters, and dimensionless parameters utilized in computations are summarized in Table 6-1. Physical properties and values of dimensionless parameters of particles of types 1 through 6 are given in Table 6-2. In order to account for additional

random motions of particles resulting from particle-microorganism interaction particle diffusivity magnitudes are taken to be larger than those found from Einstein's relation in which the diffusivity of small particles due to Brownian motion is determined.

Table 6-1. Physical properties, geometrical parameters, and values of dimensionless parameters utilized in computations

Average number density of microorganisms	\bar{n}_m	10^{12} cells/m ³
Density of water	ρ_0	10^3 kg/m ³
Specific gravity of microorganisms	$\Delta\rho_m / \rho_0$	0.05
Volume of a micro-organism	θ_m	5×10^{-16} m ³
Average swimming velocity of microorganisms	W_m	10^{-4} m/s
Diffusivity of microorganisms	D_m	5×10^{-8} m ² /s
Gyrotaxis orientation parameter	B	5 s
Kinematic viscosity of the suspension	ν	10^{-6} m ² /s
Height of the computational domain	H	0.005 m
Width of the computational domain	L	0.005 m
Dimensionless average swimming velocity of microorganisms	$W_m^* = W_m \frac{L}{D_m}$	10.000
Schmidt number	$S_c = \frac{\nu}{D_m}$	20
Gyrotaxis number	$G = \frac{BD_m}{L^2}$	10^{-2}
Rayleigh number for microorganisms	$R_m = \frac{\bar{n}_m \theta_m \Delta\rho_m g L^3}{\rho_0 \nu D_m}$	612.5
Aspect ratio	$\lambda = \frac{H}{L}$	1

Table 6-2. Physical properties and values of dimensionless parameters of particles utilized in computations

	Type 1	Type 2	Type 3
Average number density of solid particles $(\bar{n}_p)_i$	10^{11} cells/m ³	10^{11} cells/m ³	10^{11} cells/m ³

Specific gravity $(\Delta\rho_p)_i/\rho_0$	0.10	0.25	0.30
Volume of a particle $(\theta_p)_i$	$5 \times 10^{-16} \text{ m}^3$	$5 \times 10^{-16} \text{ m}^3$	$5 \times 10^{-16} \text{ m}^3$
Settling velocity of particles $(W_p)_i$	$0.5379 \times 10^{-5} \text{ m/s}$	$1.34475 \times 10^{-5} \text{ m/s}$	$1.6137 \times 10^{-5} \text{ m/s}$
Diffusivity of particles $(D_p)_i$	$5 \times 10^{-8} \text{ m}^2/\text{s}$	$5 \times 10^{-8} \text{ m}^2/\text{s}$	$5 \times 10^{-8} \text{ m}^2/\text{s}$
Dimensionless settling velocity of particles $(W_p^*)_i = (W_p)_i \frac{L}{D_m}$	0.5279	1.34475	1.6137
Rayleigh number for particles $(R_p)_i = \frac{\bar{n}_m (\theta_p)_i (\Delta\rho_p)_i g L^3}{\rho_0 \nu D_m}$	1225.0	3062.5	3675
Dimensionless diffusivity of particles $(D_p^*)_i = \frac{(D_p)_i}{D_m}$	0.1	0.1	0.1
Dimensionless average concentration of particles $(\bar{n}_p^*)_i = \frac{(\bar{n}_p)_i}{\bar{n}_m}$	0.1	0.1	0.1

TABLE 6-2 (continued)

	Type 4	Type 5	Type 6
Average number density of solid particles $(\bar{n}_p)_i$	$10^{11} \text{ cells/m}^3$	$10^{11} \text{ cells/m}^3$	$10^{11} \text{ cells/m}^3$
Specific gravity $(\Delta\rho_p)_i/\rho_0$	0.35	0.40	0.45
Volume of a particle $(\theta_p)_i$	$5 \times 10^{-16} \text{ m}^3$	$5 \times 10^{-16} \text{ m}^3$	$5 \times 10^{-16} \text{ m}^3$
Settling velocity of particles $(W_p)_i$	$1.8478 \times 10^{-5} \text{ m/s}$	$2.1516 \times 10^{-5} \text{ m/s}$	$2.42055 \times 10^{-5} \text{ m/s}$
Diffusivity of particles $(D_p)_i$	$5 \times 10^{-8} \text{ m}^2/\text{s}$	$5 \times 10^{-8} \text{ m}^2/\text{s}$	$5 \times 10^{-8} \text{ m}^2/\text{s}$
Dimensionless settling velocity of particles $(W_p^*)_i = (W_p)_i \frac{L}{D_m}$	1.8478	2.1516	2.42055
Rayleigh number for particles $(R_p)_i = \frac{\bar{n}_m (\theta_p)_i (\Delta\rho_p)_i g L^3}{\rho_0 \nu D_m}$	4278.5	4900	5512.5
Dimensionless diffusivity of particles $(D_p^*)_i = \frac{(D_p)_i}{D_m}$	0.1	0.1	0.1
Dimensionless average concentration of particles $(\bar{n}_p^*)_i = \frac{(\bar{n}_p)_i}{\bar{n}_m}$	0.1	0.1	0.1

Nonuniformities of two number density distributions may be equal in value while the two distributions are not identical. Figure 6-2 shows the difference between two number density distributions with the same nonuniformity. This is a bidispersed case with particles of types 1 and 4. Figure 6-2(a) shows the number density distribution of solid particles of type 4 at steady-state obtained by using real diffusivity in the case with bioconvection. Figure 6-2(b) shows the number density distribution of solid particles of type 4 at steady-state obtained by using effective diffusivity in the case without bioconvection. Noting that identical nonuniformities only show identical average deviations from the uniform distribution, it is plain to see from Fig. 6-2 that two entirely different distributions exist for the same nonuniformity.

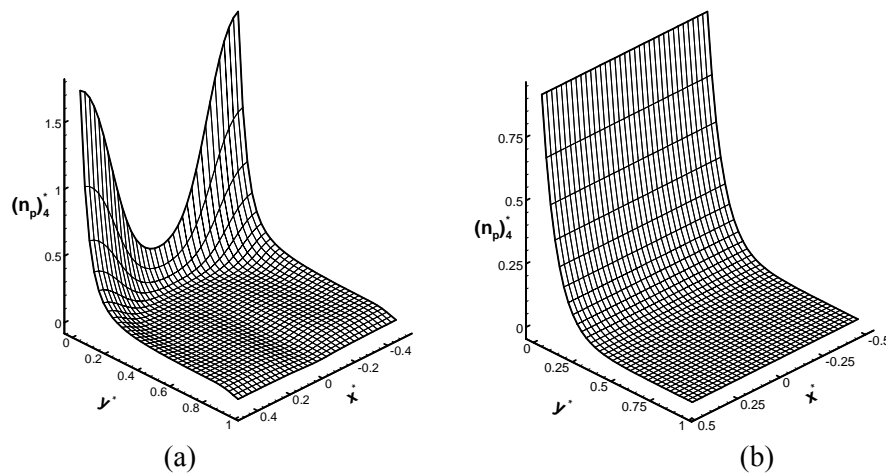
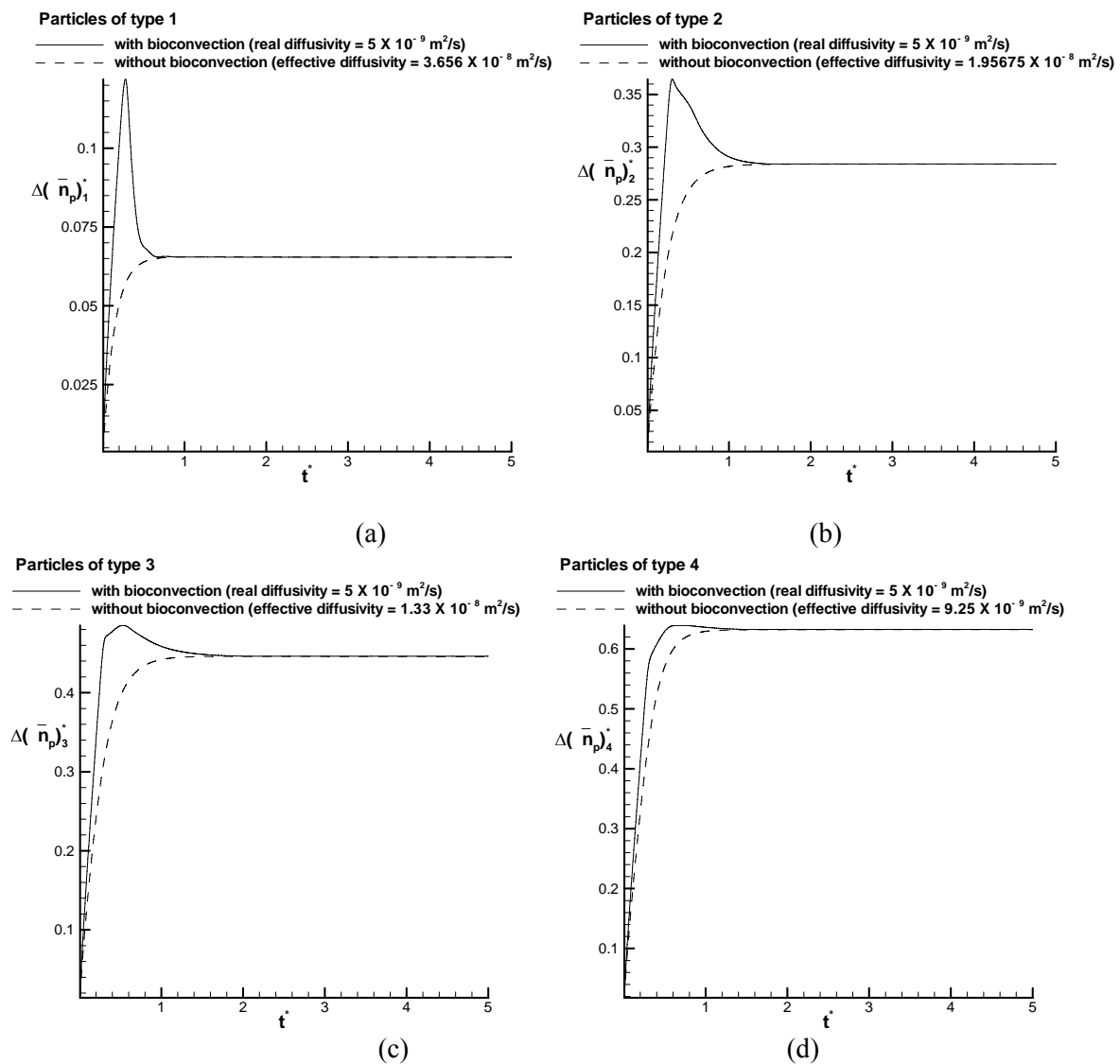


Figure 6-2. Steady state distributions of the dimensionless number density of particles of type 4 in a bidispersed suspension of particles of types 1 & 4 (a) the case with bioconvection, computations are based on real diffusivity of solid particles, (b) the case without bioconvection, computations are based on effective diffusivity of solid particles

A monodispersed suspension of small particles in the fluid that contains motile gyrotactic microorganisms is considered first. Figures 6-3(a)-(f) show the nonuniformities of number density distributions of solid particles of types 1 through 6, $\Delta(\bar{n}_p)_i^*$, versus the dimensionless time, t^* . Both cases with and without bioconvection are considered. The nonuniformities of number density distributions are zero at $t^* = 0$. The nonuniformities develop very quickly (for example, in Fig 6-3(a),

this occurs between $t^* = 0$ and $t^* = 0.275$). This is because during this short time period bioconvection does not even have a chance to develop while the solid particles are settling. After bioconvection has developed, it helps to mix particles in the suspension. This decreases the nonuniformities of solid particles and makes the number density distributions of particles more uniform. This trend is easy to see for light particles, as shown in Figs. 6-3(a) and 6-3(b). However, in Figs. 6-3(c) and 6-3(d) this phenomenon is not observed. This is because bioconvection is not effective in mixing suspensions of heavy particles.



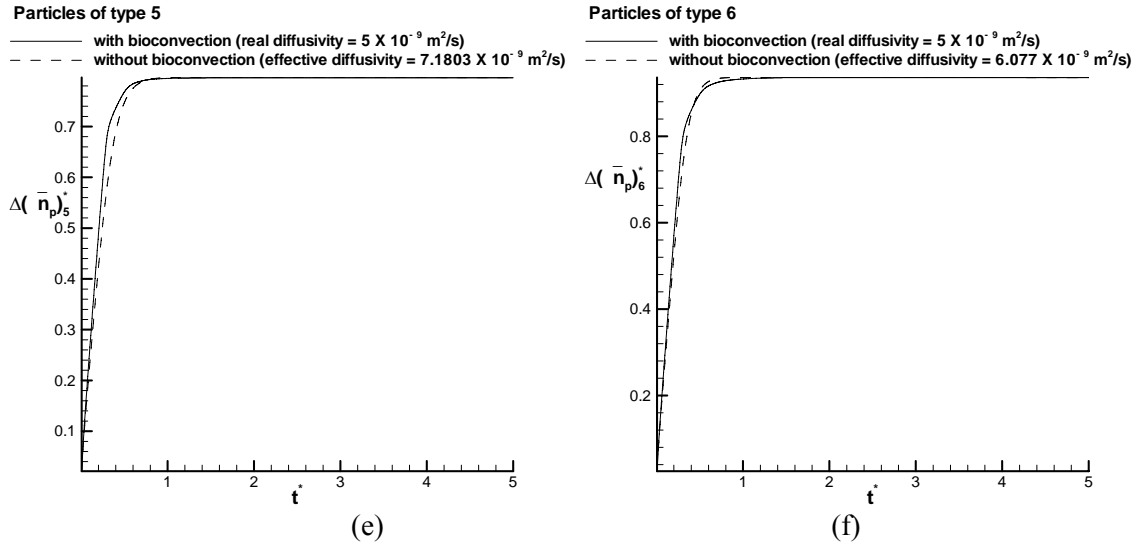


Figure 6-3. Nonuniformities of number density distributions of solid particles in a monodispersed suspension with and without bioconvection (effective diffusivities are utilized for the cases without bioconvection) (a) particles of type 1, (b) particles of type 2, (c) particles of type 3, (d) particles of type 4, (e) particles of type 5, (f) particles of type 6

Figure 6-4 shows the difference in the effect of bioconvection on mixing suspensions of light and heavy particles. In Fig. 6-4(a), the number density distribution of particles of type 1 is presented at (a1) $t^* = 0$ (the uniform distribution), (a2) $t^* = 0.275$ (the nonuniformity takes on its maximum value), and (a3) $t^* = 5$ (the steady state). In Figs. 6-4(b) the number density distributions of particles of type 6 are presented at (b1) $t^* = 0$ (the uniform distribution), (b2) $t^* = 0.5$, and (b3) $t^* = 5$ (the steady state). The nonuniformity does not have a maximum in Fig. 6-3(f) as it does in Fig. 6-3(a) because the particles are too heavy for bioconvection to have any effect on them. In Fig. 6-4(a2), most particles are concentrated at the bottom of the chamber because bioconvection is not developed yet. After bioconvection is developed, as in Fig. 6-4(a3), the distribution of the particles becomes more uniform. This phenomenon cannot be found in Figs. 6-4(b2) and 6-4(b3), which means that bioconvection is less effective in mixing suspensions of heavy particles than it is in mixing suspensions of light particles.

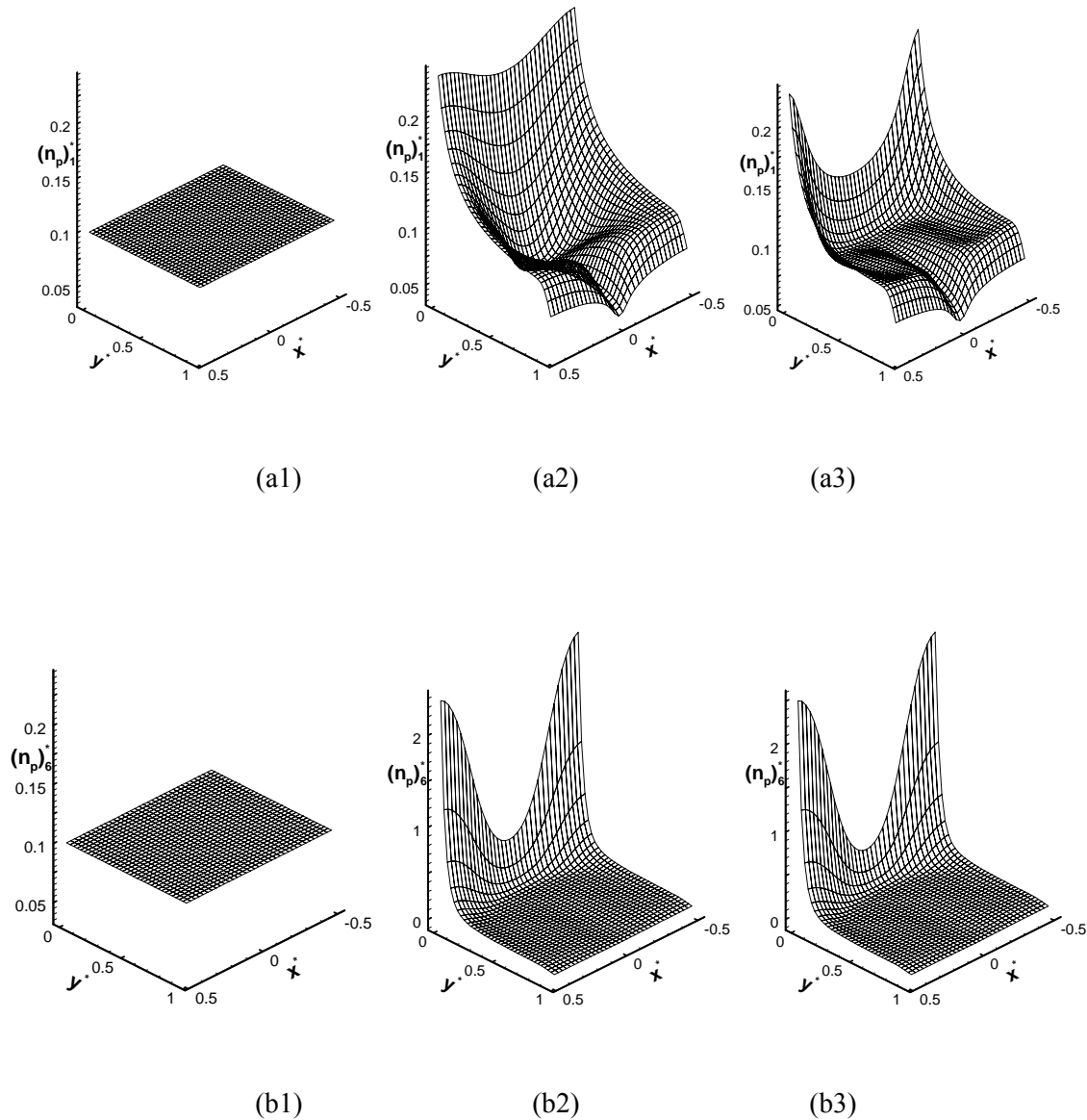


Figure 6-4. Number density distributions of particles of types 1 and 6 in monodispersed suspensions (a1) particles of type 1 at $t^* = 0$, (a2) particles of type 1 at $t^* = 0.275$, (a3) particles of type 1 at $t^* = 5.0$, (b1) particles of type 6 at $t^* = 0$, (b2) particles of type 6 at $t^* = 0.5$, (b3) particles of type 6 at $t^* = 5.0$

The solved values of effective diffusivities for solid particles of types 1 through 6 shown in Figures 6-3(a)-(f) are summarized in Table 6-3. Figure 6-5 is based on these effective diffusivities. This figure displays the effect of the particles density on effective diffusivity in a monodispersed suspension of solid particles. All effective diffusivities are larger than the real diffusivities. This means that bioconvection helps in making number density distributions of solid particles more uniform. Figure 6-

5 shows that effective diffusivities decrease when the density of solid particles increases. This is because bioconvection has less effect on heavier particles. Heavy particles settle down much faster than the light ones so that bioconvection can barely change anything. For example, effective diffusivity of particles of type 1 is more than 6 times larger than the real diffusivity while effective diffusivity of particles of type 6 is only 20% larger than the real diffusivity.

Table 6-3. Effective diffusivities of solid particles of types 1 through 6 for monodispersed cases

(a summary of data presented in Figure 6-3)

	Effective Diffusivity of Particles
Particles of type 1 in Figure 6-2(a) $(D_p^*)_1$	3.656×10^{-8}
Particles of type 2 in Figure 6-2(b) $(D_p^*)_2$	1.95675×10^{-8}
Particles of type 3 in Figure 6-2(c) $(D_p^*)_3$	1.33×10^{-8}
Particles of type 4 in Figure 6-2(d) $(D_p^*)_4$	9.25×10^{-9}
Particles of type 5 in Figure 6-2(e) $(D_p^*)_5$	7.1803×10^{-9}
Particles of type 6 in Figure 6-2(f) $(D_p^*)_6$	6.077×10^{-9}

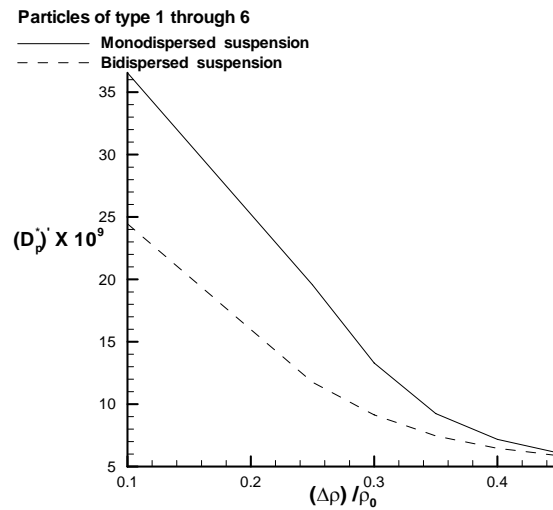
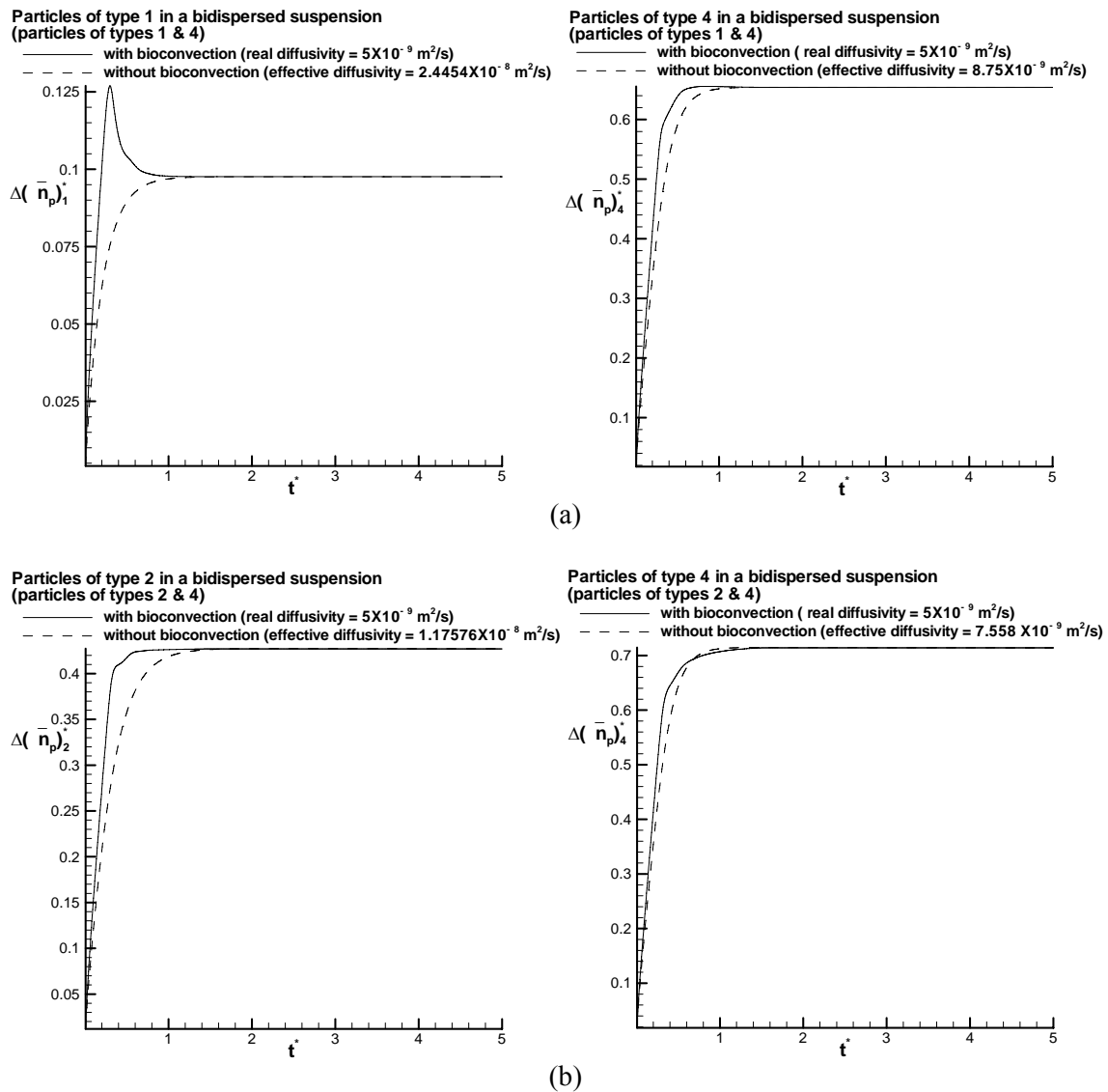
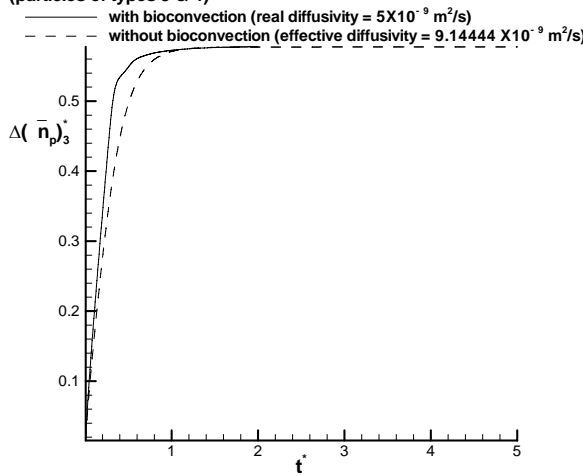


Figure 6-5. Effect of particle density on effective diffusivity of solid particles in monodispersed and bidispersed suspensions. In a bidispersed case, particles of type 4 are always presented in the suspension while the other particle type is changing from 1 to 6. This figure shows effective diffusivities of the second particle type (1 through 6), while effective diffusivity of particles of type 4 in a bidispersed suspension is shown in Fig. 6-7

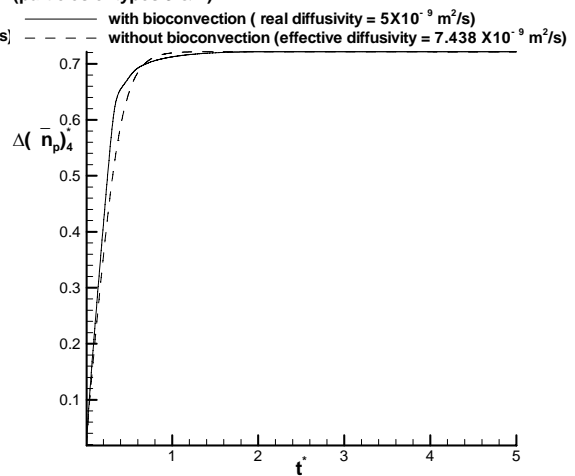
This chapter also investigates how the number density distribution of particles of one type may influence the number density distribution of particles of another type. Six different cases are considered. Particles of type 4 are in all six of them. The other type of solid particles in a bidispersed suspension is changed from type 1 through 6, respectively. Figures 6-6(a)-(f) show the nonuniformities of number density distributions of solid particles of type from 1 through 6, $\Delta(\bar{n}_p)_i^*$, and type 4, $\Delta(\bar{n}_p)_4^*$, versus the dimensionless time, t^* . The same maxima which were found in monodispersed cases are also found in bidispersed cases when the density of solid particles is small.



Particles of type 3 in a bidispersed suspension
(particles of types 3 & 4)

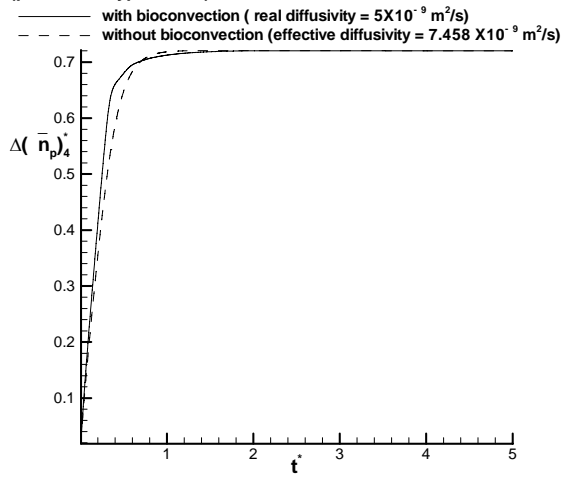


Particles of type 4 in a bidispersed suspension
(particles of types 3 & 4)



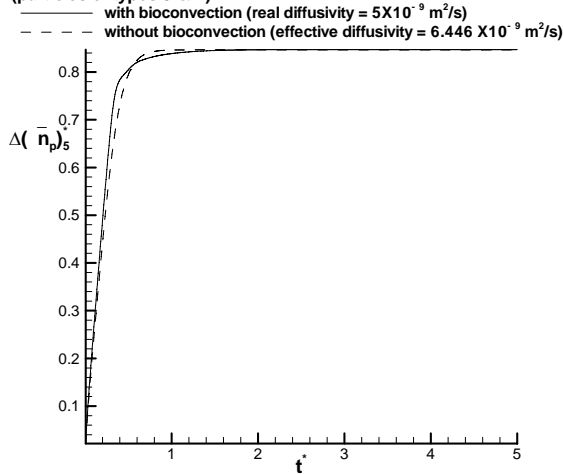
(c)

Particles of type 4 in a bidispersed suspension
(particles of types 4 & 4)

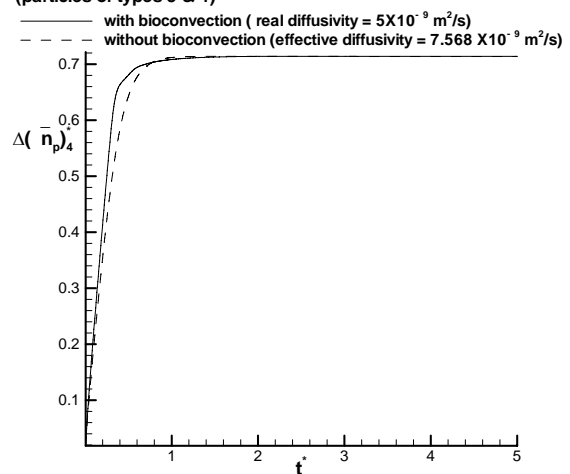


(d)

Particles of type 5 in a bidispersed suspension
(particles of types 5 & 4)



Particles of type 4 in a bidispersed suspension
(particles of types 5 & 4)



(e)

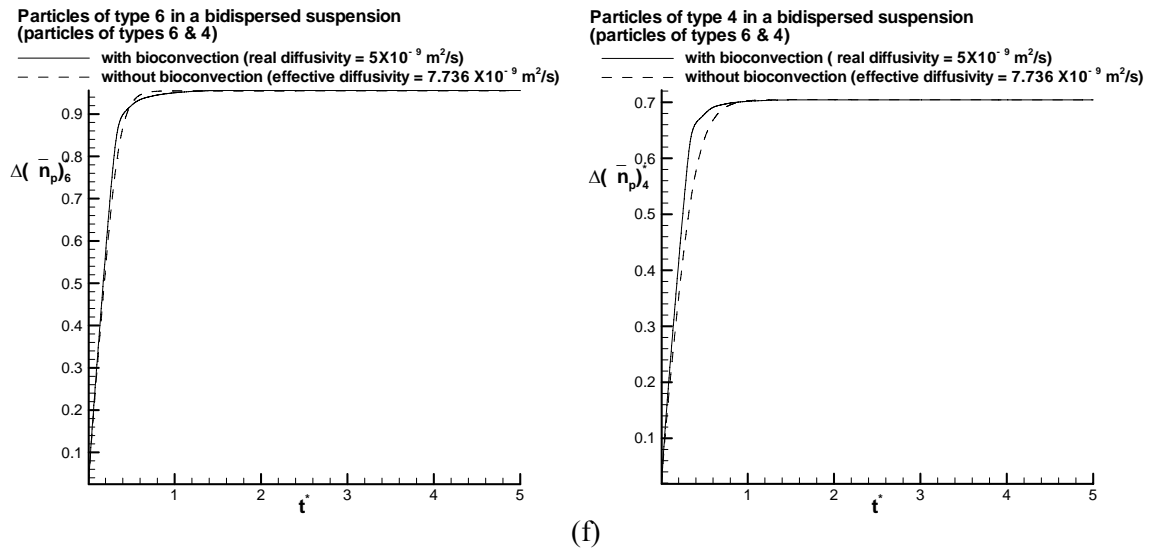


Figure 6-6. Nonuniformities of number density distributions of solid particles in a bidispersed suspension with and without bioconvection (effective diffusivities are utilized for the cases without bioconvection) (a) particles of type 1 & 4, (b) particles of type 2 & 4, (c) particles of type 3 & 4, (d) particles of type 4 & 4, (e) particles of type 5 & 4, (f) particles of type 6 & 4

The values of effective diffusivities of solid particles of type 1 through 6 in Figures 6-6(a)-(f) are summarized in Table 6-4 and are shown in Figure 6-5. All effective diffusivities decrease with an increase in the density of solid particles. An interesting observation is that all values of effective diffusivities from bidispersed cases are smaller than those from monodispersed cases. This means that the number density of particles is more nonuniform if another type of solid particles is present in the suspension. Furthermore, the difference of effective diffusivities between monodispersed and bidispersed cases is decreased when the density of particles is increased. This shows that the introduction of the second particle type has a greater effect on the diffusivities of lighter solid particles than of heavier solid particles.

Table 6-4. Effective diffusivities of solid particles of types 1 through 6 for bidispersed cases

(a summary of data presented in Figure 6-6)

	Effective Diffusivity of Particles
Particles of type 1 in Figure 6-4(a) $(D_p^*)_1$	2.4454×10^{-8}
Particles of type 2 in Figure 6-4(b) $(D_p^*)_2$	1.17576×10^{-8}
Particles of type 3 in Figure 6-4(c) $(D_p^*)_3$	9.14444×10^{-9}
Particles of type 4 in Figure 6-4(d) $(D_p^*)_4$	7.458×10^{-9}
Particles of type 5 in Figure 6-4(e) $(D_p^*)_5$	6.466×10^{-9}
Particles of type 6 in Figure 6-4(f) $(D_p^*)_6$	5.874×10^{-9}

The most interesting phenomenon is found after collecting values of the effective diffusivities of solid particles of type 4 in Figures 6-6(a)-(f) in Table 5, and showing them in Figure 6-7. Figure 6-7 displays the effective diffusivity of particles of type 4 as a function of the density of the second particle type in a bidispersed suspension. To compare the values of effective diffusivity between mono and bidispersed cases, the effective diffusivity of particles of type 4 in a monodispersed suspension is also presented in Fig. 6-7. For all computed cases, values of effective diffusivity of particles of type 4 in a bidispersed suspension are less than that in a monodispersed suspension (9.25×10^{-9} according to Table 3). This means that introducing a second particle type into the suspension makes the distribution more nonuniform. The effective diffusivity of particles of type 4 decreases initially and then increases as the density of the other particle type is increased. This shows that a minimum effective diffusivity of particles of type 4 exists. Figure 6-7 also shows that effective diffusivity of particles of type 4 in a monodispersed suspension is always larger than that in a bidispersed suspension.

Table 6-5. Effective diffusivities of solid particles of type 4 for bidispersed cases

(a summary of data presented in Figure 6-6)

	Effective Diffusivity of Particles
Particles of type 4 in Figure 6-4(a) $(D_p^*)_4$	8.750×10^{-9}
Particles of type 4 in Figure 6-4(b) $(D_p^*)_4$	7.558×10^{-9}
Particles of type 4 in Figure 6-4(c) $(D_p^*)_4$	7.438×10^{-9}
Particles of type 4 in Figure 6-4(d) $(D_p^*)_4$	7.458×10^{-9}
Particles of type 4 in Figure 4(e) $(D_p^*)_4$	7.568×10^{-9}
Particles of type 4 in Figure 4(f) $(D_p^*)_4$	7.736×10^{-9}

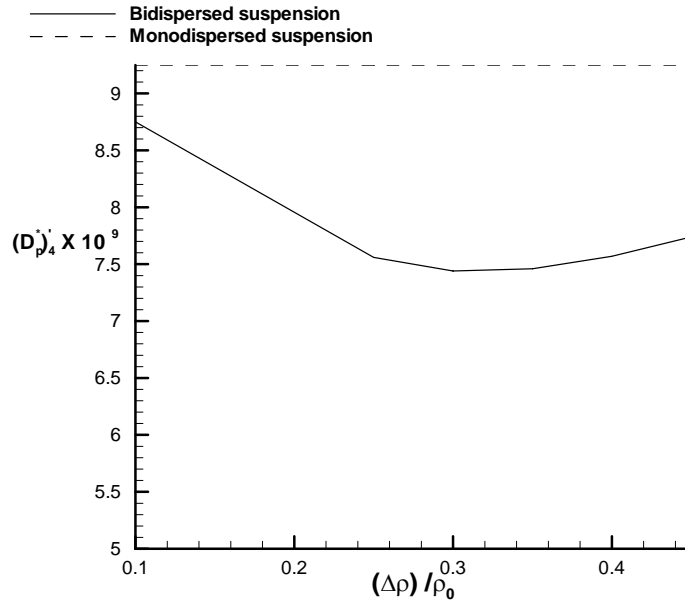


Figure 6-7. Values of effective diffusivities for solid particles of type 4 in a bidispersed suspension. (The other particle type in the bidispersed suspension is changing from 1 through 6. Their effective diffusivities are shown in Figure 5.)

6.4 CONCLUSIONS

A new parameter, called the *effective diffusivity* of solid particles, is defined in this chapter. This parameter is utilized for the analysis of monodispersed and bidispersed suspensions. Since the

effective diffusivity is found to be always greater than real diffusivity, bioconvection helps mixing between solid particles. In a monodispersed suspension, increasing the density of particles increases the nonuniformity of the number density distribution of particles, which means that bioconvection is less effective in mixing suspensions of heavy particles than it is in mixing suspensions of light particles. In a bidispersed suspension, the introduction of a second particle type decreases the effect of mixing by the bioconvective flow thus making the particle distribution more nonuniform.

ACKNOWLEDGEMENTS

AVK gratefully acknowledges the grant # NAG3-2706 awarded to him by NASA Office of Biological and Physical Research, Physical Sciences Division. Constructive comments and suggestions of Mr. Sid Becker are greatly appreciated.

REFERENCES

- 1 Batchelor, G.K., "Sedimentation in a Dilute Polydisperse System of Interacting Spheres. Part 1. General Theory", J. Fluid Mech. 119 (1982) 379-408.
- 2 Batchelor, G.K., "Sedimentation in a Dilute Polydisperse System of Interacting Spheres. Part 1. General Theory", J. Fluid Mech. 119 (1982) 379-408.
- 3 Geng, P. and Kuznetsov, A.V., "Settling of Bidispersed Small Solid Particles in a Dilute Suspension Containing Gyrotactic Microorganisms", International Journal of Engineering Science (2003), submitted.
- 4 Ghorai, S. and Hill, N.A., "Development and Stability of Gyrotactic Plumes in Bioconvection", J. Fluid Mech. **400**, 1-31 (1999).
- 5 Ghorai, S. and Hill, N.A., "Periodic Arrays of Gyrotactic Plumes in Bioconvection", Physics of Fluids **12**, 5-22 (2000).

- 6 Kashiwagi, Y. and Sakoda, K., "Evaluation of Micro-volume Sample Analysis Using *BioMajesty*® JCA-BM1650 Automated Biochemistry Analyzer", Application & Research Center, JEOL Ltd. (2001).
- 7 Kessler, J.O., "Hydrodynamic Focusing of Motile Algal Cells", *Nature* **313**, 218-220 (1985a).
Kessler, J.O., "Co-operative and Concentrative Phenomena of Swimming Microorganisms", *Contemp. Phys.* **26**, 147-166 (1985b).
- 8 Kessler, J.O., Burnett, G.D. and Remick, K.E., "Mutual Dynamics of Swimming Microorganisms and Their Fluid Habitat", in "Nonlinear Science at the Dawn of the 21st Century", P.L. Christiansen, M.P. Sorensen, and A.C. Scott, Eds., Springer, New York (2000), pp. 409-426.
- 9 Kessler, J.O., Wiseley, D.A., Remick, K.E. and Marthaler, D.E., "Individual and Collective Dynamics of Swimming Bacteria", in Proceedings of the Workshop "Traffic and Granular Flow'97", M. Schreckenberg and D.E. Wolf, Eds., Springer, New York (1997), pp. 37-51.
- 10 Kuznetsov, A.V. and Geng, P., "Effect of Bioconvection Caused by Gyrotactic Microorganisms on the Settling of Small Solid Particles", *International Journal of Numerical Methods for Heat and Fluid Flow* (2003), submitted.
- 11 Pedley, T.J., Hill, N.A. and Kessler, J.O., "The Growth of Bioconvection Patterns in a Uniform Suspension of Gyrotactic Microorganisms", *J. Fluid Mech.* **195**, 223-338 (1988).
- 12 Pedley, T.J. and Kessler, J.O., "The Orientation of Spheroidal Microorganisms Swimming in a Flow Field", *Proc. R. Soc. Lond.* **B231**, 47-70 (1987).
- 13 Pedley, T.J. and Kessler, J.O., "A New Continuum Model for Suspensions of Gyrotactic Microorganisms", *Journal of Fluid Mechanics* **212**, 155-182 (1990).

- 14 Pedley, T.J. and Kessler, J.O., “Hydrodynamic Phenomena in Suspensions of Swimming Microorganisms”, Ann. Rev. Fluid Mech. **24**, 313-358 (1992).

PART THREE

DYNAMICS OF LARGE SOLID PARTICLES IN

BIOCONVECTION FLOW CAUSED BY MOTILE

GYROTACTIC MICROORGANISMS

7. DIRECT NUMERICAL SIMULATION OF SETTLING OF A LARGE SOLID PARTICLE DURING BIOCONVECTION

ABSTRACT

Settling of a large solid particle in bioconvection flow caused by gyrotactic microorganisms is investigated. The particle is released from the top of the bioconvection chamber; its settling pattern depends on whether it is released in the center of the bioconvection plume or at its periphery. The Chimera method is utilized; a subgrid is generated around a moving particle. The method suggested by Liu and Wang [1] is further developed to account for the presence of a moving boundary in the streamfunction-vorticity formulation using the finite-difference method. A number of cases for different release positions of the particle are computed. It is demonstrated that bioconvection can either accelerate or decelerate settling of the particle depending on the initial position of the particle relative to the plume center. It is also shown that the particle impacts bioconvection plume by changing its shape and location in the chamber.

NOMENCLATURE

a	radius of a microorganism, m
B	time scale for the reorientation of microorganisms by the gravitational torque against viscous torque, $4\pi\mu a^3 / (mgh)$, s
D_m	diffusivity of microorganisms, m^2/s
g	gravity vector, $9.81 m/s^2$
G	gyrotaxis number, BD_m / L^2
h	displacement of the center of mass of a gyrotactic microorganism from its center of buoyancy, m
H	height of the chamber, m
\mathbf{J}_m^*	dimensionless flux of microorganisms, defined in equation (7.14)
L	width of the chamber, m
n_m	number density of microorganisms, $1/m^3$
\bar{n}_m	average number density of microorganisms, $1/m^3$
n_m^*	dimensionless number density of microorganisms, n_m / \bar{n}_m
$\hat{\mathbf{p}}$	unit vector indicating the direction of swimming of gyrotactic microorganisms
p_e	excess pressure (above hydrostatic), Pa
R_m	bioconvection Rayleigh number, $\bar{n}_m \theta_m \Delta \rho_m g L^3 / (\rho_0 \nu D_m)$
S_c	Schmidt number, ν / D_m
t	time, s
t^*	dimensionless time, $D_m t / L^2$
\mathbf{V}	velocity vector, m/s
\mathbf{V}^*	dimensionless velocity vector, $\mathbf{V}L / D_m$

V_x	horizontal velocity component, m/s
V_y	vertical velocity component, m/s
V_θ	radial velocity component, m/s
V_τ	tangential velocity component, m/s
W_m	average swimming velocity of microorganisms (assumed to be constant), m/s
W_m^*	dimensionless average swimming velocity of microorganisms, $W_m L / D_m$
x	horizontal coordinate, m
x^*	dimensionless horizontal coordinate, x / L
\hat{x}	unit vector in the x -direction
y	vertical coordinate, m
y^*	dimensionless vertical coordinate, y / L
\hat{y}	unit vector in the y -direction

Greek symbols

$\Delta\rho_m$	density difference between microorganisms and water, $\rho_m - \rho_0$, kg/m ³
ζ	horizontal component of vorticity, 1/s
ζ^*	dimensionless horizontal component of vorticity, $\zeta L^2 / D_m$
θ_m	volume of a microorganism, m ³
λ	aspect ratio of the chamber, H / L
μ	dynamic viscosity, assumed to be approximately the same as that of water, kg/(m s)
ν	kinematics viscosity, assumed to be approximately the same as that of water, m ² /s
ρ_0	density of water, kg/m ³
ρ_m	density of microorganisms, kg/m ³

ρ_p	density of the particle, kg/m ³
ψ	streamfunction, m ² /s
ψ^*	dimensionless streamfunction, ψ / D_m
ω	angular velocity, 1/s
ω^*	dimensionless angular velocity, $L^2 / D_m \omega$

7.1 INTRODUCTION

Bioconvection provides a powerful tool to manipulate mass transfer in microvolumes of fluids. This may have potential pharmaceutical and bio-technological applications. This chapter investigates a possible application of bioconvection to control settling of a large solid particle, which may be useful to control sedimentation in microvolumes.

Motile microorganisms swim in a particular direction because of different stimuli such as phototaxis, chemotaxis, or gyrotaxis. This chapter considers gyrotactic microorganisms, such as many species of algae. Because these microorganisms are bottom heavy, their swimming direction is determined by the balance of gravitational and viscous torques. Gyrotactic behavior results in the accumulation of these microorganisms in the regions of most rapid downflow. Since the algae are typically 3-5% more dense than water, the density in the regions of downflow becomes larger than in the regions of upflow. Buoyancy increases velocities in both upflow and downflow regions, enhancing velocity fluctuations and introducing a hydrodynamic instability (Pedley et al. [2], Ghorai and Hill [3, 4]). The induced convection fluid motion leads to the development of bioconvection plumes. Many experimental papers (Kessler [5, 6], Kessler et al. [7, 8]) have described the formation of gyrotactic plumes with regular patterns in algal suspensions.

Geng and Kuznetsov [9, 10] investigated the settling of small solid particles in a suspension of motile gyrotactic microorganisms. It was found that mixing induced by bioconvection slows down settling of such particles which leads to a more uniform number density distribution of solid particles along the height of the chamber. In these studies, the particles were small and their number was large so that they were modeled as a continuous phase having its own number density distribution.

A large number of research papers addressed moving objects in a fluid. Hu et al. [11] used the finite element method for the computation of settling a solid object in a liquid. In this study, the motion of the solid object was tracked by an Arbitrary Lagrangian-Eulerian (ALE) scheme. Gan et al. [12]

presented a direct numerical simulation of sedimentation of large solid particles in a flow field induced by natural convection. The cases of one and two large settling particles were investigated. Hsiao and Chahine [13] applied the Chimera method to simulate the bubble dynamics in a vortex flow. A moving Chimera grid was generated to describe the bubble surface motion. Russell and Wang [14] developed a Cartesian grid method for modeling multiple moving objects in a 2-D incompressible viscous flow. An underlying regular Cartesian grid was used to resolve the moving boundary problem. Boundary conditions for the moving boundary were satisfied by superposing a homogenous solution of Poisson's equation upon the initial solution for the streamfunction. The initial solution was generated by neglecting the moving object in the fluid flow.

The utilization of the streamfunction-vorticity formulation is an effective method for numerical modeling of a 2-D incompressible flow. However, its utilization to calculate the values of the streamfunction and vorticity in a domain that contains moving boundaries still provides a challenge. Liu and Wang [1] introduced a high order finite-difference method in multi-connected domains. This method provides an algorithm for computing boundary conditions for streamfunction and vorticity in a fixed multi-connected domain. In this research, the method developed in Liu and Wang [1] is extended to allow for moving boundaries in the domain filled with an incompressible fluid.

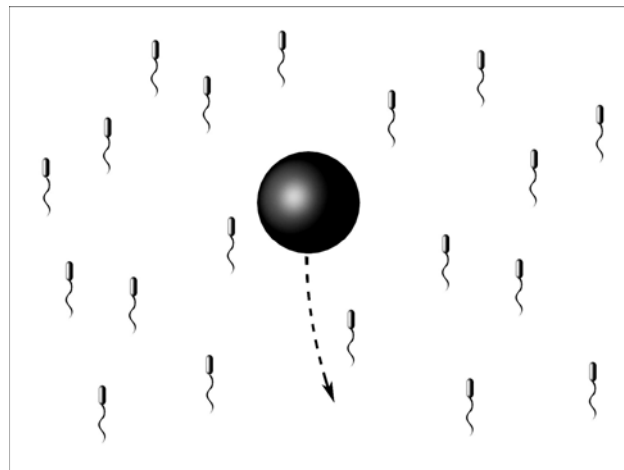


Figure 7-1. Schematic diagram of a large particle settling in developed bioconvection flow

This chapter considers a large particle (in a 2-D model utilized in this research it is represented by an infinitely long cylinder, see Fig. 1a) settling in a chamber in which the bioconvection plume is already fully developed. A finite-difference method based on the moving Chimera grid scheme is utilized. The vorticity and streamfunction are introduced into the Navier-Stokes equations to eliminate the pressure.

It is assumed that bioconvection plumes occur periodically. The two-dimensional computational domain coincides either with one or two the periodic cells (each periodic cell contains a single bioconvection plume). The height of the periodic cell is H and its width is L , where L is a typical plume spacing and $\lambda = H/L$ is the aspect ratio of the periodic cell. Ghorai and Hill [4] studied the effect of the aspect ratio on bioconvection and found that the steady-state bioconvection plume was stable for $\lambda = 1$. Increasing λ slowed down the solution's convergence to steady-state. This chapter assumes that $\lambda = 1$.

7.2 GOVERNING EQUATIONS

7.2.1 Dimensional Governing Equations

Governing equations for a bioconvection plume caused by gyrotactic microorganisms are given in Ghorai and Hill [3, 4] as:

Momentum equation

$$\rho_0 \left(\frac{\partial \mathbf{V}}{\partial t} + (\mathbf{V} \cdot \nabla) \mathbf{V} \right) = -\nabla p_e + \mu \Delta \mathbf{V} + n_m \theta_m \Delta \rho_m \mathbf{g} \quad (7.1)$$

Continuity equation

$$\nabla \cdot \mathbf{V} = 0 \quad (7.2)$$

Conservation of motile microorganisms

$$\frac{\partial(n_m)}{\partial t} = -\text{div}(n_m \mathbf{V} + n_m W_m \hat{\mathbf{p}} - D_m \nabla n_m) \quad (7.3)$$

where D_m is the diffusivity of microorganisms (this assumes that all random motions of microorganisms can be approximated by a diffusive process); n_m is the number density of motile microorganisms; p_e is the excess pressure (above hydrostatic); $\hat{\mathbf{p}}$ is the unit vector indicating the direction of microorganisms' swimming (equations for this vector are obtained in Pedley et al. [2]); \mathbf{V} is the velocity vector, (V_x, V_y) ; $W_m \hat{\mathbf{p}}$ is the vector of microorganisms' average swimming velocity (W_m is assumed to be constant); $\Delta\rho_m$ is the density difference between microorganisms and water, $\rho_m - \rho_0$; θ_m is the volume of a microorganism; μ is the dynamic viscosity of the suspension; and ρ_0 is the density of water.

The motion of the solid particle is described by Newton's second law:

$$m \frac{dV_x}{dt} = F_x, \quad m \frac{dV_y}{dt} = F_y, \quad \mathbf{I} \frac{d\omega}{dt} = \mathbf{T}$$

and

$$\frac{dx}{dt} = V_x, \quad \frac{dy}{dt} = V_y, \quad \frac{d\theta}{dt} = \omega \quad (7.4)$$

where $m = \rho_p \left(\frac{\pi d^3}{4} \right)$ is the mass of the particle, $\mathbf{I} = m \left(\frac{d^2}{8} \right)$ is the polar moment of inertia of the particle, d is the diameter of the particle, ω is the particle's angular velocity, F_x is the x -component of the total external force on the particle, F_y is the y -component of the total external force on the particle, and \mathbf{T} is the mechanical torque on the particle.

The force terms are due to gravity and the viscous force that the fluid exerts on the surface of the particle. Since the particle is symmetric, the viscous friction on the surface of the particle is the only contributor to the torque:

$$F_x = \int_{\Omega} \left(\mu \frac{\partial \mathbf{V}_\tau}{\partial \mathbf{n}} \cdot \hat{\mathbf{x}} \right) ds$$

$$F_y = \int_{\Omega} \left(\mu \frac{\partial \mathbf{V}_\tau}{\partial \mathbf{n}} \cdot \hat{\mathbf{y}} \right) ds + \frac{\rho_p - \rho_0}{\rho_p} \left(\pi d^2 / 4 \right) \mathbf{g}$$

$$\mathbf{T} = \int_{\Omega} \left(\mu \frac{\partial \mathbf{V}_\tau}{\partial \mathbf{n}} \cdot \frac{d}{2} \right) ds \quad (7.5)$$

where Ω is the surface of the particle and \mathbf{V}_τ is the tangential fluid velocity along the surface of the particle.

7.2.2 Dimensionless Governing Equations

Utilizing the streamfunction-vorticity formulation, the governing equations can be recast in the following dimensionless form:

$$\zeta^* = -\nabla^2 \psi^* \quad (7.6)$$

$$S_c^{-1} \left(\frac{\partial \zeta^*}{\partial t^*} + V_x^* \frac{\partial \zeta^*}{\partial x^*} + V_y^* \frac{\partial \zeta^*}{\partial y^*} \right) = \nabla^2 \zeta^* - \left(R_m \frac{\partial n_m^*}{\partial x^*} \right) \quad (7.7)$$

$$\frac{\partial n_m^*}{\partial t^*} = -\nabla \cdot \left[n_m^* (\mathbf{V}^* + W_m^* \hat{\mathbf{p}}) - \nabla n_m^* \right] \quad (7.8)$$

The dimensionless variables in equations (7.6)-(7.8) are defined as:

$$x^* = \frac{x}{L}, y^* = \frac{y}{L}, t^* = \frac{D_m}{L^2} t, u^* = \frac{\partial \psi^*}{\partial y^*}, v^* = -\frac{\partial \psi^*}{\partial x^*}, \mathbf{V}^* = \mathbf{V} \frac{L}{D_m},$$

$$W_m^* = W_m \frac{L}{D_m}, n_m^* = \frac{n_m}{\bar{n}_m}, S_c = \frac{v}{D_m}, G = \frac{BD_m}{L^2}, R_m = \frac{\bar{n}_m \theta_m \Delta \rho_m g L^3}{\rho_0 \nu D_m}, \quad (7.9)$$

where asterisks denote dimensionless quantities.

Ghorai and Hill [3, 4] have shown that if the inertia terms in the momentum equation are neglected (which is justified for bioconvection flows because of a very low Reynolds number), the vector $\hat{\mathbf{p}}$, which determines the swimming direction of microorganisms, can be computed as:

$$\hat{\mathbf{p}} = \begin{cases} \left(-\kappa - (\kappa^2 - 1)^{1/2}, 0 \right), & \kappa < -1 \\ \left(-\kappa, (1 - \kappa^2)^{1/2} \right), & |\kappa| \leq 1 \\ \left(-\kappa + (\kappa^2 - 1)^{1/2}, 0 \right), & \kappa > 1 \end{cases} \quad (7.10)$$

where $\kappa = B\zeta = G\zeta^*$. The parameter B is called the “gyrotactic orientation parameter” by Pedley and Kessler [15], who defined it as:

$$B = \frac{4\pi\mu a^3}{mgh} \quad (7.11)$$

where h is the displacement of the center of mass of a gyrotactic microorganism from its center of buoyancy, m is the mass of the microorganism, and a is the radius of a microorganism.

7.2.3 Chimera Grid Scheme

The Chimera grid scheme is a grid embedding technique that is utilized in both 2-D and 3-D computations (see, for example Hsiao and Chahine [13]). The Chimera scheme provides a simple

method for domain decomposition. A structured subgrid is generated around the moving particle settling in bioconvection flow field. In this chapter, a subgrid is created around the particle and a global rectangular grid is created for the global flow field, as demonstrated in Figs. 7.2a and 7.2a. Equations (7.6)-(7.8) are solved separately for the global grid and the subgrid. The communication between the global grid and the subgrid is implemented by interpolation. The unknown values of variables in the subgrid boundary points are computed by interpolating these boundary points onto the global grid with the known values on the global grid. Therefore, the computational problem for the subgrid becomes a boundary value problem. In the global grid, the same procedure is required; the only difference is that an artificial inner boundary is created around the moving particle. The problem for the global grid becomes a boundary value problem by interpolating these artificial inner boundary points onto the subgrid with known values on the subgrid. Equations (7.6)-(7.8) are transformed into a polar coordinate system for the subgrid computations.

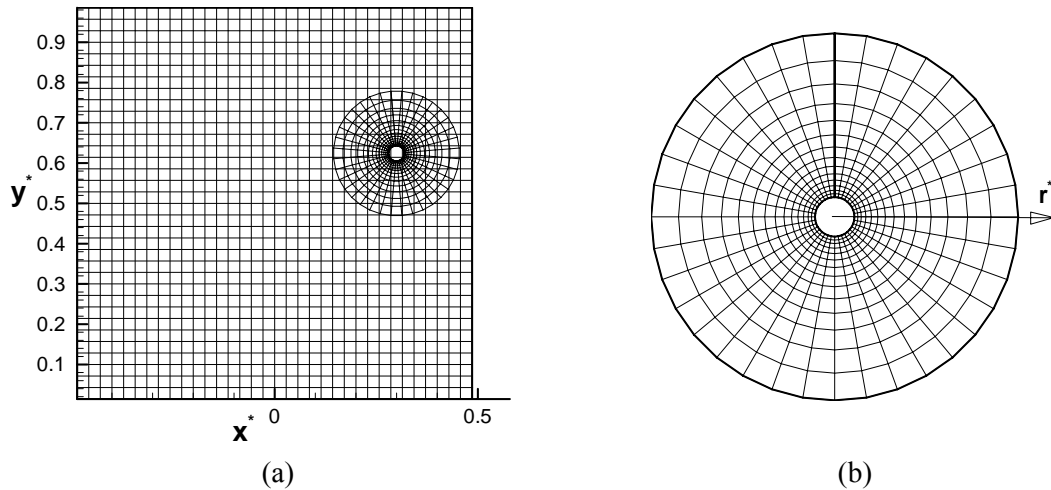


Figure 7-2. Chimera grid system: (a) global and subgrid mesh, (b) subgrid mesh

7.2.4 Initial and Boundary Conditions

Equations (7.6)-(7.8) are solved subject to the following boundary conditions. The side walls of the computational domain are assumed shear-free in order to model plumes' periodic condition. The free

surface is assumed stress-free, and the bottom wall is assumed rigid (a hydrodynamic no-slip condition is imposed there). At the surface of the settling particle, the no-slip boundary condition along with the no-penetration condition for the microorganisms is assumed. Under these assumptions, the boundary conditions at the walls of the computational domain are presented as:

$$\psi^* = 0 \text{ at } y^* = 0, \lambda \text{ and } x^* = \pm 0.5, \quad (7.12a)$$

$$\frac{\partial \psi^*}{\partial y^*} = 0 \text{ at } y^* = 0, \quad (7.12b)$$

$$\frac{\partial^2 \psi^*}{\partial y^{*2}} = 0 \text{ at } y^* = \lambda, \text{ and } \frac{\partial^2 \psi^*}{\partial x^{*2}} = 0 \text{ at } x^* = \pm 0.5. \quad (7.12c)$$

Normal fluxes of microorganisms are zero through all boundaries of the computational domain and the surface of the moving particle:

$$\mathbf{J}_m^* \cdot \hat{\mathbf{y}} = 0 \text{ at } y^* = 0, \lambda; \mathbf{J}_m^* \cdot \hat{\mathbf{x}} = 0 \text{ at } x^* = \pm 0.5; \quad (7.13a)$$

$$\mathbf{J}_m^* \cdot \hat{\mathbf{r}} = 0 \text{ at surface of the moving particle} \quad (7.13b)$$

where $\hat{\mathbf{x}}$, $\hat{\mathbf{y}}$, and $\hat{\mathbf{r}}$ are the unit vectors in the x -, y -, and r -directions, respectively, and

$$\mathbf{J}_m^* = n_m^* (\mathbf{V}^* + W_m^* \hat{\mathbf{p}}) - \nabla n_m^* \quad (7.14)$$

is the dimensionless flux of microorganisms.

To calculate the values of the streamfunction and vorticity on the moving boundary, they are defined in the polar coordinate system:

$$\zeta^* = - \left(\frac{\partial^2 \psi^*}{\partial r^{*2}} + \frac{1}{r^*} \frac{\partial \psi^*}{\partial r^*} + \frac{1}{r^{*2}} \frac{\partial^2 \psi^*}{\partial \theta^2} \right) \quad (7.15)$$

$$V_r^* = \frac{1}{r^*} \frac{\partial \psi^*}{\partial \theta}, \quad V_\theta^* = -\frac{\partial \psi^*}{\partial r^*} \quad (7.16)$$

where r^* is the dimensionless radial coordinate, r/L , (see Fig. 2b) and V_r^* and V_θ^* are the dimensionless velocity components in the polar coordinate system.

Representing $\psi^*(r^*, \theta)$ through Taylor series expansion near the moving boundary and assuming that Δr^* is constant (to simplify equations, the subgrid is constructed such that the two first grid layers around the particle are of uniform thickness; after that the grid becomes non-uniform) the following equations are obtained:

$$\psi^*(r_0^* + \Delta r^*, \theta) = \psi^*(r_0^*, \theta) + \Delta r^* \frac{\partial \psi^*}{\partial r^*} + \frac{(\Delta r^*)^2}{2} \frac{\partial^2 \psi^*}{\partial r^{*2}} + \frac{(\Delta r^*)^3}{6} \frac{\partial^3 \psi^*}{\partial r^{*3}} + o((\Delta r^*)^4) \quad (7.17)$$

$$\psi^*(r_0^* + 2\Delta r^*, \theta) = \psi^*(r_0^*, \theta) + 2\Delta r^* \frac{\partial \psi^*}{\partial r^*} + \frac{(2\Delta r^*)^2}{2} \frac{\partial^2 \psi^*}{\partial r^{*2}} + \frac{(2\Delta r^*)^3}{6} \frac{\partial^3 \psi^*}{\partial r^{*3}} + o((\Delta r^*)^4) \quad (7.18)$$

where $r_0^* = r_0/L$ and r_0 is the radius of the particle.

Eliminating $\left(\frac{\partial \psi^{*3}}{\partial r^{*3}}\right)$ between Eqs. (7.17) and (7.18) and using the expressions for V_r^* , V_θ^* , ζ^* ,

$\frac{\partial \psi^*}{\partial r^*}$, and $\frac{\partial^2 \psi^*}{\partial r^{*2}}$ from Eqs. (7.15) and (7.16), the equation for $\zeta^*(r_0^*, \theta)$ is obtained as:

$$\begin{aligned} \zeta^*(r_0^*, \theta) = & \\ & \frac{\left(-6\Delta r^* + \frac{2(\Delta r^*)^2}{r_0^*}\right) V_\theta^*(r_0^*, \theta) - (8\psi^*(r_0^* + \Delta r^*, \theta) - \psi^*(r_0^* + 2\Delta r^*, \theta) - 7\psi^*(r_0^*, \theta))}{2(\Delta r^*)^2} \\ & - \frac{1}{r_0^*} \frac{\partial V_r^*}{\partial \theta} \end{aligned} \quad (7.19)$$

Liu and Wang [1] have developed a method to calculate the boundary values of the streamfunction on a fixed boundary of a multi-connected domain. In the case of a fixed boundary, the streamfunction is constant along a surface that represents a closed contour in a 2-D space while in the moving boundary case the streamfunction is a function of location (x, y) on the surface and time t . In Liu and Wang [1], the momentum equation is multiplied by a unit tangential vector $\boldsymbol{\tau}$ to obtain the boundary condition for the streamfunction. The same idea is utilized in this study for the moving boundary problem.

Multiplying Eq. (7.1) by a unit tangential vector $\boldsymbol{\tau}$ along the moving boundary of the particle, the following is obtained:

$$\rho_0 \left(\frac{\partial \mathbf{V}_\tau}{\partial t} + (\mathbf{V} \cdot \nabla) \mathbf{V}_\tau \right) = - \frac{\partial p_e}{\partial \boldsymbol{\tau}} + \mu \Delta \mathbf{V} \cdot \boldsymbol{\tau} + n_m \theta_m \Delta \rho_m \mathbf{g} \cdot \boldsymbol{\tau} \quad (7.20)$$

Transforming Eq. (7.20) to the dimensionless form, noticing that $\Delta \mathbf{V} \cdot \boldsymbol{\tau} = - \frac{\partial \zeta}{\partial \mathbf{n}}$, and ignoring the pressure difference along the boundary of the particle (because both bioconvection and settling velocities are small), the following is obtained:

$$\frac{\partial \zeta^*}{\partial \mathbf{n}} = M \quad (7.21a)$$

$$\text{where } M = - \frac{1}{S_c} \left(\frac{\partial \mathbf{V}_\tau^*}{\partial t^*} + (\mathbf{V}^* \cdot \nabla) \mathbf{V}_\tau^* \right) - R_m n_m \hat{\mathbf{y}} \cdot \hat{\boldsymbol{\tau}} \quad (7.21b)$$

Discretizing Eq. (7.a) at the surface of the particle:

$$\frac{\partial \zeta^*(r_0^*, \theta)}{\partial \mathbf{n}} = \frac{-3\zeta^*(r_0^*, \theta) + 4\zeta^*(r_0^* + \Delta r^*, \theta) - \zeta^*(r_0^* + 2\Delta r^*, \theta)}{2\Delta r^*} = M \quad (7.22)$$

Substituting Eq. (7.19) into Eq. (22) and solving for $\psi^*(r_0^*, \theta)$:

$$\psi^*(r_0^*, \theta) = -\frac{4(\Delta r^*)^3 M - 8(\Delta r^*)^2 \zeta^*(r_0^* + \Delta r^*, \theta) + 2(\Delta r^*)^2 \zeta^*(r_0^* + 2\Delta r^*, \theta)}{21}$$

$$+ \frac{\left(6\Delta r^* - 2\frac{(\Delta r^*)^2}{r_0^*}\right) V_\theta^*(r_0^*, \theta)}{7} + \frac{8}{7} \psi^*(r_0^* + \Delta r^*, \theta)$$

$$- \frac{1}{7} \psi^*(r_0^* + 2\Delta r^*, \theta) + \frac{2}{7} \frac{(\Delta r^*)^2}{r_0^*} \frac{\partial V_r^*}{\partial \theta}$$
(7.23)

Equations (7.19) and (7.23) provide necessary boundary conditions for the streamfunction and vorticity on the surface of the moving particle.

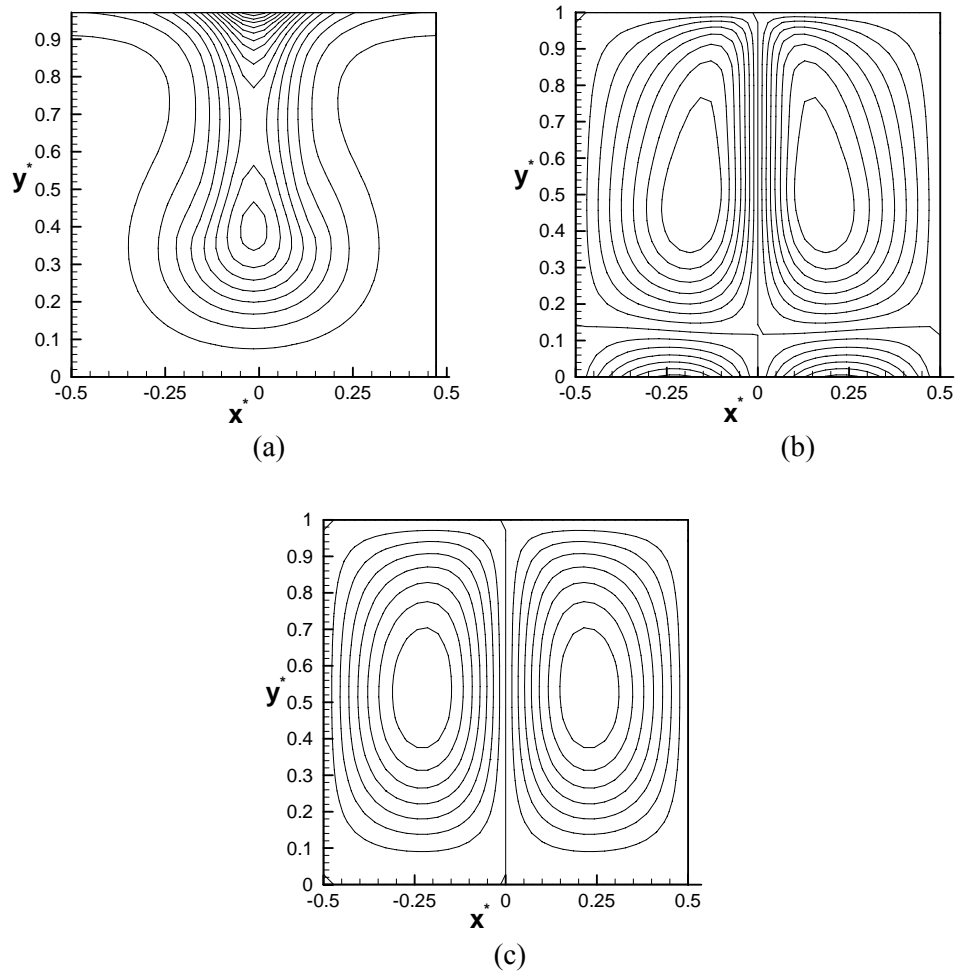


Figure 7-3. Steady-state bioconvection plume: (a) Dimensionless number density of microorganisms, (b) Contour lines of the dimensionless vorticity, (c) Contour lines of the dimensionless streamfunction

Initially, at $t^* = 0$, the bioconvection plume is fully developed (see Fig. 7.3). The particle is released with zero initial velocity at some distance beneath the free surface to keep all subgrid nodes inside the computational domain.

7.2.5 Numerical Procedure

A conservative finite-difference scheme is utilized to discretize the governing equations in both Cartesian and polar coordinate systems. An implicit scheme with Euler backward differencing in time and central differencing in space is utilized. A line-by-line tri-diagonal matrix algorithm and iteration technique with over-relaxation for the number density of microorganisms on the global grid and under-relaxation for other variables for both global and subgrid nodal points is used to solve the nonlinear discretized equations. A staggered mesh is utilized in which the streamfunction and vorticity are stored in one nodal set while the number density of microorganisms is stored in another nodal set. The mesh is chosen such that the number density nodes lie in the interior of the computational domain while the streamfunction and vorticity nodes lie in the interior and at the boundary of the domain. Computations are performed on a single 3.0 GHz Intel Xeon processor on the North Carolina State University IBM p690 supercomputer. The typical CPU time required for computing particle settling from just beneath the free surface to near the bottom of the computational domain (on a 36×36 uniform global mesh and a 15×36 non-uniform polar mesh) is approximately 50 hours. Numerical stability requires the dimensionless time step of 2×10^{-7} ; the average number of iterations per timestep is 100 (in the beginning of settling the number of iterations is large and it decreases as the settling process goes on). The convergence criterion is that the maximum relative variation of the dimensionless vorticity, streamfunction, and number density of microorganisms in every nodal point between two iterations does not exceed 10^{-7} .

7. 3. RESULTS AND DISCUSSION

Values of the physical properties, geometrical parameters, and dimensionless parameters utilized in computations are summarized in Table 7.1. One of the aims of computations is to investigate the effect of the settling particle on the bioconvection plume. Five cases (A-E) with different particle release positions, different particle densities, and different number of periodic cells (one or two) in the computational domain are investigated. Parameter values for these five cases are summarized in Table 7.2. To ensure that all subgrid point are located within the global mesh, the particle is released at some distance beneath the free surface (the vertical position of the free surface is $y^* = 1.0$, the center of the particle is initially located at $y^* = 0.8$, the subgrid extends to $r^* = 0.1674$).

Table 7-1. Physical properties, geometrical parameters, and values of dimensionless parameters utilized in computations

Average number density of microorganisms	\bar{n}_m	$10^{12} \text{ cells}/m^3$
Density of water	ρ_0	$10^3 \text{ kg}/m^3$
Density of microorganisms	ρ_m	$1.05 \times 10^3 \text{ kg}/m^3$
Volume of a microorganism	θ_m	$5 \times 10^{-16} m^3$
Average swimming velocity of microorganisms	W_m	$10^{-4} m/s$
Diffusivity of microorganisms	D_m	$5 \times 10^{-8} m^2/s$
Gyrotaxis orientation parameter	B	$5 s$
Kinematic viscosity of the suspension	ν	$10^{-6} m^2/s$
Height of the periodic cell	H	$0.005 m$
Width of the periodic cell	L	$0.005 m$
Dimensionless average swimming velocity of microorganisms	$W_m^* = W_m \frac{L}{D_m}$	10.000
Schmidt number	$S_c = \frac{\nu}{D_m}$	20

Gyrotaxis number	$G = \frac{BD_m}{L^2}$	10^{-2}
Bioconvection Rayleigh number	$R_m = \frac{\bar{n}_m \theta_m \Delta \rho_m g L^3}{\rho_0 \nu D_m}$	612.5
Aspect ratio of the periodic cell	$\lambda = \frac{H}{L}$	1
Radius of the particle	r_0	$9 \times 10^{-5} \text{ m}$
Density of the particle	ρ_p	$1.2 \sim 1.4 \times 10^3 \text{ kg/m}^3$

Table 7-2. Initial positions of the center of the particle for Cases A-E

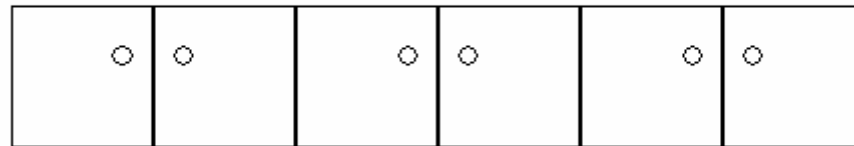
	Case A	Case B	Case C	Case D	Case E
x^*	0.0	0.3	0.5	0.3	0.3
y^*	0.8	0.8	0.8	0.8	0.8
$\frac{\rho_p}{\rho_0}$	1.2	1.2	1.2	1.2	1.4
Number of periodic cells in the computational domain	1	1	2	2	1

Bioconvection is fully developed and steady-state before the particle begins to settle. Figure 7.3 displays the steady-state bioconvection plume at $t = 0$. Figure 7.3a shows the dimensionless number density of microorganisms, Fig. 7.3b depicts contour lines of the dimensionless vorticity, and Fig. 7.3c displays contour lines of the dimensionless streamfunction. Number density of microorganisms takes on its maximum value in the center of the free surface of the computational domain while bioconvection plume is located in the center of the domain. Fluid flow is directed downward in the center of the domain and upward at its periphery.

In Case A, the particle is released in the center of the computational domain, directly in the center of the falling bioconvection plume. It is assumed that the events happening within the periodic cell are not influenced by other plumes in the neighboring periodic cells. This assumption implies that neighboring periodic cells each contain a particle settling in the center of the cell (see Fig. 7.4a). Figure 7.5 shows the dimensionless number density of microorganisms and contour lines of the dimensionless vorticity and streamfunction at different moments of time ($t^* = 0.0001$ and $t^* = 0.0007$). From Fig. 7.5 it is evident that the settling particle that goes through the bioconvection plume extends the length of the plume. Microorganisms are transported deeper into the chamber by the plume; for example, comparing Figs. 7.5a and 7.3a one can see that the local maximum of the number density of microorganisms is displaced downward from $y^* = 0.4$ to approximately $y^* = 0.3$.



(a)



(b)

Figure 7-4. Schematic diagram of neighboring periodic cells with a particle in each of them: (a) Particle is released in the center of the chamber, (b) Particle is released at one side of the chamber

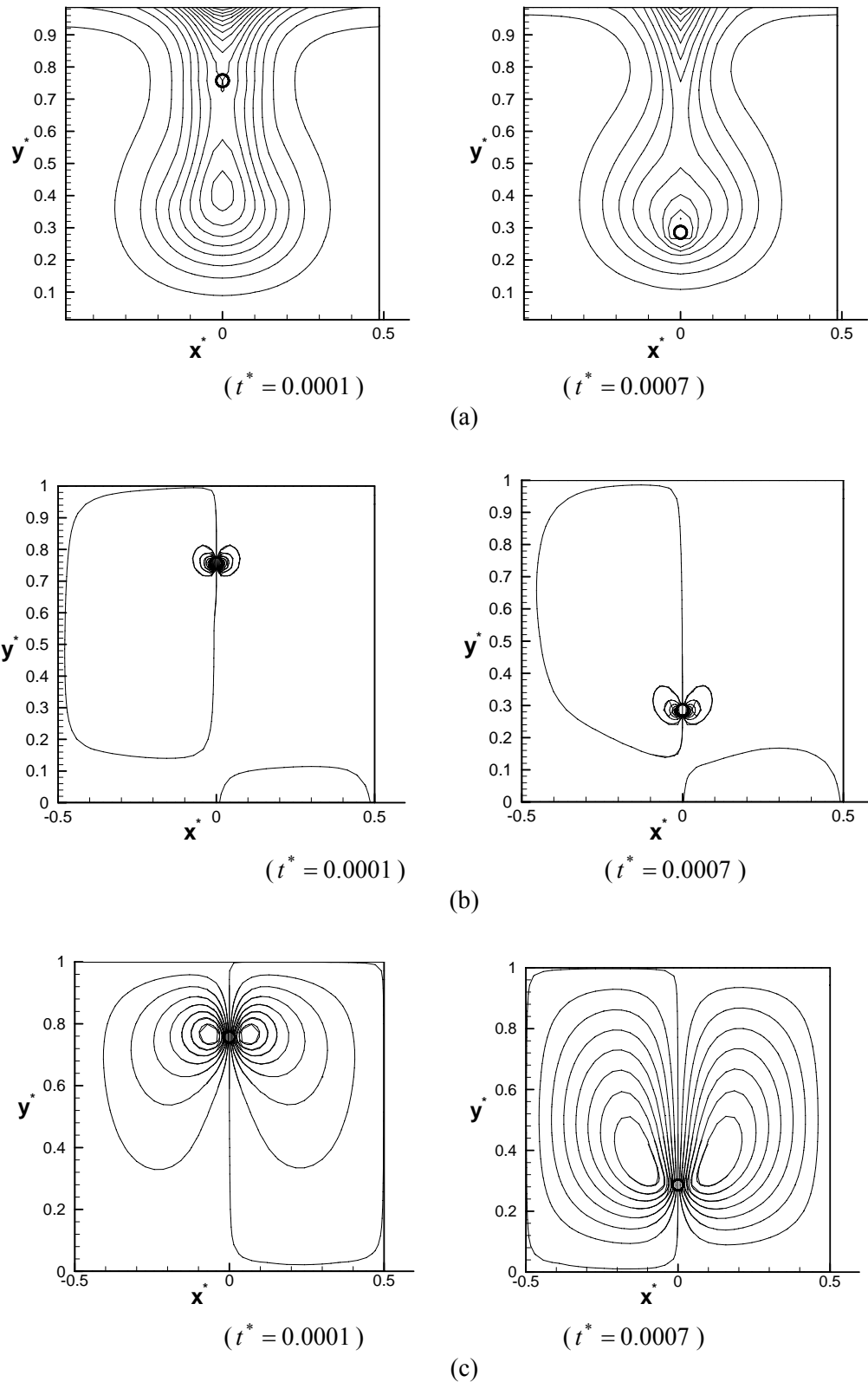


Figure 7-5. Case A: (a) Dimensionless number density of microorganisms, (b) Contour lines of dimensionless vorticity, (c) Contour lines of dimensionless streamfunction

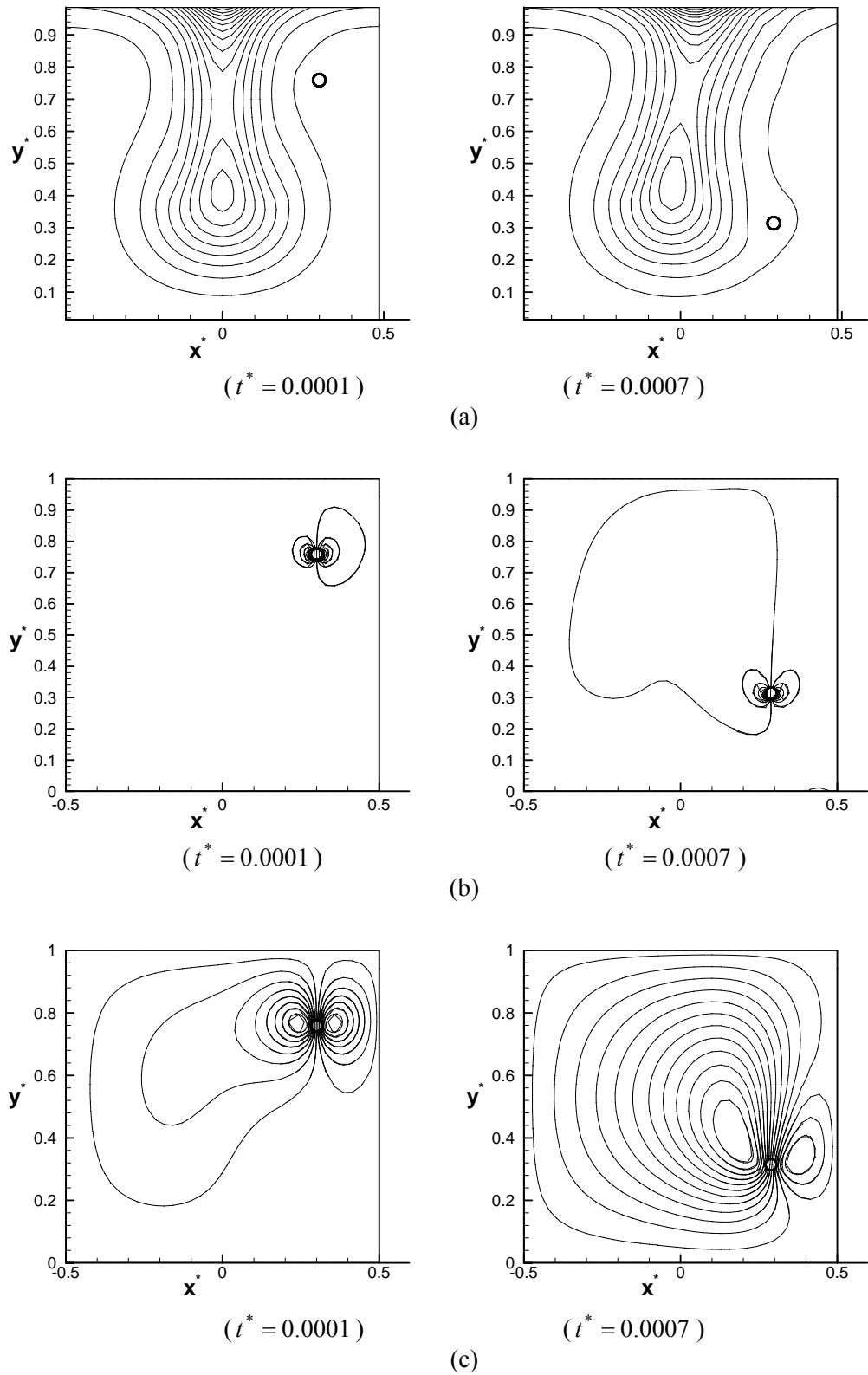


Figure 7-6. Case B: (a) Dimensionless number density of microorganisms, (b) Contour lines of dimensionless vorticity, (c) Contour lines of dimensionless streamfunction

Figure 7.6 shows the dimensionless number density of microorganisms and contour lines of the dimensionless vorticity and streamfunction at different moments of time ($t^* = 0.0001$ and $t^* = 0.0007$) for Case B. As in Case A, it is assumed that the events happening within the periodic cell are not influenced by other plumes in the neighboring periodic cells. In case B, this assumption implies that the neighboring periodic cell contains a particle whose initial position is symmetric with respect to the vertical boundary of the periodic cell (see Fig. 7.4b). The bioconvection plume is pushed away from the particle during sedimentation. This suggests that the location and the shape of the bioconvection plume can be manipulated by introducing a solid particle into the plume.

To investigate how the upward bioconvection flow affects particle sedimentation, a particle is released between two identical bioconvection plumes (Case C). To compute this case, the width of the computational domain is doubled (in case C it is $2L$) in order to include two periodic cells (see Fig. 7.7). In computing this case, the symmetry of the problem is utilized in the numerical code and the vorticity and streamfunction fields are made antisymmetric with respect to the vertical plane $x^* = 0.5$. Due to this symmetry, the x -viscous force and the torque on the particle vanish.

Figure 7.7 shows the dimensionless number density of microorganisms and contour lines of the dimensionless vorticity and streamfunction at different moments of time ($t^* = 0.0001$ and $t^* = 0.0007$) for Case C. In the beginning of the process, while the particle settles in the center of the computational domain, bioconvection plumes, which are located on both sides of the particle, keep their symmetry. As settling continues, the plumes are pushed away from the particle and are shifted to the sides of the domain; their symmetry (with respect to the centerline of the plume) is broken.

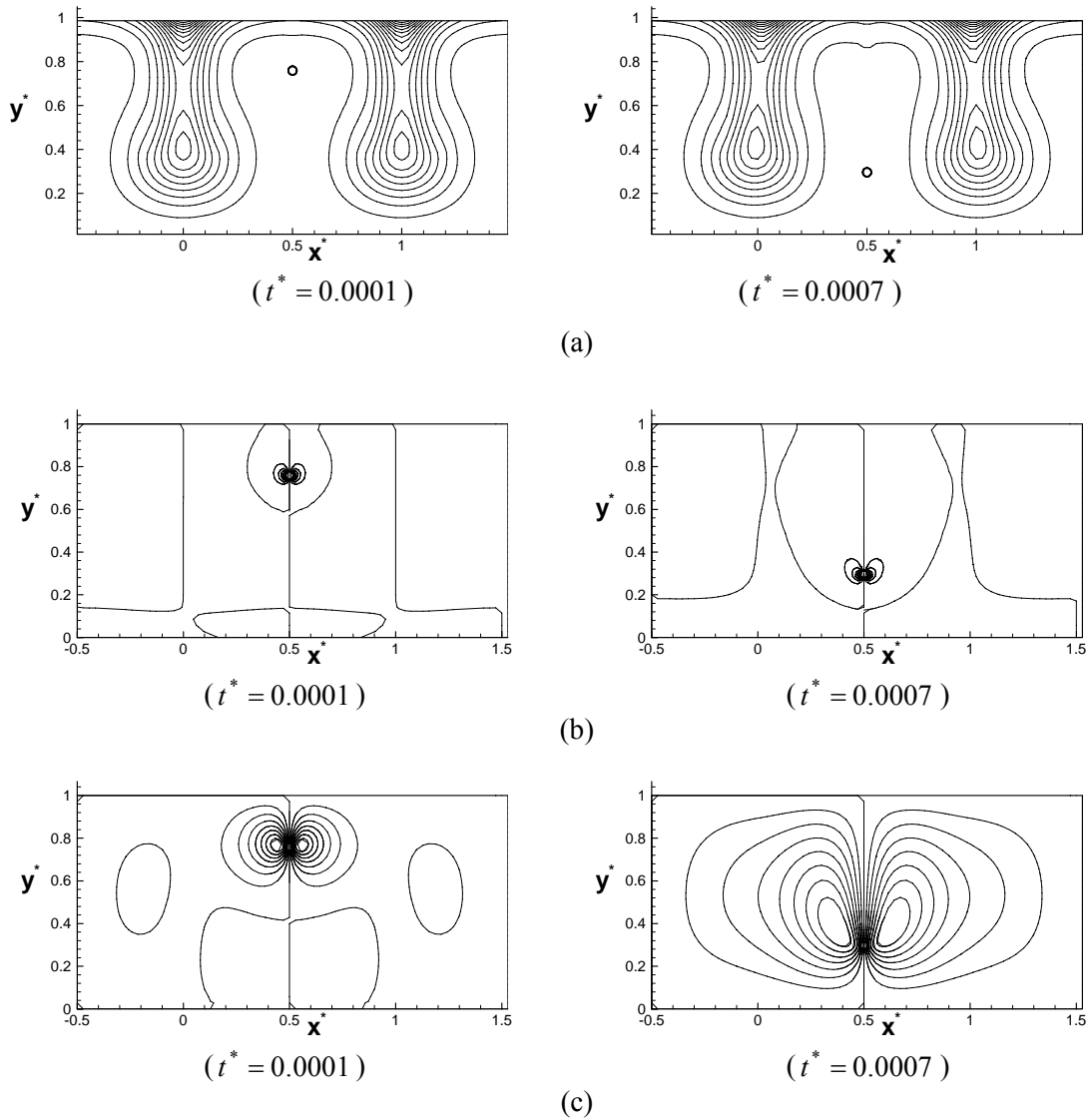


Figure 7-7. Case C: (a) Dimensionless number density of microorganisms, (b) Contour lines of dimensionless vorticity, (c) Contour lines of dimensionless streamfunction

To investigate the effect of two neighboring plumes on particle sedimentation, in Case D (as in case C) a computational domain that consists of two periodic cells is utilized, but, unlike Case C, the particle is released non-symmetrically. The dimensionless distance between the particle release position and the center of the left bioconvection plume is 0.3 and the distance between that and the center of the right plume is 0.7. Figure 7.8 shows the dimensionless number density of

microorganisms and contour lines of the dimensionless vorticity and streamfunction at different moments of time ($t^* = 0.0001$ and $t^* = 0.0007$) for Case D. The settling particle pushes both bioconvection plumes away as it settles. The left bioconvection plume is pushed farther away than the right one meaning that the particle has more effect on the plume which is closest to it.

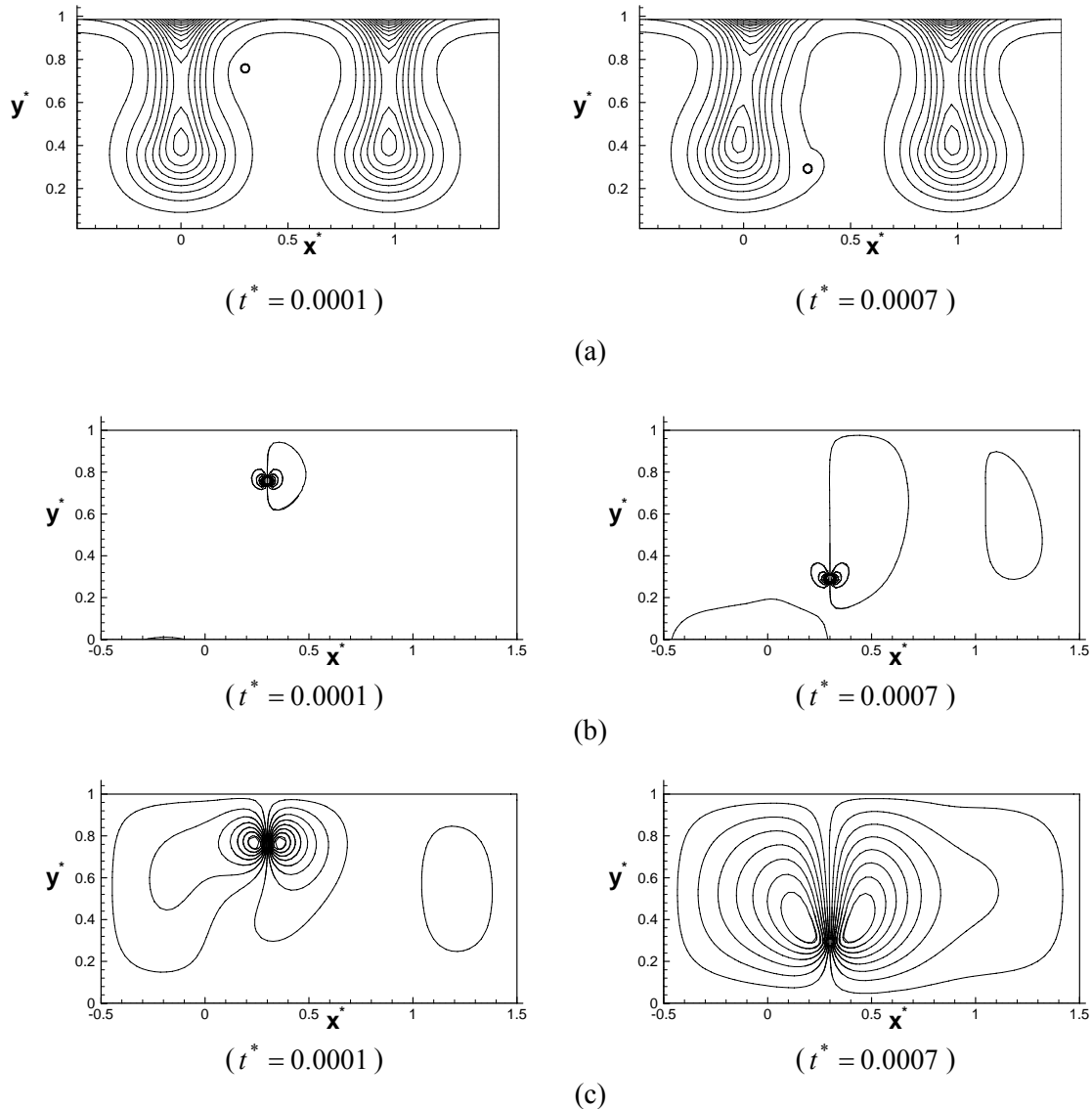


Figure 7-8. Case D: (a) Dimensionless number density of microorganisms, (b) Contour lines of dimensionless vorticity, (c) Contour lines of dimensionless streamfunction

Figure 7.9a displays the dimensionless x -velocity of the particle, V_x^* , Figure 7.9b displays the dimensionless y -velocity of the particle, V_y^* , and Figure 7.9c displays the dimensionless angular velocity of the particle, ω^* , for Cases A-C. Figure 7.9a shows that the particle in Case B has the largest x -velocity because the particle is involved in the bioconvection flow, which in Case B at the particle release position has the largest horizontal velocity of the three cases. In Case B the particle is released close to the vertical boundary of the periodic cell. Physically, the largest horizontal displacement of the particle results from the effect of this periodic boundary. In Case D it is shown that if the computational domain is enlarged to include the second periodic cell, the particle displacement in the horizontal direction becomes much smaller. In Cases A and C the bioconvection flow affecting the particle is entirely vertical (the flow is upward for Case C and downward for Case A). Although in Case A the initial position of the particle center is exactly in the center of the bioconvection plume, the particle sedimentation is not strictly vertical but shows a small (50 times smaller than in Case B) displacement in the horizontal direction. This displacement is caused by numerical inaccuracies. However, there is a different way to look at this result. As particle settles in the center of the bioconvection plume, a small disturbance (which is modeled by a numerical error in computations) can break the symmetry and make the particle shift to either side. Once the particle is shifted, its displacement from the center of the domain increases monotonically. This small horizontal velocity is not observed in Case C because, as explained above, the symmetry of the problem is utilized in numerical formulation in computing Case C.

In Fig. 7.9b, the downward velocity decreases as the particle settles. Its settling y -velocity approaches a constant value, which is the particle terminal velocity caused by the balance of gravitational and viscous forces. The viscous force is calculated using an empirical correlation provided by Sucker and Brauer [16] for a drag coefficient in a flow past a cylinder of unit length:

$$C_D = \frac{F_D}{\rho_0 U^2 r_0} \approx 1.18 + \frac{6.8}{\text{Re}^{0.89}} + \frac{1.96}{\text{Re}^{0.5}} - \frac{0.0004 \text{Re}}{1 + 3.64 \times 10^{-7} \text{Re}^2} \quad (7.24)$$

where $\text{Re} = \frac{2Ur_0}{\nu}$.

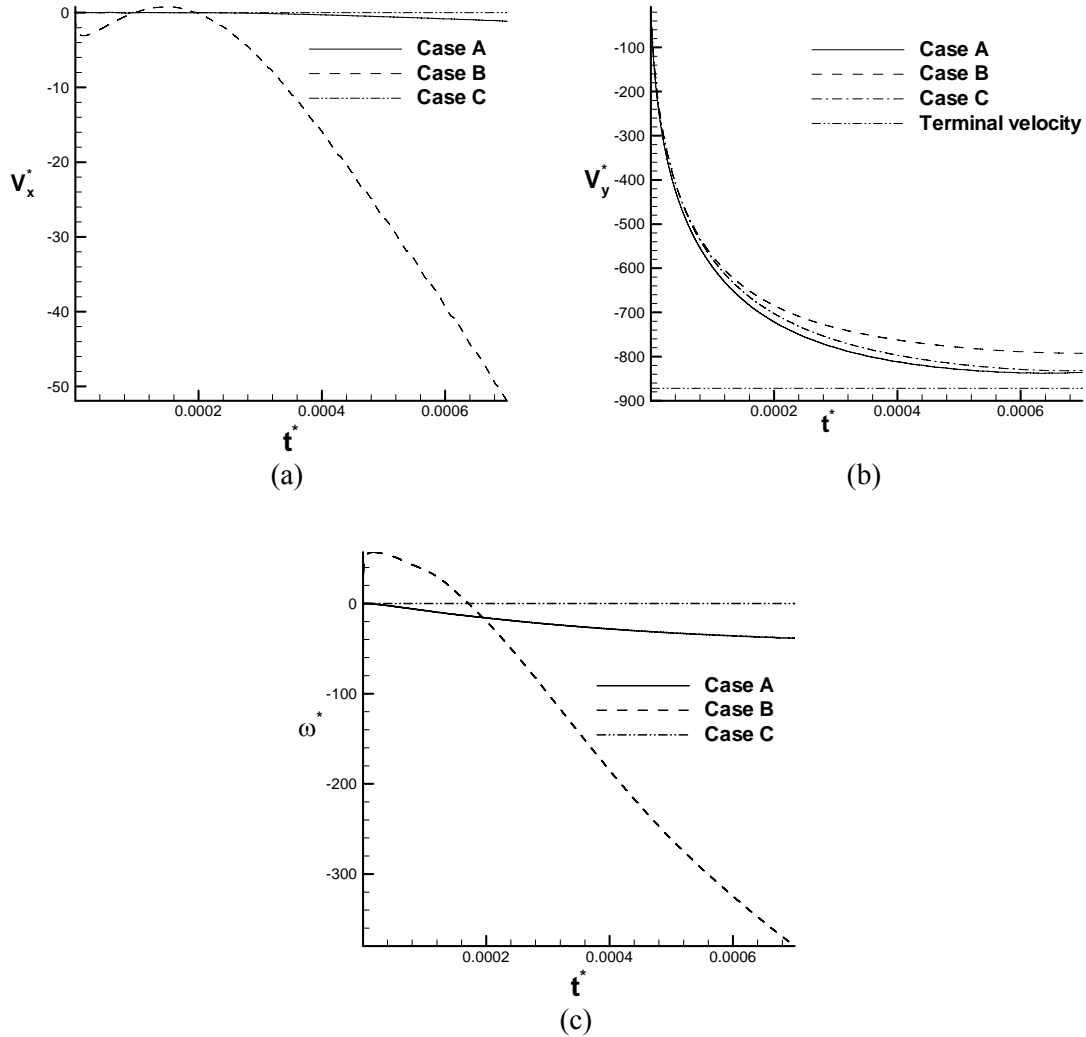


Figure 7-9. (a) Dimensionless velocity in the x direction, V_x^* , at the surface of the particle; (b) dimensionless velocity in the y direction, V_y^* , at the surface of the particle; (c) dimensionless angular velocity of the particle, ω^* , versus time for Cases A, B, and C

The particle terminal velocity, U , which is shown by a horizontal line in Fig. 8b, is found by equating gravitational and viscous forces:

$$F_D = (\rho_p - \rho_0)(\pi r_0^2)g \quad (7.25)$$

Figure 7.9b shows that particle velocities at the end of the sedimentation process approach the particle terminal velocity (obtained using experimental correlation (24)) in all Cases A-C, which validates the obtained numerical results. This figure also shows that Case A has the largest V_y ; this is because the particle release position in this case is in the center of the plume where the downward velocity of the bioconvection flow is the largest. The absolute value of the downward velocity in Case B is smaller than that in Case C; this happens because the upward bioconvection flow at $x^* = 0.3$ (particle release position for Case B) is stronger than that at $x^* = 0.5$ (particle release position for Case C).

As seen from Fig. 7.9c, the particle in Case A has a small non-zero angular velocity, which is caused by numerical inaccuracies (physically, because of the symmetry, the particle angular velocity in Case A must be zero). In Case C, the angular velocity of the particle is exactly zero because symmetry of the problem is explicitly utilized in computing this case by making the vorticity and streamfunction fields antisymmetric. In Case B, the angular velocity, ω^* , is decreasing during sedimentation (its absolute value is increasing). This means that the particle rotates in the counter-clockwise direction with an increasing speed.

To study the effect of particle density, a heavier particle is considered in Case E. In this case the particle release position and the computational domain size are identical to Case B. The paths of the particle centers during settling for Cases B, D, and E are displayed in Figure 9. The particle's path for Case E is similar to that for Case B but has larger displacements in both horizontal and vertical directions by the end of sedimentation. In Case D, the particle is displaced toward the center of the closest plume during the first half of the sedimentation process; this is caused by the direction of the

bioconvection flow in the beginning of particle sedimentation. During the second part of the sedimentation process, the direction of the bioconvection flow changes and the particle is displaced away from the center of the closest plume. The effect of the bioconvection plume in a neighboring cell is seen from comparing particle's paths for Cases B and D. Neglecting the bioconvection plume in a neighboring cell and imposing a stress-free impermeable boundary between the two cells results in a larger particle displacement away from this boundary in Case B.

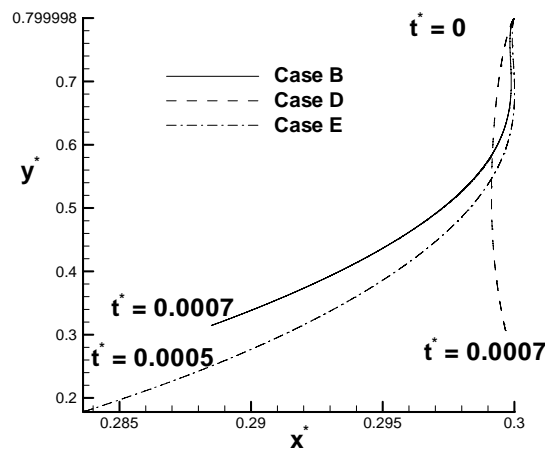


Figure 7-10. The path of the particle center for Cases B, D and E

7.4 CONCLUSIONS

A numerical method based on the streamfunction-vorticity formulation for the case of a multi-connected domain with moving boundaries is developed. This method is utilized to investigate settling of a large solid particle suddenly released in a chamber with a fully developed bioconvection flow caused by gyrotactic microorganisms. The particle settling changes the shape and location of the bioconvection plume. The particle settling is also affected by bioconvection. Because of bioconvection, the particle is pushed in both vertical and horizontal directions. Five different cases are computed with different particle release positions, different particle densities, and different sizes of the computational domain. It is found that restricting the size of the computational domain to one

periodic cell by imposing periodic boundary conditions at the vertical boundaries of the domain pushed the particle away from the periodic boundary. Numerical studies involving deeper chambers as well as physical experiments are needed to gain further understanding of this problem.

References

1. Liu, Jian-Guo and Wang, Cheng, High Order Finite Difference Methods for Unsteady Incompressible Flows in Multi-connected Domains, *Computes & Fluid*, 2004; **33**: 223-255.
2. Pedley, T.J., Hill, N.A. and Kessler, J.O., The Growth of Bioconveciton Patterns in a Uniform Suspension of Gyrotactic Microorganisms, *J. Fluid Mech.*, 1988; **195**: 223-338.
3. Ghorai, S. and Hill, N.A., Development and Stability of Gyrotactic Plumes in Bioconvection, *J. Fluid Mech.*, 1999; **400**: 1-31.
4. Ghorai, S. and Hill, N.A., Periodic Arrays of Gyrotactic Plumes in Bioconvection, *Physics of Fluids*, 2000; **12**: 5-22.
5. Kessler, J.O., Hydrodynamic Focusing of Motile Algal Cells, *Nature*, 1985; **313**: 218-220.
6. Kessler, J.O., Co-operative and Concentrative Phenomena of Swimming Microorganisms, *Contemp. Phys.*, 1985; **26**: 147-166.
7. Kessler, J.O., Wiseley, D.A., Remick, K.E. and Marthaler, D.E., Individual and Collective Dynamics of Swimming Bacteria, In Proceedings of the Workshop *Traffic and Granular Flow '97*, M. Schreckenberg and D.E. Wolf, Eds., New York, 1997: Springer, 37-51.
8. Kessler, J.O., Burnett, G.D. and Remick, K.E., Mutual Dynamics of Swimming Microorganisms and Their Fluid Habitat, In *Nonlinear Science at the Dawn of the 21st Century*, P.L. Christiansen, M.P. Sorensen, and A.C. Scott, Eds., New York, 2000: Springer, 409-426.

9. Geng, P. and Kuznetsov, A.V., Settling of Bidispersed Small Solid Particles in a Dilute Suspension Containing Gyrotactic Microorganisms, *International Journal of Engineering Science*, in press 2005.
10. Geng, P. and Kuznetsov, A.V., Introducing the Concept of Effective Diffusivity to Evaluate the Effect of Bioconvection on Small Solid Particles, *International Journal of Transport Phenomena*, **7**, 321, 2005b.
11. Hu, Howard H. and Joseph Daniel D. Direct Simulation of Fluid Particle Motions, *Theoret. Comput. Fluid Dynamics*, 1992; **3**: 285-306.
12. Gan, H., Chang, J., Feng, J. and Hu, H., Direct Numerical Simulation of The Sedimentation of Solid Particles with Thermal Convection, *J. Fluid Mech.*, 2003; **481**: 385-411.
13. Hsiao, Chao-Tsung and Chahine Georges L. Numerical Simulation of Bubble Dynamics in a Vortex Using Navier-Stokes Computations and Moving Chimera Scheme, 2001; *CAV2001*, session A10.001.
14. Russell, David and Wang Z. Jane, A Cartesian Grid Method for Modeling Multiple Moving Objects in 2D Incompressible Viscous Flow, *Journal of Computational Physics*, 2003; **191**: 177-205.
15. Pedley, T.J. and Kessler, J.O. The Orientation of Spheroidal Micro-organisms Swimming in a Flow Field, *Proc. R. Soc. Lond.*, 1987; **B231**: 47-70.

8. DYNAMICS OF LARGE SOLID PARTICLES IN BIOCONVECTIVE SEDIMENTATION

ABSTRACT

Settling of one or two large solid particles in a bioconvection flow induced by gyrotactic motile microorganisms is investigated using a 2D numerical model. The results of varying the initial positions of large particles on the bioconvection flow pattern are investigated. The Chimera method is utilized to generate subgrids around the moving particles. It is demonstrated that the introduction of a single large particle displaces bioconvection plume and changes its shape. The introduction of two particles on the same side of the bioconvection plume further displaces the plume while the introduction of two particles on opposite sides reduces this displacement. The influence of the bioconvection plume on the particles' settling paths and particles' settling velocities is investigated.

8.1 INTRODUCTION

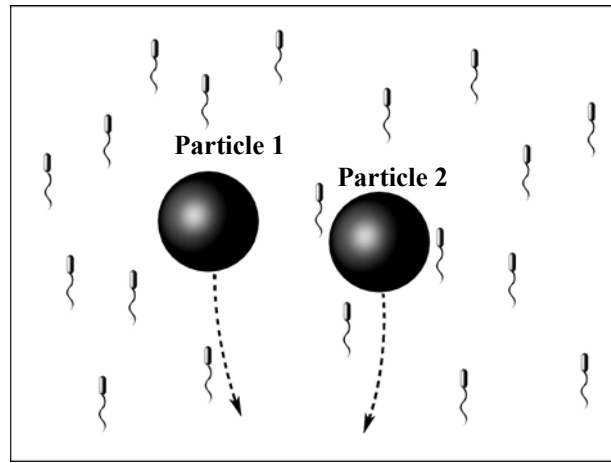
Bioconvection caused by gyrotactic microorganisms has been studied extensively, both experimentally and numerically. Bioconvection provides a method for manipulating mass transfer in microvolumes of fluids that has potential pharmaceutical and bio-technological applications. The results of this chapter bring to light the interaction between large particles and a bioconvection plume which may be utilized in controlling sedimentation in microvolumes.

Gyrotactic microorganisms, such as *Dunaliella*, *Chlamydomonas*, *Volvox*, and *Peridinium* (Pedley et al.¹), swim in a particular direction due to the balance of gravitational and viscous torques. Gyrotactic behavior causes these microorganisms to accumulate in the regions of most rapid downflow. Since these microorganisms are typically 3-5% heavier than water, the density of the suspension in the regions of downflow becomes larger than in the regions of upflow. Buoyancy increases velocity fluctuations in both upflow and downflow regions thus introducing a hydrodynamic instability (Pedley et al.¹, Ghorai and Hill^{2,3}). The induced convection fluid motion causes the development of bioconvection plumes.

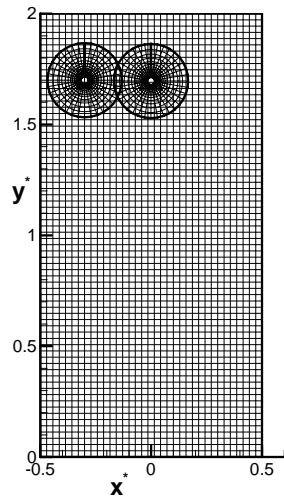
Substantial research into sedimentation has been conducted. For large particles, sedimentation velocity is related to wall separation distances (Kuusela⁴). In Liu et al.⁵ particle sedimentation and rotation near a wall is simulated. Particle-particle interactions during sedimentation are studied in Joseph et al.⁶ Singh and Joseph⁷ extend the numerical research of particle sedimentation to three dimensions. Gan et al.⁸ present a direct numerical simulation of sedimentation in a flow field induced by natural convection.

Preliminary research has been conducted involving the combined bioconvection-sedimentation problem (called here bioconvective sedimentation). Geng and Kuznetsov^{9,10} investigate the sedimentation of small solid particles in bioconvection. Sedimentation of a single large particle during bioconvection is studied in Geng and Kuznetsov¹¹.

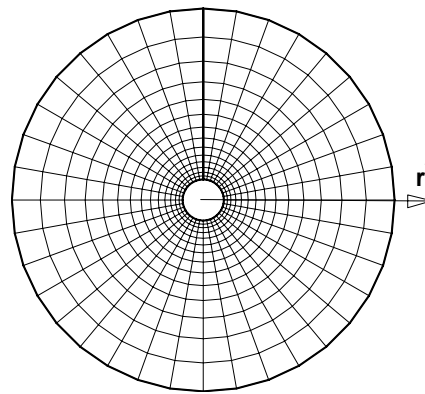
This chapter investigates sedimentation of one and two large particles in a bioconvection plume. The two-dimensional model considers two large circular particles (see Fig. 1a) settling in a chamber in which the bioconvection plume is fully developed. The height of the computational domain is H and its width is L , where L is a typical plume spacing and $\lambda = H/L$ is the aspect ratio of the chamber. This chapter uses $\lambda = 2$.



(a)



(b)



(c)

Figure 8-1. (a) Schematic diagram of two large particles settling in a bioconvection flow; (b) Chimera grid system, global and subgrid meshes; (c) Chimera grid system, subgrid mesh

The stream function-vorticity method used here is applied to a multi-connected domain that involves moving particles. In order to overcome the complication of imposing boundary conditions at moving boundaries a method similar to that used in Liu and Wang¹² is incorporated. The multiple and moving grid systems (see Figs. 1b and 1c) are formulated using the Chimera method (Chattot and Wang¹³, Houzeaux and Codina¹⁴).

8.2 GOVERNING EQUATIONS

8.2.1 Dimensional Governing Equations

Governing equations for a bioconvection plume caused by gyrotactic microorganisms are given in Ghorai and Hill^{2,3} as:

Momentum equation

$$\rho_0 \left(\frac{\partial \mathbf{V}}{\partial t} + (\mathbf{V} \cdot \nabla) \mathbf{V} \right) = -\nabla p_e + \mu \nabla^2 \mathbf{V} + n_m \theta_m \Delta \rho_m \mathbf{g} \quad (8.1)$$

Continuity equation

$$\nabla \cdot \mathbf{V} = 0 \quad (8.2)$$

Conservation of motile microorganisms

$$\frac{\partial (n_m)}{\partial t} = -\text{div}(n_m \mathbf{V} + n_m W_m \hat{\mathbf{p}} - D_m \nabla n_m) \quad (8.3)$$

where D_m is the diffusivity of microorganisms (it is assumed that all random motions of microorganisms can be approximated by a diffusive process); \mathbf{g} is the gravity vector; n_m is the number density of motile microorganisms; $\hat{\mathbf{p}}$ is the unit vector indicating the direction of microorganisms' swimming (equations for this vector are obtained in Pedley et al.¹); p_e is the excess

pressure (above hydrostatic); \mathbf{V} is the velocity vector; t is the time; (V_x, V_y) ; $W_m \hat{\mathbf{p}}$ is the vector of microorganisms' average swimming velocity (W_m is assumed to be constant); $\Delta\rho_m$ is the density difference between microorganisms and water, $\rho_m - \rho_0$; θ_m is the volume of a microorganism; μ is the dynamic viscosity of the suspension, assumed to be approximately the same as that of water; and ρ_0 is the density of water.

Applying the second Newton's law to particles, the motion of particles can be described by equations (8.4a) and (8.4b):

$$m_p \frac{dV_x}{dt} = F_x, \quad m_p \frac{dV_y}{dt} = F_y, \quad I \frac{d\boldsymbol{\omega}}{dt} = \mathbf{T} \quad (8.4a)$$

where $\mathbf{F} = (F_x, F_y)$ is the total external force on a particle, $I = m_p \left(\frac{d^2}{8} \right)$ is the polar moment of inertia of a particle, $m_p = \rho_p \left(\frac{\pi d^3}{4} \right)$ is the mass of a particle (d is the diameter of a particle), \mathbf{T} is the mechanical torque on a particle, and $\boldsymbol{\omega}$ is the particle's angular velocity vector.

$$\frac{dx}{dt} = V_x, \quad \frac{dy}{dt} = V_y, \quad \frac{d\theta}{dt} = \omega \quad (8.4b)$$

where ω is the particle's angular velocity.

In this research, the two particles are assumed to be of identical mass and size. Particle density is uniform so that the particle geometrical center is also its center of mass.

The fluid exerts a viscous force on the surface of the particles. Since particles are symmetric, the viscous friction on the surface of a particle provides the only contribution to the torque:

$$F_x = \int_{\Omega} \left(\mu \frac{\partial V_x}{\partial \mathbf{n}} \cdot \hat{\mathbf{x}} \right) ds \quad (8.5a)$$

$$F_y = \int_{\Omega} \left(\mu \frac{\partial \mathbf{V}_\tau}{\partial \mathbf{n}} \cdot \hat{\mathbf{y}} \right) ds + \frac{\rho_p - \rho_0}{\rho_p} \left(\pi d^2 / 4 \right) \mathbf{g} \quad (8.5b)$$

$$\Gamma = \int_{\Omega} \left(\mu \frac{\partial \mathbf{V}_\tau}{\partial \mathbf{n}} \cdot \frac{d}{2} \right) ds \quad (8.5c)$$

where \mathbf{V}_τ is the tangential fluid velocity along the surface of a particle and Ω is the surface of a particle.

8.2.2 Dimensionless Governing Equations

The governing equations can be recast into the following dimensionless form by utilizing the streamfunction-vorticity formulation:

$$\zeta^* = -\nabla^2 \psi^* \quad (8.6)$$

$$S_c^{-1} \left(\frac{\partial \zeta^*}{\partial t^*} + V_x^* \frac{\partial \zeta^*}{\partial x^*} + V_y^* \frac{\partial \zeta^*}{\partial y^*} \right) = \nabla^2 \zeta^* - \left(R_m \frac{\partial n_m^*}{\partial x^*} \right) \quad (8.7)$$

$$\frac{\partial n_m^*}{\partial t^*} = -\nabla \cdot \left[n_m^* (\mathbf{V}^* + W_m^* \hat{\mathbf{p}}) - \nabla n_m^* \right] \quad (8.8)$$

The dimensionless variables in equations (8.6)-(8.8) are defined as:

$$\begin{aligned} x^* &= \frac{x}{L}, \quad y^* = \frac{y}{L}, \quad t^* = \frac{D_m}{L^2} t, \quad u^* = \frac{\partial \psi^*}{\partial y^*}, \quad v^* = -\frac{\partial \psi^*}{\partial x^*}, \quad \mathbf{V}^* = \mathbf{V} \frac{L}{D_m}, \\ W_m^* &= W_m \frac{L}{D_m}, \quad n_m^* = \frac{n_m}{\bar{n}_m}, \quad S_c = \frac{\nu}{D_m}, \quad G = \frac{BD_m}{L^2}, \quad R_m = \frac{\bar{n}_m \theta_m \Delta \rho_m g L^3}{\rho_0 \nu D_m} \end{aligned} \quad (8.9)$$

where G is the gyrotaxis number, R_m is the bioconvection Rayleigh number, S_c is the Schmidt number, ν is the kinematic viscosity of the suspension, and asterisks denote dimensionless quantities.

By neglecting inertia terms in Eq. (8.1) (which is justified for bioconvection flows because of a very low Reynolds number), Ghorai and Hill^{2, 3} have shown that the vector $\hat{\mathbf{p}}$, which determines the swimming direction of microorganisms, can be computed as:

$$\hat{\mathbf{p}} = \begin{cases} \left(-\kappa - (\kappa^2 - 1)^{1/2}, 0 \right), & \kappa < -1 \\ \left(-\kappa, (1 - \kappa^2)^{1/2} \right), & |\kappa| \leq 1 \\ \left(-\kappa + (\kappa^2 - 1)^{1/2}, 0 \right), & \kappa > 1 \end{cases} \quad (8.10)$$

where $\kappa = B\zeta = G\zeta^*$. The parameter B is called the “gyrotactic orientation parameter” by Pedley and Kessler¹⁵; it is defined as:

$$B = \frac{4\pi\mu a^3}{m_m gh} \quad (8.11)$$

where a is the radius of a microorganism, h is the displacement of the center of mass of a gyrotactic microorganism from its center of buoyancy, and m_m is the mass of a microorganism.

8.2.3 Initial and Boundary Conditions

It is assumed that bioconvection plumes occur periodically. The two-dimensional computational domain coincides with a periodic cell that contains a single bioconvection plume. It is assumed that the particles do not interact with any bioconvection plumes outside the computational domain. Ghorai and Hill [3] studied the effect of the aspect ratio ($\lambda = H/L$) on bioconvection and found that the steady-state bioconvection plume was stable for $\lambda = 2$. Increasing λ slowed down the solution's convergence to steady-state; oscillations were observed for $\lambda = 5$ so that the steady-state could never be reached. This chapter uses $\lambda = 2$.

The no-slip boundary condition is utilized at the bottom wall. The top and the side boundaries of the computational domain are assumed impermeable to the fluid and stress-free. Under these assumptions, the boundary conditions for the computational domain can be presented as:

$$\psi^* = 0 \text{ at } y^* = 0, \lambda \text{ and } x^* = \pm 0.5, \quad (8.12a)$$

$$\frac{\partial \psi^*}{\partial y^*} = 0 \text{ at } y^* = 0, \quad (8.12b)$$

$$\frac{\partial^2 \psi^*}{\partial y^{*2}} = 0 \text{ at } y^* = \lambda, \text{ and } \frac{\partial^2 \psi^*}{\partial x^{*2}} = 0 \text{ at } x^* = \pm 0.5. \quad (8.12c)$$

Normal fluxes of microorganisms are zero through all boundaries of the computational domain and the surfaces of the moving particles:

$$\mathbf{J}_m^* \cdot \hat{\mathbf{y}} = 0 \text{ at } y^* = 0, \lambda, \mathbf{J}_m^* \cdot \hat{\mathbf{x}} = 0 \text{ at } x^* = \pm 0.5 \quad (8.13a)$$

$$\mathbf{J}_m^* \cdot \hat{\mathbf{r}} = 0 \text{ at surface of a moving particle} \quad (8.13b)$$

where $\hat{\mathbf{x}}$, $\hat{\mathbf{y}}$, and $\hat{\mathbf{r}}$ are the unit vectors in the x -, y -, and r -directions, respectively, and

$$\mathbf{J}_m^* = n_m^* (\mathbf{V}^* + W_m^* \hat{\mathbf{p}}) - \nabla n_m^* \quad (8.14)$$

is the dimensionless flux of microorganisms.

The streamfunction and vorticity are defined in the polar coordinate system for the subgrids created around the particles as follows:

$$\zeta^* = - \left(\frac{\partial^2 \psi^*}{\partial r^{*2}} + \frac{1}{r^*} \frac{\partial \psi^*}{\partial r^*} + \frac{1}{r^{*2}} \frac{\partial^2 \psi^*}{\partial \theta^2} \right) \quad (8.15)$$

$$V_r^* = \frac{1}{r^*} \frac{\partial \psi^*}{\partial \theta}; V_\theta^* = -\frac{\partial \psi^*}{\partial r^*} \quad (8.16)$$

where r^* is a dimensionless coordinate used around the particle (see Fig. 8.1c), and V_r^* and V_θ^* are the dimensionless velocity components in the polar coordinate system.

At the surface of the settling particles, the no-slip boundary condition is imposed. Geng and Kuznetsov [11] have shown that the values of the streamfunction and vorticity on a moving boundary in a multi-connected domain can be calculated numerically by the following procedure. Using Taylor series expansion for $\psi^*(r^*, \theta)$ near the moving boundary, $\frac{\partial^2 \psi^*}{\partial \theta^2}$ on the particle surface is expressed

as:

$$\frac{\partial^2 \psi^*}{\partial r^{*2}} = \frac{8\psi^*(1, \theta) - \psi^*(2, \theta) - 7\psi^*(0, \theta) - 6\Delta r \frac{\partial \psi^*}{\partial r^*}}{2\Delta r^2} + o((\Delta r)^4) \quad (8.17)$$

The equation to calculate $\zeta^*(0, \theta)$ on the particle surface is derived by substituted Eq. (8.17) into Eq. (8.15):

$$\zeta^*(0, \theta) = \frac{\left(-6\Delta r + \frac{2(\Delta r)^2}{r_0}\right) V_\theta^*(0, \theta) - (8\psi^*(1, \theta) - \psi^*(2, \theta) - 7\psi^*(0, \theta))}{2(\Delta r)^2} - \frac{1}{r_0} \frac{\partial V_r^*}{\partial \theta} \quad (8.18)$$

where r_0 is the radius of the particle.

To calculate the boundary values of the streamfunction on a moving boundary, Eq. (8.1) is multiplied by a unit tangential vector τ along the surface of a particle. Ignoring the pressure difference along the particle's surface, the following equation for $\psi^*(0, \theta)$ is obtained:

$$\psi^*(0, \theta) = -\frac{4(\Delta r)^3 M - 8(\Delta r)^2 \zeta^*(1, \theta) + 2(\Delta r)^2 \zeta^*(2, \theta)}{21} + \frac{\left(6\Delta r - 2\frac{(\Delta r)^2}{r_0}\right) V_{\theta}^*(0, \theta)}{7} + \frac{8}{7} \psi^*(1, \theta) - \frac{1}{7} \psi^*(2, \theta) + \frac{2}{7} \frac{(\Delta r)^2}{r_0} \frac{\partial V_r^*}{\partial \theta} \quad (8.19)$$

where

$$M = \frac{\partial \zeta^*}{\partial \mathbf{n}} = -\frac{1}{S_c} \left(\frac{\partial \mathbf{V}_{\tau}^*}{\partial t^*} + (\mathbf{V}^* \cdot \nabla) \mathbf{V}_{\tau}^* \right) - R_m n_m \hat{\mathbf{y}} \cdot \hat{\mathbf{t}} \quad (8.20)$$

Initially, at $t^* = 0$, the bioconvection plume is assumed fully developed. The two particles are released just beneath the free surface to keep all subgrid nodes located inside the computational domain. It is assumed that the particles' initial velocity is zero.

8.2.4 Numerical Procedure

In this chapter, following the Chimera method (Chattot and Wang¹³), two subgrids are created; one around each particle, and a global rectangular grid is created for the global flow field, as demonstrated in Figs. 8-1b and 8-1c. Governing equations (8.6)-(8.8) for the global grid and the two subgrids are solved separately. The exchange of information between the global grid and the subgrids is implemented by interpolation. The unknown boundary values of variables on the subgrids are computed by interpolating these boundary points onto the known global grid. Therefore, the computational problem for the subgrids is transformed to a boundary value problem. The same procedure is required for computations on the global grid except that two artificial unknown inner boundaries (projected onto subgrids) are created around the moving particles.

A conservative finite-difference scheme is utilized to discretize the governing equations in both the Cartesian and polar coordinate systems. An implicit scheme with Euler backward differencing in time

and central differencing in space is utilized. A line-by-line tri-diagonal matrix algorithm and an iteration technique with over-relaxation for the number density of microorganisms on the global grid and under-relaxation for other variables for both global and subgrid nodal points is used to solve the discretized equations. A staggered mesh is utilized in which the streamfunction and vorticity are stored in one nodal set while the number density of microorganisms is stored in another nodal set. Computations are performed on a 3.0 GHz Intel Xeon processor. Typical CPU time required to investigate particles settling from just beneath the free surface to near the bottom of the computational domain for a 36×72 uniform global mesh and two 15×36 non-uniform curvilinear meshes is 200 hours.

8.3 RESULTS AND DISCUSSION

Values of physical properties and dimensionless parameters utilized in computations are summarized in Table 1. The parameters of microorganisms are identical to those given in Table 1 of Ghorai and Hill³. Four cases with different particle initial positions are investigated. The same initial position ($x^* = -0.3, y^* = 1.8$) is used for one particle (denoted Particle 1) in all cases (A-D). In Case A Particle 1 is released by itself while in Cases B-D a second particle (denoted Particle 2) is released at varying positions. Positions of centers of the particles at $t = 0$ are summarized in Table 2. Particles are released beneath the free surface so that the subgrids are located completely inside the global grid; since the vertical position of the free surface corresponds to $y^* = 2.0$, the centers of the particles are initially located at $y^* = 1.8$.

Table 8-1. Physical properties, geometrical parameters, and values of dimensionless parameters utilized in computations

Average number density of microorganisms	\bar{n}_m	$10^{12} \text{ cells/m}^3$
Density of water	ρ_0	10^3 kg/m^3
Density of microorganisms	ρ_m	$1.05 \times 10^3 \text{ kg/m}^3$
Volume of a microorganism	θ_m	$5 \times 10^{-16} \text{ m}^3$
Average swimming velocity of microorganisms	W_m	10^{-4} m/s
Diffusivity of microorganisms	D_m	$5 \times 10^{-8} \text{ m}^2/\text{s}$
Gyrotaxis orientation parameter	B	5 s
Kinematic viscosity of the suspension	ν	$10^{-6} \text{ m}^2/\text{s}$
Height of the computational domain	H	0.01 m
Width of the computational domain	L	0.005 m
Dimensionless average swimming velocity of microorganisms	$W_m^* = W_m \frac{L}{D_m}$	10.000
Schmidt number	$S_c = \frac{\nu}{D_m}$	20
Gyrotaxis number	$G = \frac{BD_m}{L^2}$	10^{-2}
Bioconvection Rayleigh number	$R_m = \frac{\bar{n}_m \theta_m \Delta \rho_m g L^3}{\rho_0 \nu D_m}$	612.5
Aspect ratio of the computational domain	$\lambda = \frac{H}{L}$	2
Radius of the particles	r_0	$9 \times 10^{-5} \text{ m}$
Density of the particles	ρ_p	$1.1 \times 10^3 \text{ kg/m}^3$

Table 8-2. Initial positions of particle centers for Cases A-D

	Case A	Case B	Case C	Case D
Particle 1: (x^*, y^*)	(-0.3, 1.8)	(-0.3, 1.8)	(-0.3, 1.8)	(-0.3, 1.8)
Particle 2: (x^*, y^*)	No Particle 2 in Case A	(-0.1, 1.8)	(0.1, 1.8)	(0.3, 1.8)

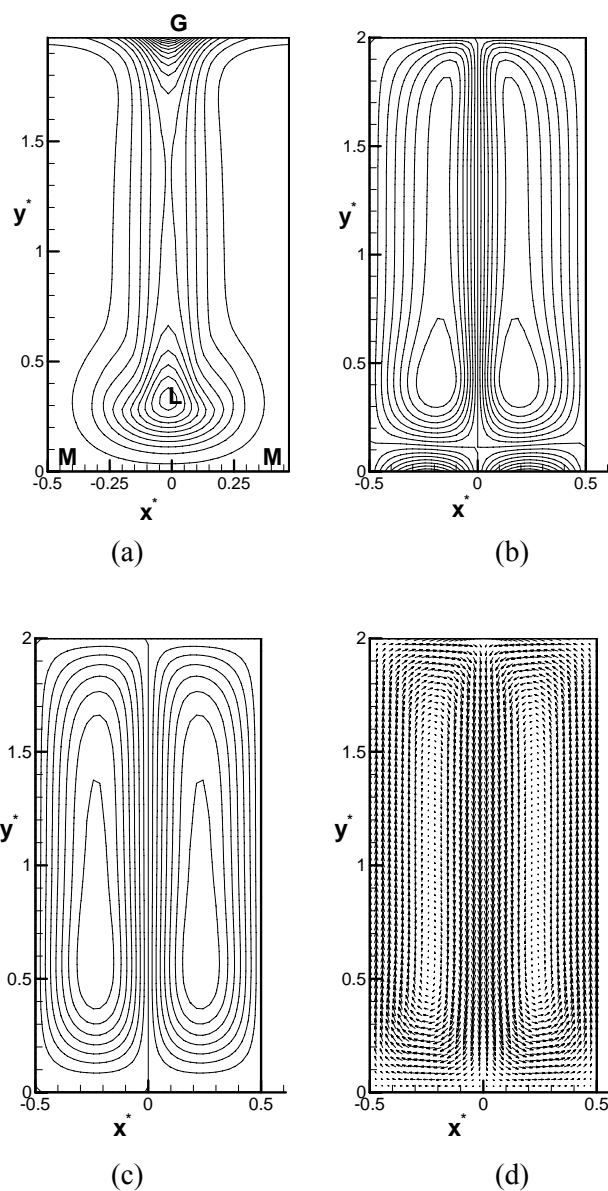


Figure 8-2. Steady-state bioconvection plume: (a) Dimensionless number density of microorganisms, (b) Contour lines of the dimensionless vorticity, (c) Contour lines of the dimensionless streamfunction, (d) Vector field of fluid velocity

To quantify the influence of particle sedimentation, a purely bioconvection flow pattern is used as a reference (depicted in Fig. 8-2). Figure 8-2a shows the dimensionless number density of microorganisms, Fig. 8-2b shows contour lines of the dimensionless vorticity, Fig. 8-2c displays contour lines of the dimensionless streamfunction, and Fig. 8-2d shows the vector field of the fluid velocity. The bioconvection plume is located in the center of the computational domain. The number density of microorganisms takes on its maximum value (a *global maximum*) in the center of the free surface (marked by G in Fig. 8-2a). The fluid flow is directed downward in the center of the domain and upward at its periphery, this flow transports microorganisms from the upper fluid layer to the bottom of the domain and causes a *local maximum* of their number density (marked by L in Fig. 8-2a). The number density of microorganisms takes on its *minimum* value at the bottom corners of the computational domain (marked by M in Fig. 8-2a).

Data presented in Fig. 8-2 are in good agreement with those plotted in Fig. 8-9 of Ghorai and Hill².

In Case A Particle 1 is released by itself in the bioconvection plume. Figure 8-3 shows the dimensionless number density of microorganisms, contour lines of the dimensionless vorticity, contour lines of the dimensionless streamfunction, and a vector field of the fluid velocity for Case A 1.0 s after Particle 1 is released. Figure 3a shows that the bioconvection plume is displaced away from Particle 1 as the particle settles on the left side of the bioconvection plume. Convective circulations are developed on both sides of the particle. The convective circulation on the right side of the particle is stronger than on the left (see Figs. 8-3c and 8-3d). From Fig. 8-3a a comparison between $t = 0.1 s$ and $t = 1.1 s$ shows that the maximum value of the number density of microorganisms is shifted from the center of the free surface to the left and is located directly above the particle (the meanings of G, L, and M in Fig. 8-3a are the same as that in Fig. 8-2a). To the left of the particle in the upper part of the computational domain the fluid velocity is directed downward while in the lower part of the domain the fluid velocity is directed upward (the shear-free boundary condition used at the domain's side walls implies that the horizontal velocity vanishes but the vertical velocity does not). Counter-

propagating vertical jets (marked by block arrows in Fig. 8-3d) collide to the left of the particle and create a horizontal jet directed to the right. Figure 8-7d shows that Particle 1 is displaced by this horizontal jet from $x^* = -0.3$ to $x^* = -0.2$ as it settles.

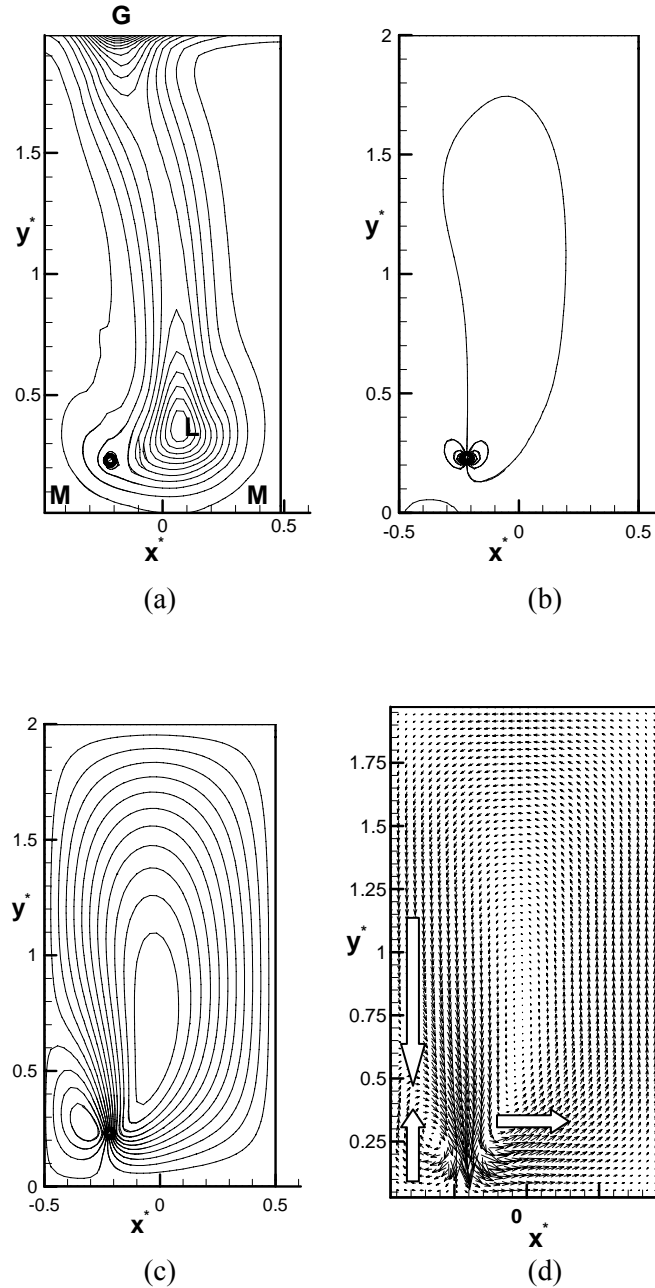
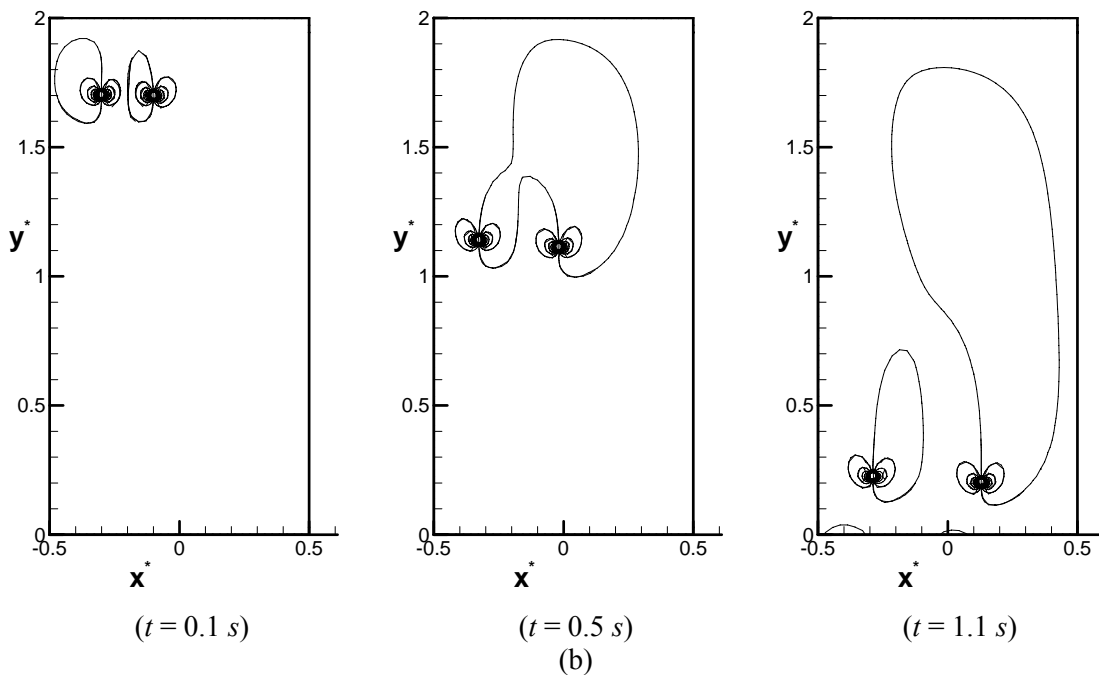
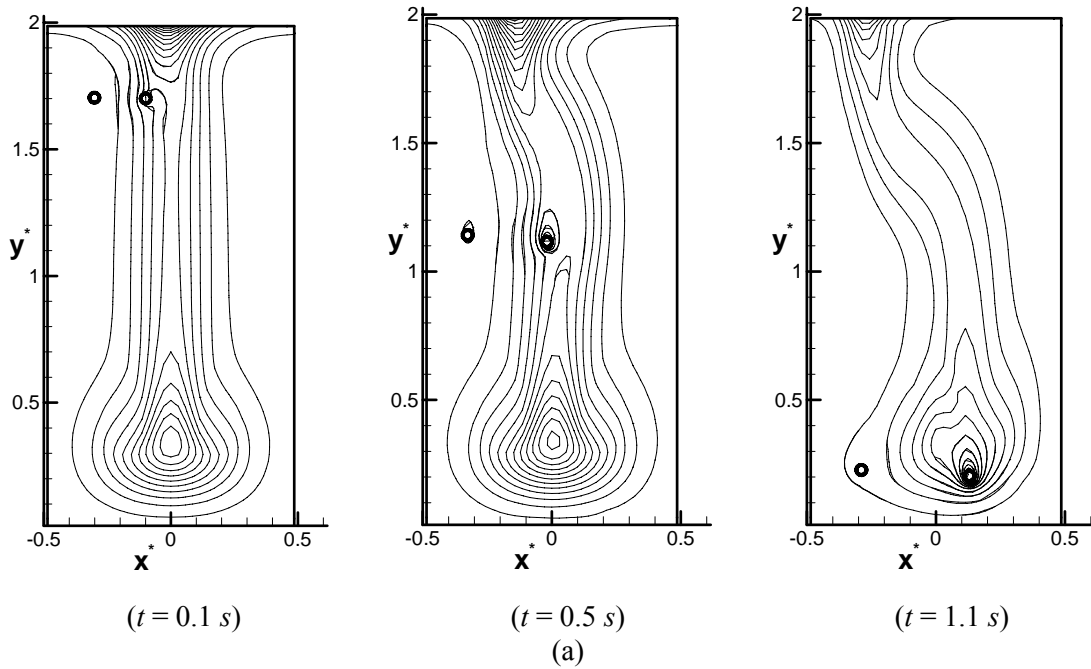


Figure 8-3. Case A, $t = 1.0$ s: (a) Dimensionless number density of microorganisms, (b) Contour lines of the dimensionless vorticity, (c) Contour lines of the dimensionless streamfunction, (d) Vector field of fluid velocity

To see how the two particles affect bioconvection as well as how they influence each other's sedimentation, Particle 2 is released simultaneously with Particle 1. Particle 1 retains the same initial position while the initial position of Particle 2 is varied (see Table 8-2).



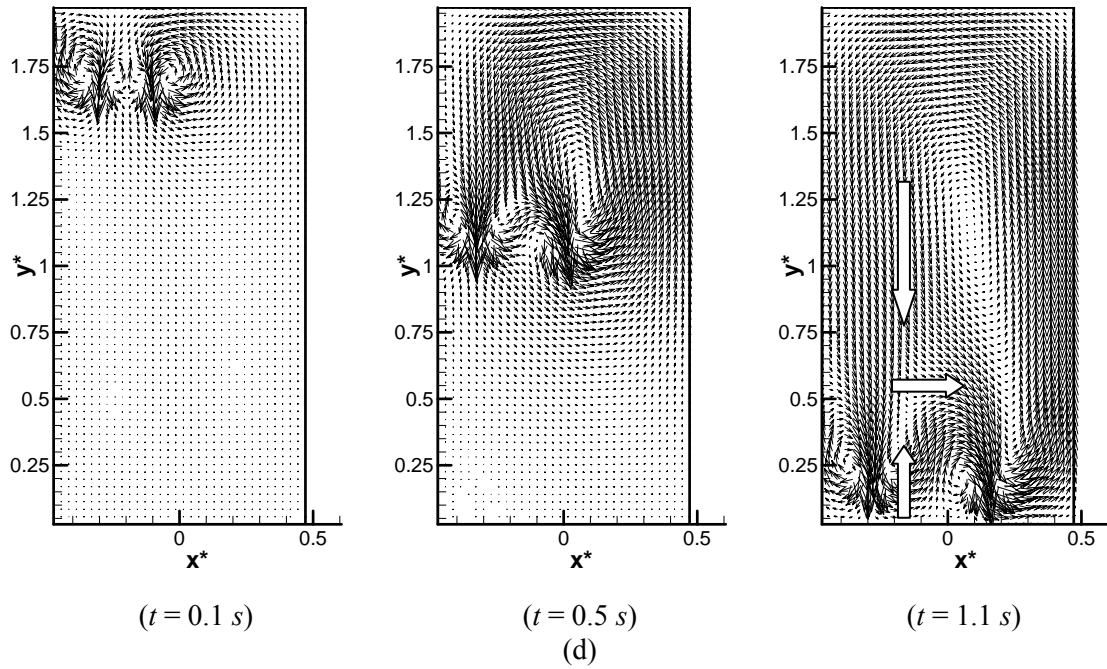
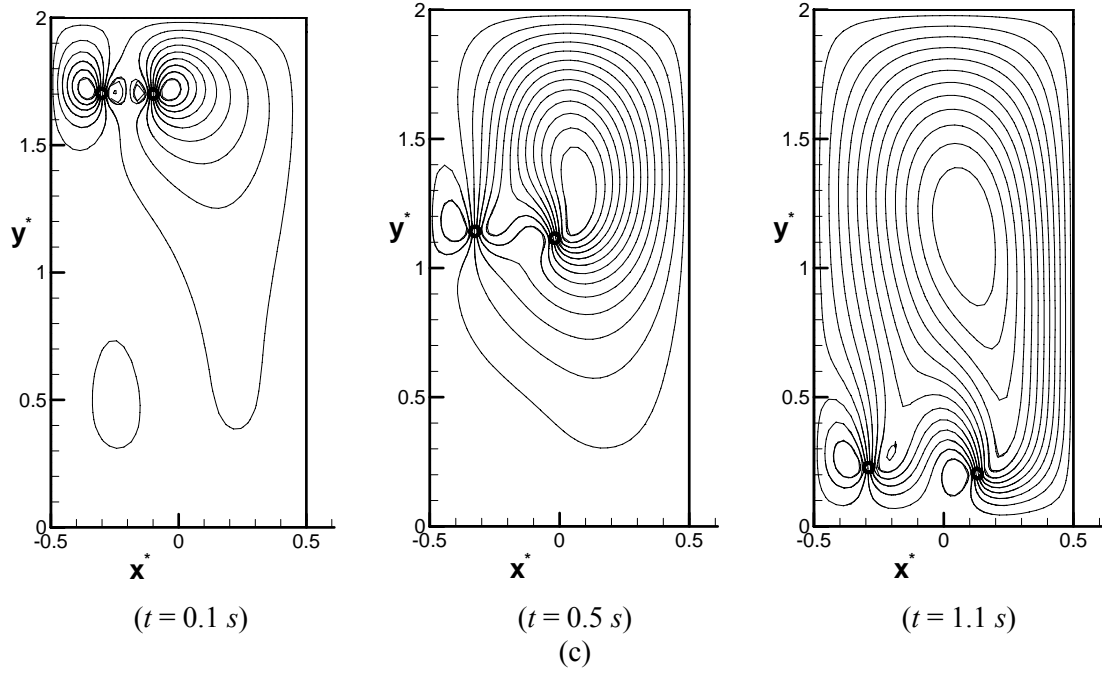


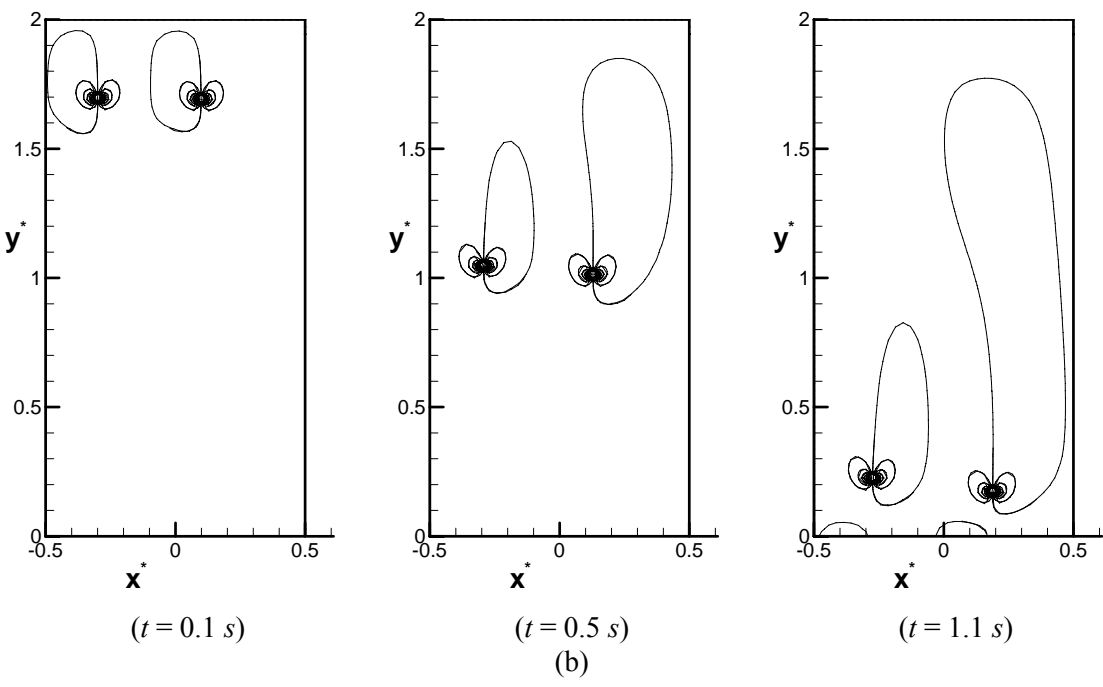
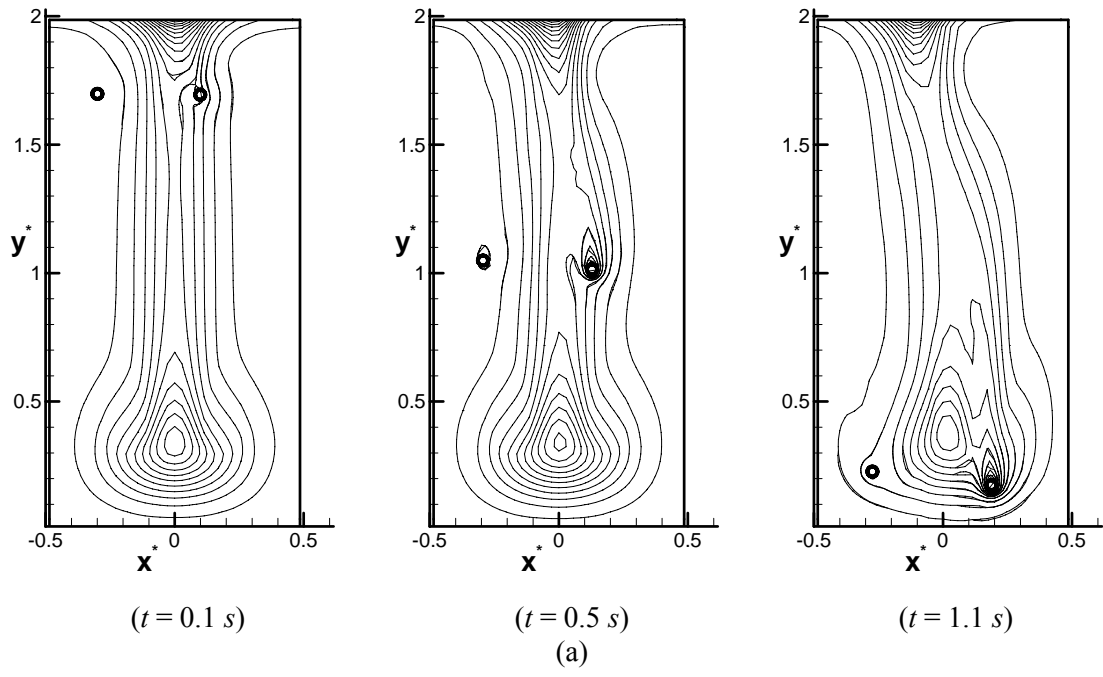
Figure 8-4. Case B: (a) Dimensionless number density of microorganisms, (b) Contour lines of dimensionless vorticity, (c) Contour lines of dimensionless streamfunction, (d) Vector field of fluid velocity

In Case B (Fig. 8-4) Particle 2 is also released to the left of the plume (at $x^* = -0.1$). The bioconvection plume is pushed to the right and away from the settling particles. By the end of sedimentation, both particles are displaced from the left side of the computational domain to the center of the domain. Figure 4a shows that at $t = 1.1$ s Particle 2 has a lower vertical position than Particle 1 reflecting a larger downward vertical velocity. This is because the bioconvection velocity is directed downward in the center of the domain and upward at its periphery. Figure 8-4d ($t = 0.1$ s) shows that convective circulation around Particle 2 is stronger than around Particle 1, so that Particle 1 is displaced to the left in the beginning of the sedimentation process (see Fig. 8-7a). In Fig. 4d ($t = 0.5$ s), similarly to case A, counter-propagating jets develop to the left of Particle 1. The fluid velocity is downward to the left of Particle 1 in the upper part of the computational domain and upward in the lower part of the domain. A horizontal jet develops displacing Particle 1 to the right (as in Case A in Fig. 8-3). Another horizontal jet is generated between the two particles because of the collision of the two vertical counter-propagating jets marked by block arrows in Fig. 8-4d ($t = 1.1$ s). This horizontal jet pushes Particle 2 to the right. The paths of the particle centers for Case B are displayed in Fig. 8-7a. As explained above, initially Particle 1 is displaced to the left by the convective circulation caused by Particle 2. Later the horizontal jet developed during sedimentation pushes Particle 1 to the right. Particle 2 is displaced to the right during the whole duration of the sedimentation process by the horizontal jet generated between Particles 1 and 2. Comparing Figs. 8-4a ($t = 1.1$ s) and 8-3a, it is evident that the bioconvection plume has larger horizontal displacement in Case B than in Case A, which means that introducing an additional particle on the same side of the plume increases the displacement of the bioconvection plume.

In Case C (Fig. 8-5), Particle 2 is released to the right of the plume, at $x^* = 0.1$, thus the convective circulations induced by the two particles are more symmetric. Figure 5a shows that the displacement of the bioconvection plume to the right is less than in Cases A and B. Particle 1, which is farther away from the center of the plume than Particle 2, has more effect on the plume displacement, implying a

direct relation between particle distance from the plume center and influence on plume displacement. Obviously, moving the particle far away from the plume will diminish this influence; therefore, it is expected that there exists an optimal distance at which the particle's effect on the plume is the strongest. Both particles move to the right during sedimentation as seen in Fig. 8-7b. The distance between the particles in Case C is too great for the convection circulation around Particle 2 to have any noticeable effect on Particle 1. Recall that this is not so in Case B (Fig. 4d) where the particles are closely spaced and the convection circulation around Particle 2 influences Particle 1 by initially displacing it to the left (Fig. 8-7a). Particle 2 has larger vertical velocity than Particle 1. The paths of the particle centers for Case C are displayed in Fig. 8-7b. Particle 2 exhibits larger horizontal displacement than Particle 1 during sedimentation.

In Case D (Fig. 8-6), the two particles are initially positioned symmetrically relative to the vertical centerline of the bioconvection plume, so that for Particle 2, $x^* = 0.3$. Sedimentation occurs symmetrically and the two particles settle without significantly changing the shape and location of the bioconvection plume. Comparing Fig. 8-2 (no particles) and Fig. 8-6a ($t = 0.5 s$), it is evident that the particles have a constrictive influence, locally reducing the width of the plume in a horizontal plane where the particles are located. No noticeable horizontal jets are found in Fig. 8-6d, which means that the horizontal displacements that the two particles exhibit are caused by bioconvection. The paths of particle centers for Case D are displayed in Fig. 8-7c. The two particles move from the periphery of the domain toward its center during sedimentation because of bioconvection. The bioconvection flow is directed toward the plume's center in the upper part the domain and away from the plume's center in the lower part of the domain. This explains why the particles are displaced toward the center of the domain during sedimentation, moving first with an increasing horizontal velocity and then with a decreasing horizontal velocity.



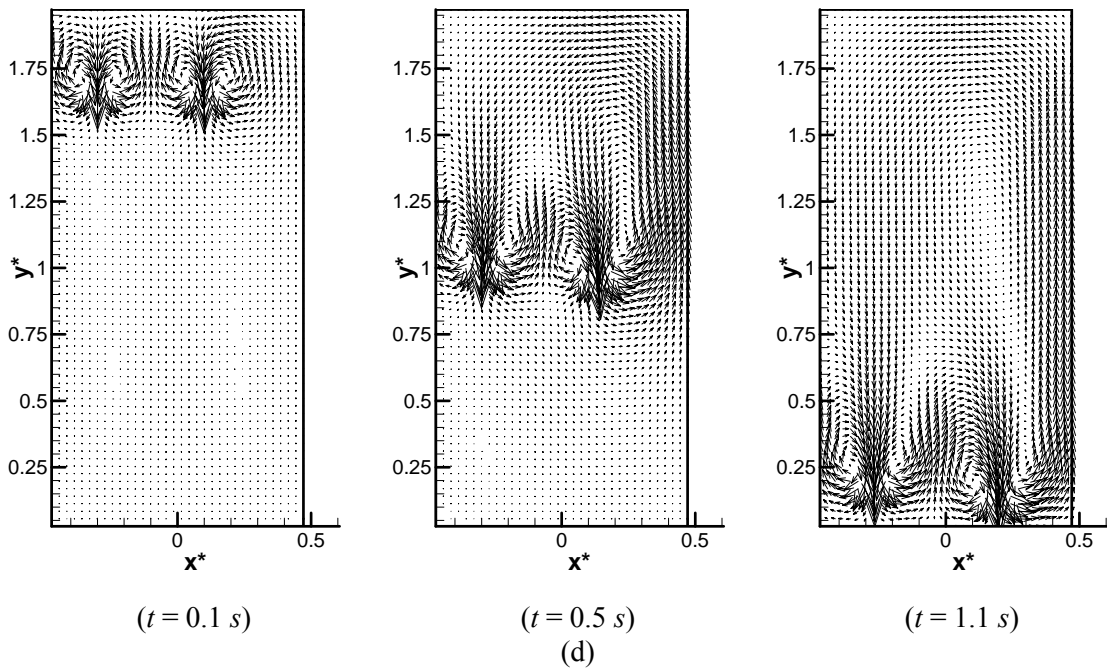
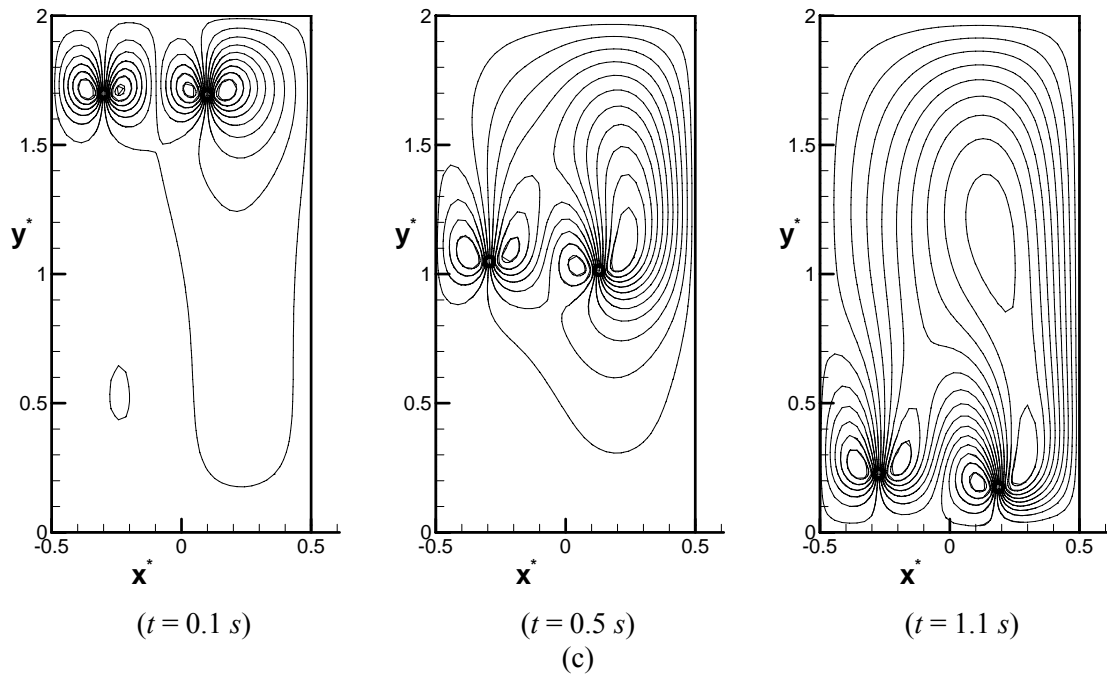
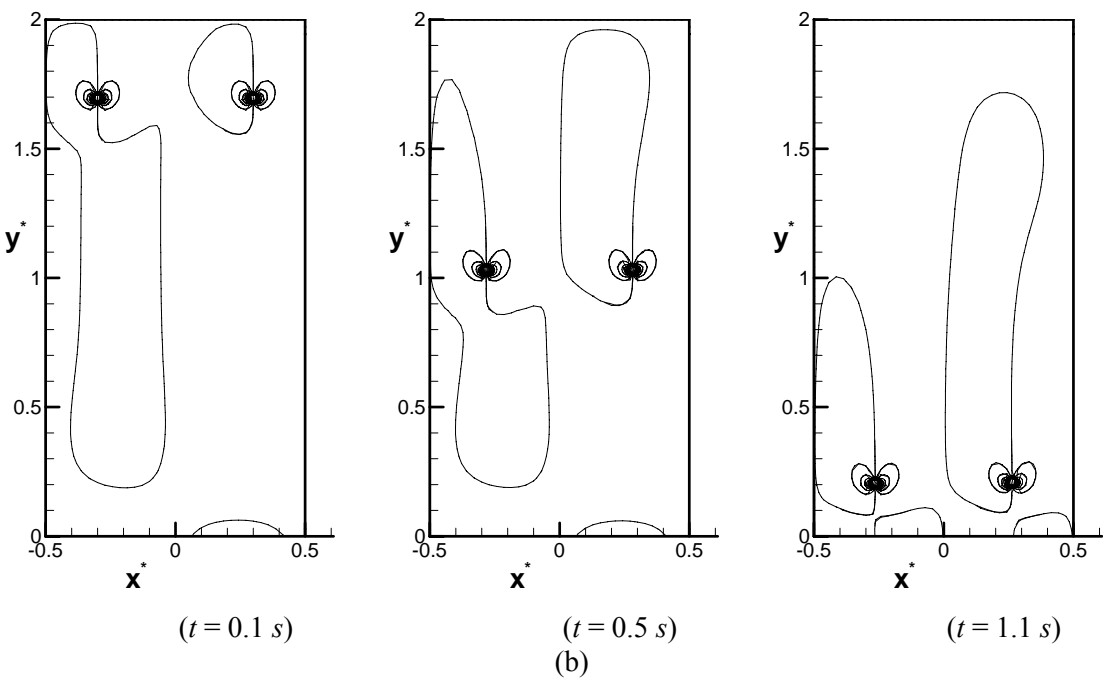
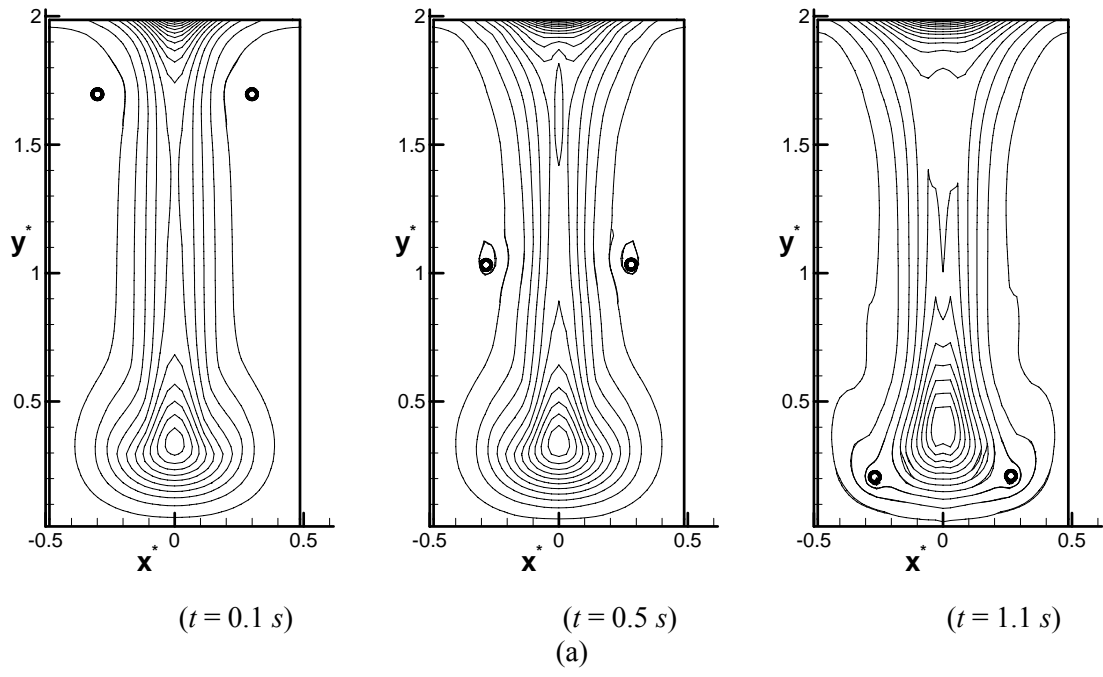


Figure 8-5. Case C: (a) Dimensionless number density of microorganisms, (b) Contour lines of dimensionless vorticity, (c) Contour lines of dimensionless streamfunction, (d) Vector field of fluid velocity



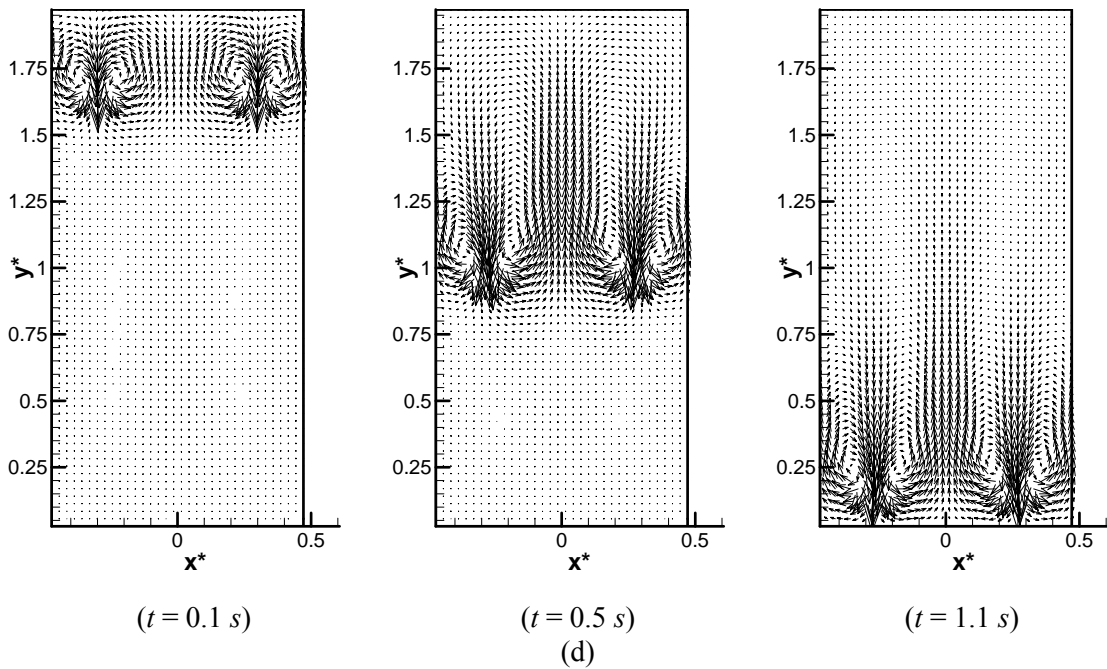
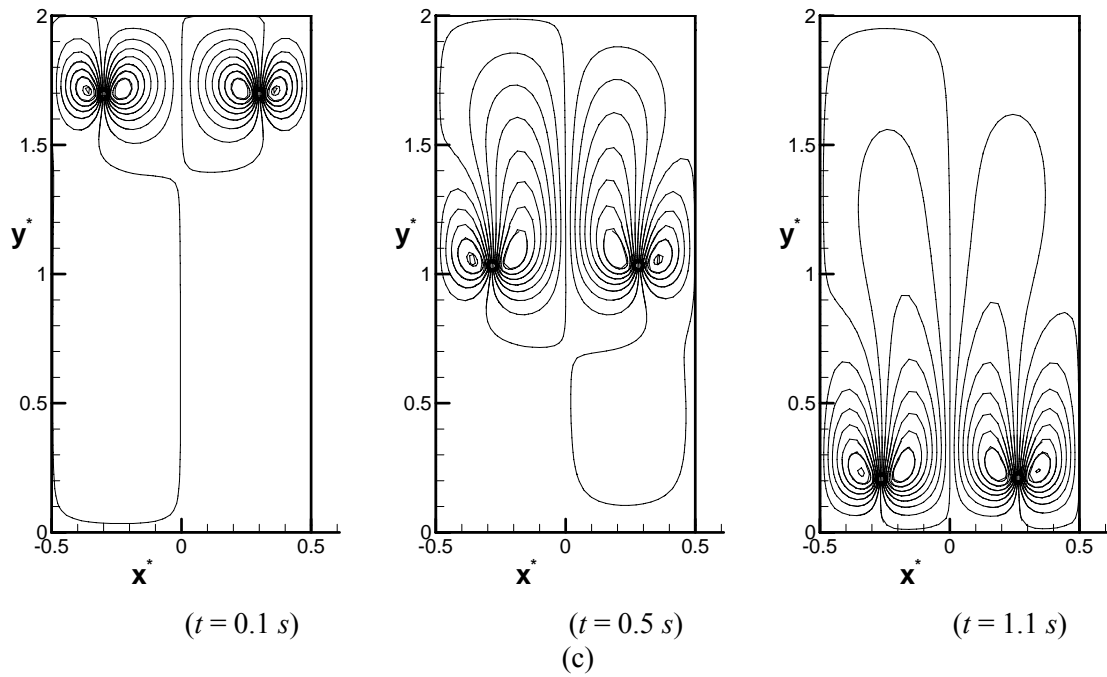


Figure 8-6. Case D: (a) Dimensionless number density of microorganisms, (b) Contour lines of dimensionless vorticity, (c) Contour lines of dimensionless streamfunction, (d) Vector field of fluid velocity

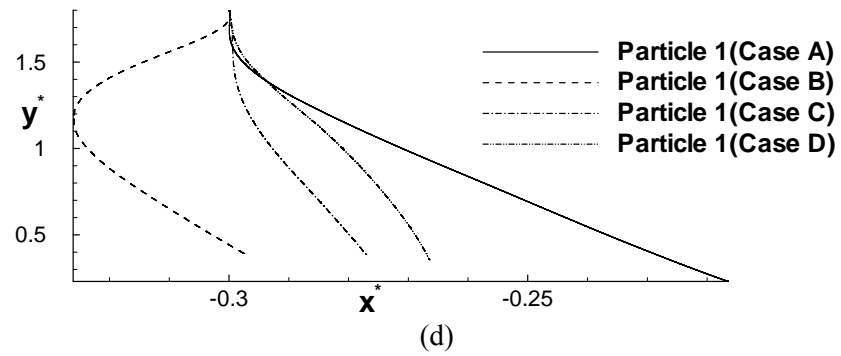
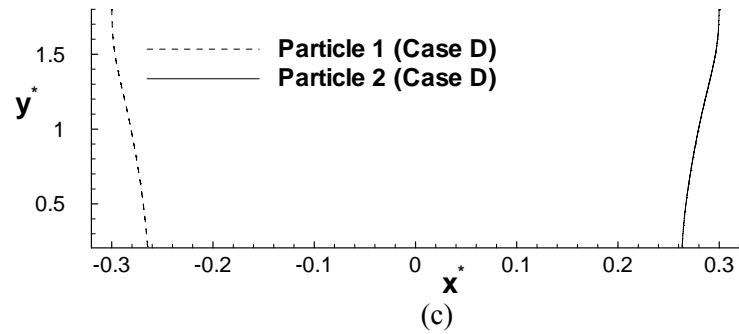
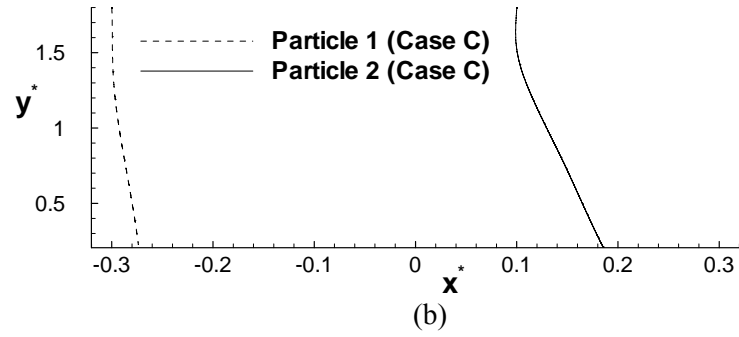
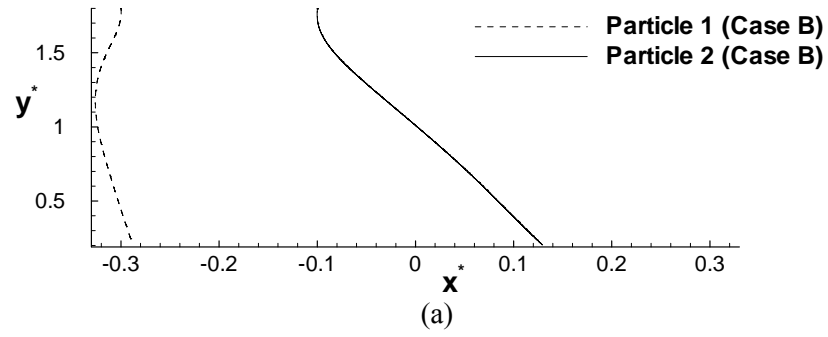


Figure 8-7. Paths of particle centers for (a) Case B, (b) Case C, (c) Case D and (d) Paths of the center of the Particle 1 for Cases A-D

The paths of Particle 1 (Cases A-D) are summarized in Fig. 8.7d. Particle 1 exhibits a large horizontal displacement in Case A while with the addition of Particle 2 in Cases B-D this displacement decreases. The presence of Particle 2 increases the symmetry of convection. The greater the distance between the two particles initially, the less Particle 1's course is altered.

In order to additionally validate numerical results, Figs. 8-8a and 8-8b displays the dimensionless y -velocity, V_y^* , of Particles 1 and 2, respectively, for various cases. The horizontal lines in Figs. 8-8a and 8-8b show the particle terminal velocity resulting from the balance of gravitational and viscous forces:

$$F_D = (\rho_p - \rho_0) (\pi r_0^2) g \quad (8.21)$$

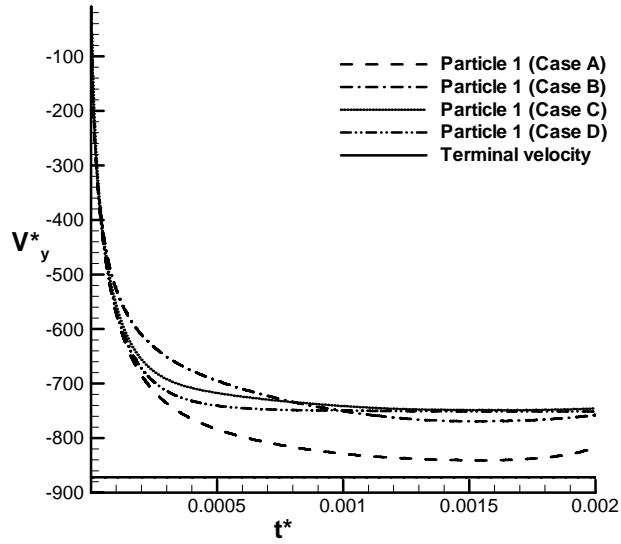
The particle terminal velocity, U , is found by substituting Eq. (8.21) into the following experimental curve-fit correlation for a drag coefficient in a flow past a circular cylinder suggested by Sucker and Brauer¹⁶:

$$C_D = \frac{F_D}{\rho_0 U^2 r_0} \approx 1.18 + \frac{6.8}{\text{Re}^{0.89}} + \frac{1.96}{\text{Re}^{0.5}} - \frac{0.0004 \text{Re}}{1 + 3.64 \times 10^{-7} \text{Re}^2} \quad (8.22)$$

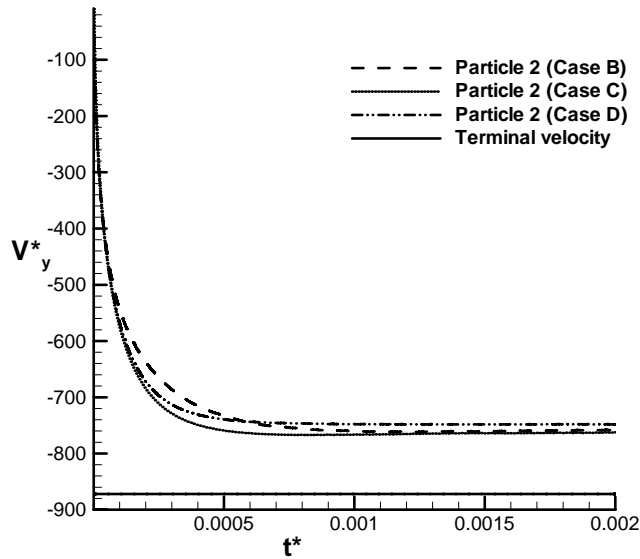
where $\text{Re} = \frac{2Ur_0}{\nu}$ and F_D is the viscous drag force on the cylinder.

Figures 8-8 show that particle velocities at the end of the sedimentation process approach the particle terminal velocity (obtained using experimental correlation (8.22)) in all Cases A-D, which validates the obtained numerical results. The settling velocity of the particles at the end of sedimentation is a little smaller than the particle terminal velocity because the bioconvection flow creates a "pillow" at the bottom of the chamber and slows down sedimentation. At the end of sedimentation, the particle velocity of the single particle case (Case A) is closer to U than that of the multiple particle cases

(Cases B-D). This is apparently a result of the interaction of the multiple particles with the bioconvection plume.



(a)



(b)

Figure 8-8. Dimensionless velocity in the y direction at the center of the particles (a) Particle 1, (b) Particle 2

8.4 CONCLUSIONS

Sedimentation of one and two large particles suddenly released in a fully developed bioconvection plume is investigated. Particle sedimentation changes the shape and location of the bioconvection plume. Settling of a single particle to one side of the plume shifts the bioconvection plume away from the particle. Increasing geometric similarity about the plume center for multiple particle sedimentation decreases plume displacement while decreasing this similarity increases plume displacement. The particles' settling is also affected by bioconvection. Because of bioconvection, particles are pushed in both vertical and horizontal directions. The direct interaction between the bioconvection plume and the particles as well as the indirect interaction between the two particles depends on the initial position of the particles. The computational results suggest evidence of an optimal distance between the vertical symmetry plane of the unit cell and the initial position of the particle at which the particle's effect on the plume is the strongest. Further numerical studies are needed to understand whether the introduction of large particles can result in the plume breaking apart, forming two or multiple bioconvection plumes. These studies should involve multiple unit cells, which would allow investigating the effect of multiple plumes on particle sedimentation.

REFERENCE

1. Pedley, T.J., Hill, N.A. and Kessler, J.O., "The Growth of Bioconvection Patterns in a Uniform Suspension of Gyrotactic Microorganisms," *J. Fluid Mech.*, **195**, 223 (1988).
2. Ghorai, S. and Hill, N.A., "Development and Stability of Gyrotactic Plumes in Bioconvection," *J. Fluid Mech.*, **400**, 1 (1999).
3. Ghorai, S. and Hill, N.A., "Periodic Arrays of Gyrotactic Plumes in Bioconvection," *Physics of Fluids*, **12**, 5 (2000).

4. Kuusela, E, "Steady-State Sedimentation of Non-Brownian Particles with Finite Reynolds Number," Dissertation of Department of Engineering Physics and Mathematics, Helsinki University of Technology (Espoo, Finland), (2005).
5. Liu, Yaoqi, Nelson, John, Feng, Jimmy, and Joseph, Daniel D., "Anomalous Rolling of Spheres Down and Inclined Plane," *J. Non-Newtonian Fluid Mech.* **50**, 305 (1993).
6. Joseph, D. D., Liu, Y.J., Poletto, M., and Feng, J., "Aggregation and Dispersion of Spheres Falling in Viscoelastic Liquids," *J. Non-Newtonian Fluid Mech.* **54**, 45 (1994).
7. Singh, P. and Joseph, D.D., "Sedimentation of a Sphere Near a Vertical Wall in an Oldroyd-B Fluid," *J. Non-Newtonian Fluid Mech.* **94**, 179 (2000).
8. Gan, H., Chang, J., Feng, J. and Hu, H., "Direct Numerical Simulation of the Sedimentation of Solid Particles with Thermal Convection," *J. Fluid Mech.* **481**, 385 (2003).
9. Geng, P. and Kuznetsov, A.V., "Settling of Bidispersed Small Solid Particles in a Dilute Suspension Containing Gyrotactic Microorganisms," *International Journal of Engineering Science* **43**, 992 (2005).
10. Geng, P. and Kuznetsov, A.V., "Introducing the Concept of Effective Diffusivity to Evaluate the Effect of Bioconvection on Small Solid Particles," *International Journal of Transport Phenomena*, **7**, 321 (2005).
11. Geng, P. and Kuznetsov, A.V., "Direct Numerical Simulation of Settling of a Large Solid Particle During Bioconvection," *International Journal of Numerical Methods in Fluids*, under review.

12. Liu, Jian-Guo and Wang, Cheng, "High Order Finite Difference Methods for Unsteady Incompressible Flows in Multi-connected Domains," *Computes & Fluid*, **33** 223 (2004).
13. Hsiao, Chao-Tsung and Chahine Georges L., "Numerical Simulation of Bubble Dynamics in a Vortex Using Navier-Stokes Computations and Moving Chimera Scheme," *Proceedings of the Fourth International Symposium on Cavitation (CAV2001)*, June 20-23, 2001, Pasadena, CA, USA, session A10.001 (2001).
14. Houzeaux, G. and Codina, R., "Dirichlet/Neumann(Robin) Coupling for the Navier-Stokes Equations," *Computer Methods in Applied Mechanics and Engineering* **192**, 3343 (2003).
15. Pedley, T.J. and Kessler, J.O., "The Orientation of Spheroidal Micro-organisms Swimming in a Flow Field," *Proc. R. Soc. Lond.* **B231**: 47 (1987).

9 CONCLUSIONS

Bioconvection is a convection motion of fluid that results from the density gradient created by collective swimming in a particular direction of motile microorganisms that are heavier than the fluid. The formation of bioconvection plume is investigated analytically. Two kinds of possible applications that utilizing bioconvection plumes are studied numerically. Applications of bioconvection in the pharmaceutical and bio-technological industries to enhance mixing in microvolumes of a fluid is modeled as utilizing bioconvection to enhance the mixing of a suspension of small solid particles. Large particles sedimentation in bioconvection is simulated as well. The numerical results of large particle settling agree well with the analytical results.

9.1 REMARKS ON FALLING BIOCONVECTION PLUME

Microorganisms may swim in a certain direction due to different stimulus such as oxytactic, phototaxis, chemotaxis, and gyrotaxis. The formation of oxytactic bioconvection plume was studied analytically in Chapter 2 and 3. These bacteria consume oxygen and swim up the oxygen gradient as they require certain minimum concentration of oxygen to be active. Microorganisms concentrate at oxygen-rich region that is close to the free surface and cause instability, result in the formation of falling plumes that carry cells and oxygen into the lower part of the chamber. Similarity solutions of governing equations are obtained. The obtained numerical solutions reveal that the cell concentration increases from the periphery of the plume toward its center.

9.2 REMARKS ON SMALL SOLID PARTICLES SETTLING IN BIOCONVECTION

A possible application of bioconvection is to use bioconvection to slow down settling and enhance mixing between particles. Small particles' sedimentation in bioconvection of gyrotactic microorganisms is studied numerically in Chapter 4-6. Gyrotaxis is the behavior typical for algae, whose swimming direction is determined by the balance of gravitational and viscous torques. Both microorganisms and particles are heavier than water. The particles are small, so that the Brownian

diffusion is not completely negligible. It was established that bioconvection makes number density distribution of solid particles more uniform (Chapter 4) Sedimentation in bioconvection with two kinds of small particles (bidispersed suspensions of small particles) that have different densities is investigated in Chapter 5. A useful method of adjusting particle concentration in bio-convection by introducing particles of a different density is suggested. A new parameter, called the *effective diffusivity* of solid particles, is defined in Chapter 6 to evaluate the effect that bioconvection has on the mixing of solid particles. It is found numerically that that bioconvection is less effective in mixing suspensions of heavy particles than it is in mixing suspensions of light particles.

9.3 REMARKS ON LARGE SOLD PARTICLES SETTLING IN BIOCONVECTION

Settling of one or two large solid particles in a bioconvection flow induced by gyrotactic motile microorganisms is numerically modeled. The results of varying the initial positions of large particles on the bioconvection flow pattern are investigated. The particle settling changes the shape and location of the bioconvection plume. It is found that restricting the size of the computational domain to one periodic cell by imposing periodic boundary conditions at the vertical boundaries of the domain pushed the particle away from the periodic boundary (Chapter 7). Increasing geometric similarity about the plume center for multiple particle sedimentation decreases plume displacement while decreasing this similarity increases plume displacement. The direct interaction between the bioconvection plume and the particles as well as the indirect interaction between the two particles depends on the initial position of the particles. The computational results suggest evidence of an optimal distance between the vertical symmetry plane of the unit cell and the initial position of the particle at which the particle's effect on the plume is the strongest (Chapter 8).

9.4 RECOMMENDATIONS FOR FUTURE WORK

It is assumed that bioconvection plumes occur periodically. The two-dimensional computational domain coinciding with a periodic cell that contains a single bioconvection plume is the typical

computational domain in researches of bioconvections. A computational domain that contains two bioconvection plumes was investigated. It is very interesting to investigate the large particles settling in the bioconvection with computational domain that contains more than two chambers. Large particles sedimentation in bioconvection was simulated in 2D model therefore the particles were treated as infinite long cylinders. 3D model is highly recommended in future research that the large particles are modeled as spheres.